Review of the T-H-M-C Properties of MX-80 Bentonite

NWMO-TR-2019-07 June 2019

David A. Dixon

Golder Associates Limited

nwmo

NUCLEAR WASTE MANAGEMENT ORGANIZATION

SOCIÉTÉ DE GESTION DES DÉCHETS NUCLÉAIRES

Nuclear Waste Management Organization
22 St. Clair Avenue East, 6th Floor
Toronto, Ontario
M4T 2S3
Canada

Tel: 416-934-9814
Web: www.nwmo.ca

Review of the T-H-M-C Properties of MX-80 Bentonite

NWMO-TR-2019-07

June 2019

David A. Dixon
Golder Associates Limited

Document History

Title:	Review of the T-H-M-C Properties of MX-80 Bentonite		
Report Number:	NWMO-TR-2019-07		
Revision:	R000	Date:	June 2019
Golder Associates Limited			
Authored by:	David A. Dixon		
Verified by:	Frank Barone		
Approved by:	George Schneider		
Nuclear Waste Management Organization			
Reviewed by:	Kenneth Birch		
Accepted by:	Chris Boyle		

ABSTRACT

Title: **Review of the T-H-M-C Properties of MX-80 Bentonite**
Report No.: **NWMO-TR-2019-07**
Author(s): David A. Dixon
Company: Golder Associates Limited
Date: June 2019

Abstract

The filling of the placement room for the Mark II geometry includes the use of both highly compacted bentonite blocks that surround and maintain spacing between the used fuel containers, as well as much-lower density granular bentonite materials that are used to fill the voids between the bentonite blocks and the surrounding rock mass. A review of information available regarding the thermal, hydraulic, gas transport, mechanical, chemical and other related properties of water-saturated MX-80 bentonite has been completed in order to identify key parameter values needed for the conduct of performance assessment modelling of bentonite installed in NWMO's Mark II placement geometry.

Evaluation of the influence of environmental conditions and processes that may affect the performance of bentonite under repository conditions has been included in the review of available information. As NWMO is considering both Sedimentary and Crystalline rock as potential host media for a deep geological repository, a very wide range of conditions must be considered in the evaluation of the engineered barriers system.

Conditions that need to be considered in the evaluation of performance of bentonite-based barriers include, but are not limited to: the effects of bentonite density, fluid saturation, pore fluid composition (salinity, pH), temperature, interaction of bentonite with corrosion products from a UFC, radiation, and bacterial activity. The parameters that will most immediately affect the physical performance of the bentonite are its density, degree of water saturation and the salinity of the water entering the system from the surrounding rock. The initially high thermal gradient across the placement rooms shortly after UFC placement will affect system behaviour, particularly prior to achieving water-saturation.

Over the longer-term, on achieving water saturation other parameters and processes such as pH change, steady-state temperature, bacterial activity, corrosion and cementation may affect the behaviour of bentonite. It would not appear that radiological conditions will physically affect the behaviour of bentonite, although release and subsequent transportation of radionuclides through the engineered barriers must be considered.

Based on the review of the properties of MX-80 Bentonite for use as a sealing material in the NWMO placement concept, there are three opportunities that exist to build further confidence in predicting parameter values and predict system performance, they are as follows:

- Addressing the combined effects of elevated temperature and high groundwater salinity on the deformation characteristics of bentonite;
- Continued correlation of the results of quality-control testing on as-received bentonite with expected performance behaviour, with the goal of making any appropriate modifications to material acceptance criteria for a production setting; and
- Conducting physical and numerical modelling of coupled T-H-M mockups of NWMO's current placement geometry in order to gain further confidence in the ability to understand and predict sealing system behaviour.

TABLE OF CONTENTS

Page

ABSTRACT ..... **iii**

DEFINITION OF TERMINOLOGY AND ACRONYMS ..... **x**

1. INTRODUCTION **1**

1.1 GOALS **1**
1.2 SCOPE **1**

2. DESCRIPTION OF NWMO'S DGR CONCEPT **3**

2.1 GENERIC CONCEPT DESCRIPTION **3**
2.2 INFLUENCE OF GEOSPHERE TYPE AND CONDITIONS **7**
2.2.1 Sedimentary Rock 8
2.2.2 Crystalline Rock Geosphere 11

3. DESCRIPTION OF BUFFER AND GAP FILL MATERIALS **14**

3.1 BUFFER MATERIALS IN NWMO'S REPOSITORY SEALING CONCEPT **14**
3.2 GAP FILL MATERIALS IN NWMO'S REPOSITORY SEALING CONCEPT **17**
3.3 INFLUENCE OF COMPONENT DENSITY ON OVERALL SYSTEM DRY DENSITY **20**
3.4 EQUILIBRATED SYSTEM **21**

4. T-H-M-C PROPERTIES OF HCB AND GFM MATERIALS **23**

4.1 BASIC REQUIREMENTS AND PROPERTIES NEEDED IN HCB AND GFM **23**
4.2 BASIC MATERIAL PROPERTIES THAT CAN BE USED TO HELP DETERMINE BENTONITE BEHAVIOUR **24**
4.2.1 Background 24
4.2.2 Mineralogy 25
4.2.3 Mineralogy-Related Materials Properties 27
4.2.4 Grain Size Distribution 28
4.3 POROSITY AND PORE-SIZE DISTRIBUTION IN GFM AND HCB **30**
4.4 GROUNDWATER CONDITIONS **33**
4.5 EFFECT OF RADIOLOGICAL PROCESSES ON BENTONITE STABILITY **34**
4.5.1 Background 34
4.5.2 Direct Radiation Damage to Mineral Structure 34
4.5.3 Alpha Radiation 35
4.5.4 Gamma Radiation 37
4.5.5 Radiolysis Effects on Montmorillonite 39
4.5.6 Summary of Literature Information Regarding Radiation Effects on Bentonite 41

5. T-H-M-C(B) PARAMETERS DETERMINATION FOR HCB AND GFM **44**

5.1 VOLUME CHANGE PROPERTIES OF HCB AND GFM **44**
5.1.1 Shrinkage During Drying 44
5.1.2 Swelling on Contact with Free Water and Drying Shrinkage 46
5.1.3 Volume Equilibration of Buffer/Gap Fill Materials 48
5.1.4 Summary of Volume-Change Behaviour 49
5.2 THERMAL PROPERTIES OF HCB AND GFM **49**

5.2.1 Key Environmental Parameters Effecting HCB and GFM Thermal Properties. ... 49
5.2.2 Thermal Properties of Bentonite ... 49
5.2.2.1 Background ... 49
5.2.2.2 Statistical Evaluation of Thermal Properties Data ... 50
5.2.2.3 Thermal Conductivity of Bentonite ... 51
5.2.2.4 Thermal Diffusivity, Specific Heat Parameters ... 56
5.2.3 Influence of Ambient Temperature on Thermal Properties ... 57
5.2.4 Influence of Pore Water Composition on Thermal Properties ... 58
5.2.5 Role of Secondary Processes (e.g. cementation, bacteria) ... 59
5.2.6 Summary of Thermal Properties ... 59
5.3 WATER ACTIVITY AND SUCTION-MOISTURE PROPERTIES ... 60
5.3.1 General ... 60
5.3.2 Water Activity (a_w): Impact on Bacteria Viability ... 61
5.4 HYDRAULIC PROPERTIES OF HCB AND GFM ... 66
5.4.1 Background ... 66
5.4.2 Advective Flow Through MX-80 ... 68
5.4.2.1 Flow Under Freshwater Conditions ... 69
5.4.2.2 Effect of Pore Fluid Salinity on Hydraulic Conductivity ... 70
5.4.2.3 Statistical Evaluation of Hydraulic Conductivity Data ... 71
5.4.3 Effect of Temperature on Hydraulic Properties of Dense Bentonite ... 73
5.4.4 Effects of Secondary Processes Such as Cementation, Mineral Dissolution and Bacteria on Hydraulic Behaviour ... 75
5.4.4.1 Cementation/Dissolution ... 75
5.4.4.2 Bentonite Erosion ... 78
5.4.4.3 Microbes ... 80
5.4.5 Summary ... 81
5.5 SWELLING PRESSURE OF HCB AND GAP FILL ... 81
5.5.1 Background ... 81
5.5.2 Swelling Pressure in MX-80 ... 82
5.5.2.1 Role of Density and Pore Fluid Salinity ... 82
5.5.2.2 Statistical Evaluation of Swelling Pressure Data ... 86
5.5.2.3 Influence of Temperature on Swelling Pressure ... 86
5.5.3 Bentonite homogenization ... 88
5.5.4 Secondary Process Effects: Cementation, Mineral Dissolution and Microbes ... 89
5.5.5 Summary ... 90
5.6 GAS TRANSPORT THROUGH HCB AND GFM ... 90
5.6.1 Gas Transport Process ... 90
5.6.2 Identification of Potential Influences on Gas Transport ... 93
5.6.3 Summary ... 94
5.7 SUCTION - MOISTURE CHARACTERISTICS OF HCB, GFM AND EQUILIBRATED SEALING SYSTEM ... 94
5.7.1 Drying Shrinkage of HCB and Gap Fill Material ... 94
5.7.2 Soil Water Characteristic Curves (SWCC) ... 97
5.7.3 Influence of Temperature on Suction in MX-80 ... 100
5.7.4 Effect of Pore Fluid Salinity on Suction in MX-80 ... 102
5.8 MECHANICAL PROPERTIES OF HCB AND GFM ... 104
5.8.1 Key Parameters associated with Mechanical behaviour ... 104
5.8.2 Uniaxial (1-Dimensional) Consolidation Behaviour ... 104
5.8.3 Tensile Strength ... 107
5.8.4 Compressive Strength ... 111
5.8.4.1 Background ... 111

5.8.4.2 Compressive Strength Testing 113
5.8.4.3 Environmental Effects on Compressive Strength 117
5.8.5 Deformation Moduli 119
5.9 ANTICIPATED SYSTEM EVOLUTION AND T-H-M PARAMETERS FOR HCB AND GFM 124
5.9.1 Anticipated Dry Density Evolution of HCB and GFM and Effects on T-H-M Properties 124
5.9.2 Summary: T-H-M Parameter Values for HCB, GFM and Equilibrated System 126

6. INFLUENCE OF LOCAL GEOSPHERE ON REPOSITORY EVOLUTION 129

6.1 Localized High Water Inflow Rate 129
6.2 Physical Erosion of Bentonite 131
6.3 Localized Shearing 132

7. SUMMARY 133

8. REFERENCES 135

APPENDICES 155

APPENDIX A. 1-D CONSOLIDATION DATA SUMMARY 156

APPENDIX B: EXAMPLES OF UNCONFINED COMPRESSIVE SHEAR BEHAVIOUR OF MX80 BENTONITE AND COMPILATION OF LITERATURE DATA 158

APPENDIX C. STATISTICAL ANALYSES OF THERMAL DATA 163

APPENDIX D. STATISTICAL ANALYSES OF HYDRAULIC CONDUCTIVITY DATA: EXPONENTIAL AND POWER FITS 174

APPENDIX E. STATISTICAL ANALYSES OF SWELLING PRESSURE DATA 188

APPENDIX F. EFFECTS OF VARYING PLACEMENT ROOM AND SPACER BLOCK DIMENSIONS ON HOMOGENIZED DRY DENSITY OF SEALING MATERIALS 195

LIST OF TABLES

Page

Table 2-1: Intact Rock and Bedding Plane Mechanical Properties for Sedimentary Formations (Radakovic-Guzina et al. 2015) 11
Table 3-1: Compaction to Produce HCB Using 100 MPa Pressure 15
Table 4-1: Semi-Quantitative X-Ray Diffraction Results for Identical Bulk MX80 Bentonite Samples (3 Laboratories) 26
Table 4-2: Major Oxides Composition of MX80 Bentonite Samples (after Dixon et al. 2018) 27
Table 4-3: MX-80 Mineralogy and Mineralogy-Related Parameters 29
Table 4-4: NWMO Reference Groundwater Compositions at Placement Level of DGR in Sedimentary or Crystalline Host Rocks. 34
Table 4-5: Summary of Internal and External UFC Gamma-Radiation for NWMO's Mark II UFC (Morco et al. 2017) 43
Table 5-1: Free Swell Index & Hydrated Density of Loose MX-80 and National Standard Bentonite in Various Groundwaters. 47
Table 5-2. Best-Fit Equations, Correlation Coefficients and Prediction Bands for Thermal Properties of MX80 Wyoming Bentonite 55
Table 5-3: Chilled-Mirror Hygrometer Test Comparing Suction and a_w (Bag 2011). 61
Table 5-4: Best-Fit Equations and Prediction Intervals for Hydraulic Conductivity of MX-80 Bentonite @ Room Temperature 72
Table 5-5: MX-80 Swelling Pressure @ 25^{o}C for Various Pore Fluid Salinities 86
Table 5-6. Curve-Fitting Functions for Air Conductivity and Air Permeability Curves. 92
Table 5-7: Fitting Parameter Values Used to Estimate Shrinkage in MX-80 97
Table 5-8: Equations Describing the SWCC Curves for MX-80 @ 25^{o}C and Various TDS Conditions 103
Table 5-9. Summary of T-H-M Parameter Values for MX-80 HCB and GFM at Approximately 20^{o}C (unless otherwise noted) 127

LIST OF FIGURES

Page

Figure 2-1: Generic Illustration of the DGR Concept for the Mark II UFC 4
Figure 2-2: Mark II UFC Proposed for Use in NWMO DGR Concept 5
Figure 2-3: Mode of Installation of Buffer Boxes and Spacer Blocks and Resultant Assembly (side view) in one variant of Concept 5
Figure 2-4: Typical Sedimentary Sequencing at the Bruce DGR Site for LILRW in Sedimentary Rock (after Crowe et al. 2016). 9
Figure 2-5: Example of Generic Layout for a DGR in Sedimentary Rock (NWMO 2018). 10
Figure 2-6: Example of Generic Layout for a DGR in Crystalline Rock (NWMO 2017). 12
Figure 3-1: Isostatic Production of HCB Blocks and Resulting Buffer Box 16
Figure 3-2: Uniaxial Compaction Characteristics of MX-80 Bentonite 16
Figure 3-3: Screw Augers Used to Evaluate Ability to Place GFM. 18
Figure 3-4: Photographs of Raw Bentonite and Materials Prepared for Use as Gap Fill 19
Figure 4-1: Side View of Dry Montmorillonite Clay Platelets and Following Limited Hydration (Karnland et al. 2006) 24
Figure 4-2: X-Ray Diffraction Trace for MX-80 Bentonite (Dixon et al. 2018) 26
Figure 4-3. Grain Size Distribution Measurements for MX-80 30
Figure 4-4: Pore-Size Distribution in Compacted Bentonite Measured Using Mercury Porosimeter (Lloret et al. 2003; Romero and Simms 2008). 31

Figure 4-5: Schematic Representations of Pore Structure of Compacted Bentonite 32
Figure 4-6: Free Porosity Calculated from Average Interlayer Distance 33
Figure 4-7: Radiation Dose Rate and Accumulated Dose for Outer Surface of Mark II UFC holding CANDU UF (Morco et al. 2017) 43
Figure 5-1: Thermo-Gravimetric Behavior of MX-80 Bentonite (Vieillard et al. 2016) 45
Figure 5-2: Free Swell Volume of MX-80 Bentonite 48
Figure 5-3: Drying Shrinkage of MX-80 at 1700 kg/m^3 Dry Density and Influence of Pore Fluid Salinity (Abootalebi 2016) 48
Figure 5-4: Thermal Properties of Bentonite: Effect of Material Source, Texture and Density on Thermal Conductivity at < 1500 kg/m^3 Dry Density 52
Figure 5-5: Thermal Properties of HCB: Effect of Material Source, Texture and Density on Thermal Conductivity at >1600 kg/m^3 Dry Density 54
Figure 5-6: Thermal Properties Analyzer (TPS) Used in NWMO Studies 55
Figure 5-7. Thermal Diffusivity and Specific Heat Parameters for HCB at 1500 and 1700 kg/m^3 Dry Density. 56
Figure 5-8: Influence of Ambient Temperature on TC of Bentonite (Abootalebi 2016) 58
Figure 5-9: Relationship Between Water Activity and TDS Concentration 63
Figure 5-10: Relationship Between a_w and Density (after Dixon et al. 2005) 65
Figure 5-11: Relationship Between a_w, Density and TDS (Dixon et al. 2005) 65
Figure 5-12: Hydraulic Conductivity of MX-80 Under Freshwater Conditions 69
Figure 5-13: Effect of Pore Fluid Salinity on Hydraulic Conductivity 70
Figure 5-14: Hydraulic Conductivity of MX-80 Under Saline Groundwater Conditions 71
Figure 5-15: Effects of Temperature on Freshwater Density and Viscosity 73
Figure 5-16: Effect of Temperature on Freshwater Hydraulic Conductivity of Bentonite 74
Figure 5-17: Effect of Temperature on Intrinsic Permeability of MX-80 Once Correction for Viscosity Change is Applied (Daniels et al. 2017) 75
Figure 5-18: Distribution of Layer Charges in a Clay Electrolyte System (Bag 2011) 82
Figure 5-19: Examples of Studies on the Influence of TDS on Swelling Pressure. 84
Figure 5-20: Influence of Density and Pore Fluid Salinity on Swelling Pressure of MX-80 85
Figure 5-21: Effect of Temperature on Swelling Pressure Developed by MX-80 Bentonite 87
Figure 5-22: Observed Patterns of Swelling Pressure Development in Bentonite 89
Figure 5-23: Effect of Density and Degree of Saturation on Air Conductivity (k_a) 92
Figure 5-24: Drying Shrinkage of MX-80 Bentonite @ 1500 and 1700 kg/m^3 Dry Density 96
Figure 5-25: Stepwise Change in Water Content as the Result of Suction (Seiphoori 2015) 98
Figure 5-26: SWCC Curves of Wetting and Drying of MX-80 Bentonite (Seiphoori 2015) 99
Figure 5-27: Air-Entry Values for MX-80 Bentonite (Seiphoori 2015) 99
Figure 5-28: SWCC for MX-80 Under Freshwater Conditions 100
Figure 5-29: Effect of Small Increase in Temperature on Suction of MX-80 101
Figure 5-30: Effect of Density and Substantial Temperature Rise on Suction in MX-80 102
Figure 5-31: Influence of Pore Fluid Salinity on SWCC 103
Figure 5-32: Derivation of the Parameters Cc, Cs in the 1-D Test (Priyanto et al. (2013) 105
Figure 5-33: Lever-Arm Oedometers Used in 1-D Consolidation Testing (Dixon et al. 2018) .. 105
Figure 5-34: 1-D Consolidation Parameters for MX80 Bentonite 107
Figure 5-35: Pull-Test, Tensile Strength Measurement of HCB (Dixon et al. 2006) 108
Figure 5-36: 3-Point Tensile Strength Test Setup (Eriksson 2016) 108
Figure 5-37: Tensile Strength Testing Device Used by Ritola and Pyy (2011). 109
Figure 5-38: Effect of Dry Density on Tensile Strength with Degree of Saturation 75-85% 110
Figure 5-39: Effect of Degree of Saturation on Tensile Strength of HCB 110
Figure 5-40: Schematic Showing Triaxial Cell and Specimen (Börgesson et al. 1995). 113
Figure 5-41: Effects of Density, Saturation and Salinity on Shear Strength of MX80 115
Figure 5-42: Effects of Density, Saturation and Salinity on Strain at Failure of MX-80. 116

Figure 5-43: Effects of Density and Salinity on Friction Angle of MX-80 at Satn. >90%.....117
Figure 5-44: Triaxial Tests on MX-80 Bentonite (after Börgesson and Hernelind 1999). 118
Figure 5-45: Effect of Temperature on Deformation of MX-80 (Börgesson et al. 1988) 119
Figure 5-46: Effects of Density and Salinity on Bulk Modulus of MX-80.....121
Figure 5-47: Effects of Density and Salinity on Shear Modulus.....122
Figure 5-48: Effects of Density and Salinity on Elastic (Young's) Modulus.....123

DEFINITION OF TERMINOLOGY AND ACRONYMS

The terminology used in this document follows that utilized by NWMO in its technical reports related to its deep geological repository (DGR) concept. The terminology used by NWMO is not necessarily identical to those used in other DGR projects and so a brief set of definitions and acronyms related to the placement room and their definition is provided below.

APM - Adaptive Phased Management

AECL – Atomic Energy of Canada Limited.

ANDRA – Implementing agency for radioactive waste disposal in France.

Backfill – An engineered clay, aggregate-clay mixture, aggregate or other material designed to fill a void in the DGR. Its composition may vary depending on its location and functional requirements. In NWMO's Mark II placement concept, placement room backfill is assumed to be composed of bentonite clay.

Bentonite – The tradename used to describe commercially marketed, smectite-rich clay, typically dominated by the clay mineral Montmorillonite.

Buffer – Highly compacted bentonite (HCB) installed immediately adjacent to the UFC (buffer box) in the IFB placement geometry.

Buffer Box – the highly compacted bentonite box and UFC that make up the basic installation package for NWMOs Mark II repository concept.

Bulkhead – a massive structure intended to provide mechanical (and hydraulic) isolation to a tunnel.

Deep Geological Repository (**DGR)** – Facility located deep underground that will be used to host permanent isolation of used nuclear fuel.

Excavation Damaged Zone (EDZ) – rock showing macrostructural change as the result of excavation and excavation-induced damage in the region immediately adjacent to the tunnel openings. Caused by combination of tunnel excavation activities and subsequent rock-stress induced damage to the rock.

Excavation Disturbed Zone (**EdZ)** – rock showing microstructural changes in its behaviour as the result of excavation and excavation-induced disturbance.

Effective Montmorillonite Dry Density (EMDD) – A normalising parameter used to express the density of the swelling clay component after factoring out mass and volume of non-swelling clay solids.

Free Swell Index (FSI) -. A parameter used to describe the volume that a material will occupy when allowed unlimited access to free water and unconfined. Parameter is usually expressed as mL/2gm of dry soil.

Gap Fill (GFM) - The granular swelling clay material installed between the buffer and the surrounding rock mass, also used to fill any other construction voids remaining within the placement room.

Geosphere - The rock environment the DGR will be located within.

Highly Compacted Bentonite (HCB) – Material produced by densely compacting bentonite clay (a dried and crushed, smectite-rich shale) into desired shapes for use immediately adjacent to the UFC (buffer box and spacer block, floor tablets). There is no specific density associated with this material, rather it is a generic descriptor for a highly densified bentonite mass. NWMO defines HCB as being 1700 kg/m^3 dry density.

Hydraulic Pressure (HP) - The fluid pressure present in the geosphere or exerted on the surface of a UFC or sealing structure.

Hydraulic Conductivity (K) - The advective flow velocity of a fluid (groundwater or porewater) through a structure or material.

Horizontal Tunnel Placement (HTP) – The UFC placement geometry proposed by NWMO for use in a sedimentary environment. It consists of a UFC installed on its side in a deposition tunnel excavated to hold a series of these UFC-HCB buffer boxes.

In-Floor Borehole (IFB) – Placement geometry whereby UFCs are installed in boreholes drilled in the floor of the placement room (reference concept for SKB and Posiva)

Isostatic Compaction – compaction method used to produce large accomplished by applying equal pressure in all directions in order to achieve compaction.

Low-Heat High-Performance Concrete (LHHPC) – specially formulated concrete that has limited heat generation during curing, exhibits high compressive strength after curing (and typically has lower pH generation).

Mark II Container - The copper-coated, carbon-steel container that holds 48 bundles of used CANDU reactor fuel. This is the reference container for the NWMO UFD concept. Nominal dimensions are 2.51 m in length and 0.56 m in diameter.

NAGRA – Translates to “National Cooperative for the Disposal of Radioactive Waste” (Switzerland).

NWMO – Nuclear Waste Management Organisation (Canada).

Pellets – Pre-manufactured, clay-based material, typically composed of bentonite-rich clay that is processed into uniformly-sized, high-density aggregations that are used to fill spaces and gaps associated with the buffer and backfill.

Permeability - The ability of a rock or soil mass to transmit water or gas

Placement Rooms – the specially-excavated tunnels in the DGR that are used to install the waste packages in. In some concepts this is also referred to as the placement room although in all cases tunnels are used.

POSIVA – Implementing agency for radioactive waste disposal in Finland

SKB - Swedish nuclear fuel and waste management company

Swelling Pressure - the mechanical pressure applied by a swelling clay on its confinement. This is not the total pressure which is the sum of swelling pressure and hydraulic pressure.

Total Dissolved Solids (TDS) – The quantity of soluble materials in a solution. Typically expressed as gm/L of solution or % of solution mass.

Thermal Conductivity (TC) – Ability of a material to conduct heat, in a DGR environment this is associated with movement of heat from UFC to the surrounding geosphere.

Used Fuel (UF) – the used fuel assemblies removed from a CANDU power reactor. These bundles will not have been physically altered or the used fuel reprocessed prior to installation in a Mark II used fuel container.

Used Fuel Container (UFC) – The corrosion-resistant component of the engineered barriers system used to hold the used fuel assemblies in NWMO's repository terminology. It is the same component as that referred to as the Canister in the SKB/Posiva concepts. In this document it is assumed that the NWMO Mark II container is used.

URL – Underground Research Laboratory.

UFC - Used-Fuel Container (holds the used-fuel bundles in repository)

1. INTRODUCTION

This document provides a summation of the current state of knowledge regarding thermal-hydraulic-mechanical-chemical (T-H-M-C) parameters for the Highly Compacted Bentonite (HCB) and Gap Fill Materials (GFM). These materials are proposed for use as engineered barriers in a placement room of the type proposed for use by NWMO in its Mark II disposal concept. A brief review of the basic Deep Geological Repository (DGR) - relevant T-H-M-C properties of sedimentary and crystalline rock is provided as a basis for discussion of the geosphere influences on the placement room sealing materials.

With definition of the material properties for the host-rock, the T-H-M-C, biological (B) and radiological (R) characteristics of the sealing materials installed in the placement rooms then need to be determined in order to develop confidence in the overall robustness of the sealing system. Confidence in robustness is developed as the result of determining the consistency and reliability of the parameter values used in evaluation sealing materials and system performance and an ability to predict system evolution with time.

1.1 GOALS

This report is intended to review and compile the key T-H-M-C (as well as B and R) properties of the bentonite materials used in the placement room in NWMO's Mark II DGR concept once water saturation has been achieved. This will include consideration of the effects of conditions expected to be present or develop at repository depth in both crystalline and sedimentary geospheres. From these bounding conditions, an overview of the current literature on the physically measured and anticipated T-H-M-C properties of these sealing materials is provided. The influence of processes associated with biological (B) and radiological (R) conditions will be only briefly considered. This review of material properties and parameter values will be used to identify key influences on the properties of the sealing materials installed in a placement room following completion of water saturation of the sealing materials and to identify areas where information is currently lacking. Where possible, suggested material properties, parameter values or relationships will be identified for the sealing system components.

The impact of material properties on the fabrication of bentonite products proposed for repository use; and on their installation in the reference NWMO placement concept will also be discussed as these are key in defining the later saturated and density-equilibrated behaviour of the sealing system.

1.2 SCOPE

In order to complete the above-listed goals, this document:

1. Briefly reviews the NWMO DGR concepts for used nuclear fuel disposal;
2. Identifies key T-H-M-C parameters for the geosphere surrounding the placement rooms in a DGR;
3. Identifies the key T-H-M-C and B-R parameters of relevance to the NWMO DGR Concept and the buffer component specifically, and outlines their anticipated range of values within the DGR placement room;
4. Using literature sources, describes how materials properties will affect fabrication of sealing system components and potentially impact their installation and use in a DGR;

5. Briefly discusses geosphere effects (e.g. mechanical deformation), beyond the chemical and hydraulic impact of groundwater; and
6. Briefly considers the role of initial buffer density on buffer-gap fill density equilibration as well as the influence of water saturation on bacterial activity in the vicinity of the UFCs.

It should be noted that this document does not include discussions of the results of modelling activities related to the prediction of the performance of sealing materials. This document is intended only to provide a summary of the as-measured properties and anticipated changes in behaviour as the result of differences in the thermal and hydro-geochemical environment in the vicinity of the HCB and GFM installed in the placement room.

2. DESCRIPTION OF NWMO'S DGR CONCEPT

NWMO has developed a generic deep geological repository approach to used fuel disposal since both crystalline and sedimentary geosphere are both seen as potentially suitable for a DGR. As noted in NWMO (2017), reference geospheres have been defined for the purposes of concept design and materials development, much of the design is the result of historic experience gained in Canada. The geosphere is an important part of the multi-barrier system as it provides a natural barrier that is hydrogeologically, geomechanically and geochemically stable on timeframes relevant to repository safety (i.e., one million years). The geosphere isolates the repository from surface conditions and provides an environment that allows for a long UFC lifespan (NWMO 2017).

2.1 GENERIC CONCEPT DESCRIPTION

The current conceptual focus for the DGR is on placement of UFCs in accordance with the generic Mark II design as illustrated in Figure 2-1. In this concept, the UFCs are encapsulated by clay-based sealing materials (Buffer Box) and installed horizontally in the placement room. Remaining voids are filled with GFM or other highly compacted bentonite components such as the spacer blocks and floor-levelling tiles. NWMO is considering both deep sedimentary and deep crystalline rock as options for the DGR. The installation geometry of the UFCs for the sedimentary and crystalline rock types are similar, with only minor differences in the dimensions of the underground openings and the spacing between the UFCs differing in these two geosphere options. This difference in opening dimensions may be needed to accommodate the difference in the mechanical properties of the rock types and UFC spacing may need to be different due to thermal properties differences of the two rock types to dissipate the heat generated by the used fuel in the containers.

From the perspective of bentonite-based sealing materials in the placement rooms, the approach to both geospheres is similar. The basic requirements for these clay-based sealing materials are:

- To fill the excavated volume of the DGR's placement room;
- To support the UFCs without experiencing unacceptable change in their location within the placement room;
- To resist physical and chemical deterioration by the local environment during the life of the DGR;
- To limit the rate of groundwater movement into and through the placement rooms; and
- To limit the transport rate of any contaminants (chemical or radioactive) originating in the placement room to the surrounding geosphere.

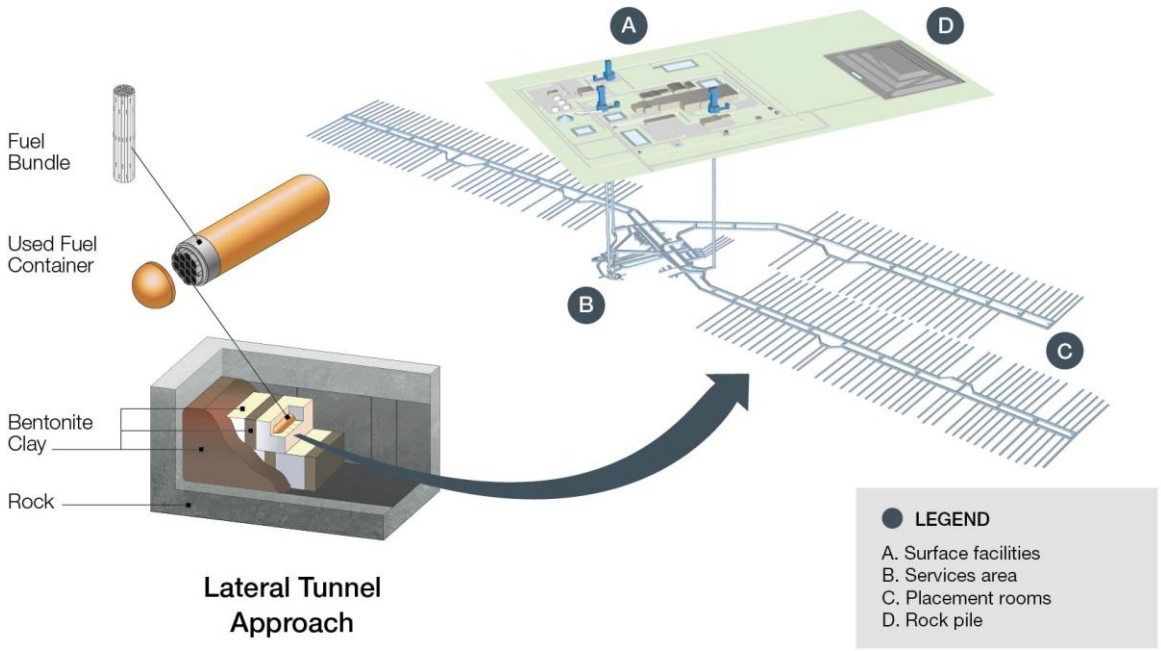

Figure 2-1: Generic Illustration of the DGR Concept for the Mark II UFC

An example of the Mark II UFC is shown schematically in Figure 2-1 and a photograph of this prototype UFC is shown in Figure 2-2 (Hatton 2015). It consists of a 2.51 m-long by approximately 0.56 m-diameter, copper-coated, hemi-head carbon-steel container holding 48 bundles of used CANDU nuclear fuel. The filled and closed container will weigh approximately 2.7 tonnes. The Mark II container is designed to withstand 45 MPa of hydrostatic load. This design is likely to change slightly as optimization occurs but is a representative mass and size that can be used for design of the surrounding sealing system.

The tunnels into which the UFCs would be installed are anticipated to be of approximately 3.2 m width by 2.2 height (Noronha 2016; NWMO 2017), with lengths varying with location and geological conditions at the repository site. Changes to the details of the sealing materials design or opening size to accommodate the installation of the UFCs may result in these nominal dimensions changing (likely slight increase in opening dimensions). These nominal tunnel dimensions reflect anticipated shape of the placement room based on rock strength and deformation characteristics for sedimentary or crystalline rocks, but final dimensions will be determined once an actual repository site is selected and site-specific rock properties are determined. Installation of the buffer boxes and spacer blocks would be accomplished as shown in Figure 2-3 (Noronha 2016). A more detailed discussion of the various components of the clay-based sealing system is provided in Section 3.

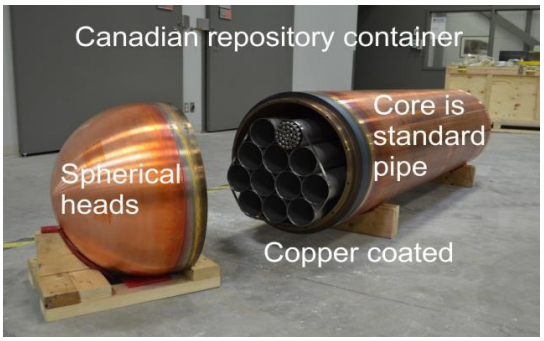

Bundles / Container	48
Total Shell Length	2.515 m
Diameter	0.565 m
Cylinder Surface Area	3.459 m^2
Lids Surface Area	1.002 m^2
TOTAL SURFACE AREA	4.462 m^2
TOTAL VOLUME	0.583 m^3

Figure 2-2: Mark II UFC Proposed for Use in NWMO DGR Concept

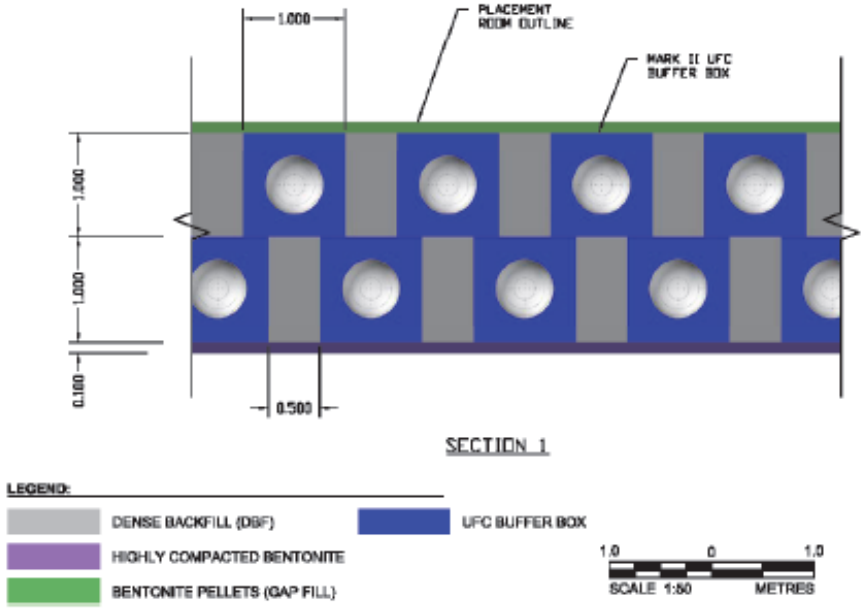

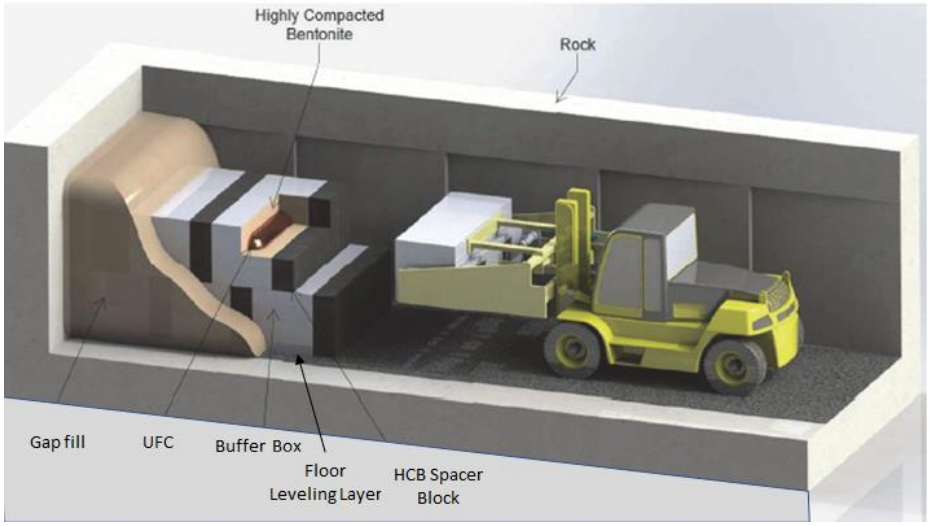

Figure 2-3: Mode of Installation of Buffer Boxes and Spacer Blocks and Resultant Assembly (side view) in one variant of Concept

Beyond the basic requirements and nominal placement room dimensions described above, the following buffer design requirements for NWMO's UFC placement concept were provided by Birch and Mielcarek (2017). The key requirements include maintaining:

- A minimum thickness of 300 mm of 100 % bentonite buffer and gap fill between UFC and geosphere;
- A minimum swelling pressure upon saturation and density equilibration of the swelling clay materials in the placement room of 100 kPa. This will provide a supporting pressure on the excavation walls, thereby limiting the amount of rock that could potentially spall from the excavation wall into a backfilled excavation;
- A maximum saturated hydraulic conductivity of 10^{-10} m/s;
- A maximum water activity (a_w) of 0.96 to suppress bacterial activity and mobility (Stroes-Gascoyne et al. 2007a,b). For groundwaters with salinity of less than 100 g/L, a_w of less than 0.96 is maintained with an average minimum buffer dry density of 1600 kg/m^3. It should be noted that a groundwater salinity of ≥ 100 g/L results in an environment with $a_w < 0.96$; and
- A maximum UFC surface temperature of <100 °C.

Based on these more detailed requirements, a 100 % bentonite buffer has been selected for use in isolating the UFCs. Isolation would be provided through use of:

- A “buffer box” consisting of highly compacted bentonite (HCB) clay produced by isostatic compaction. This box consists of two segments of 2.9 m length (x) by 0.5m height (y) and 1m depth (z) as viewed from the front face of the block assembly. These segments will be machined so as to provide a tight-fitting enclosure for the UFC.
- Highly compacted “spacer” blocks consisting of the same type of HCB blocks as were used for the buffer box. They differ from the buffer box in that their dimensions will be 2.9m x 1m x (0.3 to 0.7 m). The depth (z) will be between 0.3 and 0.7 m with no machined voids. Increasing the depth of the spacer blocks will increase the distance between the UFC’s and so provide for a lower heat loading, allowing temperatures to be controlled in the placement room and surrounding geosphere. The final dimensions of these blocks will be determined by the actual thermal conditions in the geosphere location chosen for the repository as well as the distance between the placement rooms.
- Highly compacted bentonite “floor tablets” will be installed immediately below the buffer box and spacer blocks. These tiles will be compositionally identical to the other HCB materials. Their dimensions are not clearly defined but their height (y) is expected to be in the order of 0.15 m. These tiles are intended to provide a greater spacing between the UFC and the tunnel floor as well as providing a partial “sacrificial” layer to ensure that any adverse chemical interactions between the floor leveling material(s) and the UFC does not extend into the buffer-box materials. It is assumed that roughly 0.05 m of this tablet material will lose its swelling and sealing capacity. In this manner the 0.3 m thickness of functioning bentonite is maintained.
- The use of drill and blast or other means of tunnel excavation will always result in some degree of roughness or unevenness in the floor. In order to provide for a very smooth and suitably level floor for subsequent placement of HCB floor tablets, buffer boxes and spacer blocks a means to level the floor is required. At present, one solution would be through the installation of an approximately 0.1m-thick concrete floor smoothing layer. The formulation of this concrete will be such that its potential to adversely affect HCB

behaviour will be limited and extend no further towards the UFC than the thickness of the floor tablets.

- The remaining gap between each of the walls and roof of the tunnel and the installed HCB/UFC components is required to be no more than 0.3 m at lookouts (points of deepest excavation caused in drill and blast excavation). This gap between the rock and HCB blocks is additionally specified to be at least 0.15 m in width. Hence there is a 0.15 to 0.3 m wide gap that will need to be filled. NWMO is planning to use a granulated material (GFM) produced from compacted bentonite and this material will be installed using a special auger.

It is currently required that the bentonite-filled regions provide an average dry density that is ≥ 1600 kg/m^3. The reasons for this specification are discussed in the body of this document but are primarily associated with generating an environment that meets the buffer requirements listed above and in particular, precludes discernible bacterial activity in the immediate vicinity of the UFC. In order to achieve the required average buffer dry density (based on complete density homogenization), the minimum dry densities established for the two bentonite components (highly compacted bentonite blocks and granular bentonite material) are:

1700 kg/m^3 for HCB components; and

1410 kg/m^3 for GFM Material.

The ability of existing block compaction and gap fill placement technology to meet these targets is discussed in this document, as are the key T-H-M parameter values associated with the reference installation geometry.

2.2 INFLUENCE OF GEOSPHERE TYPE AND CONDITIONS

As noted previously, NWMO is considering locating a DGR for used reactor fuel in either a sedimentary or crystalline rock geosphere.

There are a number of features that will have particular influence on the sealing materials installed to isolate the UFCs and the overall geometry of the DGR (e.g. placement room geometry, UFC spacing and distances between placement rooms). The geosphere conditions of most importance in defining these properties include:

- Rock stability – mechanical strength, deformation characteristics, ability to transfer stress to the sealing materials,
- Rock hydraulic properties – presence of water-bearing fracture features, bulk hydraulic conductivity, connected versus unconnected porosity,
- Rock chemical properties – chemical composition of rock, ability of minerals to dissolve, migrate or influence the local geosphere,
- Thermal characteristics of rock – ability to conduct UFC-supplied heat to the surrounding geosphere, and
- Rock pore fluid – the chemical composition, pH and other properties that could influence the behavior of the sealing materials and/or the robustness of the UFCs

Once the T-H-M-C properties of the host rock is established, the T-H-M-C (and B-R) characteristics of the materials installed in the placement rooms are needed in order to model system evolution and develop confidence in the overall robustness of the sealing system. Confidence in robustness is developed as the result of determining and demonstrating sealing materials performance and an ability to predict system evolution with time.

2.2.1 Sedimentary Rock

The sedimentary geosphere option under consideration by NWMO involves repository construction in deep sedimentary rock formations of the type found in Ontario. Although a site has not been selected, a generic geosphere has been identified and is as described in detail by Gobien et al. (2018).

For the purposes of conceptual design and generic planning, it is anticipated that the type of sedimentary sequencing anticipated to be present at a repository site will be similar to that found at the Bruce Site in Ontario (Figure 2-4). This site was proposed to host a DGR for Ontario Power Generation's low and intermediate level radioactive wastes (LILRW) (NWMO 2011a). The target sedimentary horizon proposed to host this DGR is located at a depth of approximately 680 m in a massive limestone formation. This type of geological site provides a deeply buried location where the massive host formation is directly overlain by ~200 m of very low permeability shale and a further 425 m (at the Bruce Site) of cap-rock. This sequencing is expected to provide excellent isolation to the repository level at the LILRW DGR site.

Figure 2-5 shows a generic layout for NWMO's DGR for used fuel (UF) in sedimentary rock (NWMO 2018). The layout illustrates the anticipated massive, intact nature of the host rock and its lack of hydraulic or other structural features that would discernably alter the room layout. The spacing of the placement rooms is nominally 20 to 25 m, but this is subject to change once the thermal characteristics of the host rock at the actual repository site are characterized, the heat generation of UF to be installed is known and thermal conditions are modelled for the site.

Sedimentary rock of the type considered for use in a DGR for used fuel isolation has a number of T-H-M-C properties that will help in defining the nature of the materials best suited for use in the placement room buffer. The limestone formations of the type considered for use (Cobourg Formation) have the following T-H-M-C properties, as provided by Radakovic-Guzina et al. (2015) Nasseri and Young (2014) and Noronha (2016). These values do not represent required materials properties for a DGR but are values that are felt to be representative of conditions that might be encountered.

Thermal:

- Thermal conductivity 2.27 W/m^{o}C
- Specific heat capacity 1.63 MJ/m^{3} ^{o}C

Hydraulic:

- Hydraulic conductivity of the limestone rock matrix is in the order of 10^{-14} m/s.

Mechanical Properties:
The mechanical properties of sedimentary formations will vary substantially, values for sedimentary units of the type likely to be encountered in Southern Ontario are provided in Table 2-1 (from Radakovic-Guzina et al. 2015).

Chemical Characteristics:
The key chemical properties for the reference sedimentary groundwater composition for deep limestone (SR-L) are as follows:

- Pore fluid composition, TDS of approximately 223 g/L comprised primarily of Na, Ca and Cl ions (Dixon et al. 2018).
- pH – anticipated to be "neutral (~7). Measured pH in artificial SR-L groundwater is 6.7 (Dixon et al. 2018)

Greater detail regarding chemical composition of the reference sedimentary groundwater is provided in Section 4-4.

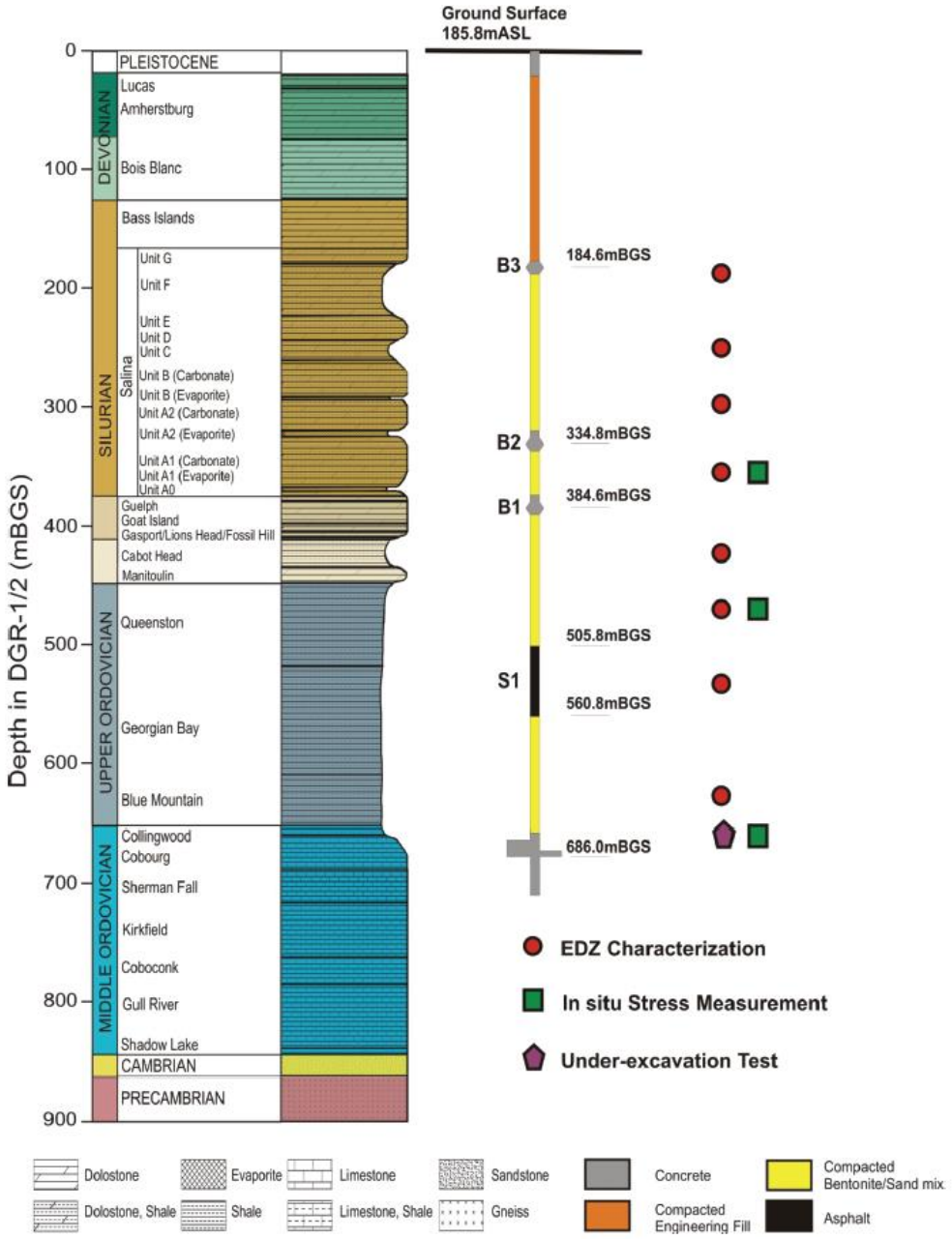

Figure 2-4: Typical Sedimentary Sequencing at the Bruce DGR Site for LILRW in Sedimentary Rock (after Crowe et al. 2016).

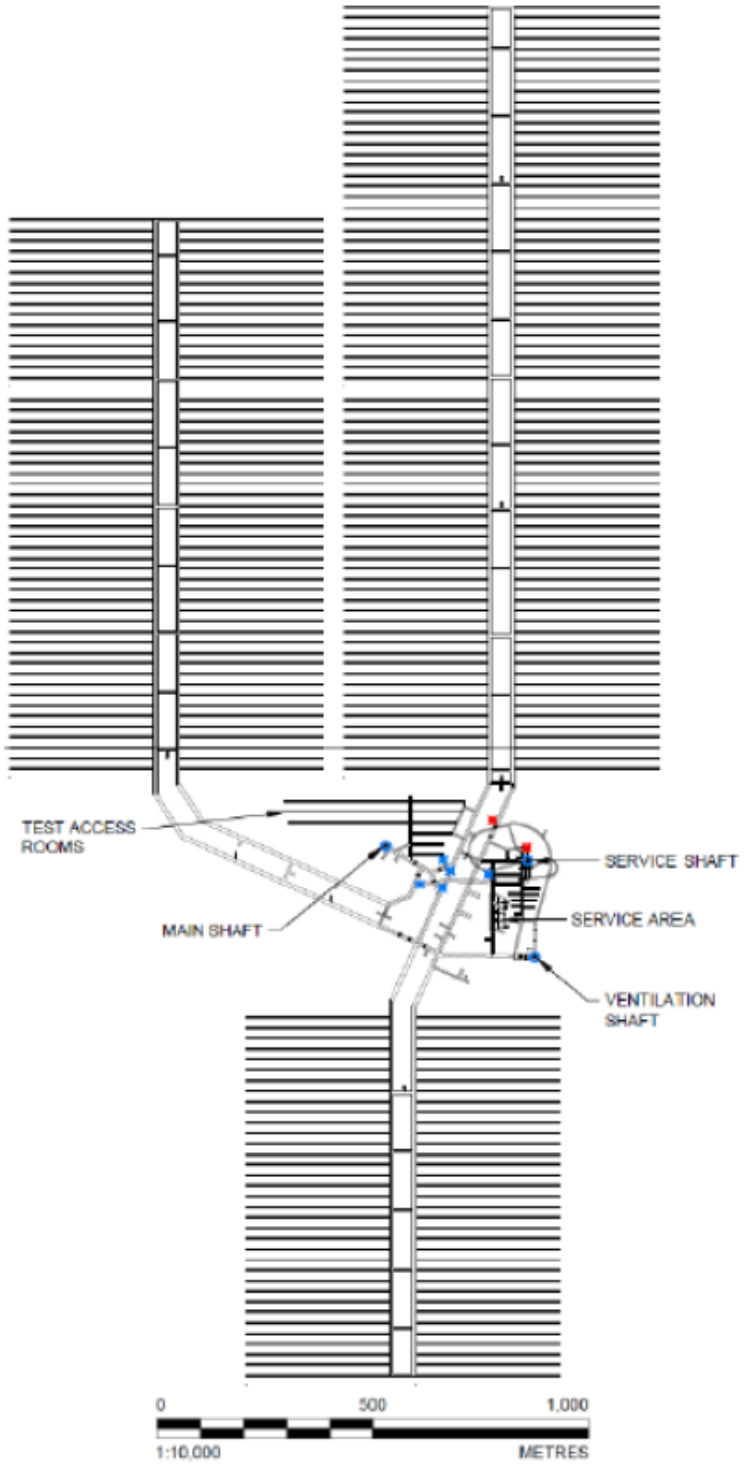

Figure 2-5: Example of Generic Layout for a DGR in Sedimentary Rock (NWMO 2018).

Table 2-1: Intact Rock and Bedding Plane Mechanical Properties for Sedimentary Formations (Radakovic-Guzina et al. 2015)

	Intact Lab		Hoek Brown parameters					Rock mass			Mohr Coulomb		
Unit	**UCS MPa**	**Ei GPa**	**GSI**	**mi**	**mb**	**S**	**a**	**Erm GPa**	**σ_{cm} MPa**	**σ_3 [3] MPa**	**C MPa**	**ϕ deg**	**Bedding kn GPa/m**
Georgian Bay[1]	34	9.04	76	10.1	4.3	0.069	0.501	7.51	11.4	10.1	3.04	37	
Blue Mountain[1]	34	9.64	77	6.0	2.6	0.078	0.501	8.14	10.1	12.1	3.16	31	
Collingwood[1]	117	36.9	76	10.0	4.2	0.070	0.501	30.7	39.2	12.8	6.66	44	1157
Cobourg[2]	121	43.5	89	11.4	7.7	0.295	0.5	41.4	67.3	9.4	11.1	49	1157
Cobourg – Lower[2]	101	39.1	89	7.2	4.8	0.295	0.5	37.2	52.4	14.1	11.4	42	1157
Sherman Fall	76	38.8	87	11.0	6.9	0.236	0.5	36.5	38.7	14.8	7.76	44	

Note: 1 – a part of Georgian Bay and Blue Mountain Formations
2 – a part of Cobourg Formation
3 – overburden weight

Bedding Plane Mechanical Data for Cobourg Limestone

Peak Cohesion MPa	Peak Friction Angle Deg.	Residual Cohesion MPa	Residual Friction Angle Deg.	Tensile Strength MPa
3.31	38.3	0	38.3	0.66

2.2.2 Crystalline Rock Geosphere

NWMO is also considering an alternative location for the DGR for UF in the ancient, Precambrian crystalline rock of the Canadian Shield. As described by Noronha (2016), NWMO (2017), the 'reference geosphere' for a crystalline rock setting has attributes that closely match those of a typical Canadian Shield site containing a body of good quality rock. The geosphere is assumed to be elastic, isotropic and homogeneous in nature.

Within the volume occupied by the repository, the rock mass is assumed to be of a very good quality with a bulk hydraulic conductivity of about 10^{-11} m/s or less. It is possible that the near surface rock will be of a lower quality and have permeable features. The geological structure of a crystalline rock of the type that could be considered for use as a repository will vary with the site considered and so a generic profile is not readily available, for illustration purposes a conceptual layout previously considered by NWMO is provided in Figure 2-6.

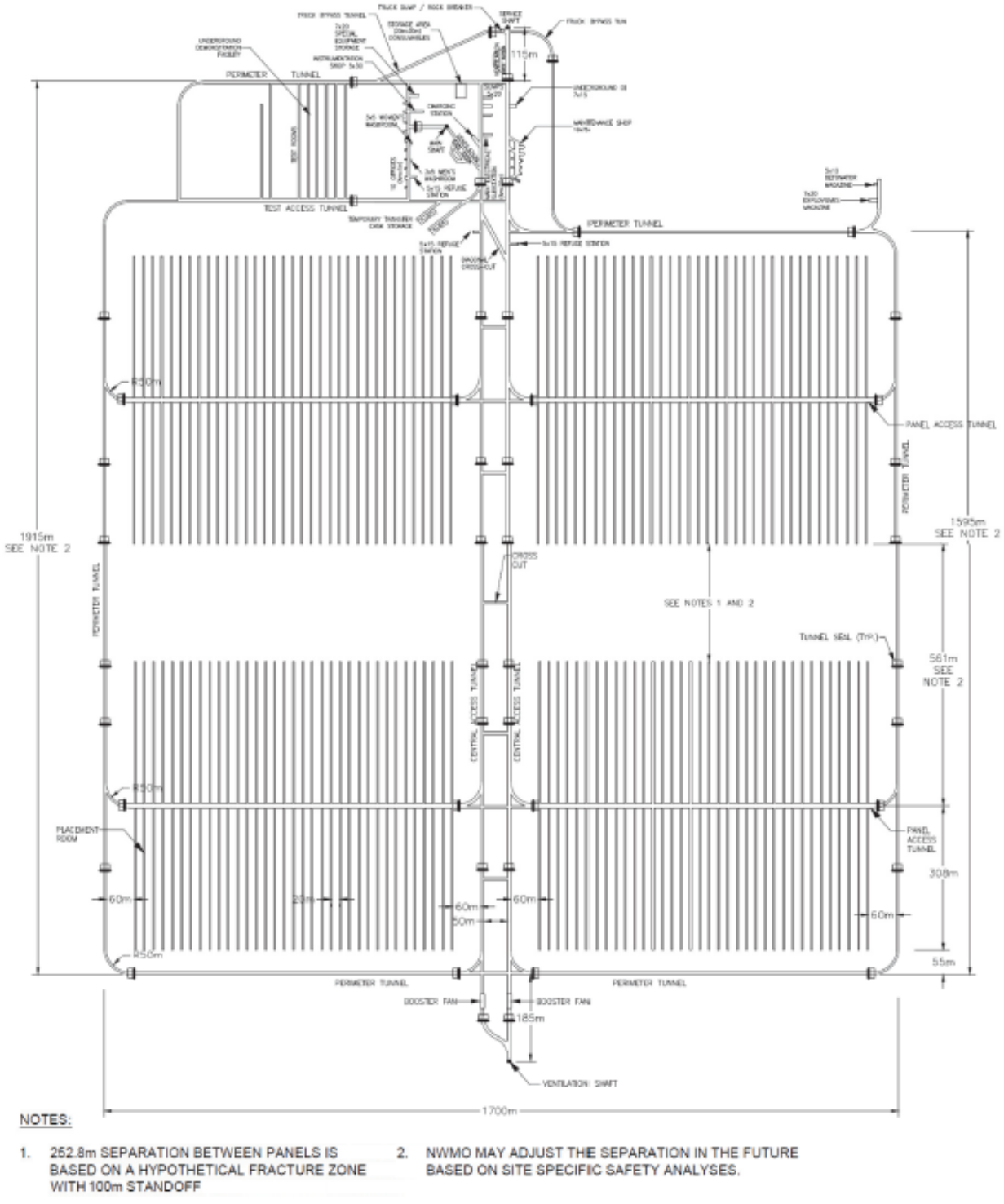

Figure 2-6: Example of Generic Layout for a DGR in Crystalline Rock (NWMO 2017).

Typically referenced T-H-M-C properties for granitic rock of the type anticipated to be present at the location of a DGR are provided by Radakovic-Guzina et al. (2015) and are as follows:

Thermal:

- Thermal conductivity 3.00 $Wm/^oC$
- Specific heat capacity 2.28 $MJ/m^3{}^oC$
- Linear coefficient of thermal expansion 10^{-5} $1/^oC$

Hydraulic:

- Hydraulic conductivity of bulk massive granite $<10^{-11}$ m/s

Mechanical:

- Rock mass peak UCS 105 MPa
- Cohesion 14 MPa
- Friction angle 59^o
- Tensile strength 1.7 MPa
- Young's Modulus, E_{rm} 39.1 GPa

Chemical

- Pore fluid composition – site dependent but reference crystalline rock pore fluid CR-10 has a TDS of 11 g/L and is comprised primarily of NaCl and $CaCl_2$. Other granitic sites within the Canadian Shield have been determined to have TDS contents approaching as high as 80 g/L (Gascoyne et al. 1987).
- pH – will vary with site condition but is anticipated to be between 7 and 8 based on site specific conditions.

3. DESCRIPTION OF BUFFER AND GAP FILL MATERIALS

3.1 BUFFER MATERIALS IN NWMO'S REPOSITORY SEALING CONCEPT

NWMO proposes use of Wyoming-type bentonite for filling the placement room volume not occupied by the UFCs. A commercial product, MX-80 Bentonite, produced by Colloid Environmental Technologies Company (CETCO), is the reference material chosen for use by NWMO, although much work has and continues to be done using alternative bentonite products. MX-80 has the advantage of having been used extensively as a reference material in repository programs in Europe and elsewhere, providing for an extensive complimentary source of materials behavior information. Mineralogical and physical properties of MX-80 are provided in Section 4.

Target physical conditions of as-placed buffer.

NWMO's repository concept requires that HCB buffer, spacer and floor tablet blocks have a minimum dry density of 1700 kg/m^3. The most effective means to produce such large blocks to consistent density is the use of isostatic compaction technology. The gap fill component of the placement room fill is produced from the same raw materials as the HCB. In order to maximize the density to which this gap fill can be placed, a carefully graded blend of densified particles is used. As the maximum grain size of the gap fill is small (< 8 mm), there is no need to use large blocks of materials in its manufacture. An effective means to generate the graded gap fill material is through the use of small, roller-compacted ribbons of compacted bentonite that can be crushed and graded to the required specifications. The manufacture of these materials is described in more detail below.

Method of HCB manufacture.

The buffer box concept for isolation of the Mark II container adopted by NWMO requires the manufacture of very large blocks of high density bentonite. Blocks large enough to be machined to the estimated 1 m x 0.5 m x 2.8 m dimensions (Noronha 2016) are not readily produced in lifts using dynamic or static compaction and blocks manufactured using those methods are prone to issues related to density homogeneity and structural stability. The remaining method to generate such large blocks of high-density bentonite is utilization of large volume isostatic pressing. NWMO has explored the viability of isostatic compaction of large blocks and their subsequent machining to produce highly consistent blocks as well as to subsequently machine voids of size suitable for installation of a UFC. Figure 3-1 shows the press used in manufacturing of full-size HCB blocks for use in Buffer Boxes and Spacer Blocks (Mielcarek and Birch 2016a; Birch and Mielcarek 2017).

The bentonite density achievable using isostatic or uniaxial compression is dependent on the parameters of moisture content and compaction pressure. The physical stability of the manufactured blocks is also sensitive to the post-manufacturing environment they are exposed to. It has been noted that blocks tended to exhibit some physical cracking if left exposed to very dry or very moist atmospheric conditions for an extended time (Arvidsson et al. 2014, Birgersson and Goudarzi 2015; Sandén et al. 2016). This is related to the high suction of the HCB clay and either uptake of atmospheric moisture or its loss due to desiccation. Storage in a moisture-controlled environment until they are ready to be used is therefore a requirement.

The NWMO production trials of isostatically-compacted, full-sized buffer blocks for use in manufacture of prototype buffer boxes has successfully generated large HCB blocks suitable for use in encasing a UFC. Following uniaxial compaction trials to establish a potentially suitable

compression pressure to produce HCB blocks (Figure 3-2), isostatic compaction trials of full-scale blocks were undertaken. Birch and Mielcarek (2017) determined that full-scale HCB blocks produced by isostatic compaction at 100 MPa achieved very consistent internal density and average block densities ranged from 1727 to 1747 kg/m^3 dry density, averaging 1743 kg/m^3. The NWMO blocks could be readily machined to the dimensions required of the 2-piece Buffer Box as shown in Figure 3-1c,d. This provides confidence that buffer and spacer blocks of adequate density can be produced using existing technology.

Data related to isostatic compaction demonstrations is summarized in Table 3-1. Ritola and Pyy (2011) reported dry densities in the order of 1791-1871 kg/m^3 using MX-80 bentonite and 100 MPa isostatic compaction, although they used a lower compaction moisture content than currently being used by NWMO in their compaction trials which may have contributed to the slightly higher density. The main difference in the materials used in these studies was the much higher initial moisture content in the NWMO studies. This shows that there is still perhaps room for NWMO to achieve higher block densities using lower moisture content material, but this would need to be considered with respect to the influences on block mechanical stability and the actual density needed to accomplish effective isolation of the UFCs.

The placement schedule for an operational DGR will require approximately 10 buffer boxes and associated spacer blocks to be installed each day. This translates to 20 buffer box blocks plus approximately 10 spacer blocks that need to be produced to accomplish this placement rate. Prototype manufacturing trials require approximately 10 minutes of pressing once a filled mold is installed. Following unloading of the press, machining is required to produce blocks of the correct size (and voids for UFC). Optimization of the production process (and use of several isostatic presses) will reduce the time required for buffer manufacture. Pre-production of blocks will provide for effective UFC packaging and placement but establishing what storage conditions are required and the mechanical stability of blocks stored for extended periods still need to be determined.

Table 3-1: Compaction to Produce HCB Using 100 MPa Pressure

	MX-80 PB1460-1*	MX-80 PB1460-5*	IBECO RWC PB1460-6*	MX-80**
Volume (m^3)	1.5644	1.7586	1.7502	1.45
Bulk Density (kg/m^3)	2131	2093	2013	
Water Content (%)	12.9	16.5	16.2	20
Dry Density (kg/m^3)	1888	1797	1732	
Subsamples				
Bulk Density (kg/m^3)	2111	2086	2008	2092
Dry Density (kg/m^3)	1871	1791	1729	1743±5.5
Saturation (%)	75.4	84.9	75.4	97.1
Void Ratio	0.470	0.536	0.591	0.561

*Isostatic compaction by Ritola and Pyy (2011)

** Isostatic compaction by Birch and Mielcarek (2017), average of 3 blocks

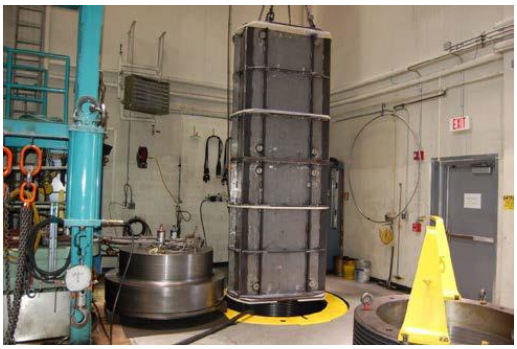

(a) Isostatic Press

(b) HCB after machining to block size

(c) HCB machined to fit UFC

(d) Blocks and UFC "Buffer Box"

Figure 3-1: Isostatic Production of HCB Blocks and Resulting Buffer Box
(Birch and Mielcarek 2017)

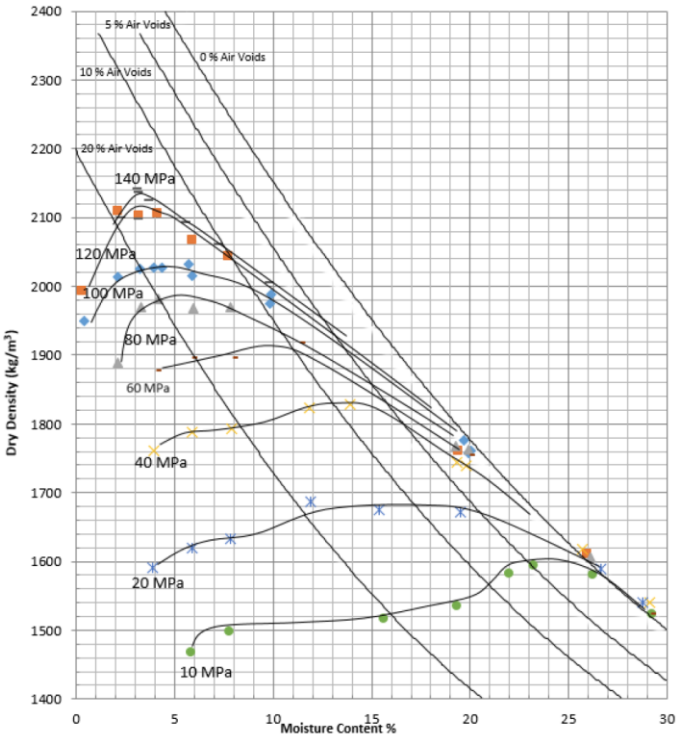

Figure 3-2: Uniaxial Compaction Characteristics of MX-80 Bentonite
(Birch and Mielcarek 2017)

Stability of Compacted HCB materials

The HCB needs to be mechanically stable in order to accomplish safe handling and installation of the buffer boxes and spacer blocks in the placement room. In the Swiss concept this is accomplished through use of HCB blocks of moderate dry density (~1720 kg/m^3) and relatively high moisture content (15%) (Seiphoori, 2015). This is very close to the conditions proposed for use by NWMO in the Mark II disposal concept (1700 kg/m^3 and moisture content in the order of 20%). It was noted by Seiphoori (2015) that at higher density (1870 kg/m^3) and lower (10.1%) moisture content that the physical stability of the blocks was poor with cracking and splitting of the blocks occurring soon after manufacture and exposure to atmospheric conditions. This is explained in part by the suction-moisture behaviour of the bentonite comprising the blocks and interaction with atmospheric moisture as discussed in Section 5.3. This is also evident in the effect of moisture content on tensile behaviour of compacted bentonite (see Section 5.8)

3.2 GAP FILL MATERIALS IN NWMO'S REPOSITORY SEALING CONCEPT

The gap fill materials (GFM) proposed for use in NWMO's Mark II placement geometry are high-density granulate of suitable particle size gradation and density to allow for its installation to a minimum dry density of 1410 kg/m^3. The GFM will be installed in the space remaining between the buffer box / spacer block assembly and the walls and roof of the placement room using a screw-type auger, similar to that shown in Figure 3-3 and reported on by Mielcarek and Birch (2016b) and Birch and Mielcarek (2017). A similar approach to GFM installation, also shown in Figure 3-3, is proposed by NAGRA for use in their pedestal placement concept in sedimentary rock (Muller et al. 2017).

In trials of GFM production and installation (Birch and Mielcarek, 2017), MX-80 bentonite, delivered at a gravimetric water content of approximately 10% was dried to the required 2 to 3 %. The dried MX-80 bentonite was then fed through a roller compaction/granulation process. Figure 3-4 shows the raw MX-80 bentonite, compacted ribbons of densely compacted bentonite and the subsequently crushed materials. The granulated material was size-separated using a series of screens in a process sifter that separates the individual crushed particles to produce a blend of the desired particle size distribution with the largest particles being less than 8mm in size. In this manner a consistent product can be produced in a process that could be done at industrial scale.

In order to demonstrate that the 1410 kg/m^3 dry density targeted by NWMO was achievable, a prototype placement auger was designed and constructed, with a series of placement trials were completed by Birch and Mielcarek (2017). In eight GFM placement trials undertaken by NWMO, GFM was demonstrated to be able to be placed to 1489 to 1595 kg/m^3 (average of 1556 kg/m^3) in 100 mm-wide vertical gaps between the HCB and the walls of a tunnel mock-up. A further series of 6 placement trials were undertaken to examine the density to which the GFM could be placed in the wider horizontal gap between the buffer blocks and the roof. The as-placed dry density of the GFM was measured to be 1480 and 1557 kg/m^3 and averaged 1524 kg/m^3 (Birch and Mielcarek 2017). Further trials using a smaller test volume achieved GFM dry densities of 1490±21 kg/m^3. All of these trials exceeded the density specification currently set for the GFM, providing room for future modification of GFM density specifications if required.

Granulated bentonite materials have also been produced by Nagra for use in surrounding their waste container in a horizontal pedestal placement geometry (Müller et al. 2017). This geometry has substantial differences from the NWMO concept, for example they propose use of a much larger container, the use of a smaller circular tunnel, a pedestal consisting of HCB blocks that acts as a cradle to support the waste container and filling of the majority of the

tunnel volume with crushed bentonite materials. Figure 3-3 shows the type of machine proposed for use by NAGRA and Figure 3-4 shows the material proposed for installation. The auger system proposed is similar to that of NWMO and the granulated bentonite is also produced by the crushing of HCB materials. The NAGRA concept uses a coarser gap fill material as a result of the larger volume to be filled with granulated material and also a more complex auger system, again largely as a result of the difference in the geometries considered. The reference as-placed pellet dry density for NAGRA is 1450 kg/m^3 and they report achieving average densities of 1490 to 1530 kg/m^3.

NWMO prototype (Birch and Mielcarek 2017)

Nagra Prototype showing UFC placement geometry (Müller et al. 2017)

Figure 3-3: Screw Augers Used to Evaluate Ability to Place GFM.

SKB and Posiva are considering a geometry that is different than NWMOs Mark II concept, with installation of their Used Fuel Canisters in boreholes drilled in the floor of the placement rooms (IFB). The boreholes and placement rooms will need to be backfilled. This is expected to be achieved using a combination of HCB blocks and extruded bentonite pellets as gap fill. The placement of the pellets in the KBS-3 placement geometry considered by SKB and Posiva will need to be accomplished in gaps of similar dimension to that of the NWMO concept (Wimelius and Pusch 2008). The current reference pellet materials proposed for use by SKB and Posiva differ from those of NWMO and Nagra in that the pellets are larger, composed of extruded, rod-shaped pellets as seen in Figure 3-4. There are several reasons for the difference in pellet size and shape difference, including a smaller proportion of pellets to HCB and the need for the gap

fill in the SKB and Posiva concepts to be able to deal with potentially substantial localized water inflow during backfilling operations. The NWMO and Nagra concepts are focused on geosphere conditions where, after any needed preliminary grouting in carried out, there is little to no discernible water inflow to the openings during backfilling operations. Where there is a discernible water inflow to the placement room, the rod-shaped gap fill proposed by SKB and Posiva allows for greater initial water redistribution within the gap filled volume, reducing risk of short-term disruption of the placed materials (Sandén and Jensen 2016). In placement trials for extruded pellets it was determined that they could be reliably installed to an average dry density of approximately 950 kg/m^3 (940 kg/m^3 Arvidsson et al. 2014; 860-997 kg/m^3 Sandén and Jensen 2016) with slight differences in density based on the type of bentonite used in the pellet manufacturing.

Based on gap fill placement experiences gained by NWMO and other organizations, it would seem reasonable to expect that the type of GFM proposed for use in the Mark II repository concept can be installed to densities substantially higher than the 1410 kg/m^3 specified in NWMO's placement concept. This is a desirable situation as this provides for a greater degree of confidence that the average density of the materials installed in the placement room will exceed the 1600 kg/m^3 average specified in the current reference concept. Higher density of the as-installed blocks and gap fill materials should not be problematic as this will allow additional margin to the system should localized material loss by erosion, or non-uniform equilibrated dry density of the system.

Raw MX-80 Bentonite
Rautioaho & Korkiala-Tanttu (2009)

Dense bentonite chips and subsequently granulated materials considered by NWMO (Birch and Mielcarek 2017)

Granulated bentonite mixture considered by Nagra (Müller et al. 2017)

Extruded bentonite pellets of type used by SKB and Posiva (Johnsson & Sandén 2013)

Figure 3-4: Photographs of Raw Bentonite and Materials Prepared for Use as Gap Fill

3.3 INFLUENCE OF COMPONENT DENSITY ON OVERALL SYSTEM DRY DENSITY

Although the topic of influence of component density change from the current reference dry densities for the HCB blocks and gap fill materials will be discussed with respect to their T-H-M-C and (B) properties in Section 5, a brief discussion is also provided below to illustrate the impact of as-placed component variation. For the purposes of discussion, it is assumed that there are no unfilled voids, component volume and density is uniform throughout the filled volumes. Additionally, for discussion purposes it is assumed that there is no loss of material from the regions where they were installed.

The placement room proposed for use in NWMOs DGR concept will have nominal dimensions of between 3.2 and 3.35 m width by 2.2 and 2.55 m height (cross-section of 7.04 – 8.54 m^2). The final dimensions will be established based on site-specific and other operational considerations. With the exception of the Gap Fill, the materials installed in the placement room are expected to be of fixed volume and dimension. Options exist regarding these fixed dimensions, (e.g. the width of spacer blocks), but once a container spacing is decided on (it will be determined in part by the geological conditions present at the actual repository site and the allowable thermal loading of the UFCs), they will also be of fixed dimensions. The volume occupied by each Buffer Box is approximately 2.9 m^3 and it contains a single UFC of approximately 0.58 m^3.

Spacing between the Buffer Boxes (and hence UFCs) can be adjusted by changing the thickness of the Spacer Blocks. The dimension of the spacer blocks will therefore determine the thermal loading per m of tunnel length and so is important to evaluate during conceptual design and repository design phases of planning.

For the purposes of analysis and design, there are two Spacer Block sizes currently being evaluated (0.5 m and 0.3 m thick), as shown in Figure 3-3.

- For a 0.5 m thick spacer block, there will be approximately ~1.33 Buffer Boxes and ~1.33 spacer blocks per m of placement room length.
- For a 0.3 m thick spacer block, Buffer Box loading increases to ~1.51 per m of placement room length.

From these dimensions it is possible to estimate the amount of gap fill required per tunnel m-length. It should be noted that the volumes estimated in this document do not take into account the presence of construction voids (or gaps) between the Buffer Boxes and the Spacer Blocks. These voids will result in slight reduction in the calculated homogenized dry clay density for the system.

Based on the excavation and placement block dimensions provided above, scoping calculations were undertaken in order to determine the effects of varying Buffer Box spacing, opening dimension and density of the GF material installed on the homogenized clay density in the placement room. Summary spreadsheets containing the results of calculations are provided in Appendix F.

The data provided in Appendix F can be summarized as follows:

- For a 0.3 m or 0.5 m spacing between Buffer Boxes in the current base-case:
    - There are 8 Spacer Blocks and 8 Buffer Boxes and 8 UFCs per 5.2 m of tunnel for 0.3 m Spacer Blocks.
    - There are approximately 8 Buffer Boxes and 8 Spacer Blocks, and 8 UFCs for every 6 m of tunnel length for 0.5 m thick Spacer Blocks,

- the average dry density for the HCB-GFM components is between 1616 kg/m^3 and 1665 kg/m^3 for the extremes of placement room dimensions considered (2.2-2.55 m height and 3.2 – 3.35 m width).
- The average dry density of the clay component exceeds the 1600 kg/m^3 required of the placement room fill.

For the purposes of comparison, the effect on average density of using higher as-placed clay component densities (1480 and 1730 kg/m^3 for GFM and HCB respectively) were evaluated (Appendix F). These component densities have already been demonstrated as being achievable but require considerably more effort to accomplish this level of densification. As expected, the average bulk dry density of the HCB-GFM system increases slightly when these higher-density components are used. Average dry density ranged from 1657 to 1700 kg/m^3 depending on tunnel and spacer block dimensions selected.

Further increase of the GFM component density to 1550 kg/m^3 is a possibility based on placement trials reported by Birch and Mielcarek (2017), but this results in only a further 10 kg/m^3 increase in the average density of the tunnel fill. The improvement of the GFM's as-placed dry density is therefore not particularly important to the average homogenized density of the tunnel fill, it is however of significance with respect to the thermal, hydraulic and mechanical behavior of the as-placed GFM. It should also be noted that local density variation will be also be of importance with respect to the potential for biological processes to be active.

Again, it should be noted that for all the cases examined, the calculated average bulk dry density of the placement room fill exceeds the 1600 kg/m^3 target currently set for the NWMO Mark II placement concept. The influence of these slightly higher densities will be discussed for each of the T-H-M parameters discussed in this report. The density state of the bentonite material will need to be further assessed once the equilibrium density conditions are determined and the placement room dimensions are formally established.

3.4 EQUILIBRATED SYSTEM

It is recognized that for the purposes of design and system modelling, that the placement room fill is assumed to come to density homogeneity over the longer-term. It is unclear if full density homogenization will actually occur. In reviewing available information on this topic, (Dueck et al. 2010, 2014, 2016; Kim and Priyanto 2011; Kobayashi et al. 2014; Åkesson et al. 2010a,b), it can be concluded that if the bentonite used in construction of the blocks and pellets are very similar compositionally, the HCB-Spacer Block-GFM system will evolve towards a more homogeneous mass than was present at the time of construction. This does not mean that the system will come to full density homogeneity, only that the lower density components (GFM) will be consolidated to some degree by swelling and compression of the denser (HCB) components.

As the current NWMO placement room concept calls for use of the same bentonite materials (100% bentonite from the same source), in the manufacture of buffer boxes, spacer blocks and GFM, it can be assumed that some degree of density equilibration will occur. Based on the reports by Dueck et al. (2010, 2014, 2016, 2019); Kim and Priyanto (2011); Kobayashi et al. (2014) and Åkesson et al. (2010a,b), it would seem unlikely that the GFM will reach exactly the same dry density as the HCB block-filled regions. Depending on local interactions between the HCB and its surroundings, there may also be some degree of anisotropy that persists over the long-term.

The final density state of the HCB-GFM system will be primarily controlled by the proportions of each component present and their as-placed dry densities and their behaviour will be strongly influenced by regional hydraulic and groundwater conditions. Density anisotropy will be present in the materials installed in the placement room for a very long time after system saturation has been achieved. The magnitude of this anisotropy is as-yet uncertain as is its potential influence on system performance. This uncertainty highlights the desirability of installing the component to as high an initial dry density as is practical. As can be seen in Table 3-2 and Table 3-3, the density of the GFM will not substantially affect the average density of the placement room fill, but it is desirable to have the GFM installed to sufficiently high density that it will require only minor consolidation by the adjacent HCB to ensure that the entire system will meet performance requirements early in the equilibration process. It should be noted that the calculations summarized in Appendix F use slightly larger placement room dimensions than provided by Noronha (2016) and NWMO (2017) and so provide densities lower than would be achieved in the previously quoted placement rooms. These larger dimensions were used to address recent thinking regarding installation of HCB tiles on the floor of the placement rooms (which will add height to placement room opening needed), and additional placement room width to accommodate equipment movement.

It can also be noted that increasing the as-placed dry density of the GFM and HCB components from the currently proposed minimum values of 1410 and 1700 kg/m^3 respectively, to the already demonstrated as being achievable values of 1480 and 1730 kg/m^3 will result in a modest increase (~40 kg/m^3) in the average density of a density equilibrated system. Within the range of placement room dimensions and material densities considered under the current geometries, the average placement room fill dry density will be between 1615 and 1675 kg/m^3, all of which exceed the current reference of 1600 kg/m^3. It should also be recognized that final dry density within the placement room will be impacted by variances in room dimensions due to rock overbreak during excavation. As a result, on achieving water saturation some variation in the dry density throughout the room is likely since it is unlikely that the system will come to full density equilibrium. It will therefore be important to establish what the range of local density variation will be rather than relying on estimated average density.

4. T-H-M-C PROPERTIES OF HCB AND GFM MATERIALS

4.1 BASIC REQUIREMENTS AND PROPERTIES NEEDED IN HCB AND GFM

The prediction of the long-term T-H-M-C(B) behavior of the placement room fill is based on several basic assumptions regarding initial and long-term properties and performance of HCB and GFM.

The basic requirements for these clay-based sealing materials are:

- To fill the excavated volume of the DGR's placement room. In order to accomplish this the buffer (HCB and GFM) must have the ability to swell and fill any unfilled voids left after sealing materials installation and also provide some active support to the surrounding rock. The requirement of a minimum swelling pressure of 100 kPa in the placement room is set to establish the rock support conditions. With a swelling pressure comes the ability of the sealing materials to expand into any voids adjacent to them;
- To support the UFCs without experiencing unacceptable change in their location within the placement room. This will require that the sealing materials (HCB) located below and around the UFCs exhibit adequate strength, stiffness and deformation characteristics;
- To provide an environment where the maximum temperature at the surface of the UFC is kept below 100^{o}C at all times after its installation,
- To resist physical and chemical deterioration by the local environment during the life of the DGR. This requires knowledge of;
    - Movement of groundwater in the vicinity of the placement rooms,
    - Influence of regional conditions on the materials T-H-M-C behaviour, i.e.;
        - Ability of the sealing materials to limit water movement and mass transport of contaminants to diffusional levels. A bulk hydraulic conductivity of $<10^{-10}$ m/s has been set to reflect this requirement,
        - Ability of the sealing materials to resist relocation or dissolution by the groundwater it comes in contact with,
        - Chemical interactions between sealing materials and other installed materials (concrete floor, UFC) and how these might affect system behaviour,
        - Chemical interactions caused by radiolysis (radiation exiting surface of UFC),
        - Biological processes that could affect contaminant migration or biochemical degradation of the minerals or UFC. In order to suppress bacterial activity and migration to levels where they will not impact UFC or buffer performance, a maximum water activity (a_w) of 0.96 has been identified (Stroes-Gascoyne et al. 2007a,b). For groundwater with salinity of less than 100 g/L, a_w of less than 0.96 is achieved with an average weighted minimum buffer dry density of 1600 kg/m^3. It should be noted that a groundwater salinity of ≥ 100 g/L results in an environment with $a_w < 0.96$.

4.2 BASIC MATERIAL PROPERTIES THAT CAN BE USED TO HELP DETERMINE BENTONITE BEHAVIOUR

4.2.1 Background

A number of basic characterization tests have been developed for use in geoscience and geotechnical engineering that are readily utilized in determining basic material properties and that allow for screening of candidate materials. These tests can also be used in evaluation of any changes in behavior that occurred as the result of conditions that the sealing materials were exposed to. As NWMO has selected a particular bentonite product (MX-80) as its reference material for research, design and development, discussion of materials properties will focus on this material. The general considerations outlined for MX-80 will be applicable to other products but the values obtained for those materials will be different.

The montmorillonite family of minerals exhibit certain properties that make their behavior unique. The material referred to commercially as bentonite is typically composed of a montmorillonite-rich clay shale that has been excavated, dried and crushed. The characteristic properties of each source will therefore vary depending on its geological history, composition of its source materials and its processing.

Montmorillonite-type minerals have a sheet-like structure with very large and very highly charged surfaces. These surfaces will, if not confined, take free water (and ions) into the spaces between their unit cells and in so doing will expand. The ability to expand is dependent on factors such as the magnitude of the surface charge, minor differences in the chemical composition of the mineral structure, the composition of the water surrounding them, and other environmental factors such as cementation of adjacent mineral layers. More detailed descriptions of mineralogy and mineralogical considerations is provided by Karnland et al. (2006 and Karnland (2010). A schematic showing a conceptualized side view of two montmorillonite layers is provided in Figure 4-1.

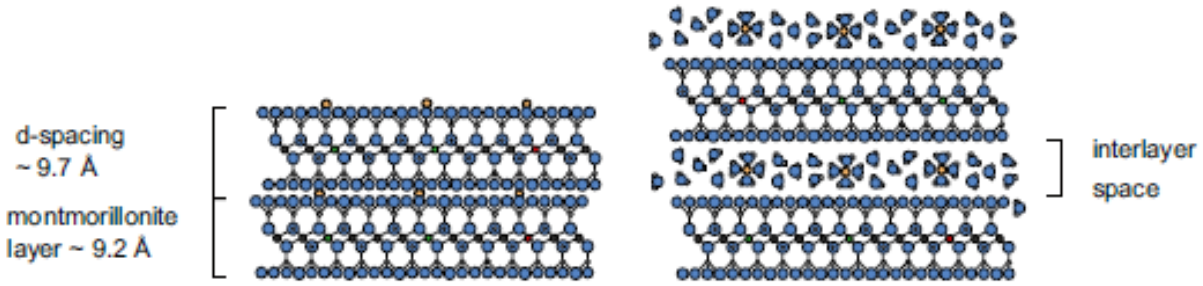

Figure 4-1: Side View of Dry Montmorillonite Clay Platelets and Following Limited Hydration (Karnland et al. 2006)

Some of the basic material properties of relevance to the sealing materials installed in a placement room include:

Mineralogically Dominated Properties:

- Mineral components present,
- Chemical composition of mineral solids,
- Surface area of minerals,
- Cation Exchange Capacity (CEC),

- Exchangeable cation composition (EC), and
- Water Activity (a_w).

Mechanical Properties:

- Grain-size distribution.

4.2.2 Mineralogy

Wyoming-type bentonites including MX-80 are the product of hydrothermal alteration of volcanic ash laid down during the Cretaceous period in the large, shallow, brackish water-filled region occupying what is now much of the central portion of the United States of America, extending north into Canada (Dixon and Miller 1995; Dixon et al. 1996a). These ash deposits were subsequently buried by further sedimentary actions and underwent geochemical alteration to form layers of montmorillonite-rich clay shale. The MX80 bentonite is a hydrous aluminum silicate comprised of clay minerals of the smectite group including montmorillonite, nontronite and sodium aluminum silicate hydroxide. Although very consistent over large areas, they are natural sedimentary deposits and so are subject to variability with respect to their composition and properties of the subsequently mined clay shales. This makes knowledge of the mineralogical and geochemical composition of the materials critical as the mineralogy of the bentonite used in manufacture of the HCB or GFM components is a key parameter in subsequent HCB and GFM production and the behavior of these materials. The amount of montmorillonite, its chemical structure and the nature of associated cations or cations adsorbed on its surfaces will define most of the T-H-M-C behavior of the HCB and the GFM.

Mineral Content of MX-80

Mineralogy is commonly determined through use of x-ray diffraction (XRD) analysis. This involves comparison of the peaks present on an x-ray diffraction pattern of a specimen to those of reference materials of known composition. This is now done routinely through computer peak-matching software, resulting in highly consistent methodology for mineral identification and quantification. An example of an XRD trace for MX-80 is provided in Figure 4-2. Determination of the quantity and type of swelling clay minerals in a sample of bentonite, as shown in Table 4-1, allows general predictions regarding material behavior since it is the montmorillonite content that determines bentonite behavior. These patterns and analyses can also provide indications of the presence of undesirable minor mineral components. Detailed discussion related to mineralogical determination of MX-80 bentonite is provided by Karnland (2010). As can be seen in Table 4-1, even subsamples of a single sample of MX-80, can show considerable variability in their analytical results. Table 4-1 presents the results obtained from three laboratories, with variability particularly evident for minor components. This illustrates the challenge of establishment of the exact mineral content of bentonite specimens. Some of the variation may be attributable to laboratory preparation, methodology or analytical method but some may reflect localized variability of the material itself. This goes along with observations that hydration state and density of the bentonite will also affect the XRD patterns, making quantification challenging (Muurinen 2009).

The bulk chemical composition of the bentonite can be determined via x-ray florescence (XRF) which provides a measure of the main cations present in the specimen and provides information related to the structure of the clay as well as what minor components such as soluble iron or calcite are present. Examples of XRF data for 3 identical MX-80 Bentonite samples is provided in Table 4-2 Dixon et al. (2018). These data also show variations in the results obtained, further illustrating the differences that can be encountered when examining subsamples of a single sample of natural bentonite.

Table 4-1: Semi-Quantitative X-Ray Diffraction Results for Identical Bulk MX80 Bentonite Samples (3 Laboratories)

Mineral	Activation Labs (%)	Hutton Institute (%)	SRC (%)	Average or range (%)	SKB Karnland et al. (2006) (%)
Montmorillonite	94.8	88.5	79	87.4±8.0	81.1-85.8
Calcite	2.2	3	3.6	2.9±0.7	0.1-0.5
Dolomite	-	TR	-	TR	-
Quartz	1.6	2.3	3.5	2.5±1.0	4.6-7*
Biotite	1.4	-	-	<1.4	-
Muscovite (+illite)	-	0.3	7.1	0.3-7.1	2.1-3.9
Plagioclase	TR	0	6.8	0-6.8	1.8-4.2
K-Feldspar	TR	3	-	<3	0.3-2.1*
Siderite	-	1.9	-	<2	-
Pyrite	-	0.6	-	<0.6	0.5-0.6
Gypsum	-	0.4	-	<0.4	0.5-1.3
Iron minerals**	-	-	-	-	0.8-2.6
Total	100	100	100	99.9	

Note: TR = trace; '-' = not detected
* values are sum of polymorphs of the indicated mineral group (e.g. quartz, cristobalite and tridymite; microcline and orthoclase feldspars)
** sum of iron minerals goethite, hematite, magnetite and lepidocrocite

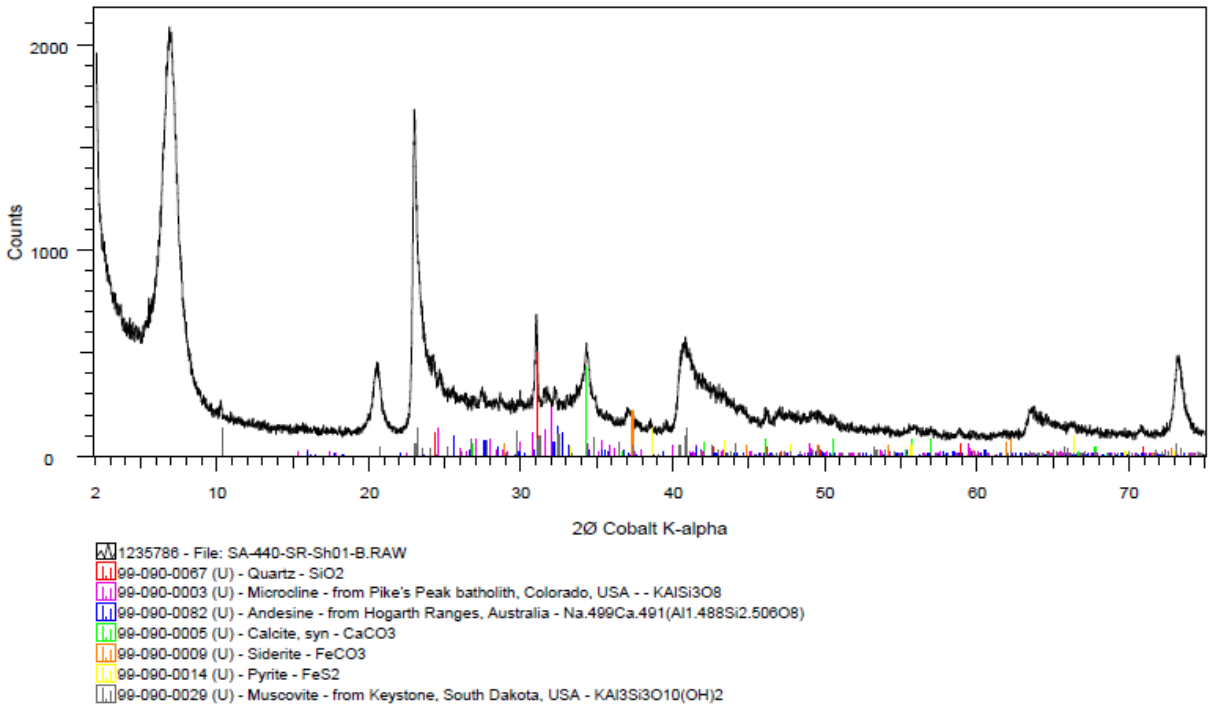

Figure 4-2: X-Ray Diffraction Trace for MX-80 Bentonite (Dixon et al. 2018)

Table 4-2: Major Oxides Composition of MX80 Bentonite Samples (after Dixon et al. 2018)

	Activ. Labs	Adj. value*	Hutton Instit.	Adj. value*	SRC 1	Adj. value*	SRC 2	Adj value*	MT***	Adj. value*	Average Adj. Value	STDev	Adjusted literature values+
Oxides													
Na_2O	1.87	2.29	1.98	2.41	1.49	1.78	1.56	1.88	1.97	2.32	**2.14**	0.26	**2.53**
MgO	3.16	3.87	3.09	3.76	2.25	2.68	2.26	2.72	2.7	3.18	**3.24**	0.50	**3.30**
Al_2O_3	18.57	22.76	18.24	22.20	18.80	22.42	18.80	22.60	20.51	24.18	**22.83**	0.70	**21.78**
SiO_2	51.46	63.06	51.76	63.01	54.40	64.87	53.10	63.84	54.13	63.81	**63.72**	0.67	**66.31**
P_2O_5	0.10	0.12	0.07	0.09	0.06	0.07	0.06	0.07	0.03	0.04	**0.08**	0.03	**tr**
K_2O	0.16	0.20	0.61	0.74	0.43	0.51	0.41	0.49	0.36	0.42	**0.47**	0.18	**0.55**
CaO	2.07	2.54	2.21	2.69	1.82	2.17	1.87	2.25	1.2	1.41	**2.21**	0.44	**1.21**
TiO_2	0.16	0.20	0.16	0.19	0.19	0.22	0.18	0.21	0.22	0.26	**0.22**	0.02	**0.18**
MnO	0.02	0.02	<0.05	0.06	0.03	0.03	0.03	0.03	0.02	0.02	**0.03**	0.01	**-**
V_2O_5	<0.003	-	<0.05	0.06	-	-	-	-		-	**-**	-	**-**
Cr_2O_3	<0.001	-	<0.05	0.06	-	-	-	-		-	**-**	-	**-**
Fe_2O_3	3.78	4.63	3.86	4.70	4.20	5.01	4.59	5.52	3.47	4.09	**4.79**	0.47	**3.74**
FeO	-	-	-	-	-	-	-	-			**-**	-	**tr**
C	-	-	-	-	-	-	-	-		-	**-**	-	**0.11**
S	-	0.00	-	0.00	0.16	0.19	0.17	0.20	0.21	0.25	**0.13**	0.11	**0.22**
LOI**	17.41	17.62	17.19	17.40	15.80	15.99	15.90	16.09	15.12	15.30	**16.48**	-	
Total	98.8	99.7	99.2	100.0	99.6	99.9	98.9	99.8	99.9	100.0	**99.9**		99.9

* Value is adjusted to remove water, removing variability in received water content from data.
** Loss on ignition (heating to 1000C). This removes all water, carbonate, gypsum and organic matter from the specimen.
*** Data provided by Minerals Technologies (Am. Colloid Company)
+ Data from Karnland et al. (2006); Kiviranta and Kumpulainen (2011), Dixon (1994) and Dixon and Miller (1995).

4.2.3 Mineralogy-Related Materials Properties

Surface Area of Bentonite Clay

Surface area (SA) of the clay is a means used to estimate the potential of the clay to chemically react with its surroundings. Montmorillonite materials have very high surface area per gram of clay and so can be expected to interact substantially with their surroundings. Measurement of SA, typically done using the Methylene Blue Test (ASTM C837) can be used to provide an indication of the surface reactivity of the clay and hence its likely suitability for use. Changes to SA as the result of exposure to harsh environments (e.g. high or low pH) or high charge cations can result in discernible changes in SA available to react with pore fluid. Both of these conditions may result in undesirable changes in the H-M behavior of the system. Values determined for this parameter are provided in Table 4-3.

The large surface area and large negatively-charged clay surfaces allows for exchange of cations between the mineral surface and the surrounding pore fluid. Cation Exchange Capacity (CEC), Exchangeable Sodium Percent (ESP) and Exchangeable Cation (EC) parameters provide an indication of the clay's ability to attract, bond and release cations from its hydrated surfaces as noted below;

- The CEC measured for a clay provides an indication of the theoretical maximum degree of cation exchange that could occur.
- The ESP is the total adsorbed sodium (meq) that is present divided by the CEC. As a result the higher the ESP, the more chemically reactive is the bentonite.
- The EC measures the actual amount of adsorbed cations that will readily exchange with their surroundings. This EC value is a more relevant measurement when assessing the

reactivity of the bentonite, since strongly adsorbed cations (such as divalent Ca, Mg, Fe, Cu) will not readily exchanged with the surrounding pore fluid once adsorbed on the clay surface.

Low CEC, ESP or EC values indicate that the clay will have a lower swelling capacity, fewer exchange sites to accommodate changes in pore fluid composition and potentially a higher ability for advective flow. This also has significance to the DGR environment should strongly adsorbing cations become available and then react with the bentonite to reduce barrier sorption ability. Typical values of CEC and EC determined for MX-80 bentonite are provide in Table 4-3 and based on the information available a set of suggested reference values have been developed. With further evaluation, these reference values may provide a good basis for quality specifications or screening values for MX80 materials proposed for repository use.

4.2.4 Grain Size Distribution

Grain size distribution in bentonite products is almost entirely a function of the mining and processing of commercial bentonite from its source clay-shale formations. The size distribution of the dry bentonite particles used to produce HCB and GFM can affect the compaction characteristics of the clay and in extreme cases unsuitable material could result in production of unacceptable block or granulate. A second consideration is associated with the fines component. The particles in the bentonite used in the manufacturing of sealing system components include fines that are dominated by the strongly hydrating montmorillonite-type minerals. These fines can have a disproportionate influence in the rate of water uptake and initial sealing behavior of installed materials such as GFM, particularly if the GFM used is in pellet form (Sandén and Jensen 2016). Granularity is therefore an important factor in both the production of block and granules for use in HCB or GFM and needs to be defined.

MX-80 is the reference source material for NWMOs HCB and GFM component and has been used extensively as a reference research material in the repository sealing programs of Finland, Sweden and Switzerland. As indicated by its product name, MX-80 is a material that has a target particle size of 80 mesh (0.177 mm) and for the majority of its mass to be contained between 30 and 80-mesh screens. Figure 4-3 provides three examples of the grain-size distribution measured for the as-received reference bentonite (MX-80) (Dixon et al. 2018; and Wang et al. 2012).

There are a number of factors that will affect the grain-size distribution of the MX-80 bentonite delivered for use, including:

- processing during manufacture (moisture content at time of manufacture, durability of the crushed clay-shales particles, effectiveness of particle screening);
- storage and handling of the commercial product (moisture change during transport and storage, and segregation during handling); and
- mechanical breakage of granules as the result of movement and handling of materials.

All of these can result in changes to how the material will respond during manufacture of HCB, GFM and other components as well as the initial reactivity of the GFM since a high proportion of fines will result in a more rapid initial rate of bentonite swelling at the site of water inflow. Hence, grain-size distribution can affect the initial water uptake rate and distribution, particularly in the lower-density GFM with its more heterogeneous granularity, and this has been documented in studies of the pellet GFM produced for use by SKB/Posiva (Sandén and Jensen 2016). Nevertheless, over the longer-term hydration, subsequent swelling and density

equilibration of the GFM and HCB, the system should minimize the effect of granularity of the source materials or as-placed GFM on overall system performance.

Table 4-3: MX-80 Mineralogy and Mineralogy-Related Parameters

Parameter	Misc Values	Carlson (2004)	Kim et al. (2012)	Abootalebi (2016)	Karnland et al. (2006) Karnland (2010)	Dixon et al. (2018)	**Possible Reference Value**
Mineralogy (%)							
Montmorillonite*	65-82[a] 75[f] 79.2[i] 92[c] 85[d]	80-85	75-85	84.6	81.1-85.6	79-94.8	**>80**
Illite	3[t]	tr			2.1-3.9	0.3-7.1	
Quartz	15.2 2.8[i] 3[c]	*4–12*		8.6	4.6-7	1.6-3.5	
Feldspar	5-8 11.2[i]	*5–8*			2.1-6.3	3-6.8	
Calcite	0.7/0.6[i]					2.2-3.6	
CEC (meq/100g)	88-110[b] 84-104[f] 76.7-78[f] 71-77* 60-80[e] 75[g]	80-110	75		80-88 75-78		**>75**
EC (meq/100g) Na Ca Mg		 61 10 3			 49-67 11-15 4-6		 **>50** **<15** **<6**
Liq. Limit+ (%)	457.1[h] 397[d] 423[d]		450-550	322		350	**>350**
Plastic Lim. (%)	32[e] 65[d]			35		33	**>30**
Plasticity Index	365[e] 358[d]			287		318	**>310**
Specific Surface (total), (m^2/g)	512[a] 523[d] 562[f]				750[8]		**>500**
Specific Gravity	2.82[a] 2.74[d]		2.78		2.62-2.78[g] 2.75-2.78	2.72	**2.75**

* Montmorillonite family of minerals;
** These values were from testing in various liquids, highlighting sensitivity to method of measurement.
+ value obtained is very sensitive to source material texture (fines) and method of preparation. It is also for untreated, natural bentonite. Chemical treatment can substantially increase this value.
a. Villar and Gómez-Espina 2008; b. Pusch 2002; c. Tang et al. (2008a);
d. Seiphoori 2015; e. Davies et al. 2017. f. Bradbury and Baeyens (2011)
g. Keto et al. 2009. h. Johannnesson and Börgesson 2002; i. Montes et al. 2003;

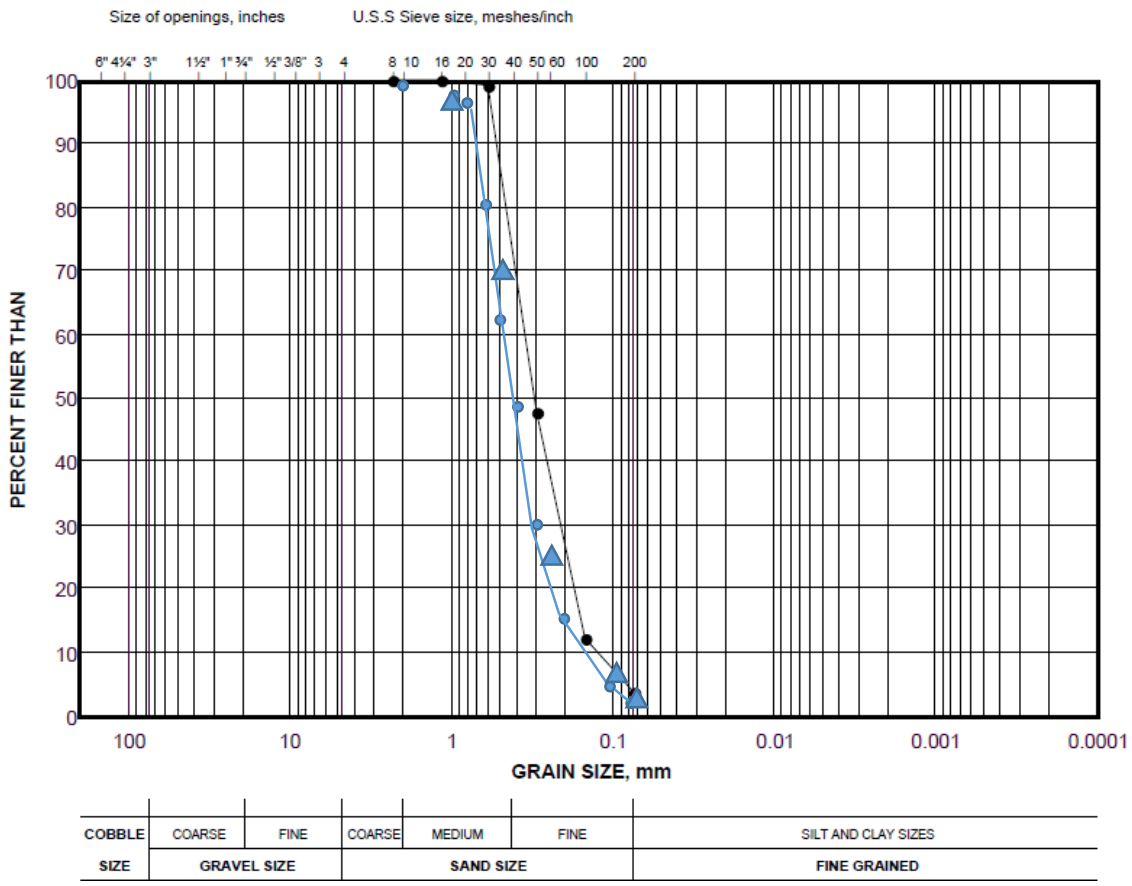

Figure 4-3. Grain Size Distribution Measurements for MX-80

4.3 POROSITY AND PORE-SIZE DISTRIBUTION IN GFM AND HCB

The thermal, hydraulic, swelling and air movement characteristics of the GFM and HCB are strongly affected by the nature of the pore spaces, particularly their size and size distribution. The determination of the pore space available for mass transport has been studied by numerous investigators (Holmboe et al. 2012; Muurinen 2009; Pusch et al. 1990; Pusch 2002; Suzuki et al. 2004) and the role of this parameter is briefly summarized below.

The pore spaces in a bentonite material can be broken down into two major sub-categories, firstly the macro-pores (greater than approximately 25 nm), between the larger clay particles and secondly, micro-pores (less than approximately 10 nm), consisting of the interlayer and diffuse double layer (DDL) water components (Figure 4-4). The micro-porosity is often inaccessible for use in movement of water through the clay mass but plays a very important role in development of swelling pressure and later hydraulic conductivity.

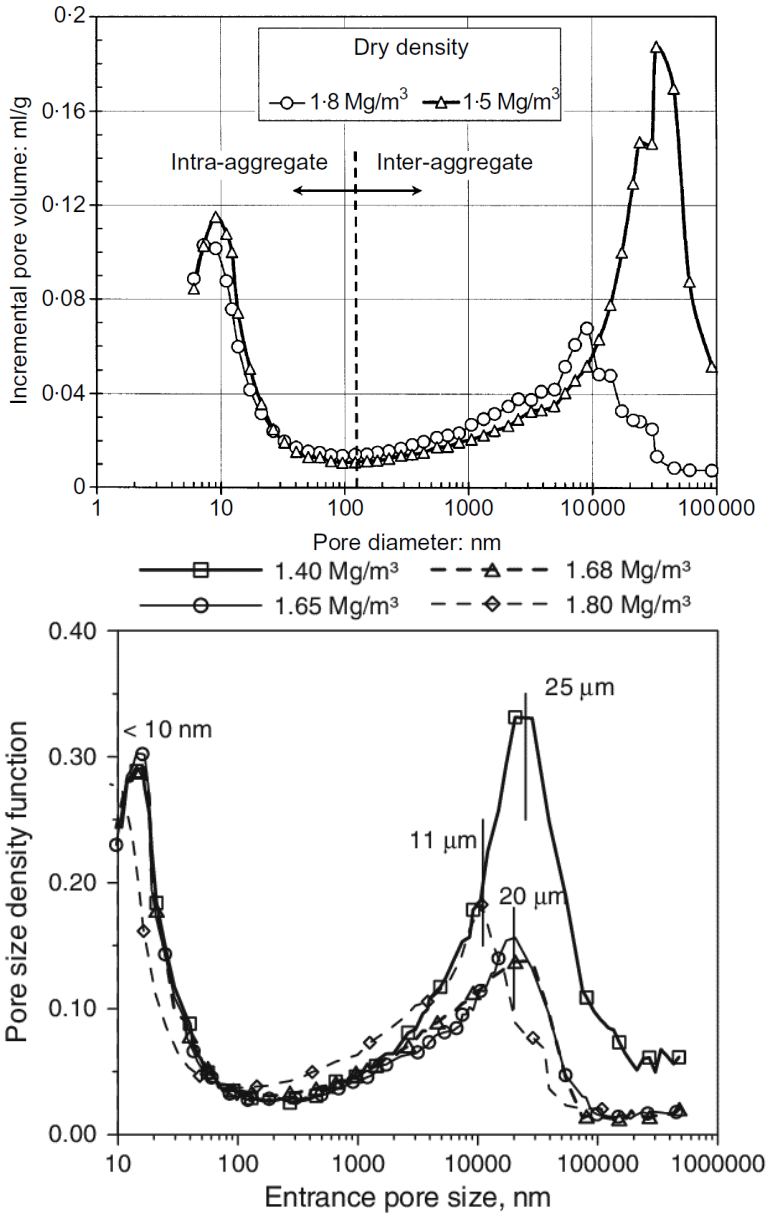

Figure 4-4: Pore-Size Distribution in Compacted Bentonite Measured Using Mercury Porosimeter (Lloret et al. 2003; Romero and Simms 2008).

The proportion and distribution of the micro- and macro-pores may also affect movement of gas through the clay. Figure 4-5 shows several schematic representations of the pore structure in a compacted bentonite clay and how these pore sizes might be distributed. What should be noted is that the distribution of these pore sizes within a clay is a result of the texture of the source material, compaction method and conditions as well as the density to which the bentonite is compacted. It is also subject to change with time, hydration state and stress history. Holmboe et al. (2012) described the response of bentonite pore size distribution with increasing densification as being largely associated with reduction of macro-pore presence and corresponding increase in interlayer voids. The proportion of such macro-voids is substantial for dry density of < 1800 kg/m^3 and at density approaching 1350 kg/m^3 the proportion of macro-voids is about of 22% of the total porosity (Suzuki et al. 2004).

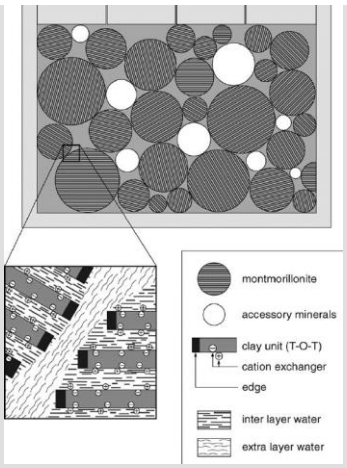

Pore structure in loosely compacted bentonite (Wersin 2003)

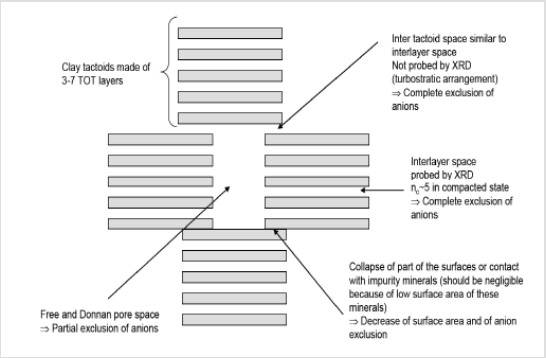

Montmorillonite microstructure at high density (Muurinen and Carlsson 2013)

Dense clay with A) large and B) small void with "external water", C) stack of flakes, D) interface between stacks (Pusch et al. 1990)

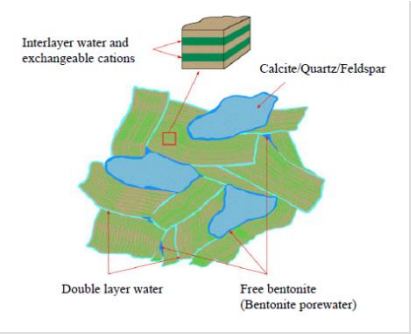

Interlayer water, double layer water & free water (Bradbury and Baeyens 2011)

Figure 4-5: Schematic Representations of Pore Structure of Compacted Bentonite

Figure 4-6 shows the estimated "free porosity" (non-structural or DDL water component) in a variety of bentonites and bentonite density conditions. Data for MX-80 indicates a change in free porosity from approximately 8-10% at dry density of 1400 kg/m^3 to < 3% at 1600 kg/m^3 or higher (Holmboe et al. 2012). Such changes in pore size distribution can be seen in changes in hydraulic and gas transport characteristics. A general conceptual model for this process has been provided by Pusch et al. (1990, 2002), Muurinen and Carlsson (2013) and Muurinen (2009).

Beyond conceptual models for clay microstructure and porosity, determined indirectly using XRD or neutron scattering techniques, pore size and pore size distribution can be measured through use of fluid (mercury) or gas intrusion measurement into compacted bentonite. Figure 4-6 shows an example of the pore volume analytical results obtained using this method and clearly shows the bi-modal distribution of pore sizes and the loss of the macro-pore component as the result of densification in bentonite materials (Lloret et al. 2003). A similar reduction is observed where hydration is ongoing, with the larger pore size component reducing in proportion as the clay swells into the larger voids (Kochmanova and Tanaka 2011). The presence of a substantial sand-sized component in association with the bentonite shifts this pattern to a tri-modal distribution with a third, larger component being associated with the sand particles (Siemens et al. 2007).

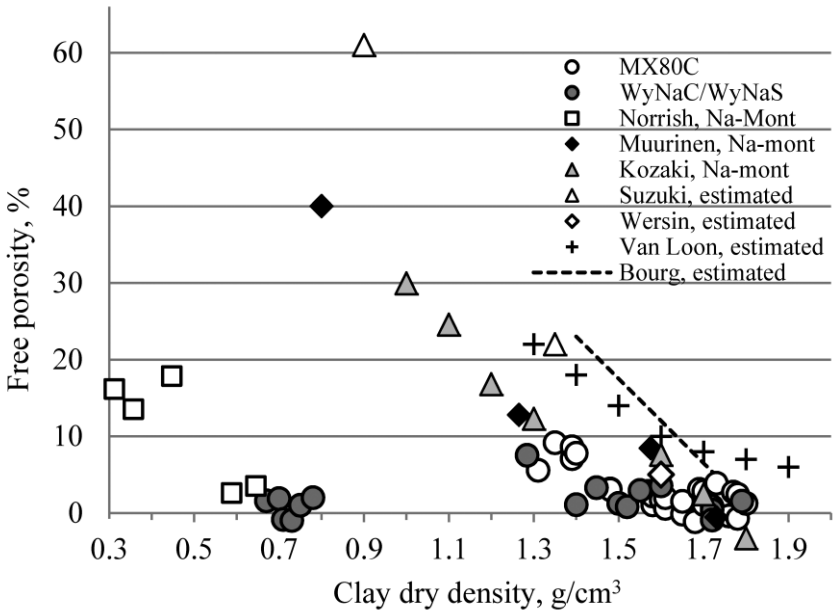

Figure 4-6: Free Porosity Calculated from Average Interlayer Distance
(Holmboe et al. 2012)

4.4 GROUNDWATER CONDITIONS

In a sedimentary geosphere the conditions encountered in the Queenston Shales that overly the Cobourg limestone unit at the Bruce site in Ontario have been selected to represent the highest salinity environment likely to be encountered. The Queenston Shale and Cobourg Limestone have TDS values in the order of 336 g/L and 272 g/L respectively (See Gobien et al. 2018, Table 7-2). Since the shafts of the DGR will pass through the more saline shale formation it is assumed that the porefluid encountered with the sealing materials are essentially saturated brines and are dominated by Na, Ca, and Cl. NWMO has generated reference formulations that are representative of the types of groundwater that are anticipated to be encountered at a DGR site. Compositional summaries for several of these pore fluids and they are presented in Table 4-4. Other sites may have less concentrated pore fluid conditions, but the issue of the more saline fluids in materials characterization and performance prediction provides a conservative bounding condition for evaluating system behavior. The depth and geological setting of the Cobourg limestone unit makes it unlikely that there will be any substantive interaction between groundwater of the biosphere with the deeper limestones (presence of overlaying low permeability sedimentary units, presence of ancient salt formations in sedimentary units overlying the limestones).

In a crystalline (granitic) geosphere, the groundwater conditions are expected to be much less saline with values of 10-80 g/L TDS anticipated at the placement level (Gascoyne et al. 1987). The interaction of the granitic formation with water originating in the biosphere is potentially higher (glacial low TDS melt water driven downwards by glacier-induced gradients (Hedstrom et al. 2015), or more saline deeper groundwaters being drawn upwards to repository level (Lofman et al. 2010) than for the sedimentary case. In the sedimentary site, the presence of large volumes of overlying highly-saline sedimentary formations, including salt deposits as well as low permeability shales will act to isolate the repository from groundwater perturbations induced by surface processes.

Actual groundwater salinity varies with depth and location in both sedimentary and crystalline rock formations. Examples of these data are presented in reports by Hobbs et al. (2011), NWMO 2011b) and NWMO (2018) for sedimentary sites and Gascoyne et al. (1987), Gobien et al. (2016), NWMO (2017) for crystalline rock conditions. These data illustrate the changes that occur with depth at various locations. For the purposes of evaluating sealing system performance, a set of bounding groundwater conditions have been defined for use in estimating influences in system performance and these are provided in Table 4-4. As noted above, granitic rocks in the Canadian Shield can exhibit higher salinity levels than the 11 g/L TDS of CR-10, reaching concentrations of 55 g/L (Frape et al. 1984) or higher (~89 g/L at 420m- depth at CNL URL site, Gascoyne et al. 1987). Therefore, the salinity at any location being considered will need to be taken into consideration when defining swelling, hydraulic and other properties for performance modelling purposes. These effects are discussed in more detail in Section 5.

Table 4-4: NWMO Reference Groundwater Compositions at Placement Level of DGR in Sedimentary or Crystalline Host Rocks.

Parameter	CR-10*	SR-L**	SR-Sh***
pH	7.0	'neutral'	'neutral'
Na	1900	46000	55200
Ca	2130	19400	48100
K	15	17600	19500
Mg	60	4860	6080
Cl	6100	135100	205600
SO4	1000	480	96
TDS	11205	223440	334576

Note: Units are in mg/L, except for pH.
*Crystalline (granitic) rock
** Limestone at depth in Ontario
*** Shale units overlying limestone formations in Ontario

4.5 EFFECT OF RADIOLOGICAL PROCESSES ON BENTONITE STABILITY

4.5.1 Background

A brief review of literature that assesses the influence of radiological-induced processes on bentonite stability and performance is provided in this section. As noted by Safi (2017), until radionuclides are released from the UFC, the possibility of their transport through the barrier is irrelevant. However, if/when UFC failure occurs, there needs to be an assessment of the effects of direct radiation and/or radiation induced processes on the microstructure of bentonite before the breach occurred. As the HCB and water adjacent to the UFC will be exposed to an extended period of irradiation by the alpha and gamma radiation being generated by the decay of the UF, the possible effects of this prior to UFC breaching still needs to be evaluated as part of a long-term degradation process.

4.5.2 Direct Radiation Damage to Mineral Structure

The potential for radiation reaching the bentonite adjacent to the UFC to change or damage the microstructure of the montmorillonite minerals has been identified as a concern regarding

barrier durability and performance. In its most severe form, radiation-induced alteration of the crystalline minerals in the bentonite results in formation of amorphous silica and alumina compounds. This was identified as an issue important for the radionuclide retention properties of smectite clays as cumulative doses may alter the mineral structure and hence properties such as sorption, swelling or water retention of clay minerals. Alternatively, formation of such an amorphous material could also result in a reduction in the porosity of the surrounding materials, thereby reducing transport capacity.

The influence of alpha and gamma radiation on the microstructure of bentonite has been evaluated by numerous researchers over the past 40 years, unfortunately much of this work has been done under very different and often not relevant boundary conditions (e.g. unrealistically high radiation levels, massive short-term irradiation, highly elevated temperature (>300^{o}C)). In order to try and avoid confusion related to these studies, the results of several key papers related to radiological effects on bentonite are summarized below in order of the date of publication with the main observations from each underlined. Where possible the units of radiological measurement have been converted to units of Gray (Gy).

4.5.3 Alpha Radiation

The Mark II UFC is very effective in self-shielding for alpha and beta radiation. It is assumed that there is effectively no alpha-radiation that makes it through to the outer surface of the UFC so long as it remains intact. This is important in that the alpha radiation is generally recognized as being most able to interact negatively with the HCB. The radiation dose rate is typically referenced in Grays (Gy), which is a derived unit of ionizing radiation dose in the International System of Units (SI). It is defined as the absorption of one joule of radiation energy per kilogram of matter. The results of various studies examining alpha radiation are summarized below in order of their publication date:

Reed et al. (1987) reviewed several studies that had examined the effect of alpha radiation on the crystallinity of bentonite. Tests were done at extremely high alpha radiation fields (2.2 x 10^{7} Gy/h) (as well as at significantly lower fields (1% and 0.1% of the original tests). There was damage to the bentonite only in the high-dose experiment with reported loss of crystallinity, low permeability and high expansivity of the clay. The sorption capacity was also reportedly higher after irradiation. The dose rates and total doses the bentonite was exposed to in the high dose experiments was estimated to be some 2000 to 10^{7} times that expected for a container installed in the basalt repository being considered in that report. It was concluded that the most representative data with respect to NWMO's DGR was for the lower dose-rate conditions examined and no structural damage was reported for the bentonite.

Allen and Wood (1988) reviewed several studies on the effects of sodium montmorillonite exposure to alpha doses. It was concluded that high alpha irradiation can lead to structural damage, but only if the container failed and there was a substantial alpha dose to the clay.

Sorieul (2003) examined cumulative alpha radiation damage to montmorillonite produced by ionizing radiation including MX-80 derived montmorillonite. The importance of the iron content of the montmorillonite minerals (or other accessory minerals) was identified. MX-80 derived minerals were reported to contain 4% iron in its structure. Ionizing irradiation was reported to induce two main effects:

- Firstly, paramagnetic point defects were identified in irradiated montmorillonite as trapped holes located on oxygen atoms of the smectite structure. These defects are

characterized by different thermal stabilities, according to annealing experiments. Their creation is limited by saturation curves with maximum damage around 100 MGy.

- Secondly, there were substantial modifications of the oxidation state of structural iron observed that were sample and dose-dependent. Irradiation was reported to induce reduction and oxidation of iron, but the intensity of redox effects varied significantly with the nature of the interlayer cation and less with the interlayer water content.

It was concluded by Sorieul (2003) that the alpha irradiation of montmorillonite has the potential to strongly modify the layer charge of the montmorillonite owing to the production of positive holes and oxidized iron. This conclusion was supported by observed changes of cation exchange capacity made using He ion irradiation. The absorbed radiation dose required to induce amorphization was measured and found to vary with the nature of interlayer cations and density charge in the minerals.

Sorieul et al. (2008) discussed the potential for cumulative doses of radiation (alpha and gamma) to degrade the mineral structure of montmorillonite to an amorphous state with alteration of their sorption, swelling, and water retention properties. They reported that the maximum effect occurs at about 300−400 °C, with temperature-induced dehydroxylation enhancing amorphization, but the exact relationship depends on the interlayer cation.

At ambient temperature, ionizing radiation and alpha-decay events do not show the same efficiency of causing amorphization. At ambient temperature, ionizing radiation in the order of 10^{10} to 10^{11}Gy is required to amorphize bentonite, which is much higher than the total radiation dose expected from the wasteform and packaging considered in 10^6 years. In contract alpha decay radiation will amorphize clays at doses consistent with those generated over 1000 years. It is noted that the limited penetration of alpha particles and recoil nuclei is limited to the 100 nm - 20 μm range. This will minimize crystal structure damage in the clays further from the source of irradiation.

Sorieul et al. (2008) concluded that montmorillonite clays will not be amorphized unless the waste package is breached and released actinides are heavily sorbed onto the clay.

Wilson et al. (2011) examined existing literature and summarized the issue of radiological influence of alpha radiation on bentonite properties as follows:

- High doses of alpha radiation can have some impact through degradation of the clay mineral structure should certain radionuclides migrate through the bentonite, especially if the migration paths are narrow.
- It was noted that SKB has considered the effect of alpha-damage on a bentonite buffer (SR-Can assessment, KBS-3 disposal facility, SKB 2006a) assuming early canister failure, and SKB concluded that only a small part of the buffer would be affected (and that this would not be substantial). It was also noted by Wilson et al. (2011) that Nagra also concluded that alpha-damage and deleterious effects were unlikely.
- Several clay mineral properties such as solubility, specific surface area, and exchange capacity can be altered by local damage produced by radiation, but the effects on properties appear significant only for high doses and remain relatively limited in distribution, being concentrated closest to the UFC.

Xie et al. (2012) concluded that the impact of alpha radiation on clay minerals (such as smectite) is primarily related to changes in its microstructure and can be understood by

considering the mechanisms for cation diffusion. Alpha radiation is expected to cause structural disintegration along the migration paths. It was reported that experiments have shown that montmorillonite that has been saturated with a radioactive solution that yielded around $5x10^{18}$ α g^{-1}, is completely destroyed and converted to an amorphous, siliceous mass. Xie et al. (2012) referenced other studies that reported that an alpha dose of around $4x10^{18}$ α g^{-1} is required to completely destroy the crystal structure of montmorillonite. Crystal structure disruption as the result of exposure to gamma radiation was expected to cause reduction of the size of the crystallites and a related increase in specific surface area.

Author note: Converting these alpha doses to units of Gy is somewhat problematic since the paper lacked some specific information regarding the energy of these alpha particles. However, assuming an energy of 6 MeV/alpha particle, and 1 MeV being equal to 1.602E-13 joule, a value in Grays can be estimated as 1 Gray = 1 Joule/kg. From this, the alpha doses used and referenced by Xie et al. (2012) is approximately 4.8×10^9 and 3.849×10^9 Gy. These alpha values are so high as to have limited relevance to the NWMO DGR, particularly as the NWMO UFC is essentially self-shielding with respect to alpha and beta radiation while it remains intact (Morco et al. 2017).

Safi (2017) undertook a review of the effects of radiation or radiation induced processes on the bentonite barrier. It was noted that the dose rate and energy of the particles in the studies so far differ substantially from those the bentonite will be exposed to in the KBS-3 repository. In some studies, for example, alpha radiation has been used to study the response of clay minerals and this is not particularly relevant for a UFC where the range of alpha radiation may not be long enough to reach the bentonite barrier. In other studies, conditions expected in the repository have not been considered properly. For example, bentonite response to electron radiation is often studied under much higher temperatures than those expected at the surface of the UFC in the KBS-3 (or NWMO) repository.

Author note: This means that the results reported by Safi are also incompatible with the conditions anticipated in NWMO's repository where fields will be comparable to those anticipated by SKB.

Safi (2017) further concluded that even though amorphization of smectite minerals is unlikely under ionizing radiation with moderate energies (alpha particles, beta and gamma rays) (Gournis et al. 2000, Allard and Calas, 2009; Allard et al. 2013), it is possible that once radioactive material is released following UFC failure, the radiation (alpha recoil nuclei) from escaped transuranic elements may be able to induce amorphization of the montmorillonite. This conclusion was however based on using rapidly accumulated radiation doses in laboratory tests to simulate what the barriers might receive during the lifetime of the repository (Safi 2017). It was concluded by Safi (2017) that since amorphization has a significant influence over the dissolution kinetics of smectite, and thus on its radionuclide-retention properties, it is important that the behavior of the montmorillonite clay under exposure to long-term radiation should be considered in safety analyses. This conclusion was also reached by Sorieul et al. (2008); Fourdin et al. (2010); Meunier et al. (1998) and Haire & Beall, (1979).

4.5.4 Gamma Radiation

Gamma radiation is capable if passing through the walls of the UFC and interacting with the HCB surrounding it. The radiation dose rate is typically referenced in Grays (Gy), which is a derived unit of ionizing radiation dose in the International System of Units (SI). It is defined as the absorption of one joule of radiation energy per kilogram of matter. The conclusions reached by various researchers are provided below and it should be noted that they are not entirely consistent. These studies examining the effects of gamma radiation are presented in order of their publication date:

Allen and Wood (1988) examined the results of several studies related to the effects of sodium montmorillonite exposure to gamma radiation and concluded that there was no evidence of damage under high gamma irradiation. In a study for the HLRW canister considered for use in the USA during the 1980's, it was determined that the radiation would be almost exclusively gamma, with a 1000-year total absorbed dose of 10^7 to 10^8Gy occurring. In a second referenced study it was observed that a total absorbed dose of $3x10^8$ Gy of ^{60}Co gamma radiation resulted in no detectable crystallographic changes. The third study referenced by Allen and Wood (1988) had a $3x10^7$ Gy total absorbed dose of ^{60}Co gamma radiation plus heating to 300^{o}C. It was concluded that no changes beyond those attributable to heating alone occurred.

Gournis et al. (2000) examined the effects of total doses of 8.4×10^4 and 4.2×10^5 Gy gamma irradiation on montmorillonite clays. It was concluded that the interaction of gamma-rays with smectite clays induced no noticeable changes in the structure of the minerals.

Negron et al. (2002) examined the effect of high doses (up to $2x10^6$ Gy) of gamma-radiation on the short-range structural organization in montmorillonite using infrared (IR) spectroscopy and solid-state high-resolution ^{27}Al and ^{29}Si nuclear magnetic resonance (NMR). No change attributable to irradiation was observed. A small variation in the water content was noted but it is not systematic. The results showed that the montmorillonite structure can accumulate high doses of gamma radiation without damage and therefore was suitable for use in the safe disposal of radioactive waste.

Plotze et al. (2003) evaluated the influence of gamma-irradiation ($1.1x10^6$ Gy, absorbed dose using ^{60}Co) on the physicochemical parameters ("crystallinity", specific surface, cation exchange capacity, main layer charge) of montmorillonite. The influence of gamma-irradiation on the physicochemical properties was observed to be generally weak. A reduction of lattice iron during irradiation could be measured, which causes decreasing values of cation exchange capacity (CEC) and main layer charge of the smectites. A weak loss of "crystallinity" of kaolinite was noted and it was concluded that the structure of clay minerals is stable even at high gamma-irradiation doses.

Sorieul et al. (2008) examined the effect of cumulative doses in the order of 10^{11} Gy which is an order of magnitude higher than they estimated would occur in a repository in 10^6 years. The dose rate used in this study was 4 to 8 orders of magnitude higher than would be expected in most repository conditions. It was concluded that montmorillonite clays will not be radiologically amorphized unless the waste package is breached and released actinides are heavily sorbed onto the clay overpack.

Huang and Chen (2004) noted that in a high-level waste repository, it is expected that most of the alpha and beta radiations are attenuated in the fuel, while the gamma radiation can penetrate to interact with the UFC and buffer materials. According to the Swedish evaluation, the initial gamma dose rate is estimated to be 0.350 Gy/h outside the canister and declines with time. Since the main contributor to the radiation dose rate is ^{137}Cs, the gamma radiation will have decayed to very low levels within 300 years. To evaluate the effects of strong gamma radiation on the swelling of buffer materials, Zhisin clay was exposed to a cumulative dose of between 1.05 and 1.06 $x10^8$ Gy gamma radiation. The irradiated clay was then used to prepare specimens for free swelling test and reduced swelling capacity was observed. It should be noted that this is some 20 times the irradiation amount considered by Plotze (2003 or Negron (2002) and more than 1000 times that of the NWMO Mark II container with its CANDU used fuel

(10^5 year cumulative gamma-dose of approximately 5.1 - 3.1 x 10^5 Gy for 30 and 50 year-cooled used fuel at the time of UFC installation (based on values provided by Morco et al. 2017)).

Wilson et al. (2011) reviewed experiments with bentonite under gamma-radiation and concluded that many of these studies didn't identify any structural alteration of bentonites under repository-conditions. It was noted that:

- Faster migration from an iron plate into clay occurred under radiation (Pusch 1993),
- CEC of montmorillonite increased (Grauer 1986).
- Solubility, specific surface area, and exchange capacity can be altered by local damage produced by radiation. Structural breakdown of montmorillonite can potentially result from radiolytic damage due to a severe ionizing radiation and clay minerals can be amorphized under electron or ion beams (Allard and Calas 2009; Allard et al. 2013).

It was concluded that these effects on the T-H-M properties of montmorillonite appear significant only for high doses and remain relatively limited under conditions anticipated to occur in SKB's DGR. Wilson et al. (2011) summarized the issue of radiological influence on bentonite properties as follows:

- Gamma radiation is less likely to result in damage to smectite crystallites.
- Several clay mineral properties such as solubility, specific surface area, and exchange capacity can be altered by local damage produced by radiation, but the effects on properties appear significant only for high doses and remain relatively limited is distribution, being concentrated closest to the UFC.

Xie et al. (2012) examined several studies that concluded that the exposure to gamma radiation would disrupt the crystal structure as the result of cause reduction of the size of the crystallites and a related increase in specific surface area. Although dose rates were not provided it was concluded that only a small part of the buffer would be affected and appear only to be substantial where radiation dose is high.

Jonsson (2012) summarized the situation regarding radiation effects on water and bentonite associated with the waste canister proposed for use in disposing of used nuclear fuel in Sweden. In a repository, bentonite will be exposed to gamma and neutron radiation even when the canister is intact. The maximum dose rate will be the same as for the copper surface of the canister. The total gamma-dose for the KBS-3 UFC will be in the order of 0.40–2.0 x 10^5 Gy and it was concluded that even at very high doses of several MGy, only small or insignificant effects have generally been found on both physical and chemical properties of bentonite and montmorillonite.

Author Note: In comparison, the UFC considered by NWMO will have a 10^5 year cumulative gamma-dose of approximately 5.10 and 3.10 x 10^5 Gy for 30 and 50 year-cooled used fuel at the time of UFC installation (based on values provided by Morco et al. 2017).

Safi (2017) concluded that even though amorphization of smectite minerals is unlikely under ionizing radiation with moderate energies (alpha particles, beta and gamma rays) (Gournis et al. 2000; Allard & Calas 2009; Allard et al. 2013), it is possible that once radioactive material is released following UFC failure, the radiation (alpha recoil nuclei) from escaped transuranic elements may be able to induce amorphization of montmorillonite.

4.5.5 Radiolysis Effects on Montmorillonite

As with the evaluation of the direct effects of ionizing radiation on the structural stability of montmorillonite provided in Sections 4.5.3 and 4.5.4, there is also the need to consider the

effects of radiolysis on this material. A series of brief summaries extracted from studies of the radiolysis process and its interaction with the HCB is provided below.

Gournis et al. (2000) examined the effects of gamma irradiation on montmorillonite clays, concluding that for sodium-montmorillonite, Mössbauer spectra show that gamma-irradiation causes a partial reduction of trivalent iron to the divalent state due to hydrogen radicals production from the radiolysis of interlayer water but that the clay maintained the two molecular layers of water associated with the clay faces and therefore concluded that the radiolysis of interlayer water causes no measurable changes in the architectural organization of the interlayer environment.

Bradbury et al. (2012) discussed the issue of radiolysis with respect to possible undesirable water oxidation effects on used fuel. Here, the main concern was the potential effect of water radiolysis on other components in the near-field. Radiolysis by alpha and beta particles is limited to a thin (a few tens of µm-thick) layer of water in direct contact with the fuel surface (or its corrosion products). Gamma radiation is more penetrating. However, most of the energy transfer in water (and therefore the production of radiolytic species) occurs only within a few cm distance from the gamma-radiation source.

It was noted that gamma-radiolysis produces mostly short-lived chemical radicals that rapidly decay to redox-neutral species, mainly water. In anoxic water, molecular oxidants (H_2O_2) are not produced in detectable amounts. For these reasons, it was concluded that water radiolysis is not likely to affect the external components of the near-field system, notably the bentonite buffer for installations involving either SF or vitrified HLW or SF. It was additionally noted that any radiolytic oxidants produced will not play a role in interactions with the bentonite since they will be consumed by reaction with $H_2(g)$ produced during the anaerobic corrosion of steel or because of the strongly decreased decay in the later stages of repository evolution. They also note that the alpha radiation field generated from vitrified waste is always 1 – 2 orders of magnitude weaker than for SF, and so radiolysis will also not be an issue in that environment.

Xie et al. (2012) discussed the effect of **r**adiolysis of porewater with its resultant production of H-bearing radicals and oxygen compounds (including ozone and hydrogen peroxide). These radiolysis products may take part in chemical reactions affecting pH and oxidizing canister metals. Oxygen compounds (in gaseous form) may occupy larger voids in the HCB and could delay or inhibit water saturation of the HCB and hence contribute to heat-induced desiccation of the buffer adjacent to the UFC. This was concluded to be of particular concern in HCB in a very tight repository host media, such as argillaceous (sedimentary) rock and very fracture-poor crystalline rock. Xie et al. (2012) concluded that radiolysis on its own is unlikely to result in a significant build-up of gas pressure in the repository with most of the gas generated being the result of iron corrosion.

Safi (2017) considered change or damage to the clay as the result of radiologically-induced chemical processes (radiolysis). As discussed by Safi (2017) montmorillonite is a 2:1 phyllosilicate mineral with an alumina octahedral sheet sandwiched between two tetrahedral sheets of silica. The octahedral sheet has aluminum as the central atom while the lower and upper tetrahedral sheets have silicon as the central atom. The aluminum in the octahedral site is partly substituted by (mainly) magnesium and silicon atoms in the tetrahedral sheets are replaced by aluminum. The montmorillonite particles may also contain Fe, mostly as a substituting atom for aluminum in the octahedral sheet, but also in other forms. It may be found as iron oxides sorbed onto the surface of the layer and as hydroxyl complexes on the layer surface located the edge of the montmorillonite layer. MX-80 has a 3 wt% Fe content.

The composition and distribution of the accessory minerals in bentonite have great influence on the long-term geochemical evolution of the buffer in the repository environment. The oxidation state of the different species may have influence on different properties of montmorillonite. The water-radiolysis products formed by radiation from the UF may alter the redox conditions in water in the bentonite and at the copper-bentonite interface leading to changes in oxidation states of the different species. Safi (2017) noted that in a relatively recent study that gamma-radiation with doses within the levels expected at the bentonite surface may alter $Fe(II)/Fe_{tot}$ ratio. The oxidation state of iron in the crystal structure of smectite minerals changes their physical-chemical properties. The alteration of $Fe(II)/Fe_{tot}$ ratio by radiation from the UF may greatly influence a number of physical properties, such as cation exchange capacity (CEC), swelling pressure, total layer charge and specific surface area, of montmorillonite. One of main oxidants among the water-radiolysis products is H_2O_2 which undergoes different processes at a solid-liquid surface in relation to the processes taking place in the bulk water. It has for example been reported that H_2O_2 adsorbs on the surface of metal oxides such as UO_2 and undergoes catalytic decomposition. It has also been noted that H_2O_2 may be associated with the changes in the observed $Fe(II)/Fe_{tot}$ ratio under gamma-radiation. Safi (2017) concluded that the role of radiolytically produced H_2O_2 in the bentonite pore and layer water content as well at the copper-bentonite interface needs to be investigated further.

4.5.6 Summary of Literature Information Regarding Radiation Effects on Bentonite

It should be noted that the NWMO UFC, like most containers proposed for use in deep geological disposal provides substantial self-shielding, and so it is likely that the amount of gas produced by radiolysis of the clay minerals will be small compared with the amount that will be produced as a result of corrosion of the steel or cast iron internal components of the UFC.

As can be seen in Section 4.5, the available literature on the influence of radiation on the structure and behaviour of bentonite under conditions relevant to the NWMO UFC is limited. Much of the literature involves tests undertaken under radiological conditions either orders of magnitude more severe than will occur or else under massive short-term exposures that do not simulate field conditions. To summarize the relevant information, radiation effects will be associated with two very different conditions:

- The first stage in radiation interaction between the UF in the UFC and the surrounding HCB occurs while the UFC is intact and radiation emitting from its surface is limited to gamma. Gamma has been concluded to have very limited effects on the structure or behaviour of the bentonite, even under conditions much more severe than will occur in the DGR. The HCB immediately adjacent to the UFC will therefore have undergone little or no radiologically-induced degradation before the UFC is breached.

- The second stage of radiological damage to the HCB will be associated with alpha radiation. This will not begin until the UFC is breached, and alpha radiation or alpha-emitting radionuclides escape to allow for short-range interaction with the clay. Alpha radiation has the potential to induce greater mineralogical damage to the bentonite, but the zone affected by this process is generally concluded to be limited due to the poor penetrating ability of this radiation and the ability of the bentonite to retard movement of ions through it. The literature is not consistent with respect to either the degree to which radiolysis will influence bentonite (Safi 2017) or if it will at all (Bradbury et al. 2012). Much will depend on minor elements (e.g. iron) in the bentonite since these have a controlling effect on the chemical processes arising from radiolysis. Additionally, it is

recognized that gas generation as the result of radiolytic processes will be very small relative to that associated with the corrosion of the steel insert components once water enters the UFC.

Each UFC will have a slightly different surface field, depending on the specifics of the used fuel bundles it contains (age and radiological component composition of the fuel bundles as determined by the fuel history). The field that the bentonite closest to the UFC will experience is also decreasing with time as the UF decays. The radiation fields present in the various waste forms and containers considered by each national program differ substantially, as do the testing conditions to evaluate effects of radiation on bentonite. The discussion below is therefore generic in nature and intended only to provide indicative information regarding radiological influences on bentonite. It should also be noted that detailed consideration of chemical and radiochemical reactions and transport processes related to water radiolysis or interaction of radiological elements released from a breached UFC with bentonite are not included in this discussion.

To evaluate what is likely to occur in the case of NWMO's UFC, the first consideration is the actual radiation field that will be experienced by the bentonite rather than how unrealistically severe experimental conditions can be demonstrated to cause changes. Actual radiation contacting the bentonite will of course depend on factors such as age of the UF, shielding effect of the massive steel UFC shell, the thick copper coating on its surface and hydration state of the bentonite. The Mark II UFC holds 48 bundles of used CANDU reactor fuel. In NWMO's repository concept, before being packaged into a UFC, this fuel has been cooled for a period of 30 to 50 years after its removal from the reactor. The result of this cooling time is a very substantial decrease in the radiation field (and heat generation) associated with it. This is illustrated in Figure 4-7 and Table 4-5. The cooled UF is ultimately installed in the massive steel UFC shown previously in Figure 3-2. The steel provides a very high degree of self-shielding to the UFC, effectively eliminating alpha and beta radiation beyond the UFC's outer surface so long as the UFC remains intact. Any damage to the HCB beyond the UFC would therefore be as a result of gamma radiation.

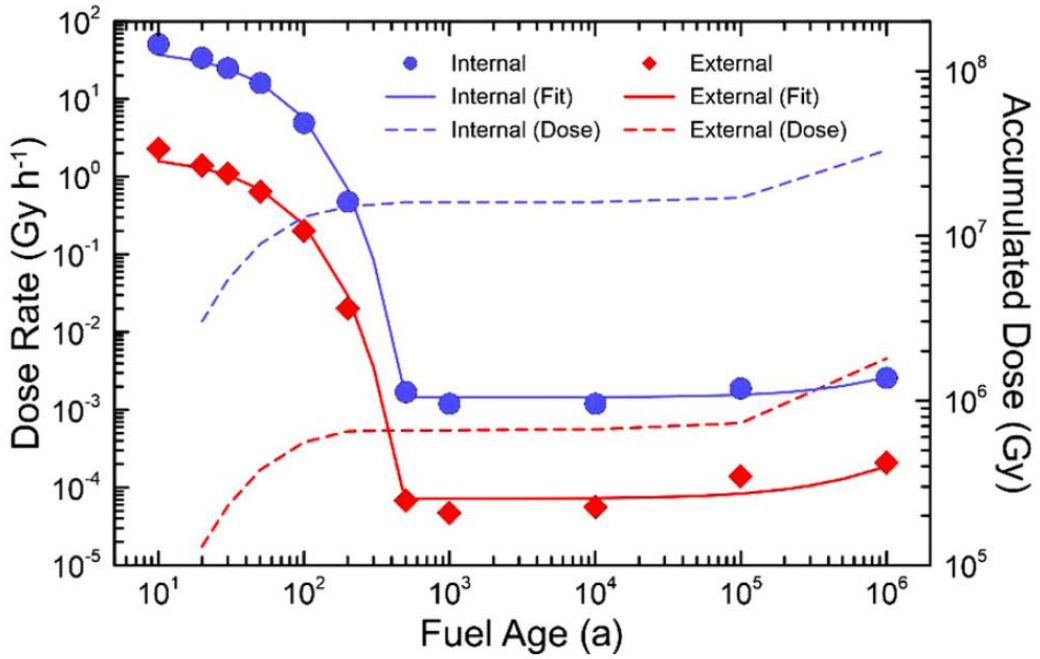

Figure 4-7: Radiation Dose Rate and Accumulated Dose for Outer Surface of Mark II UFC holding CANDU UF (Morco et al. 2017)

Based on Figure 4-7, the gamma radiation exiting the surface of NWMO's intact UFC is estimated to be in the order of 5.6 to 9.6 x 10^3 Gy/a for 50 and 30 year-cooled UF at the time of installation in a UFC (Morco et al. 2017). Based on these same data, after 10^5 years following placement of the UFCs, the cumulative gamma dose at the contact with the surrounding buffer would be in the order of 3.10 to 5.10 x 10^5 Gy for the 50 and 30 year cooled fuel. By 10^6 years this dose would have increased to approximately 1.6 to 1.8 x 10^6 Gy for the 50 and 30-year cooled fuel respectively. This level of gamma irradiation is considerably less (2 to 7 orders of magnitude), than has been applied in the studies summarized in Sections 4.5.3 and 4.5.4. Even those studies having 2 orders of magnitude higher gamma exposure were concluded to have caused little to no substantive damage to the bentonite. Based on this, it is assumed that the Thermal-Hydraulic-Mechanical properties determined for bentonite materials under conditions of no-radiological field will persist in the repository.

Table 4-5: Summary of Internal and External UFC Gamma-Radiation for NWMO's Mark II UFC (Morco et al. 2017)

Fuel age *a*	Internal surface[a] Gy h^{-1}	External surface Gy h^{-1}
10	5.1×10^{1}	2.3×10^{0}
20	3.4×10^{1}	1.4×10^{0}
30	2.5×10^{1}	1.1×10^{0}
50	1.6×10^{1}	6.4×10^{-1}
100	4.9×10^{0}	2.0×10^{-1}
200	4.8×10^{-1}	2.0×10^{-2}
500	1.7×10^{-3}	6.8×10^{-5}
1,000	1.2×10^{-3}	4.7×10^{-5}
10,000	1.2×10^{-3}	5.6×10^{-5}
100,000	1.9×10^{-3}	1.4×10^{-4}
1,000,000	2.6×10^{-3}	2.1×10^{-4}

[a]Includes assumed contribution from back-scattered β-radiation near the internal surface.

Fuel age refers to the time since the fuel was removed from the reactor.

5. T-H-M-C(B) PARAMETERS DETERMINATION FOR HCB AND GFM

Based on the outlined DGR design, anticipated geosphere conditions, and repository T-H evolution, the properties of the HCB and GFM components have been estimated. These parameter values (and ranges) assume that MX-80 bentonite is used and that the reference as-placed dry densities of the HCB and GFM components are 1700 and 1410 kg/m^3 respectively. Discussion is also provided regarding the impact of varying the as-placed and equilibrated buffer mass densities on key behavioural parameters.

5.1 VOLUME CHANGE PROPERTIES OF HCB AND GFM

5.1.1 Shrinkage During Drying

The HCB blocks and GFM components will be installed in the placement room in a condition that is assumed to match their target as-built state (1700 and 1410 kg/m^3 respectively). The as-placed condition of the buffer/GFM system is not expected to remain unchanged for very long after material placement, with drying occurring at least locally adjacent to the UFC. This is the result of the heat generated by the UFC driving moisture outwards towards the cooler perimeter of the placement room. The degree of drying and its duration are variables that will be determined largely by the amount of water entering the room from the surrounding rock. In the sedimentary environment discernible inflow will not occur for an extended time following UFC placement and so the amount of water removed from the central HCB regions will be notable. In a wetter environment such as a crystalline geosphere, the amount of drying will be lower since water will have been supplied to the perimeter from the rock, limiting the amount of water that can be relocated from the region adjacent to the UFC. With drying there will be some shrinkage of the HCB in the vicinity of the UFC, but this may not be immediately evident since swelling of the materials at the perimeter may have compensated for this shrinkage.

The volume change of HCB materials as the result of drying is strongly affected by the initial density of the material, its degree of water saturation when drying starts, the composition of its pore fluid and temperature it is exposed to.

Density affects shrinkage in that a dense material will have lower porosity and hence lower potential for volume shrinkage during drying. Additionally, in denser materials the particles will be in closer physical proximity and hence the room for volume reduction before mineral-to-mineral contact occurs (and further volume change ceases) is limited.

Unlike most clay and non-clay minerals, swelling clays have very high surface charge (Table 4-3), resulting in a strong affinity to moisture. The water associated with the charged surfaces is strongly held and therefore removal of this adsorbed water requires more energy than is needed to vaporize free water. The gradual loss of moisture by drying also results in the remaining water being more strongly held by the bentonite, this sorptive behavior is related to the increasing suction that will be developed by a bentonite material as drying progresses. This suction-moisture relationship will result in the development of increasing shrinkage forces as water content decreases.

The drying shrinkage is also related to the temperature at which drying occurs. In a system where the clay's pore fluid is a brine, there is a need for more energy input in order to release the water from the brine solution and energy required increases as the brine becomes more concentrated. Hence the shrinkage behavior of a bentonite in a low temperature environment will be different than is observed in one where the local temperature is higher. This is of

importance when evaluating the behavior of bentonites in that the amount of water that can be released during drying at 100°C will be very different than that at 90°C (lower) or 110°C (higher) with extensive drying continuing until all the adsorbed water is lost (see Figure 5-1). This is illustrated in thermogravimetric measurements where water loss occurring at various temperatures are measured. Figure 5-1 shows examples of the dehydration behavior of a high-surface charged, swelling clay (montmorillonite). The peaks on the left side of the figures are associated with loss of (a) weakly bonded surface water at temperature below approximately 90°C, then the diffusive double layer water layers at temperatures of approximately 90-130°C and (b) on the right side of the figure spikes in the graphs are associated with structural collapse of the minerals at very high (>500°C) temperature.

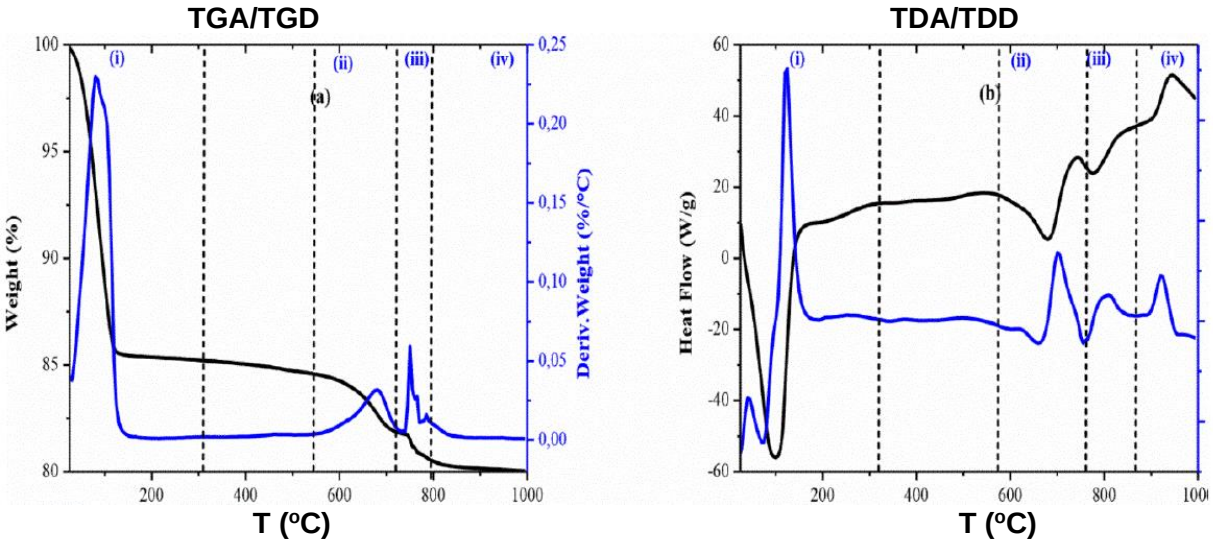

Figure 5-1: Thermo-Gravimetric Behavior of MX-80 Bentonite (Vieillard et al. 2016)

Shrinkage of bentonite materials can be presented as volume change as the result of temperature change or as the result of desiccation induced by reduced relative humidity (increased suction) in its environment.

The effects of porewater chemistry on the temperature-induced drying volume change characteristics of HCB and GFM-type components has been extensively studied. As noted in the discussion of mineralogy, the swelling clay minerals making up the majority of the volume of the bentonite are highly influenced by the composition of the water within and surrounding it as well as how close the individual particles are to one-another (density). In extreme cases, where the pore fluid salinity is very high, HCB materials may show reduced drying shrinkage. This is a result of the salt gradually coming out of solution to form a new solids phase that resists contraction of the clay. Additionally, as salinity increases so does the force with which it attempts to draw in (or hold) water. The role of suction on bentonite behavior is discussed further in Section 5.3.

The influence of change in relative humidity on the volume of bentonite is most relevant to the HCB since it is installed as massive blocks that could be subjected to substantial changes in the local relative humidity as the result of temperature-gradient and moisture migration towards the cooler rock surfaces.

The granular GFM is unlikely to see substantial drying during system evolution unless rock desaturation occurs. The nature of the GFM is such that in its as-placed condition (dry

granulate), it will behave much as an inert granular material and hence be little effected by localized drying. Should the GFM undergo a drying phase following its hydration it could be expected that it would then experience a degree of volumetric shrinkage and potentially mechanical disruption in the form of drying cracks. Of greater concern regarding drying of GFM and HCB is the tendency of these materials to become more brittle as desiccation progresses. In the pre-installation phase this might be reflected in an increased risk of HCB blocks cracking or breaking. In this situation, the GFM particles may also reduce in size with development of a higher dust component, which is more of an operational (health and safety) concern than a performance issue.

5.1.2 Swelling on Contact with Free Water and Drying Shrinkage

The effect of water supplied to the HCB and GFM components within the placement room reflects a complex H-M interaction between bentonites of very different density, initial degree of saturation and compressive behavior. Added to this is the effect of the chemical composition of the free water component that is entering the placement room.

Swelling capacity of bentonite can be evaluated through several simple tests where the volume occupied by a fully-hydrated material is measured. The swelling capacity can be assessed based on interaction of a loose bentonite material and the volume the hydrated bentonite occupies. This will provide a measure of void volume that bentonite could swell into before there is no further capacity to expand. This is not a situation that is anticipated to exist in a placement room as it will be carefully filled with HCB and GFM, the techniques are of more relevance to assessment of delivered raw bentonite as part of a quality assurance program.

The commonly-used “free-swell” test used to provide index values for bentonite materials is based on a standard methodology (ASTM D-5890-11), used to determine the water uptake capacity of soils. Use of this method on bentonite has some limitations as the values obtained are very sensitive to the granularity of the material, operator bias regarding visualization of hydrated volume and also the nature of the water available for uptake. The Free-Swell Index (FSI) is obtained by adding a known mass (2 g) of oven-dried bentonite slowly to 100 cm^3 of water (or solution) and then determining the volume occupied by the fully hydrated gel that settles out of solution.

As noted previously, the crystal structure and high surface charge of montmorillonite-type minerals results in a strong affinity to drawing water into the spaces between clay platelets. In a low salinity environment this results in development of an extensive hydration layer on the platelet faces and hence a high swelling capacity. However, if the pore fluid is saline the cations in solution will tend to sorb on the clay particle faces, reducing the strength of the charged surface and hence a lowering of the amount of water that will be drawn into the interparticle spaces and hence a lower volumetric swelling capacity. The presence of high salinity groundwater results in near-elimination of the development of hydration layers on the mineral surfaces. It is therefore very important to test free swell capacity in groundwater conditions relevant to the repository site. Table 5-1 and Figure 5-2 present some representative free-swell data and it can be clearly seen that it does not require very much in the way of porewater salinity to substantially reduce the swelling capacity of MX-80 bentonite. Similarly, the granularity of the material added to the sedimentation column will affect the results, with very fine-grained materials tending to form larger hydration flocs and occupy a larger volume. Coarser-grained materials will tend to settle quickly to the bottom of the test cylinder where they will hydrate less effectively and occupy a smaller volume as a hydrated gel.

The results of a free swell test provide an indication of the minimum field density that might develop in a location where there is a large unfilled void and no discernible mechanical consolidation of the loose bentonite is achieved by adjacent denser materials. The zero-free-swell condition also provides an estimate of the density to which the GFM would need to decrease before it is unable to expand into an adjacent void. Additional discussion of the role of solution composition is provided by Birgersson et al. (2009) where the role of cation type and concentration are examined.

Table 5-1: Free Swell Index & Hydrated Density of Loose MX-80 and National Standard Bentonite in Various Groundwaters.

FSI (cm^3/[2g])	Freshwater	CR-10 (Granitic) (11g/L)	SR-160 (160 g/L)	SR-L (223 g/L)	SR-Sh (335 g/L)
MX80[*]	32.6 ± 1.6	7.2 ± 0.4		4.2 ± 0.2	3.6 ± 0.4
MX-80	34.8, 28[**]				
MX-80	34-42[+++]				
Wyoming Bentonite	27[+], 22-30[++]	10.5[+]	6.5[+]		4[+]
Possible Reference Value	**>25**	**7-10**	**7**	**4**	**4**

[*] Dixon et al. 2018; [**]Davies et al. 2017; [+] Priyanto et al. (2013); [++] Oscarson and Dixon (1996b); [+++] Kim et al. (2012).

Figure 5-3 presents the drying shrinkage behaviour of MX80 bentonite determined by Abootalebi (2016). This provides an indication of the volume change that might occur if a fully-saturated HCB material were to be exposed to a temperature of 110ºC and moisture released by the heated material were able to escape from the system. Movement of water could occur through vapour transport from the warmer regions adjacent to the UFC to the cooler areas adjacent to the surrounding rock. It would seem possible that a fully-saturated MX80 material at initial dry density comparable to the HCB could shrink as much as 10%.

The data presented in Figure 5-3 also shows the effect of a highly saline pore fluid on drying shrinkage. Shrinkage resulting from drying at 110ºC resulted in approximately 3% shrinkage. It should be noted that Abootalebi (2016) also noted that a finely ground (200-mesh) Wyoming bentonite, exhibited similar drying shrinkage with freshwater pore fluid, but nearly 6% drying shrinkage when a saline pore fluid was present. This indicates that there are factors (i.e. particle size) other than salinity that will affect shrinkage behaviour of smectites. These tests do however provide some bounding values for use in evaluating the potential mechanical effects of bentonite desiccation.

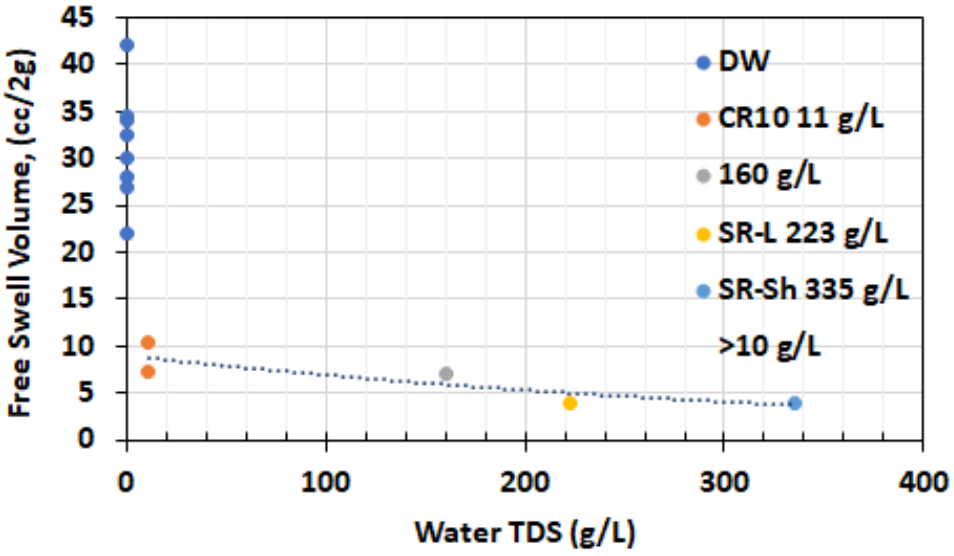

Figure 5-2: Free Swell Volume of MX-80 Bentonite

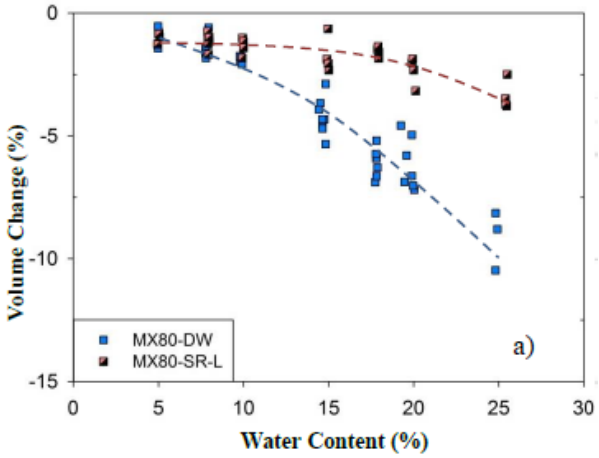

Figure 5-3: Drying Shrinkage of MX-80 at 1700 kg/m^3 Dry Density and Influence of Pore Fluid Salinity (Abootalebi 2016)

5.1.3 Volume Equilibration of Buffer/Gap Fill Materials

The issue of volumetric equilibration of the HCB and GFM in a placement room requires consideration of a large number of H-M-C factors. This was briefly introduced in Section 4.3 and it was concluded based on literature review (Dueck et al. 2010, 2014, 2016, 2019; Kim and Priyanto 2011; Kobayashi et al. 2014; Åkesson et al. 2010a,b), that the GFM will undergo some consolidation by the HCB components, but that this will likely not result in a fully-homogeneous sealing system. The degree and rate of GFM consolidation by the HCB will be a function of the following factors:

- Dry density of GFM and HCB,
- Chemistry of the water present to hydrate the bentonite,
- Rate of water uptake, and
- Mass or Volume Ratio of HCB to GFM

Also, as noted in Section 3.3, there is a likelihood that there will be some degree of density anisotropy between the HCB and GFM occupied regions. This makes optimizing (maximizing) of the as-placed density of the GFM important as there is a need to allow for some degree of density anisotropy in the equilibrated buffer-GFM system. These factors are discussed later in sections discussing H-M properties of the sealing materials.

The bounding density values can be estimated based on the range of materials volumes and as-placed density for the range of placement room dimensions. From those values, the degree of consolidation of the GFM by the HCB can be estimated using the mechanical (consolidation) behavior of the GFM.

5.1.4 Summary of Volume-Change Behaviour

The ability of the density-equilibrated HCB-GFM volume to maintain an ability to swell into any adjacent voids or voids that might develop as the repository evolves, is very important to the safety case for the DGR. The volume change capability of the HCB and GFM under the range of groundwater conditions anticipated to develop in a DGR in crystalline or sedimentary rock has been evaluated. The swelling capacity of the sealing materials is related to the swelling pressure and hence the swelling clay content and groundwater composition.

5.2 THERMAL PROPERTIES OF HCB AND GFM

5.2.1 Key Environmental Parameters Effecting HCB and GFM Thermal Properties.

One of the primary roles of the buffer and GFM components is to provide for effective transfer of heat from the UFC to the surrounding geosphere where dissipation occurs. Presence of a placement room fill material that has inadequate thermal transfer capacity could result in development of undesirably high temperatures at the UFC surface or in the HCB closest to the UFC.

In the placement room, the fill materials are 100% MX-80 bentonite, initially in the form of HCB and GFM. The thermal properties of these materials are primarily affected by their density, water content (degree of saturation), and to a lesser extent the nature of the pore fluid present in these materials. The movement of heat through the HCB and GFM is primarily via conduction and this can be adversely affected by the presence of gaps or voids in the space between the UFC and the surrounding geosphere. Other factors such as non-bentonite components in the compacted bentonite (e.g. sand or graphite) will also affect movement of heat through the placement room fill, however the NWMO concept does not include such materials and so discussion of these factors is not included in this study.

5.2.2 Thermal Properties of Bentonite

5.2.2.1 Background

The measurement of thermal properties of materials proposed for use in isolating UFCs in a DGR has been completed in numerous studies by NWMO and elsewhere. As noted above, the primary influences on thermal conduction in these materials is density, water content and pore fluid composition. It should also be noted that each bentonite material will have slightly different thermal behavior as a result of differences in mineralogical composition and granularity. Since NWMO has selected MX-80 as its reference bentonite product, these considerations are less important since this product has shown long-term consistency in its composition and granularity. Should a different material be selected for use, there could be expected to be slight differences in its thermal properties.

The HCB used as buffer boxes, spacer blocks and floor tablets in a placement room are expected to be the same density and degree of water saturation at the time of their installation. The GFM is also to be placed at a known initial condition. From these as-placed conditions, the system will begin to undergo density, saturation and pore fluid composition evolution. This may include localized drying (HCB adjacent to UFC), saturation (GFM initially and then HCB closer and closer to UFC), changes in the density of the HCB and GFM (as GFM is consolidated by expanding HCB). The pore fluid in the bentonite materials will also be changing as water moves away from the regions closest to the UFC initially, coupled with water uptake by the GFM from the surrounding rock (and/or the HCB). All of these changes in density and water content will result in changes in the thermal properties of the HCB and GFM.

The key thermal properties parameters of concern in the bentonite materials are thermal conductivity, thermal diffusivity and specific heat. They are related by the following equation:

$$\boldsymbol{\lambda = C\rho\kappa} \qquad \textbf{5-1}$$

where λ is thermal conductivity, C is volumetric heat capacity, κ is thermal diffusivity and ρ is density.

Each component of the engineered barrier system has its own set of thermal characteristics, and each needs to be characterized in order to accurately predict the thermal evolution of the UFC-bentonite system and then the broader thermal evolution of the DGR over time. There is a comprehensive body of information collected by a variety of means on bentonite materials as well as bentonite-sand mixtures (e.g. Abootalebi 2016; Abootalebi and Siemens, 2017; Börgesson et al. 1994; Dixon et al. 2018; Graham et al. 1997; Kim et al. 2012; Lee et al. 2016; Madsen 1998; Man et al. 2011; Ould-Lahoucine et al. 2002; Radhakrisha et al. 1989; Suzuki et al. 1992; Tang et al. 2008a,b). Baumgartner (2006) estimated the thermal conductivity and specific heat capacity of bentonite materials based on their composition and density and this provided a useful means of estimating TC for use in modelling thermal evolution of the DGR. Description of the thermal behaviour of bentonite materials is ideally provided as a series of sinusoidal curves for thermal conductivity as a function of degree of saturation for a given density as shown by Baumgartner et al. (2006). The information provided in the many thermal properties studies indicate general trends for thermal conductivity, but a considerable scatter exists in the data. Scatter would seem to be attributable to differences in mineralogy (Tang et al. 2008), texture and the method used to prepare the materials for testing. The test method used to obtain thermal properties may also result in differences in the measured values (although in theory this should not be the case).

5.2.2.2 Statistical Evaluation of Thermal Properties Data

The thermal properties data presented in Section 5.2.2.3 and Section 5.2.2.4 and whose best-fit equations are provided in Tables 5-2 and 5-3, were statistically analysed in order to determine their regression equations, correlation coefficient (R^2), confidence and prediction bands. The results of these analyses are provided summarized in Table 5-2 and provided in Appendix C.

A MS-Excel based program was created by Priyanto (2012) was used to perform statistical analyses to determine 95% confidence and prediction bands for the best-fit lines. This program was based on the equations described in Kleinbaum & Kupper (1978) and the assumptions that the variation of the parameter of interest follows normal Gaussian distribution at each value of dry density. The excel formulations have been modified to evaluate the effects of dry density on

parameters of current interest. The definitions of confidence and prediction bands, confidence intervals are taken from those provided at (http://en.wikipedia.org/) and as they were applied by Priyanto (2012) and to this study are summarized below.

- "The **confidence interval** is an interval estimate of a population parameter and used to indicate the reliability of an estimate. It is an observed interval and calculated from the observations (data). Confidence intervals indicate how well the mean (i.e., best-fit point) is determined for a given data set. For example, assuming the 95% degree of confidence, repeating the calculation of the confidence interval of the mean from each data point, one would expect about 95 % of those intervals to include the true value of the population mean. The confidence interval indicates the likely location of the true population parameter."
- **"Confidence bands** are used in statistical analysis to represent the uncertainty in an estimate of a curve or function based on limited or noisy data. Confidence bands are often used as part of the graphical presentation of results in a statistical analysis. Confidence bands are closely related to confidence intervals, which represent the uncertainty in an estimate of a single numerical value."
- **"A prediction interval** is an estimate of an interval in which future observations will fall, with a certain probability, given what has already been observed. It indicates where the next data point would be. The prediction interval shows the distribution of values, not the uncertainty in determining the population mean. A larger population size normally will lead to a better estimate of the population parameter. Prediction intervals must account for both the uncertainty in knowing the value of the population mean, plus data scatter. So, a prediction interval is always wider than a confidence interval. "
- **"Prediction bands** are related to prediction intervals in the same way that confidence bands are related to confidence intervals. Prediction bands commonly arise in regression analysis. The goal of a prediction band is to cover with a prescribed probability the values of one or more future observations from the same population from which a given data set was sampled. Just as prediction intervals are wider than confidence intervals, prediction bands will be wider than confidence bands." (Priyanto 2012).

5.2.2.3 Thermal Conductivity of Bentonite

In order to minimize the effects of method and material differences in determining the thermal conductivity of GFM and HCB of interest to NWMO, data was collected for well documented source materials (MX-80 and National Standard Bentonite). These data are provided by Borgesson et al. (1994); Knutsson (1983); Man and Martino (2009), Man et al. (2011), Kim et al. (2012), Dixon et al. (2018) and Abootalebi (2016); Abootalebi and Siemens, (2017) and Tang et al. (2008a,b). The studies by Man et al. (2011), Man and Martino (2009), Kim et al. (2012), Dixon et al. (2018); Abootalebi (2016) were done using the same measuring device and similar methodology but by different laboratories (thereby providing an indication of the reproducibility of the results).

The densities of particular interest to NWMO are 1410 kg/m^3 (Gap fill); 1700 kg/m^3 (HCB blocks) and 1600 kg/m^3 (anticipated density at full homogenization of GFM and HCB). For the purposes of completeness, a wider range of densities (1300 – 1800 kg/m^3) was examined. This provides a set of regression equations that leaves room for subsequent modification of the reference densities of the bentonite materials used in the NWMO repository concept.

Figure 5-4a presents the thermal conductivity data for materials of interest for GFM, identifying both the dry density and the type of bentonite used to produce the test specimens. Figure 5-4b combines these data based solely on dry density so as to allow statistical analysis and determination of data variability. The data clearly shows the increase in TC with increasing degree of water saturation and also the effect of increase in density from 1400 kg/m^3 to 1500 kg/m^3 but little difference between behaviour at 1300 kg/m^3 and 1400 kg/m^3.

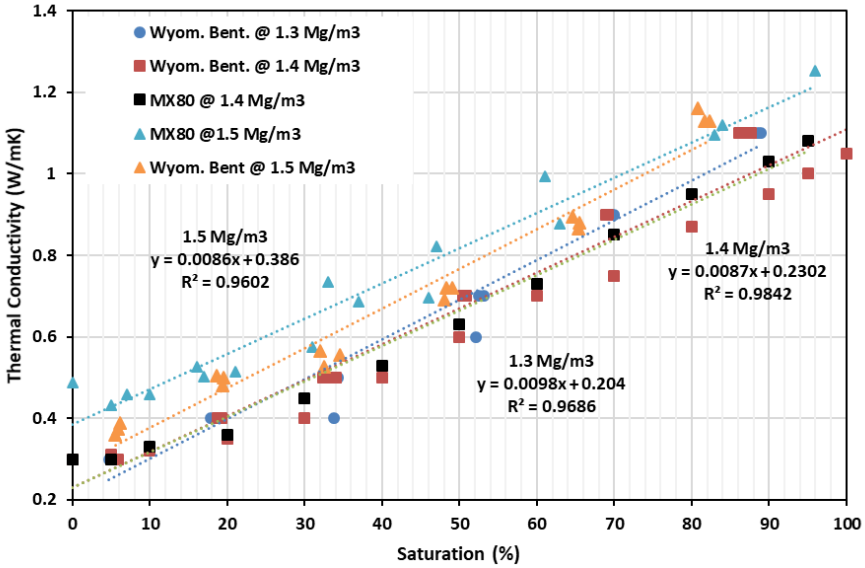

(a) Data showing effects of source material and texture

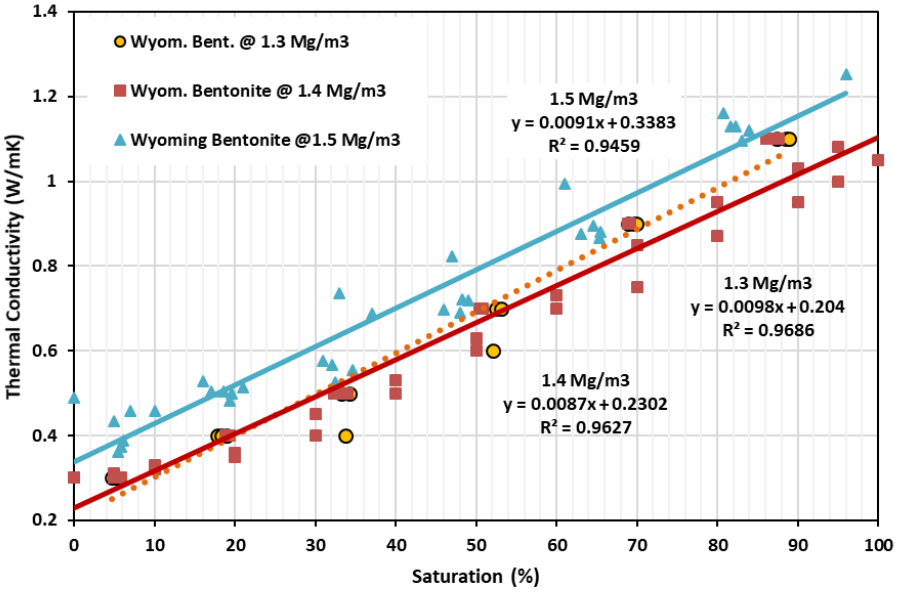

(b) Data showing effects of dry density on thermal conductivity

Figure 5-4: Thermal Properties of Bentonite: Effect of Material Source, Texture and Density on Thermal Conductivity at < 1500 kg/m^3 Dry Density

The apparent effect of material texture at low (<70%) water saturation is seen in Figure 5-4a. Thermal data for compacted materials of 1400 and 1500 kg/m^3 dry density that were produced using fine-grained (~200 mesh) source materials (identified as Wyoming Bent or HCB), and the coarser grained MX80 (80 mesh) are presented. The data shows a slightly lower thermally conductivity in materials produced from finer-textured bentonite than materials produced from coarser MX80 materials. However, the difference is relatively small and the data overlaps.

The coarser GFM granules proposed for use by NWMO tends to produce a less uniform soil matrix, and hence a potentially heterogeneous initial as-built distribution of voids within it, particularly in the small specimens used in laboratory testing. The result would be an initially poorer thermal conduction performance. This effect would be expected to be less pronounced over a larger scale where local variations are less of an influence on overall system behaviour and as the material increased in saturation.

The statistical fit to the data is provided in Table 5-2, with confidence and prediction limits also calculated. The data fit equations in Figure 5-4 and Table 5-2 are provided as linear best-fit equations as these are the simplest mathematically and more complex regressions do not provide substantively better regression coefficients (as can be seen in the test data provided in Appendix C).

It is anticipated that the HCB material making up the buffer box, spacer blocks and floor tiles in the placement room will be of the same composition and initial dry density (1700 kg/m^3). Achieving this manufactured HCB density is well demonstrated (see Section 3-1). With hydration of the HCB and subsequent compression of the GFM component, the average dry density of the bentonite in the placement room is expected to be no less than 1600 kg/m^3. In order to assess the changes in the TC of the bentonite-filled volume, a compilation of data obtained using the same measuring device and similar testing methodologies is provided in Figure 5-5. All the data follow the same general trend of increasing TC with increasing degree of saturation and all data was collected using the hot-disk thermal properties analysis (HD-TPA) device (Figure 5-6), excepting that of Knutsson (1983) who tested materials of higher density than reported elsewhere (1860 - 1930 kg/m^3) and used a thermal probe device. The thermal conductivity of the data from Knutsson (1983) falls within the scatter of values obtained for materials having dry density of 1700 to 1800 kg/m^3.

The data presented in Figure 5-5 for HCB shows the same type of increasing TC with density and saturation as was observed for the lower density materials, but HCB has a higher TC for a given degree of water saturation. As can be seen in Figure 5-5, for the data collected using the TPS measuring device, the uncertainty in the TC value generated from the best-fit equations over the entire range of saturation is likely no more than about 0.12 to 0.17 W/mK. The data also indicates that there is little improvement in the TC of the bentonite materials for a given degree of water saturation when dry density increases beyond approximately 1700 kg/m^3 and degree of saturation exceeds approximately 60%. The fitting of regression lines to the data shown in Figure 5-5 showed little discernible difference in R^2 if linear or polynomial fits were used and so for the purposes of mathematical simplicity the linear best-fits are provided. Table 6.2 provides the regression equations and correlation coefficients for the TC as a function of degree of specimen saturation with freshwater. The data, and subsequently-determined confidence and predictive limits are provided in Appendix C. The consistency of the data associated with MX80 and other high-quality Wyoming bentonites shown in Figure 5-5a allows for the data sets to be combined to produce a generic TC versus freshwater saturation plot (Figure 5-5b) and regression equations.

Summary of TC Behaviour

As noted in Section 3-1, the as-placed densities assumed in the current reference GFM and as-built HCB materials are readily achieved using currently available technologies and could be improved to a limited degree. The data provided in Figure 5-4 and Figure 5-5 indicates that an increase in average dry density of the placement room fill will result in an increase in its TC, but this improvement would not be substantial. The increase in TC for the GFM at a dry density of 1410 kg/m^3 would only be in the order of 0.075 W/mK per 100 kg/m^3 increase in dry density. A

smaller improvement of the TC of the HCB could be expected for an increase from 1600 to 1700 kg/m^3 average density of the system, less than approximately 0.05 W/mK per 100 kg dry density increase. The data also indicates that there is little discernible improvement in the TC of HCB when dry density exceeds approximately 1800 kg/m^3.

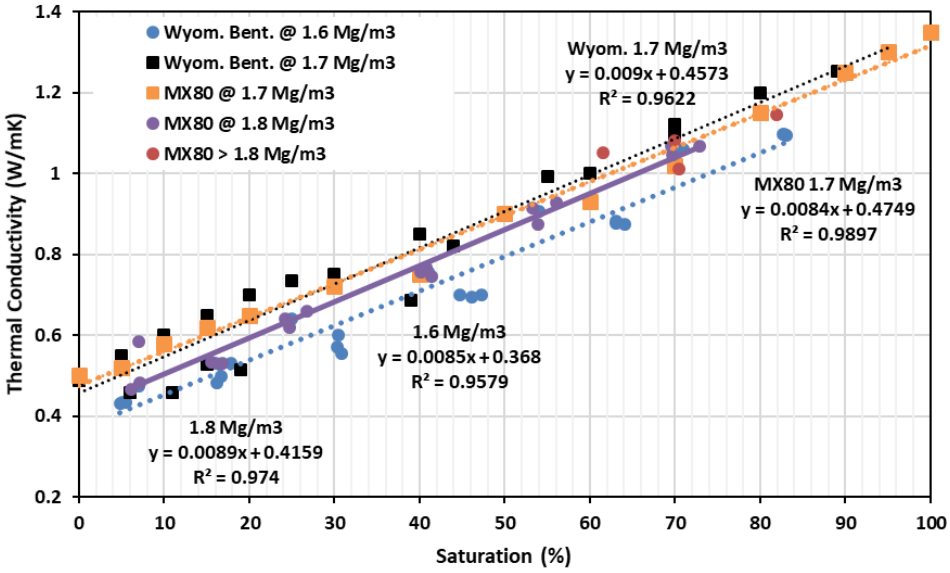

(a) Data showing effects of source material and texture

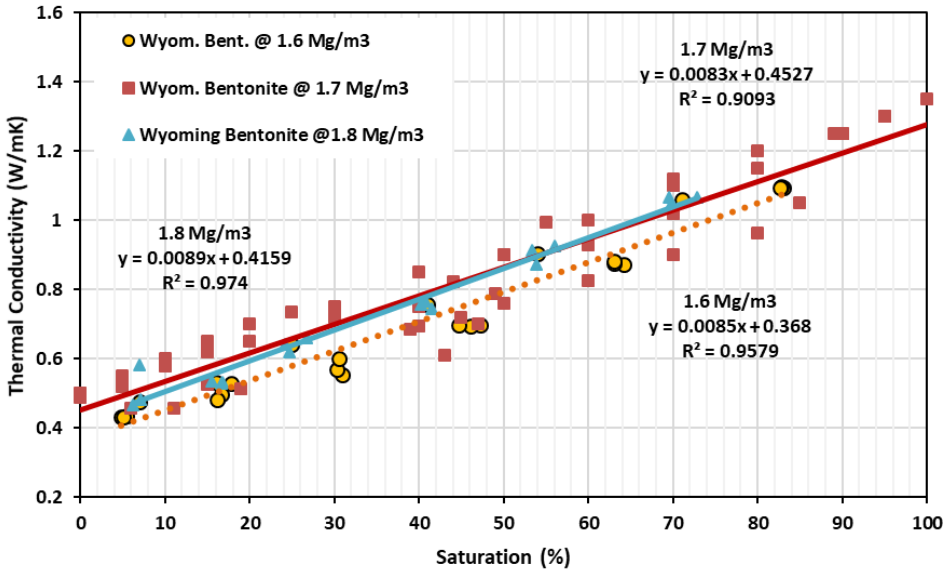

(b) Data showing effects of dry density on thermal conductivity

Figure 5-5: Thermal Properties of HCB: Effect of Material Source, Texture and Density on Thermal Conductivity at >1600 kg/m^3 Dry Density

Table 5-2. Best-Fit Equations, Correlation Coefficients and Prediction Bands for Thermal Properties of MX80 Wyoming Bentonite

Dry Density (kg/m^3)	Equation	Prediction Band^{++} (±)	R^2
1300*	TC = 0.0098S + 0.204 SH = No data found TD = No data found	0.14	0.969
1400$^+$ (as-placed GFM)	TC = 0.0087S + 0.230 SH = 0.0246S + 0.998 TD = No data found	0.13 0.40	0.963 0.966
1500**	TC = 0.0084S + 0.400 SH = 0.01445S + 1.534 TD = 0.0015S + 0.221	0.17 1.05 0.17	0.937 0.480 0.282
1600** (equilibrated placement room fill)	TC = 0.0085S + 0.368 SH = 0.0090S + 1.092 TD = No data	0.12 0.47	0.958 0.573
1700* (as-placed HCB)	TC = 0.0084S + 0.475 SH = 0.0130S + 1.822 TD = 0.0016S + 0.295	0.17 0.72 0.11	0.990 0.640 0.554
1800*	TC = 0.0089S + 0.4159		0.974

* Compiled literature data Borgesson et al. (1994); Knutsson (1983); Man and Martino (2009), Kim et al. (2012); Abootalebi (2016); Abootalebi and Siemens (2017) and Tang et al. (2008a,b).
** Data from Dixon et al. (2018), Kim et al. (2012) and Man and Martino (2009)
$^+$ Abootalebi and Siemens et al. (2017)
$^{++}$ Band ± in which 95% of data can be found for a specific degree of saturation
TC is in W/m^{o}K; S is % saturation; SH is specific heat in MJ/m^{3}K; TD is thermal diffusivity in mm^2/s.

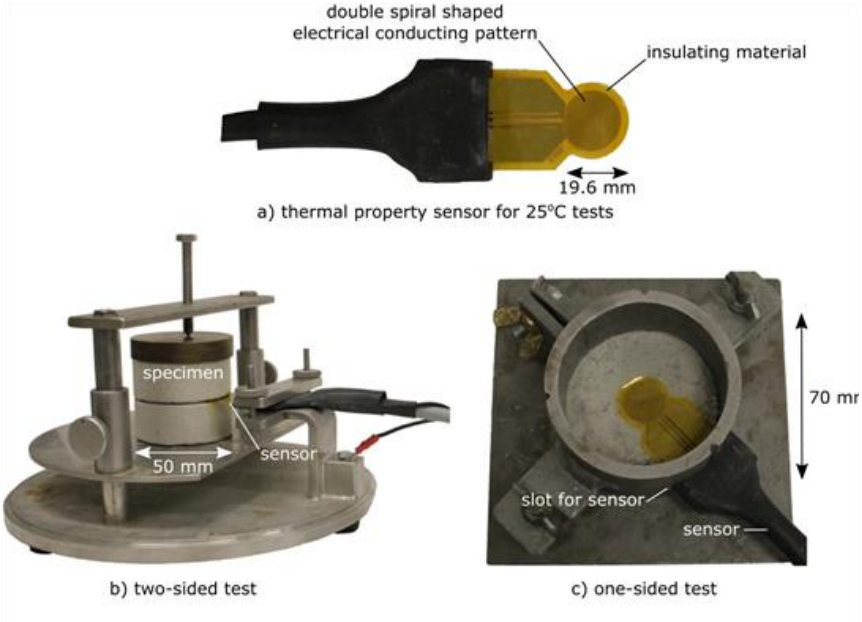

Figure 5-6: Thermal Properties Analyzer (TPS) Used in NWMO Studies
(Abootalebi 2016; Abootalebi and Siemens 2017)

5.2.2.4 Thermal Diffusivity, Specific Heat Parameters

The thermal diffusivity and specific heat capacity parameters are linked as shown in Equation 5-1. These parameters are less often reported in the literature but a recent study by NWMO examined MX80 materials prepared with freshwater to densities of 1500 and 1700 kg/m^3 (Dixon et al. 2018). Figure 5-7 presents the data associated with these tests as well that that from Man and Martino (2009) who examined a Wyoming bentonite of similar composition but finer texture (200-mesh) than MX80 (80-mesh) and also show the 95% confidence and predictive limits. The data associated with these tests are provided in Appendix C and the statistical best fits and coefficients of correlation are provided in Table 5-2.

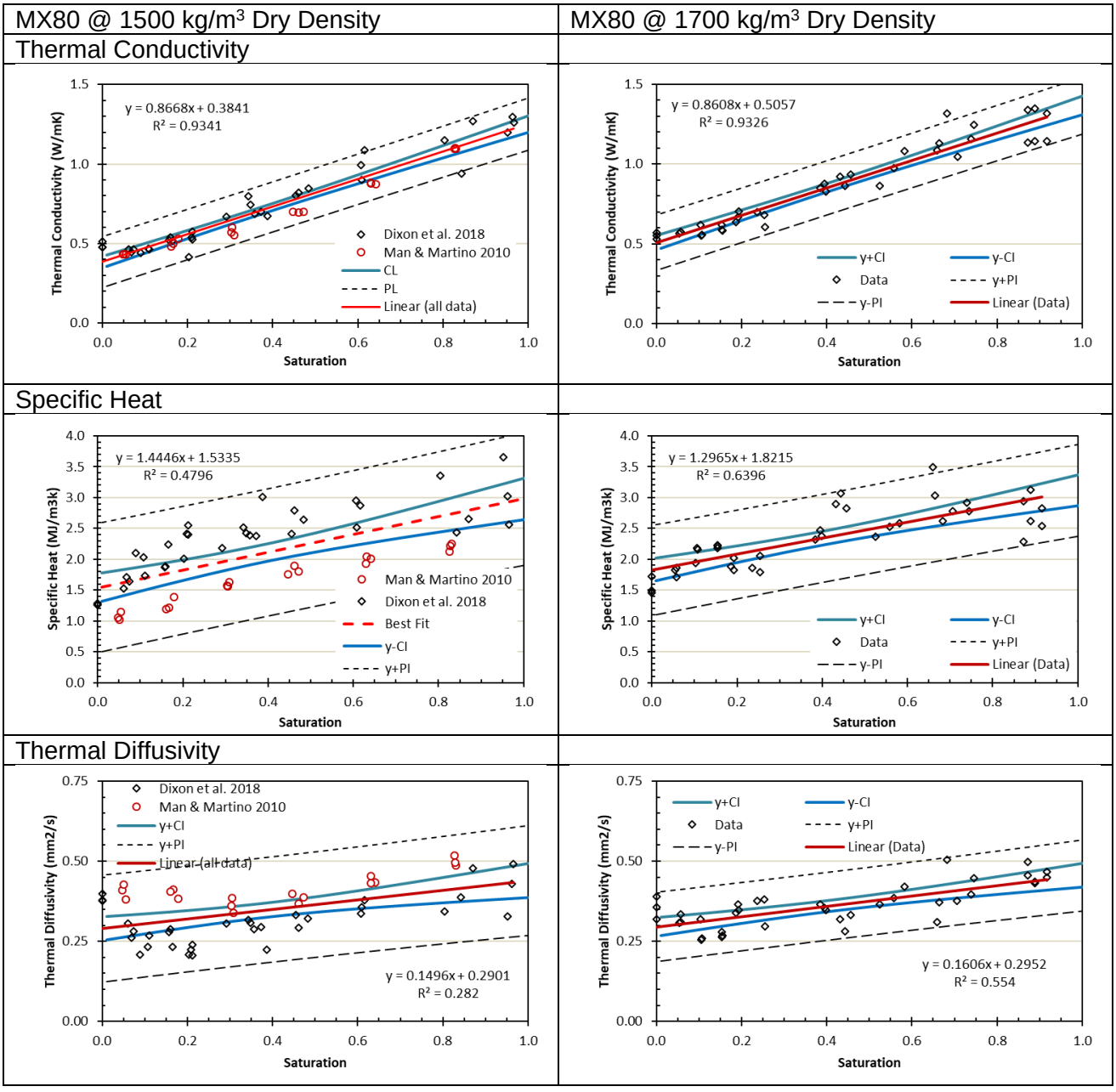

Figure 5-7. Thermal Diffusivity and Specific Heat Parameters for HCB at 1500 and 1700 kg/m^3 Dry Density.

The data presented in Figure 5-7 show that the high-quality Wyoming bentonites examined (MX80 and 200 mesh) show a very consistent pattern of increasing TC with increasing degree of water saturation and modest increase in TC with increased dry density as well as a slightly lower TC for finer grained source material. In terms of the parameters of specific heat (MJ/m^3k) and thermal diffusivity (mm^2/s) the data shows the following:

- Specific heat shows a trend of increasing values with increased degree of saturation but also an apparent influence of the original granularity of the bentonite with finer-grained source material exhibiting a lower specific heat.
- Specific heat values show considerable scatter and as a result broad predictive bands are present.
- Thermal diffusivity shows a very weak trend of increasing value with increasing degree of saturation and a great degree of scatter in the available data.
- Thermal diffusivity shows no discernible change with density for a given water saturation.

5.2.3 Influence of Ambient Temperature on Thermal Properties

Each repository program considering the use of GFM is examining materials of differing granularity and installed density. The potential for change in the TC of the GFM or HCB as the result of thermal conditions within the DGR needs to be known in order to ensure that thermal evolution of the DGR can be accurately estimated and predicted. For NWMO's Mark II DGR concept it is anticipated that the temperature within the bentonite-filled region will be <80°C. Figure 5-8 presents the data available regarding NWMO's GFM, together with some additional data generated for GFM in other DGR programs. The majority of thermal testing on bentonite materials has been done under room temperature conditions (~25°C). In a repository environment this may be close to the conditions present at the time of placement room filling, but it will not persist for long as the heat generated by the UFCs will result in a rise in the far-field temperature conditions. Over the relatively short-term it is expected that the temperature at the surface of the UFC will approach 100°C and that much of the bentonite-filled volume adjacent to the UFCs will experience temperatures in the order of 80°C.

There have only been a few studies that systematically examined the effects of ambient temperature on thermal properties. Pusch (2002) indicated that the effect of temperature on the TC of buffer (HCB) will be small. A more recent study of the effect of temperature on TC has been completed by Abootalebi (2016) on the bentonite materials (Wyoming-type and MX-80) of interest to NWMO. The results of these measurements are provided in Figure 5-8 and include both GFM and HCB materials. In the HCB materials generated using MX-80 there was only a small change in TC as the result of ambient temperature conditions, while for HCB fabricated from finer textured bentonite there was no discernible change in TC. The apparent difference in TC of MX80 HCB at 25 and 80°C can be attributed to the coarser texture of MX-80 source material. This results in a slightly less uniform microstructure and a higher number of larger pores, resulting in greater influence of thermal conditions on heat conduction.

The GFM data shows a small (~0.1 to 0.2 W/m°C) increase in thermal conductivity with increase in ambient temperature from 25 to 80°C for materials having a degree of saturation greater than 20%, produced using either MX-80 or a finer-grained Wyoming bentonite. There is limited increase in TC for degree of saturation 0% to 20%, which is consistent with the Boltzmann sigmoidal curve predicted by Baumgartner (2006). At this low saturation level, the limited water present is tightly bonded to the mineral surfaces and so the system acts primarily as a "solid" mineral assembly, hence there would be little expectation of changing TC with ambient temperature. Once there is a notable moisture content (>20% saturation), there is easier movement of the fluid phase within the GFM, and hence better heat transport capacity and

increasing the apparent thermal conductivity with higher ambient temperatures (Beziat et al. 1988; Abootalebi 2016)). In a relatively loose system like the GFM there is a notable macro-pore component and so there will be a higher air void fraction and water void fraction compared to HCB and this may be the source of the apparent increase in TC with increase in temperature. It should also be noted that the TC of the GFM produced from MX-80 or 200 mesh bentonites is essentially identical.

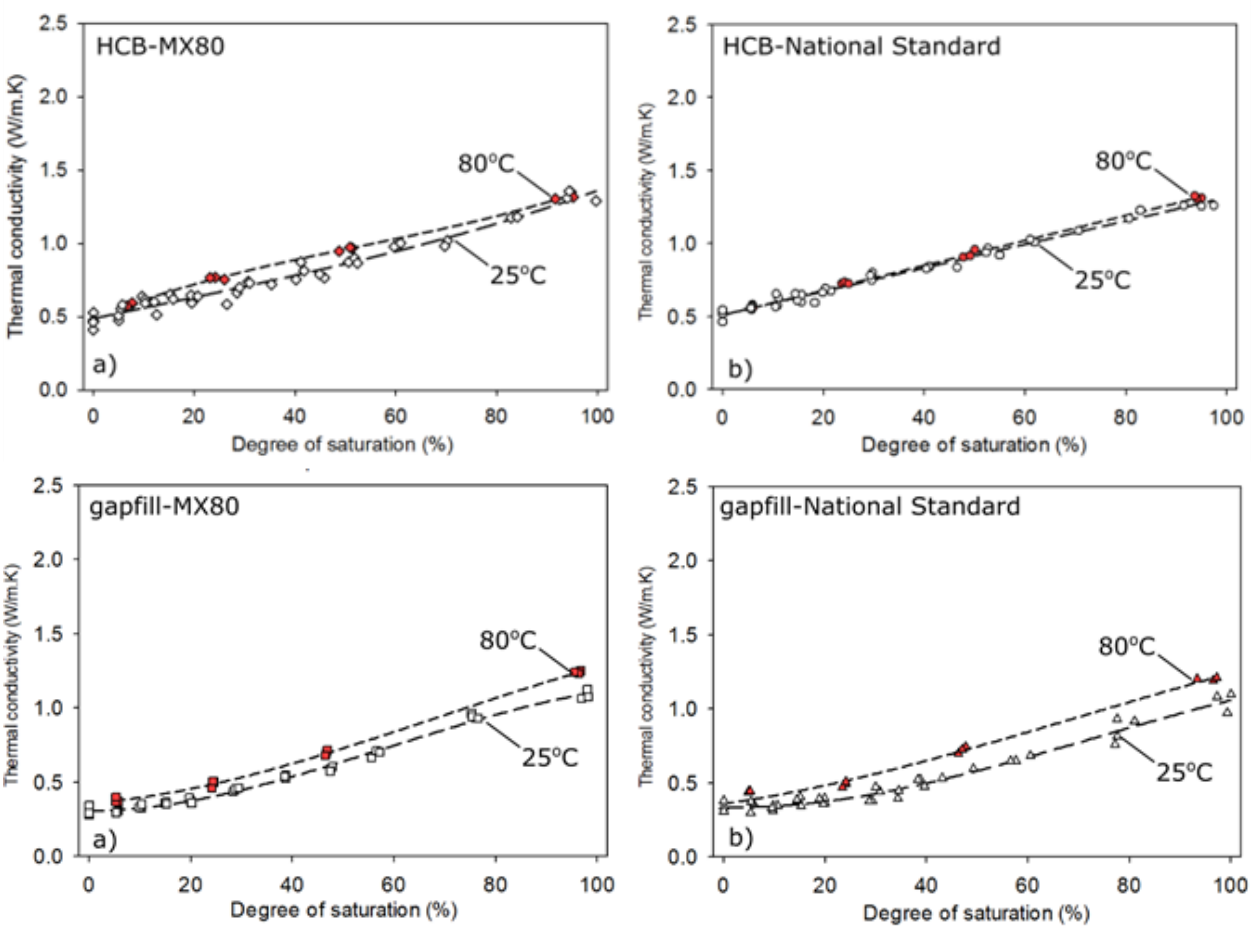

Figure 5-8: Influence of Ambient Temperature on TC of Bentonite (Abootalebi 2016)

5.2.4 Influence of Pore Water Composition on Thermal Properties

The evolution of the placement room fill will involve the eventual influx of groundwater from the surrounding geosphere. The rate of influx will be highly site specific and so the HCB/GFM system may experience a period of unsaturation and relatively fresh pore fluid conditions. In this phase the TC conditions described in Section 5.2.3 will persist. Over the longer-term water will enter the placement room and be taken up by the bentonite, ultimately resulting in bentonite saturation. With water uptake the thermal conductivity will increase, however there is an as-yet undetermined role that pore fluid salinity will have in the thermal behavior of the bentonite system. The thermal conductivity of pure water is commonly referenced to be approximately 0.6 W/(mK) at 20°C and increases to approximately 0.67 W/(mK) at 100°C. In a saline system (NaCl) the TC decreases with increasing TDS, and at ~236 g/L concentration is approximately 0.557 at 20°C and 0.643 at 80°C. This represents an approximate reduction in TC of 7% at 20°C and 4% at 80°C in a fully-saturated system, based on data from Ozbek et al. (1977). As there is no readily available information on thermal properties of HCB or GFM under saline

groundwater conditions, these values provide only some general guidance regarding a saturated placement room fill having a high TDS content.

An additional and reverse influence consideration regarding the influence of pore water composition on thermal behavior is the influence of cations in solution on the water associated with the clay particles. With increasing TDS in the pore fluid, the amount of readily mobile porewater increases and hence an increase in TC might be expected as the system evolves. If extremely accurate values regarding TC in brine are needed there is a need to develop a set of materials properties parameters related to the thermal properties of the GFM and HCB under the range of groundwater compositions of concern in a DGR.

5.2.5 Role of Secondary Processes (e.g. cementation, bacteria)

Beyond the intrinsic thermal properties of the bentonite materials, there can be changes in the thermal properties as the result of processes going on in and around the bentonite. The process of greatest potential influence to thermal behavior is the precipitation (or dissolution) of minerals within the buffer and gap fill. As solid minerals have higher thermal conduction properties than air, gas or liquid the replacement of those components by precipitated minerals, or conversely the loss of minerals through dissolution will result in an increase or decrease in the thermal conductivity respectively. There is no literature information available that clearly demonstrates the influence (or lack of influence) of cementation on the thermal properties of HCB or GFM.

The other potential effect on the thermal characteristics of the HCB and GFM is related to the development of biofilms or extensive quantities of organic material within or surrounding the buffer. The presence of substantial organic material in the clay could in theory result in a degree of thermal insulation, but the total and organic carbon component of MX-80 bentonite is in the order of 0.72% and 0.11% respectively (Marshall and Simpson 2014), making it very unlikely that it could discernibly alter the thermal behaviour. The HCB-GFM system is also designed so as to minimize/preclude the activity micro-organisms by maintaining a sufficiently high dry density, thereby limiting any potential influence of this on system TC. The nature of biological materials in the HCB and GFM are presented in papers by Stroes-Gascoyne et al. (2005; 2006; 2007a, b; 2010a, b); and Pederson et al. (2000).

5.2.6 Summary of Thermal Properties

Sections 5.2.2 through 5.2.4 have provided a basic outline of the thermal characteristics of HCB and GFM of the types considered for use by NWMO. The currently established thermal properties of MX-80 GFM and HCB materials have been estimated and predictive equations were provided in Table 5-2. The greatest effects on thermal properties of the GFM and HCB have been confirmed to be density and degree of water saturation. It would also appear that increasing the dry density of the HCB beyond approximately 1700 kg/m^3 does not result in any substantive increase in its TC for a given degree of water saturation. Other factors such as groundwater salinity are anticipated to have only a secondary influence, possibly with materials having high salinity exhibiting slightly lower TC, but this has not yet been established through TC testing. There is no demonstrated influence of bacterial activity on thermal behavior of the GFM or HCB.

Statistical treatment of available data shows that there is a notable degree of data scatter in the literature, this results in a range in the prediction interval for thermal properties that needs to be considered when using these parameters in predictive or performance modelling.

5.3 WATER ACTIVITY AND SUCTION-MOISTURE PROPERTIES

5.3.1 General

The movement of water into or out of a bentonite barrier, particularly during the pre-saturation period is largely controlled by the suction-moisture behaviour of the bentonite. This is dominated by the interaction between water (liquid or vapour) and the mineral surfaces as the montmorillonite tries to balance or reduce the strong surface charges, by taking on water from the surrounding atmosphere in order to increase the spacing between particles (swelling). The result is a high suction potential associated with clay particles and a tendency to draw moisture in from its surroundings. If the clay can physically expand, water uptake will occur due to the osmotic gradient present between adjacent particles and with expansion and increasing water saturation the suction will reduce.

Water activity (a_w) is defined as the ratio of vapor pressures of the solution and a solvent.

$$a_w = P / P_o \qquad \textbf{5-2}$$

Where P is vapor pressure in solution and Po is the vapor pressure in the solvent.

In bentonite systems, a_w is primarily associated with the degree to which the water from the surrounding environment is drawn to the highly charged mineral surfaces where it becomes strongly held. The clay surfaces generate a high suction effect on their surroundings, particularly when the system is unsaturated. The result of this in unsaturated conditions is the reduction of the relative humidity (rH) in the air phase. This is accompanied with the suction generated by water tension in the larger pore spaces. As a result, bentonite will tend to reduce the vapour pressure of the air associated with it, generating a system where water is pulled towards the bentonite surfaces. This suction will reduce in magnitude as the bentonite hydrates and once sufficient hydration occurs (and if physical conditions allow), the bentonite will expand provided water supply continues.

The suction – moisture relationship for bentonite is therefore directly related to water activity as the suction generated by the montmorillonite particles will reduce the rH of the atmosphere immediately surrounding the clay. This generates a lower ratio between the vapour pressure in solution (or soil and porefluid) and the solvent (e.g. fluid within an organism). The relationship between the repulsive forces between montmorillonite particles and its confinement under saturated conditions is the source of swelling pressure in bentonite. Similarly, in an environment where water is being driven off as the result of thermal conditions (drying), water adsorbed to the particle surfaces is lost but the force with which the remaining water is held increases. This can result in a tightening of the soil matrix and shrinkage of the bentonite as shown previously in Figure 5-3.

As noted by Bag (2011), the total suctions of bentonite-water mixture can be calculated from the measured water activity and temperature using the Kelvin's equation expressed as:

$$\textbf{Total suction, } \psi = (RT/M) \ln(a_w) \qquad \textbf{5-3}$$

where R is the universal gas constant (Jmol-1K-1), T is the laboratory temperature (^oK), a_w is the water activity and M is the molecular mass of water. The water content, temperature, water activity and suction results for MX-80 measured in freshwater by Bag (2011) are presented in Table 5-3. Based on these results, the a_w of bentonite remained below the required maximum value of 0.96 for the entire range of tests, excepting the wettest (0.967 @ 32.8 % water content). At that water content, the maximum dry density (at water saturation)

would correlate to 1446 kg/m^3, essentially the as-placed state of the GFM in NWMO's concept. Since salinity will also act to depress the a_w value, it could be expected that a bacteria-unfriendly environment would be maintained.

Table 5-3: Chilled-Mirror Hygrometer Test Comparing Suction and a_w (Bag 2011).

Final Water content (%)	Temperature (°C)	Water activity	Suction (MPa)
(1)	(2)	(3)	(4)
11.0	20.8	0.783	98.83
12.8	20.8	0.557	79.23
15.5	20.8	0.650	58.32
17.4	20.8	0.723	43.91
20.0	20.7	0.826	25.87
22.6	20.7	0.891	15.62
25.3	20.8	0.927	10.26
28.1	20.7	0.944	7.80
32.8	20.8	0.967	4.54

5.3.2 Water Activity (a_w): Impact on Bacteria Viability

Of concern over the longer-term in a DGR is the potential for microbial activity to create an environment that is detrimental to the UFCs. The microbial risk to the UFC is primarily associated with microbially (bacterially)-induced corrosion (MIC) of carbon-steel (but also to a lesser-extent copper). This process has been investigated by numerous investigators including Stroes-Gascoyne et al. (2005; 2006); Johnson and King (2002); Motamedi (1999); Pedersen et al. 2000 and Bengtsson et al. (2015). In order to avoid potential issues related to MIC, achieving and maintaining a high density in the bentonite-filled volume is necessary. At high density the fluid saturated bentonite has very small pore spaces, making bacteria movement or activity difficult, but more importantly the water activity (a_w) is low enough to preclude (or severely limit bacterial activity (although bacteria might persist in a non-active (spore) state).

As bacteria of concern in the DGR can generally not tolerate a_w of less than 0.96 the combination of solution salinity, suction associated with the clay particle surfaces and soil matrix will have a very substantial effect on bacteria viability. There is a relatively narrow range of water activity (a measure of vapour pressure difference from that of the environment, maintained by the organism), where bacteria can persist as active, growing organisms, generally set as a_w > ~0.96 (Stroes-Gascoyne et al. 2006). When a_w decreases below this level the cell membranes are not able to maintain hydration within the cell and the bacteria either dies as the result of desiccation or if possible, will move into an inactive "spore" phase until environmental conditions again become favorable for metabolic processes to re-activate. These spores are typically much smaller in size than the active organism and so can persist in smaller pore spaces.

The simplest means to controlling bacteria activity is through maintaining a sufficiently elevated temperature and a dry (unsaturated) environment where the combination of high clay suction associated with dry clay and temperature is sufficient to result in no growth by the bacteria. Reliance on container heating to dry the sealing materials as an ongoing control over bacteria activity in the long term is however not a viable approach. It was observed by Stroes-Gascoyne and Hamon (2010) that bacteria survived in the Alternative Buffer Material (ABM) experiment conducted by SKB where temperatures reached 95^{o}C to 135^{o}C, although most likely as spore-forming organisms. They noted that at such temperatures little survival of vegetative cells is expected and spore-form does not pose a direct danger to the longevity of containers in a future repository because spores by their nature are not active. A concern expressed that the presence of a significant population of such spore-formers represents a potential for future increased bacteria activity, if and when conditions become more favourable. With improved environmental conditions (more moderate temperatures, reduced density and supply of low salinity water), spores could become vegetative cells, with an active metabolism that could produce corrosion-inducing metabolic by-products, such as organics acids, or in the case of Sulfate Reducing Bacteria (SRB), sulphides (Stroes-Gascoyne and Hamon 2010). This is consistent with the results provided by Stroes-Gascoyne et al. (2006) where it was concluded that in order to keep culturable (not necessarily active), bacteria at or below the background levels in the as-sourced bentonite, for a 100% bentonite system, one or more of the following criteria need to be achieved:

- An a_w value less than or equal to 0.96 This would result from an in situ dry density of at least 1600 kg/m^3 (EMDD≈1400 kg/m^3); or
- A swelling pressure value of >2000 kPa is present; or
- Porewater salinity in excess of 60 g/L.

Consistently present in the patterns observed by Stroes-Gascoyne (2005), Motamedi (1999) Pedersen et al. 2000 and Bengtsson et al. (2015) was a rapid decline in the quantity of viable bacteria as density increases in repository-relevant MX-80 materials. The anticipated supply of high-pressure groundwater from the surrounding rock mass (crystalline environment) or more gradual uptake of water by the bentonite (sedimentary environment) all lead to an expectation that the system will achieve saturation, possibly over the relatively short term. The temperature at the surface and in the vicinity of the UFC's surface will also be decreasing with time within a relatively short time of repository closure (maximum temperature is 92^{o}C at UFC surface at 47 years following placement (Guo 2018)). As a result, maintaining bacterially-hostile conditions will require maintaining sufficiently high bentonite density, particularly under groundwater conditions where TDS is lower than ~60 g/L.

Stroes-Gascoyne (2010b), Stroes-Gascoyne et al. (2005; 2006; 2007a,b; 2010b) and Pedersen et al. (2000) all indicate that if the a_w can be maintained at less than approximately 0.96, bacteria should be inactive. Such low a_w environments can be achieved by using water-saturated, bentonite-based materials with high dry density or where there is a high salinity. For applicability to bentonites of differing montmorillonite contents, the a_w can also be related to effective montmorillonite dry densities (EMDD) (Dixon et al. 2005; Stroes-Gascoyne et al. 2005). EMDD is a measure of the density of the montmorillonite component once the mass and volume occupied by non-montmorillonite solids are excluded. The non-montmorillonite components are treated as inert filler materials that have no influence on the H-M behaviour of the compacted bentonite. EMDD was developed to allow for normalization of the behaviour observed for bentonites of differing montmorillonite content.

EMDD is defined as follows:

$$\mathbf{EMDD = M_m / (V_m + V_v) = (M_T - M_{nm}) / (V_T - V_{nm})} \qquad \mathbf{5\text{-}4}$$

where M_m = dry mass of montmorillonite clay; M_{nm} = mass of non-montmorillonite mineral component; M_T= total dry mass of specimen; V_m = volume of the montmorillonite; V_{nm} = volume of non-montmorillonite mineral solids; V_T = total volume; and V_v = volume of voids.
As described by Stroes-Gascoyne et al. (2005 ; 2006 ; 2007a.b ; 2010b)), water activity a_w is affected by pore water salinity as follows: (1) increasing salinity results in decreased swelling pressure of the montmorillonite and (2) increasing salinity of the pore fluid reduces the value of a_w as presented by Robinson and Stokes (1959) as shown in Figure 5-9. Figure 5-10 shows the relationship between a_w, EMDD and dry density of MX-80 bentonite where montmorillonite content is assumed to be 80%. For systems having a montmorillonite content greater than 80% the dry density value will shift to the left for a given EMDD. Figure 5-10 shows that for a groundwater TDS of approximately 70-80 g/L the environment will be unable to support meaningful bacteria activity, regardless of the effects of the bentonite component.

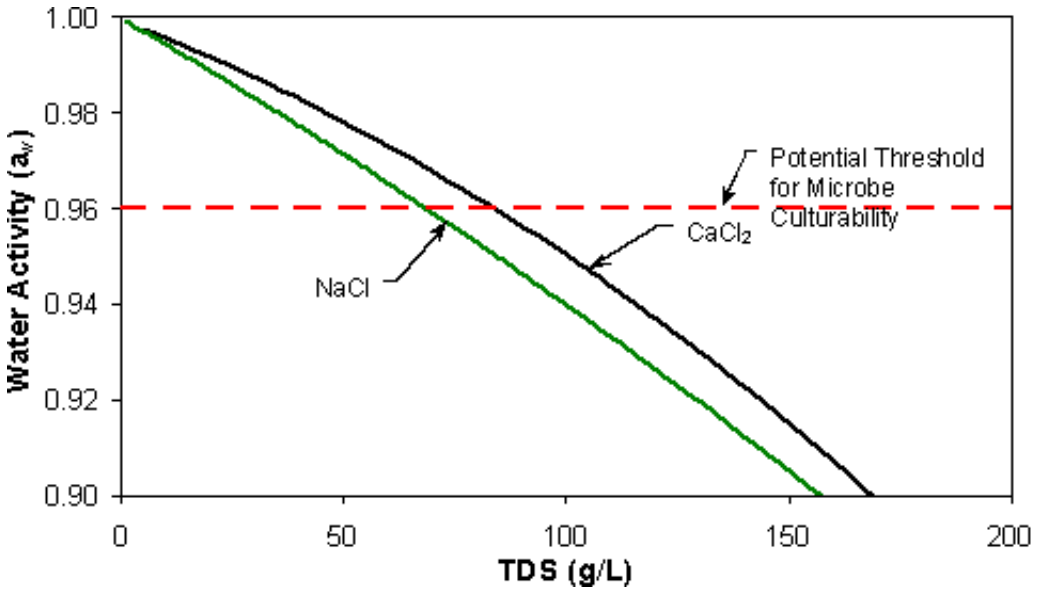

Figure 5-9: Relationship Between Water Activity and TDS Concentration
(Dixon et al. 2005)

Combining the swelling pressure (osmotic suction forces that draw water into the clay interstices and result in swelling pressure development) and solution concentration effects on a_w, results in the relationship shown in Figure 5-10 (Dixon et al. 2005; Stroes-Gascoyne et al. 2006). Density in Figure 5-10 is shown in terms of both dry density and EMDD (for MX-80 having 80% montmorillonite content). This means that a way of dealing with bacteria activity over the longer term (saturated environment) can be developed through density control of the placement room bentonite. From these plots it was estimated that at an EMDD greater than 1350 kg/m^3 (MX-80 dry density of approximately 1500 kg/m^3) and in a freshwater environment, bacteria would be inactive. The actual density at which this condition occurs will be influenced by factors such as montmorillonite content (which affects a_w), and perhaps the pore-size conditions in a particular material. It is also likely that the bentonite-filled volume will be non-homogeneous, with regions of slightly higher- and lower-than-average density persisting over the longer-term. This could give rise in conditions where bacterial activity is not entirely supressed at an “average” dry density of 1500 kg/m^3. Given that the groundwater conditions in a DGR will certainly be saline to

some degree, in order to achieve an a_w of less than 0.96, the dry density of the MX-80 will need to be closer to 1600 kg/m^3 in an environment having groundwater salinity of less than ~70 g/L TDS as discussed in Stroes-Gascoyne et al. (2007b) and Dixon et al. (2005). It should be noted that environments with TDS > 70 g/L can have dry densities less than this 1600 kg/m^3 value while maintaining bacterially-hostile conditions.

Studies using MX-80 bentonite by Stroes-Gascoyne and Hamon (2008) and Stroes-Gascoyne et al. (2010a,b,c) reported generally similar results to those reported in Dixon et al. (2005) and Stroes-Gascoyne et al. (2007b), but:

- The 2008 study concluded that the threshold dry density and salinity that will result in bacteria culturability at or below that the source material could likely be lowered to 1400 kg/m^3 at salinity of greater than 50 g NaCl/L;
- The 2010 study concluded that in a low salinity environment a dry density of 1600 kg/m^3 and high swelling pressure is required to suppress bacteria growth. It was also concluded that in a high salinity (≥ 100 g/L TDS) environment dry density of > 1000 kg/m^3 was all that was needed to suppress microbial activity.

There are also recent data that indicate that the critical dry density required to suppress sulphate-reducing bacteria may be in the order of 1350-1400 kg/m^3 for MX80 bentonite Bengtsson et al. (2016). This is a much lower density than 1500-1600 kg/m^3 previously reported by Dixon et al. (2005); Stroes-Gascoyne et al. (2010b) and Bengtsson et al. (2015). The actual density at which SRB activity is severely surpressed needs further evaluation as part of establishing a density specification for the bentonite components

Consistent with the observations of Stroes-Gascoyne et al. (2007b), Bengtsson et al. (2015) noted a substantial decrease in the number of culturable bacteria when saturated density was increased from 1750 to 2000 kg/m^3 in a low salinity (<10 g/L TDS) groundwater. These saturated densities correspond to dry densities of approximately 1200 and 1580 kg/m^3 respectively, the higher density is comparable to the density threshold identified in Figure 5-11 as well as an a_w of 0.96. Figure 5-11 describes the “swelling pressure” effects on water activity as described in Dixon et al. (2005), the high swelling pressure present at EMDD greater than approximately 1400 kg/m^3 results in the compression of gaps, voids or pore spaces present in the as-placed system, the resulting pore spaces are very small and represent an environment that is hostile to bacterial activity since there is insufficient room for them to persist as viable, active organisms. It should also be noted that in Figure 5-10 and Figure 5-11 that the term “microbe” is actually referring to bacteria. Other organisms such as fungi were not included in these studies and have yet to be assessed with regards to their potential effects and viability in the repository environment.

The preceding summary of studies to determine the roles of density, salinity and other environmental factors on water activity and bacterial viability show that despite all the laboratory data and conceptual descriptions described above, the conditions required to ensure a low bacterial viability is not entirely clear. General patterns of bacteria response to their environment have been identified with increasing density and salinity clearly having an adverse effect but the thresholds where these lead to non-viability or non-culturable bacteria are not clearly established. This topic requires further evaluation in order to clearly establish the environmental conditions that will preclude significant bacteria activity.

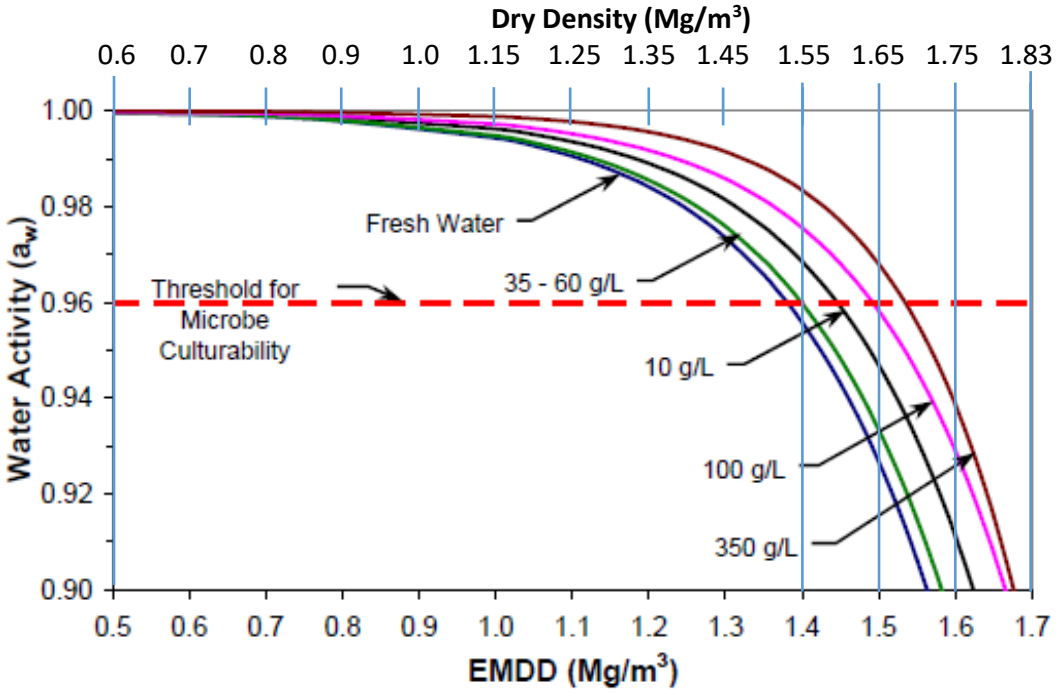

Figure 5-10: Relationship Between a_w and Density (after Dixon et al. 2005)

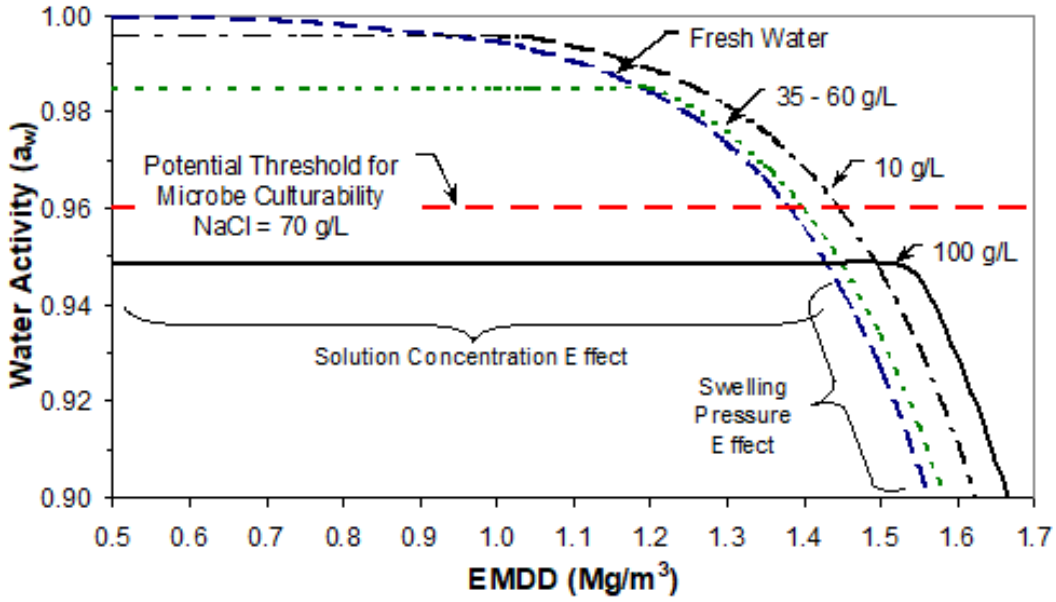

Figure 5-11: Relationship Between a_w, Density and TDS (Dixon et al. 2005)

5.4 HYDRAULIC PROPERTIES OF HCB AND GFM

5.4.1 Background

One of the most important parameters in evaluating the safety of a DGR is the ability of the water-saturated sealing materials to restrict movement of contaminants within the placement room to diffusion-dominated rates. In the bentonites considered for use in the HCB and GFM, this corresponds to an advective flow rate of $<10^{-10}$ m/s in a water-saturated system.

Influencing the movement of water within the as-placed barrier materials is the strong suction present in the unsaturated materials. A portion of the suction forces is related to the physical arrangement of the particles and the matric suction associated with the hydration and dehydration of the voids. The more substantial suction force is the osmotic suction associated with the highly charged particle surfaces and the resultant drawing in, or retention of water. These forces are greatest in dry materials and suction decreases as hydration progresses. The basic effect of suction forces in unsaturated materials is an initial rate of water uptake that is higher than would be expected under the local groundwater conditions, with inflow rate decreasing as saturation is approached. The suction forces in an unsaturated bentonite can also result in local desaturation of the surrounding host rock if it has inadequate ability to supply water. This can result in subsequent disturbance of the T-H-M characteristics of the rock, particularly subsequent supply of water to the bentonite-filled region. The suction generated by the clay therefore has a substantial influence on the early T-H-M evolution of the placement room.

In an environment where water supply to the bentonite is sufficient to avoid rock desaturation, water uptake by an unsaturated bentonite is controlled by water interaction with the clay particle surfaces and soil porosity (suction), this includes a strong influence of the ionic composition of that water. The movement into or presence of a pore fluid of high ionic strength results in a decrease in the extent of the osmotic forces in the clay-water system as the high negative charges on the mineral surfaces are neutralized by nearby cations or hydrated cation complexes provided by the pore fluid. With surface force neutralization, water movement through the clay becomes easier since the pore space available for movement has increased, interaction with particle surfaces is reduced and flow can then be described using conventional advective flow relationships. Other factors that affect the pore volume available to conduct fluid movement, pore structure or fluid movement include the precipitation or dissolution of minerals within the clay. Besides reducing pore space available for water movement, microbes if present and active can also potentially affect the movement of ions within the clay through development of chemical concentration gradients associated with their metabolic processes or by generating corrosion-inducing by-products.

The pore structure of the HCB or GFM components can be conceptualized as presented in Section 4.3, with several pore size groupings present in compacted bentonite. Much of the micro pore volume is associated with the strongly adsorbed (diffuse double layer (DDL)), water between clay platelets as described in Mitchell (1993) or is otherwise unavailable to take part in advective flow. Movement of water through the soil's pore spaces is such that flow through micropores is highly restricted with most flow occurring through the larger (macro) pores. Changes in the distribution of the macro/micro porosity distribution as the result of macro-strain (volume expansion or consolidation) could therefore be expected to influence the nature of water movement through the bentonite. Such changes will be most evident in low-density systems where strain is more readily accomplished, higher-density systems will be less readily affected. It should be noted that for the purposes of modelling diffusive transport through clays,

a single porosity model has been developed and is described by Idiart and Pekala (2015). This model is a numerical means of trying to reproduce behaviour observed in diffusion tests, with diffusion of ions assumed to occur through the entire interlayer phase. This is inconsistent with the generally accepted assumption of anion exclusion from the interlayer as referenced by Idiart and Pekala (2015).

As a result of the complex interaction of all the above-listed processes, the movement of water into, out of or through the bentonite is subject to a degree of variability beyond that attributable to density alone. This may be the source of the scatter in the measured hydraulic conductivity values and is further complicated when cations in solution interact with both the clay surface and the water molecules surrounding them. The interaction can be briefly summarized as follows:

- Development of a diffuse double layer (DDL) on the particle surfaces actually reduces the porosity available for mass transport (effective porosity). In cases where the free pore water cation concentration is low, the thickness of this DDL is large and the surrounding water molecules become strongly associated with the clay particles, restricting the ability to transmit water through this part of the porosity. High surface charge and a low ionic concentration will also result in the presence of strong repulsive forces acting between the platelets. This will encourage the particles to move further apart (swelling), reducing the macro-pore volume available for water movement.
- Should the pore water subsequently become more saline, the DDL will reduce and the porosity available for flow will increase (as will hydraulic conductivity, k). Saline pore fluid actually becomes more Newtonian in nature as TDS increases (Swartzendruber 1962) changing the way it moves through the soil matrix.
- When cation concentration in the free pore fluid is high to begin with, the thickness of the DDL layer is small, with higher k and reduced swelling capacity.

The physical structure of the bentonite porosity will therefore depend on the particle charges, the type of cations initially present in the double layer (adsorbed cations) and free porewater regions, as well as the cation concentration in the free pore water.

The Darcy equation for flow through porous media is the most commonly used means to present the hydraulic behaviour of bentonite.

Darcy Equation at constant temperature is:

$$\mathbf{Q = kiA} \qquad \mathbf{5\text{-}5}$$

Where Q is quantity of flow per unit time (m^3/s), k is hydraulic conductivity (m/s), i is the hydraulic gradient (m/m) which is determined by the hydraulic head difference (m) across the specimen's length, and A is the cross-sectional area (m^2) of the specimen being tested.

It is important to note that many of the basic assumptions associated with applicability of Darcy's Law are not maintained in bentonite systems and so care must be used in interpreting changes in flow behaviour using this relationship. Darcy's law implicitly assumes that:

- Isotropic soil structure exists,
- Soil fabric does not change,
- Fluid viscosity is constant,
    - Brine solutions are more viscous than freshwater,

  - The viscosity of water is a constant 1.005 mPa.s at 20°C,
  - Freshwater viscosity will change with temperature and at 90°C it is approximately 0.315 mPa.s (Pramudiya 2011),
- Fluid density is constant. Brine solutions are of higher density than freshwater, but also experience density reduction and viscosity decrease with temperature rise (Ozbek et al. 1977),
- Laminar fluid flow occurs,
- Non-pressure gradients and counter-gradients (e.g. chemical or microbial osmotic gradients) are not present,
- A constant temperature is present, and
- Water density is constant, when various conceptual models for water flow were examined.

It was observed by Dixon (1995) that the Poiseuille equation can be used to predict hydraulic behaviour in bentonite-based materials (Lambe and Whitman 1979; Mitchell 1976, 1993; Yong and Warkentin 1975). The Poiseuille equation is based on flow through tubular pore channels, providing further support to the concept that flow is dominated by the limited number of macropores. The basic Poiseuille equation for flow through a tube is presented below as Equation 5-6:

$$v_{ave} = p_w R^2 i_h / 8\eta \qquad 5\text{-}6$$

Where v_{ave} is the average fluid velocity, R is the tube radius, ρ_w is the mass density of the permeating water, i_h is the hydraulic gradient and η is the water viscosity.

However, in order to provide a more representative model for flow through soils, the Poiseuille equation has been modified (Mitchell 1976). The modified Poiseuille equation provided below gives a good predictive estimate of water flow and allows for evaluation of changing environmental conditions (temperature, porosity, salinity effects on fluid viscosity and density parameters can be changed). The estimation of flow requires knowledge (or estimation) of numerous parameters associated with the soil and so can prove challenging to use.

$$q = C_s V_s^2 \rho_w e^3 S^3 i_h A / (\eta S_o^2 (1+e)) \qquad 5\text{-}7$$

where (q) is flow rate as it allows for consideration of factors such as degree of saturation (S), pore shape coefficient (Cs), porosity (e), specific surface of particles (S_o), particle volume (V_s), fluid density (ρ_w), water viscosity (η), and the cross-sectional area of the specimen (A).

Despite the apparent limitations of using Darcy's law as a predictive tool, flow data processed using this relationship has been demonstrated to provide a consistent means of comparing the gross changes in flow as the result of changes in the density, thermal or chemical conditions. Hydraulic conductivity (k) as generated using Darcy's law is the way in which most literature presents flow behaviour and changes in flow behaviour and so it is maintained in this discussion.

5.4.2 Advective Flow Through MX-80

On achieving water saturation and internal structural equilibrium of the pore spaces, the physical advective movement of water as well as dissolved minerals or contaminants becomes a process that can be described by Darcian flow under constant temperature conditions. Darcy's law for advective flow in soils (Equation 5-5) is generally used to describe flow in water-saturated bentonites although it may not be readily applied under low gradient or very low density conditions since the quantity of mobile water may change as a result of the diffuse double layers (DDL) associated with montmorillonite particles (Dixon 1995; Dixon et al. 1999).

The DDL is discussed further in Section 5.5. Since pore fluid TDS will affect the porosity available to transfer fluid (or gas), k will vary with groundwater conditions, even where the density of the clay is the same. It is therefore important that the groundwater composition and anticipated salinity conditions during the repository lifetime be known so that accurate estimation of k can be accomplished.

5.4.2.1 Flow Under Freshwater Conditions

Measurements of the advective flow behavior of bentonites of the type used as the reference clay by NWMO (MX-80) have been reported in numerous research reports including; Barone et al. 2014; Bennett 2014; Bucher et al. 1986; Daniels et al. 2017; Dixon 1995, Dixon and Miller 1995; Dixon et al. 1987, 1996a,b, 1999, 2016, 2018; Man and Martino 2009; Oyang and Daemen, 1992; Pusch 1980b; Studds et al. 1998; and Westsik et al. 1982. Figure 5-10 shows the effect of density under freshwater conditions on the hydraulic conductivity of MX-80. There is a very substantial and consistent decrease in k as the density increases, a behavior that is consistent with what would be expected where macro-pore volume decreases, and micro-pore volume is unchanged. Ultimately there is effectively no macroporosity and what flow occurs is forced through the micropores and interlayer water associated with particles (as discussed in Section 4.3). There is a degree of scatter in the data, as would be expected when testing is undertaken by different labs using slightly different testing equipment, test methodologies and materials sourced over several decades, but this does not affect the overall trend in behaviour observed. The hydraulic conductivity is less than 10^{-11} m/s for the density range shown in Figure 5-12.

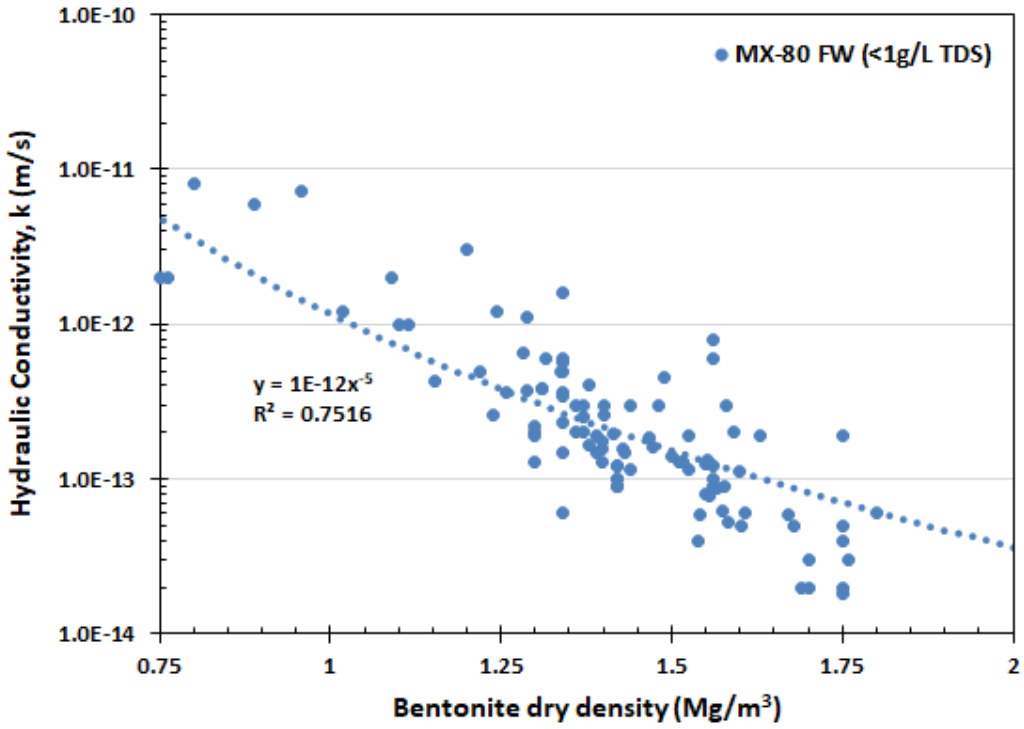

Figure 5-12: Hydraulic Conductivity of MX-80 Under Freshwater Conditions

As noted earlier in this document, bentonites are natural materials that are typically mined and processed (crushed, dried and sometimes chemically treated) for industrial use. This means that materials sourced from different locations, and perhaps even within the same deposit will

vary compositionally. This is reflected in a considerable range of montmorillonite-type clay mineral content and variations in their chemical composition and surface charges. As well the nature of the cations present in the natural clay will affect the ability of the clay to swell (e.g. monovalent Na versus multi-valent Ca, Mg, Fe, Cu) when provided with water. Monovalent cations generally result in a higher swelling capacity. In order to provide a means to compare the behavior of these different bentonites as well as bentonite-aggregate mixtures a parameter known as Effective Montmorillonite Dry Density (EMDD) was developed (Dixon et al. 2003). This parameter allows for prediction of the hydraulic properties of clays of differing source based on their montmorillonite content. This parameter also allows for prediction of the hydraulic characteristics of bentonite – aggregate contents. As this report focusses on the behavior of 100% MX-80 bentonite the EMDD parameter is not used and data is presented as dry density.

5.4.2.2 Effect of Pore Fluid Salinity on Hydraulic Conductivity

The presence of dissolved solids (salts) in the pore spaces of a bentonite clay has a well-documented effect on the movement of water through the system. With increasing TDS comes an increase in hydraulic conductivity for a given clay density. The magnitude of this effect is generally agreed upon to be greatest at low dry density, likely as the result of space being available for clay-cation interaction as well as the larger porosity being available for water movement. Figure 5-12 shows examples of the pattern of changing k with salinity observed for low density bentonite systems (Studds et al. 1998) and high density materials (Villar et al. 2005). In Figure 5-13 void ratios of 1.0 and 2.0 correspond to bentonite dry densities of approximately 1380 kg/m^3 and 920 kg/m^3 respectively. Similar behaviour has been observed for denser bentonite systems (e.g. Barone et al. 2014; Dixon 2000 ; Dixon et al. 1999, 2003, 2018; Khan 2013; Pusch 1980b; Villar et al. 2005; Alonso and Ledesman 2003; Cui 2017; Johannesson et al. 2015; Martikainen and Schatz 2011; Priyanto et al. 2013; Westsik et al. 1982).

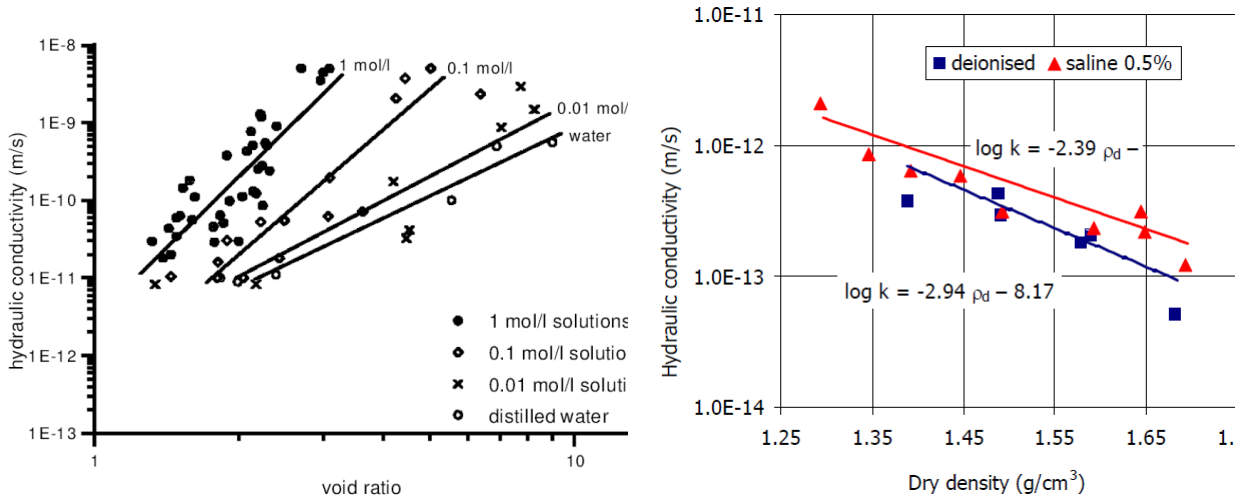

Figure 5-13: Effect of Pore Fluid Salinity on Hydraulic Conductivity
(Studds et al. 1998; Villar et al. 2005)

While literature clearly shows the effect of increasing salinity on hydraulic conductivity, when the results of different studies are combined, it becomes more difficult to quantitatively determine the impact of salinity. Figure 5-14 presents combined literature related to the effects of ionic strength on the hydraulic behavior of MX-80 bentonite, clearly showing the increased ability of a material exposed to brine conditions to conduct fluid but also the overlap in the available data,

particularly as density increases. The greatest effects of changing porewater composition on k are observed at low to moderate salinity. Based on limited data, it would appear that once salinity increases beyond approximately 100 g/L there is limited additional influence of Total Dissolved Solids (TDS) increase on hydraulic behavior. At high TDS concentration, the volume of pore space effected by surface charge on the clay platelets has been greatly reduced and the quantity of structured water/cations on the surface is small. As a result, additional concentration of cations in solution do not result in further change in the porosity available for advective flow. The exponential and power best-fit equations for the hydraulic conductivity-density data provided in Figure 5-14 are summarized in Table 5-4. Plots of the data used to derive the regression lines and correlation coefficients are provided in Appendix D.

It should also be noted that the density-hydraulic conductivity data presented does not extend to extremely low density conditions (<500 kg/m^3 dry density), where estimation of k is complicated by development of extremely large hydration layers around the particles under freshwater conditions. Such low density conditions are not particularly relevant to a DGR where materials will be placed at much higher densities (1400 to 1700 kg/m^3).

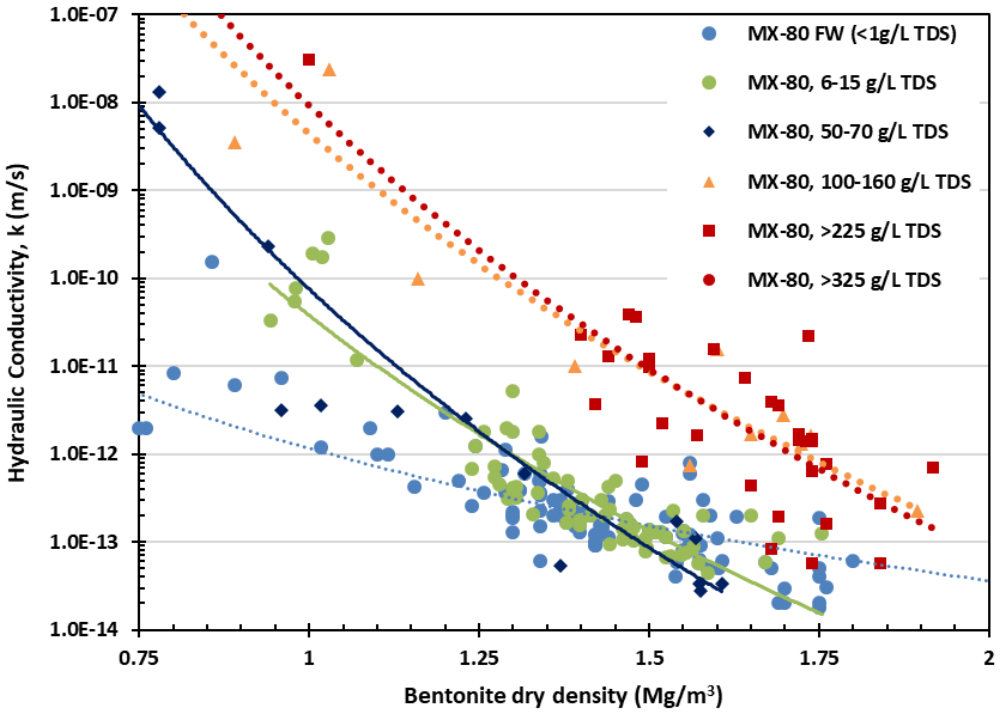

Figure 5-14: Hydraulic Conductivity of MX-80 Under Saline Groundwater Conditions

5.4.2.3 Statistical Evaluation of Hydraulic Conductivity Data

The hydraulic conductivity data presented in Section 5.4.2.2 and whose best-fit equations are provided in Table 5-4 were statistically analysed in order to determine their confidence limits as well as their prediction bands. These analyses were undertaken using the methodology outlined in Section 5.2.2.3 and are summarized in Appendix D. From these plots the predictive bands for data can be seen for the range of groundwater salinity of interest in a DGR. In some cases, there is limited data available for use in these analyses and as a result the confidence and predictive bands are quite large, particularly when densities are substantially above or below the reference values.

Table 5-4: Best-Fit Equations and Prediction Intervals for Hydraulic Conductivity of MX-80 Bentonite @ Room Temperature

Solution	Best-fit Equation	R^2	K at 1.4 Mg/m^3 (m/s)	K at 1.6 Mg/m^3 (m/s)	K at 1.7 Mg/m^3 (m/s)
MX-80 in Freshwater	$k = 1E\text{-}12 \times DD^{-4.62}$ $k = 5E\text{-}11e^{-3.694DD}$ PI	0.740 0.709	 3.0E-13 3.4E-14 to 2.6E-12	 1.4E-13 1.6E-14 to 1.2E-12	 9.8E-14 1.1E-14 to 8.5E-13
MX-80 in 5-15 g/L TDS	$k = 2E\text{-}11 \times DD^{-11.19}$ $k = 4E\text{-}08e^{-7.929DD}$ PI	0.671 0.607	 5.7E-13 3E-14 to 1.1E-11	 1.2E-13 6E-15 to 2.3E-12	 5.3E-14 2.7E-15 to 1E-12
MX-80 in 50-70 g/L TDS	$k = 4E\text{-}11 \times DD^{-16}$ $k = 8E\text{-}04e^{-15.68DD}$ PI	0.813 0.794	 3.6E-13 5.2E-17 to 2.4E-9	 1.1E-14 7E-19 to 1.8E-10	 2E-15 8E-20 to 5.4E-11
MX-80 in 100-160 g/L TDS	$k = 2E\text{-}10 \times DD^{-7.623}$ $k = 2E\text{-}07e^{-6.521DD}$ PI	0.695 0.775	 2.2E-11 4.2E-12 to 2.2E-8	 5.9E-12 1.3E-13 to 2.4E-8	 3.1E-12 6.8E-14 to 2.6E-8
MX-80 in >223 g/L TDS	$k = 2E\text{-}09 \times DD^{-14.2}$ $k = 3E\text{-}04e^{-11.55DD}$ PI	0.839 0.808	 2.9E-11 3.1E-13 to 2.6E-9	 2.8E-12 3.1E-14 to 2.6E-10	 9E-13 9.6E-15 to 8.4E-11
MX-80 in > 325 g/L TDS	$k = 1E\text{-}08 \times DD^{-16.82}$ $k = 1.36E\text{-}02e^{-13.66DD}$ PI	0.967 0.946	 6.7E-11 4.1E-12 to 1.1E-9	 4.4E-12 2.7E-13 to 7.1E-11	 1.1E-12 6.6E-14 to 1.9E-11

Where DD is dry density of MX-80 expressed as Mg/m^3 and k is in m/s; PI is 95% prediction interval.

Potential reasons for the scatter in literature data for MX80 bentonite are numerous. The most likely are associated with:

- The natural variability of the composition of bentonite. It is a natural material subject to localized differences in its montmorillonite content as well as its soluble salts and minor mineral composition.
- Different testing methods and equipment are used in each lab providing measurements. While the basic concepts for testing and equipment design are similar, variations will result in differences in the measurements obtained.

5.4.3 Effect of Temperature on Hydraulic Properties of Dense Bentonite

In addition to the effects of density and pore fluid salinity, the movement of water through the GFM and HCB materials is influenced by temperature. In the early evolution of the placement room, the movement of moisture will be driven in part by the thermal gradient from the heat-generating UFC to the rock contact beyond the GFM. With time and water uptake from the surrounding rock, the bentonite filled regions will move towards saturation. The hydraulic conductivity of the water-saturated bentonite is influenced by the effects of ambient temperature, largely as the result of change in fluid viscosity with change in temperature. The Darcy equation for flow in porous media recognizes the influence of changing water viscosity with temperature, and so k will change with temperature. Figure 5-15 shows how a temperature increase from 20 to 90°C results in a reduction in water viscosity (1000 to 350 mPa.s), making it easier for water to move through the clay matrix as temperature increases. As can also be seen in Figure 5-15, the density of pure water decreases from 1000 to approximately 965 kg/m^3 as temperature rises from 20°C to 90°C (Pramuditya 2011; Anton-Paar 2011). This can also have a substantial effect on the pore pressures generated in a fully-saturated very low permeability system if temperature changes more rapid than the system's ability to move fluid into or out of its pores.

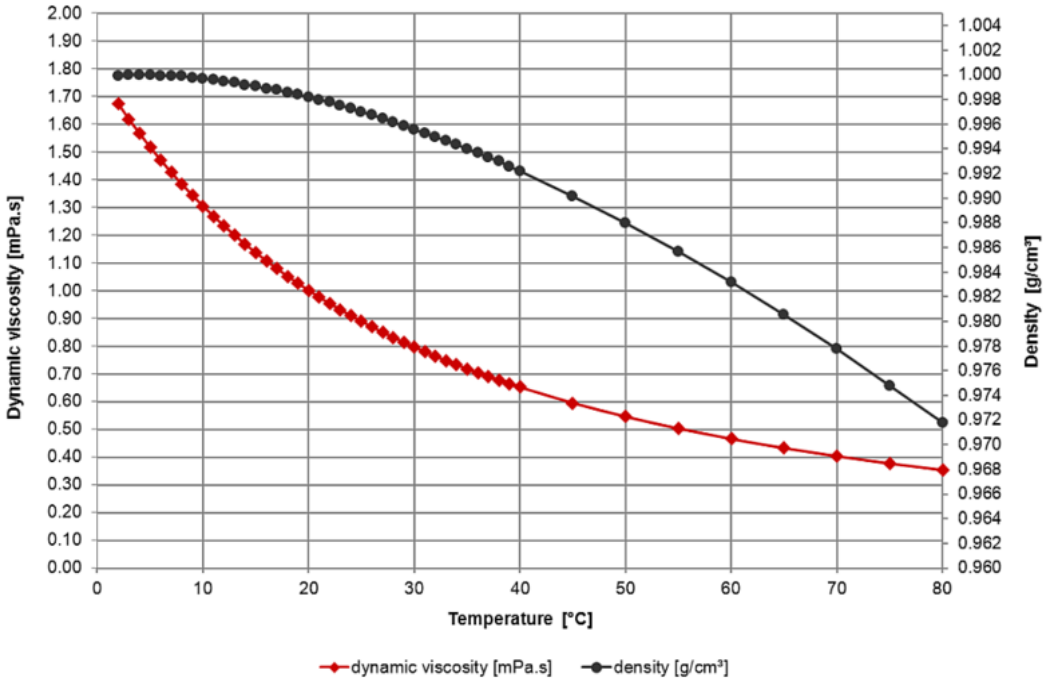

Figure 5-15: Effects of Temperature on Freshwater Density and Viscosity
(Anton-Paar 2011) https://wiki.anton-paar.com/en/water/

Viscosity-dominated change in hydraulic conductivity has been observed in measurements made by numerous researchers (Bennett 2014; Cho et al. 1999, 2000; Dixon 1995; Dixon et al. 1987, 1996a,b; Daniels et al. 2017; Oscarson and Dixon 1990; Villar et al. 2010; Zihms and Harrington 2015). All of these studies noted a significant increase in the hydraulic conductivity with temperature increase. Figure 5-16 shows examples of the observed changes in the hydraulic conductivity of bentonites having similar mineralogical compositions as the result of temperature change. Literature data and theory all indicate that hydraulic conductivity increases with increasing temperature and can be explained primarily by change in water viscosity, although the data is not entirely consistent. Although change in viscosity of water is the dominant factor, there are other factors such as mineral surface charge, surface area, adsorbed cation composition, flow path tortuosity and pore size distribution that affect flow.

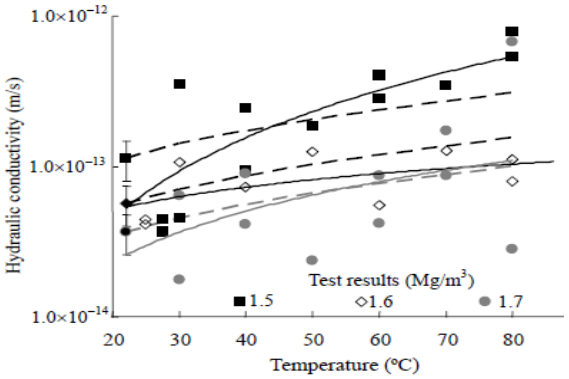

(MX-80 Villar et al. 2010)

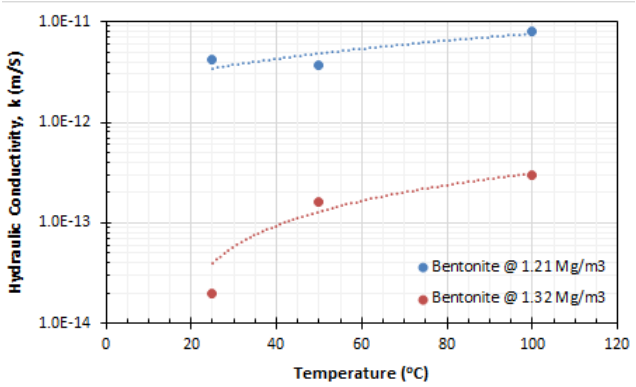

(Sask. Bentonite, after Dixon et al. 1987)

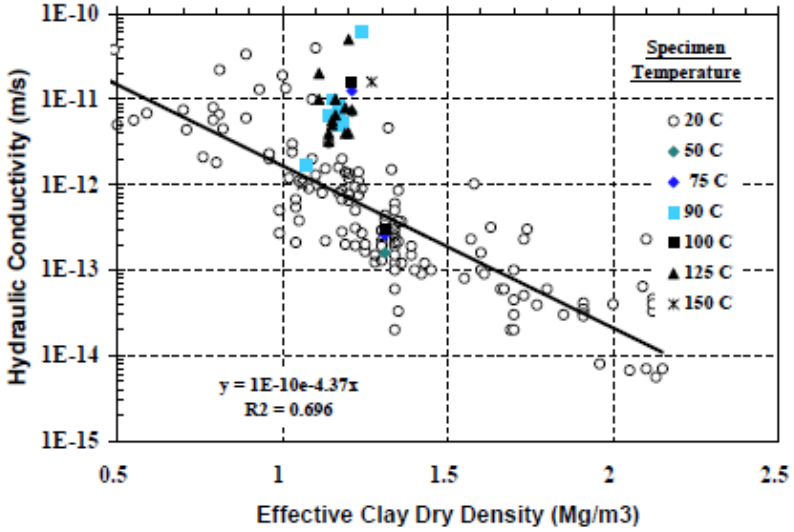

(Oscarson and Dixon 1989, 1990 as presented in Dixon et al. 1997)

Figure 5-16: Effect of Temperature on Freshwater Hydraulic Conductivity of Bentonite

Although temperature change clearly affects the hydraulic conductivity of compacted bentonite, there is also the question as to whether these changes in flow velocity are associated with any intrinsic ability of the bentonite to conduct water. Daniels et al. (2017) examined flow through MX-80 bentonite having a dry density of 1560 kg/m^3 at temperatures from 20 to 170^{o}C with the results shown in Figure 5-17. From these data it would appear that for the temperature range of

interest (<100°C), there is no substantial change in the permeability with change in temperature once viscosity of water is considered. At temperatures in the >100°C to <150°C range, the permeability seems to exhibit a reduction (~2% / °C) with temperature rise. The change in hydraulic conductivity (or permeability) is not exactly accounted for by water viscosity and this may be associated with changes in solid-liquid volume ratio as the result of thermal expansion of solids. Additionally, water movement may be influenced by changes in the macro-micro void ratios as the result of thermal expansion and gradual changes in the soil microstructure with time, hydration and water movement. The dashed lines shown for very high temperature shown in Figure 5-17 are for readings associated with equipment malfunction and so are not considered representative of real behaviour. The results of Daniels et al. (2017) are consistent with the conclusions of Oscarson and Dixon (1990) who examined the effects of elevated temperature and also exposure to and subsequent cooling of initially unsaturated and saturated bentonite-sand mixtures having clay dry density of 1000 to 1300 kg/m^3. In that study there was no discernible irreversible effect of thermal cycling and temperature, behaviour is attributable to changes in water viscosity, porosity and water density.

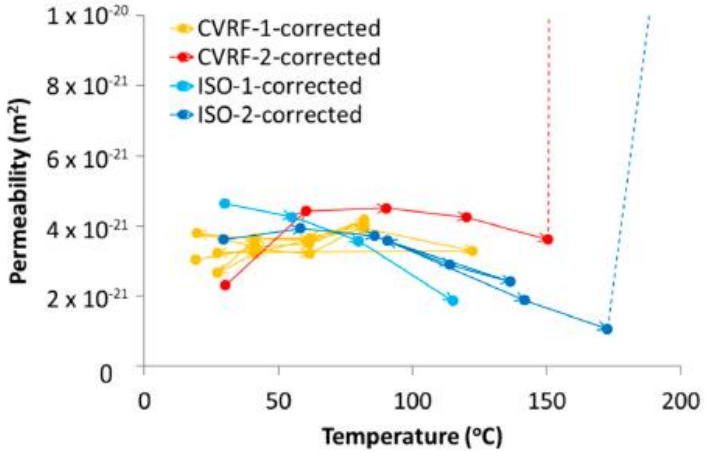

Figure 5-17: Effect of Temperature on Intrinsic Permeability of MX-80 Once Correction for Viscosity Change is Applied (Daniels et al. 2017)

5.4.4 Effects of Secondary Processes Such as Cementation, Mineral Dissolution and Bacteria on Hydraulic Behaviour

The hydraulic properties of the HCB and GFM system can also be affected by a number of secondary process that could develop over the longer term. These include but are not limited to:

- Cementation of the soil matrix through precipitation of materials within the clay.
- Dissolution of minerals in the clay and subsequent alteration of the porosity of the clay or changes to the ability of montmorillonite to restrict water movement.
- Development of microbial colonies.

5.4.4.1 Cementation/Dissolution

Cementation or dissolution of materials within the bentonite-filled volume are secondary processes associated with changes to the chemical environment surrounding and within the GFM or HCB. Cementation of the clay particles will require either transport into and precipitation of soluble materials within the clay-filled volume, or local dissolution and

reprecipitation of a portion of the original clay or accessory minerals (not necessarily the swelling clay). Cementation across particle boundaries could result in loss of swelling capacity and subsequently adversely affect self-sealing of the HCB-GFM volume. Cementation could also however result in clogging of key pathways for water (and contaminant) movement, reducing the ability of contaminants to move through the system. This process was described by Pusch (1977) and discussed with respect to internally-occurring, silica cementation in bentonite systems by soluble silica naturally present within the bentonite, with a conclusion that cementation would not be able to produce brittle behavior in dense bentonite. Other sources of potentially cementitious material include:

- Gypsum, which occurs naturally within bentonite and is readily soluble.
- Calcite, which occurs naturally within bentonite. Calcite or gypsum (calcium sulphate) are readily dissolved or precipitated materials that are likely to move within the bentonite as temperature conditions evolve, and so may play a role in longer-term alteration in the bentonite swelling or hydraulic behaviour.
- Amorphous iron naturally present in the bentonite or from iron-rich materials left behind during repository closure (e.g. rock bolts, reinforcing bars in concrete, UFC).

The presence of natural iron in the bentonite is very limited and of more concern is the introduced iron-bentonite reaction and the potential subsequent reduction in swelling pressure. Carlson et al. (2006) and Wersin et al. (2008) examined iron-bentonite reactions with respect to the UFC and the surrounding bentonite. The results by Carlson et al (2006) were not clearly conclusive, while Wersin et al. (2008) concluded that iron migration into bentonite was unlikely to be very substantial (only a few cm), even over a very long time. Bradbury et al. (2012) indicates that montmorillonite alteration at temperatures less than 100^{o}C in the relatively freshwater conditions in Nagra's repository concept would see little alteration as the result of conversion to Fe-smectites, although there is still some uncertainty regarding effects of other possible alteration products such as iron-chlorite. Davies et al. (2017) also reviewed thermal (20-300^{o}C) and corrosion-related processes in very high TDS / MX-80 systems and noted that corrosion-alone does not appear to significantly affect swelling behaviour of bentonite. It was noted that in mixed ion systems (such as natural high-salinity groundwaters) that interlayer exchange of cations was accelerated under elevated temperature conditions. They also concluded that in their gel-consistency specimens that salinity will have a greater influence on the bentonite than will corrosion products, with corrosion products generally forming poorly crystalline precipitates within the clay matrix rather than altering the adsorbed ion composition. Over the short-term Davies et al. (2017) noted that this increased the swelling capacity of the clay but over longer duration (2yr), a reduction in the swelling capacity was observed. It should be noted that these results are for materials tested as clay-fluid suspensions and so may not be representative of processes that can occur under actual field conditions (e.g. high density, low porosity).

Laine and Karttunen (2010) identify two processes that may lead to changes in swelling pressure, hydraulic conductivity, ionic diffusivity and loss of plasticity of the buffer as precipitation of SiO_2 and/or montmorillonite transformation to non-expandable minerals such as illite. Arthur & Zhou (2005) attribute cementation in natural bentonite formations to be mainly a result of the smectite/illite conversion reaction which has occurred over the many millions of years since it was initially deposited as silica-rich volcanic ash. Cementation can also be the result of precipitation of agents other than Si, such as iron-oxides, calcite or gypsum.

The buffer in the placement room will have a temperature gradient across it as the result of the heat-generating UFCs. These may cause migration of dissolved compounds inwards or outwards within the bentonite and if they reach a temperature, pH and other conditions where

the precipitation is possible they will come out of solution and fill part of the pore volume as well as potentially cementing the clay particles together (Pusch et al. 1998, Pusch 2001, Pastina & Hellä 2006, Wersin et al. 2007). Similarly, if conditions become less favourable, they may also redissolve and migrate elsewhere in the bentonite or repository volume. Each potential cementing agent will have a unique condition under which it will precipitate.

In the study by Wersin et al. (2007), temperature related cementation was summarized as follows:

- No significant cementation seems to occur below the temperature 110 ºC.
- Slight cementation at 130 ºC.
- Significant cementation at 150 ºC and perhaps also smectite to illite transformation.

Wersin et al. (2007) also referenced a study on Kinnekulle bentonite as a natural analogue data which indicated that bentonite retains low hydraulic conductivity even after extended exposure to elevated temperatures and substantial illitization and cementation has occurred. A more recent review of montmorillonite stability under near-field repository conditions relevant to Nagra's sedimentary repository concept as well as for the SKB and Posiva crystalline rock repository concepts was completed by Nagra (Leupin et al. 2014). These three repository concepts all have relevance to NWMO's repository concept as both sedimentary and crystalline rock concepts are being considered by NWMO and bentonite is proposed for use as a sealing system component immediately surrounding the used fuel containers and similar temperature conditions are expected to exist. It was concluded that for realistic geochemical and thermal conditions that so far as swelling or cation adsorption is concerned there would be little change and that the fundamental physical and chemical properties of the smectite will be preserved over the longer-term.

The conclusions of Leupin et al. (2014) are consistent with the earlier finding reported for the FEBEX project where evaluation of the effect of five years of contact of highly compacted bentonite with a cast concrete plug was examined (Enresa 2006). The FEBEX installation was operated in a granitic geosphere at elevated temperature (~65ºC at concrete-bentonite contact) and water in the system migrated towards these contacts where essentially saturated conditions existed. At the end of the five years of testing, extensive mineralogical, geochemical and chemical analysis was undertaken on the bentonite and the porefluid associated with it. The mineralogical composition of the bentonite was not discernibly altered although some minor mineral phases (gypsum and calcite) were evident at the time of decommissioning.

As noted by Laine and Karttunen (2010), silica polymorphs (quartz, cristobalite and amorphous silica) can precipitate over a wide temperature range. The precipitation temperatures were identified to range from 18 to 500 ºC depending on the prevailing salinity/pH conditions. SiO_2 content in groundwater in the repository was identified as being controlled by the following processes and are relevant to the MX-80 immediately adjacent to the UFCs:

- Dissolving of smectite and other minerals of bentonite,
- Dissolving of minerals of host rock,
- Dissolving of cement-based construction materials, and
- Dissolving of silica based grouting material.

Chemical dissolution of smectite is assumed to be a temperature-related reaction (Wood 1983, Pusch et al. 1998), that is also affected by the solid/liquid ratio of the system and pH. The dissolution of smectite may release silica and aluminum. Released Si may later function as a cementing agent in bentonite when a suitable site for reprecipitation is encountered. In a

particularly aggressive environment, where very high pH conditions (>11) exist, dissolution of some of the mineral component of the bentonite may occur. There is however no currently identified mechanism whereby such an environment would persist in a DGR.

The presence of cementitious materials (e.g. concrete) in contact with the bentonite materials will result in a localized increase in the pH conditions to between 9 and 11 for the period immediately following the concrete and bentonite placement if specially formulated low pH cementitious materials are used. The duration of this pH anomaly will depend on many factors but predominantly on the formulation of the cementitious materials used, the number of pore volume exchanges that occur and neutralizing reactions with the clay and surrounding rock mass. The reaction process associated with cementitious materials has been studied by Onofrei and Gray (1990), Kim et al. (2011) and considerations regarding their use has been reviewed by (Hansen 2004; Kim et al. 2011). In order to deal with potential long-term interaction, the general approach has been to allocate a portion of the bentonite thickness as a sacrificial zone where bentonite alteration (and or cementation) occurs based on the quantity of concrete present. For example, in Nagra's tunnel placement concept where the concrete-lined tunnels will result in an anticipated <0.13 m of bentonite alteration to illite, hydroxides, carbonates, calcium silicate hydrates and aluminosilicates, over a 1 million year period (Bradbury et al. 2012). A subsequent report by Savage (2013) loss of bentonite in concrete-lined tunnel was estimated. For concrete thickness of 150-250 mm (similar to thickness of NWMO placement room floor), it was estimated that bentonite alternation would extend some 38 to 67 mm beyond the original contact. This is substantially less than that predicted by Bradburry et al. (2012) and also less than the estimated 150 mm thickness of the bentonite floor tablets present between the concrete and the lower surface of the buffer box in NWMO's placement rooms. The swelling pressure and contaminant retention properties of this alteration zone would be reduced but not zero.

In a study to identify the magnitude of the effect of high pH on the properties and behaviour of bentonite, Oscarson et al. (1996a) examined the effects of bentonite exposure to high (0-5% by dry weight) concentrations of $Ca(OH)_2$, followed by percolation with freshwater. The results were not able to detect any changes in the swelling pressure or hydraulic conductivity of the bentonite, although conversion from a sodium to a calcium bentonite was observed.

Additionally, a study by Lehikoinen (2009) examined the possible extent of mineralogical alteration as the result of continued exposure of bentonite to elevated pH (12.2; 11.6 and 9.7) and it was concluded that while extended exposure would result in mineralogical damage, it would be confined to the region close to the interface between the clay and high pH material and would likely result in clogging of the pores in that region.

5.4.4.2 Bentonite Erosion

The loss of substantial quantities of bentonite from the placement room via conventional erosion cannot readily occur in a placement room unless there is very substantial water inflow occurring during the placement process. Physical erosion involves the relocation of bentonite as the result of water flow through the placement room, either during UFC installation or immediately following placement room closure. The loss of bentonite during UFC installation is a potential concern only in that situation. It is not anticipated that discernible water inflow will occur during UCF installation in a sedimentary environment such as that considered by NWMO (similar to what is anticipated for other sedimentary concepts in Belgium, France and Switzerland). Water-induced mechanical erosion is a possibility in crystalline rocks such as considered by Canada, Sweden and Finland and is discussed by Sandén et al (2008). If inflow is locally substantial,

means to control water inflow such as grouting or installation of water drainage systems or structures can be used (Åkesson et al. 2016; Koskinen 2015; Koskinen and Sandén (2014), Sandén 2016; Sandén and Börgesson 2014; Sandén et al. 2008). These will allow for UFC and sealing material installation to continue under conditions of modest water inflow, should inflow be too high to deal with those placement rooms (or sections of placement rooms) would not be used. Under conditions of low to moderate water inflow, the potential exists for water to relocate some of the bentonite installed in the tunnel, this would be a local phenomenon and should not result in a substantive alteration in the density of the installed bentonite. However, this factor needs to be carefully considered when undertaking UFC installation in a wet environment.

The intrusion of bentonite into small fissures or cracks in the surrounding rock mass can occur to a limited extent, the depth of penetration will depend on many local physical and environmental factors. It will ultimately be restricted through the development of filter layers as coarser particles clog the openings, limiting further movement of material into the rock. Birgersson et al. (2009) note that for Na-montmorillonite pore sizes of <0.5 to 0.2 um will stop bentonite movement while a Ca-montmorillonite will require pore sizes > 100um to migrate.

Bentonite erosion through “chemical” means other than chemical dissolution has been suggested as being possible under conditions of hyper-freshwater intrusion to repository depth, combined with contact of bentonite with this solution in a water-conductive geological feature (fracture or fault) (Birgersson et al. 2009). This type of “erosive” loss by the formation of “bentonite sol” is the result of ongoing dispersion of colloidal sodium bentonite (<20% Ca in exchange sites), into the moving hyper-fresh groundwater. There is a dramatically lower capability for this type of sol formation where the bentonite is in the Ca/Na form or Ca is the dominant (90%) exchangeable cation. In a Ca form the montmorillonite is not prone to formation of sols. The sedimentary formations considered by NWMO are located below and within hyper-saline structures (see Table 4-4 for groundwater composition), that have survived multiple glaciations without evidence of dilution of their pore fluid to hyper-fresh conditions.

As noted by Birgersson et al. (2009) the critical coagulation concentration (CCC) for Wyoming-type bentonite is in the order of 25 mM (1.17 g/L) in a pure NaCl form. At higher concentrations the bentonite will coagulate and become a non-colloidal particle that is less mobile. In mixed Na/Ca systems the CCC is even lower. It is unlikely that this type of mechanism would be encountered in the sedimentary rock formations considered by NWMO as the overlying and target installation-level structures all contain substantial natural concentrations of salt in their pore fluid, with evidence that there has been little interaction of the deeper (>330 m depth) at the Bruce Site in Ontario groundwater with surface water over many millions of years (Clarke et al. 2013, 2015 and Al et al. 2015).

Formation and subsequent movement of bentonite in a colloidal form requires the presence of hyper-freshwater in order for this process to become discernible. Tests by Birgersson et al. (2009) indicated that TDS levels in the order of 1-5 mM (0.05 – 0.42 g/L) of sodium or Na/Ca chlorides were sufficient to prevent erosion of Na-dominated bentonite. It was concluded by Birgersson et al. (2009) that for the situation in the Grimsel site, located in granitic rock that glacier-generated meltwater would be insufficient to trigger colloidal release from the bentonite. Hence in the type of geological conditions anticipated in a DGR located within the granitic rocks of the Canadian Shield, conditions that could lead to colloidal release by the bentonite is highly unlikely given the depth, hydraulic gradient conditions and also the presence of a substantially higher natural groundwater TDS concentration than is present at the Grimsel site.

5.4.4.3 Microbes

The presence of a viable and active microbial (bacteria, fungi) population has been determined as being able to alter the hydraulic properties of clay soils, typically by generation of biofilms or intrusive growth into the pore space between particles. As a result, microbiological activity is typically something that will decrease water flow through soils. The potential therefore exists for microbial activity to influence water movement and have some influence on the hydraulic behavior of the sealing system. The environmental conditions required to allow for bacterial activity are not however generally found in the HCB and is unlikely to persist in the GFM for long after density equilibration begins. This bacteria-unfriendly environment is caused by a number of factors (Stroes-Gascoyne et al. (2005; 2006; 2007a, b; Stroes-Gascoyne and Hamon 2008; 2010), Stone et al. (2016) with the main factors being:

- The very high porewater suction present within the bentonite in the pre-saturation phase makes it difficult for bacteria to survive in an active form;
- The very small pore spaces in which the bacteria would need to exist precludes their active presence although they may persist as spores;
- The very low water activity (a_w) conditions induced by highly saline fluid; and
- Elevated temperatures adjacent to the UFC (Stroes-Gascoyne and Hamon 2010).

The role of these factors in discouraging bacterial activity is discussed in detail by Stroes-Gascoyne 2005; Stroes-Gascoyne and Hamon 2008, 2010; Stroes-Gascoyne et al. 2005; 2006; 2007a, b; Stone et al. 2016). It was conservatively estimated that in order to have essentially no bacterial activity in a low salinity bentonite environment that a dry density of greater than approximately 1600 kg/m^3 must be present. This condition is met in the HCB component and with consolidation of the GFM by swelling of the HCB, this potentially viable density condition may not persist within the perimeter bentonite for very long. Alternatively, if low density persists or develops a region that previously had no viable bacteria population may see re-establishment of microbial activity (Stroes-Gascoyne and Hamon 2010).

A study of the effects of bacterial action on advective flow through compacted bentonite was included in the work by Stroes-Gascoyne et al. (2006) and it was concluded that bacterial activity was not a discernible influence on water flow through bentonite, and that presence of a saline (68 g/L TDS) pore fluid resulted in a very substantive reduction in bacterial presence in and around the bentonite. In the studies by Stroes-Gascoyne and Hamon (2008, 2010), the presence of an initially active and viable bacterial population within the loose bentonite before compaction into HCB did not persist and although still present at the interface between the HCB and filter stones on the upper and lower faces of the specimen, there was no discernible change in the hydraulic conductivity (or swelling pressure) measured. This has particular relevance to a DGR since there will be contact interfaces between the HCB, GFM and surrounding rock mass at a sufficient distance from the UFC surface that temperature will be substantially lower than at the surface of the UFC. The result will be a less-harsh environment that might be more conducive to bacterial growth. Hence, based on the laboratory tests where a more microbe-friendly environment was present and no discernible effect on Ps or k was observed, it might be concluded that this situation will also occur in the placement room.

The temperature at the HCB-UFC contact will rapidly increase to approximately 90^{o}C. Stroes-Gascoyne and Hamon (2010) examined the effects of temperature and density on the culturability of bacteria native to Wyoming MX-80 bentonite. It was noted that there was a five-order of magnitude decrease in the culturable cells when temperature was 60^{o}C although there was still some cell viability at 80^{o}C. Once temperatures were raised to >121^{o}C the bentonite was essentially sterilized although there was still a very low level of aerobic culturability

detected once temperature decreased. Stroes-Gascoyne and Hamon (2010) also noted that viability was also influenced by clay density with higher viability at lower densities.

5.4.5 Summary

The advective flow behaviour of bentonite is primarily controlled by the dry density of the clay and the salinity of its pore fluid. Relationships describing the swelling pressure-density of MX-80 bentonite behaviour have been developed and provided in Table 5-5. The effects of further increasing TDS concentration of the pore fluid seem to be limited when they exceed approximately 100 g/L. Factors such as exchangeable cation composition, cation ratio and bacteria will have a limited discernible effect when the density of the bentonite is high. When the density of the bentonite is low, secondary processes and effects become more easily identified. At elevated temperature the advective flow velocity (hydraulic conductivity) will change primarily as a function of changing water viscosity. Fluid flow may change with time depending on the presence of processes leading to erosion, cementation/precipitation and bacterial activity but at present, under conditions relevant to the DGR, none of these processes have been clearly demonstrated to be present at levels that would substantially alter fluid flow (and hence contaminant migration). A further evaluation of processes likely to be of importance will need to be undertaken once a repository site is selected and site-specific groundwater information is available as well as site-specific thermal evolution following UFC installation and facility closure.

5.5 SWELLING PRESSURE OF HCB AND GAP FILL

5.5.1 Background

Swelling pressure is defined as the mechanical load per unit area of surface of a rigidly-confining medium. In the DGR swelling pressure is the pressure applied to the rock or UFC by a fully-hydrated bentonite.

As a result of the high negative surface charge present on the faces of the bentonite particles there is a strong repulsive force developed between the plates. This repulsive force is evidenced by a swelling potential (pressure) where there is no means to allow the particles to move apart (saturation has not been achieved or material is rigidly confined). Where water is supplied to the bentonite and volume strain can occur, the water and cation-water complexes allows the particles to hydrate and move apart. The force developed by this repulsion can be very substantial and the closer the particles are required to remain to one-another the higher is this repulsion. As discussed previously, the presence of balancing cations in the water between the particle surfaces reduces the magnitude of the repulsive forces and hence decreases the force developed on the confinement. This is described in greater detail in Dixon 1995; Karnland 1997, 1998 and Bag 2011. Figure 5-18 shows the diffuse-double-layer concept with the various forces and regions of structured water associated with parallel clay particles. In dense systems the majority of the water associated with the bentonite is held in a structured form and so is not entirely free to move through the clay. The strength of the electro-chemical bonding will vary with factors such as internal structure of the clay particles, distance between particles and the presence and composition of the cations present in the free water phase. Factors such as temperature, hydraulic pressure and bacterial activity may also play a role in determining the swelling pressure that a confined bentonite will develop.

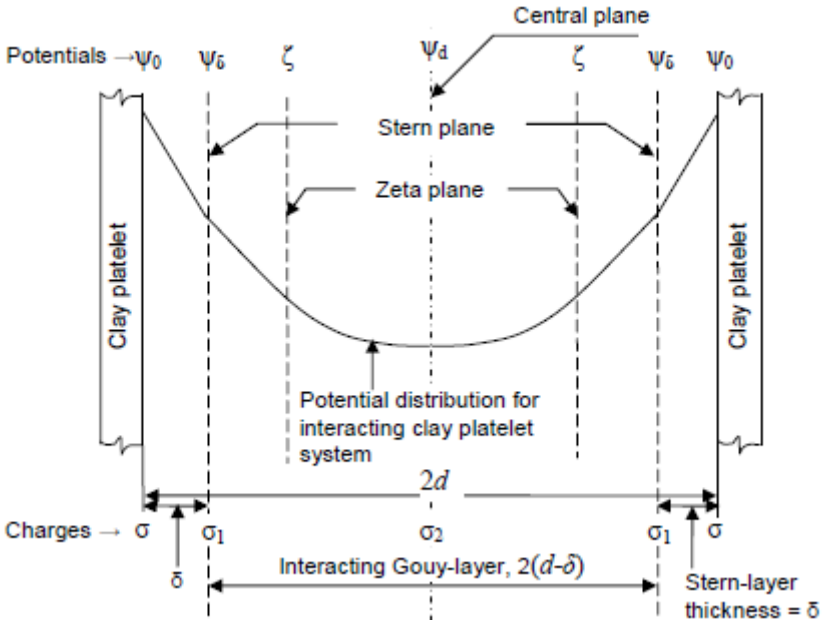

Where Ψ_o is the electrical potential at the mineral - water phase contact and is mainly associated with oriented water dipoles on the clay surfaces (known as Stern water layer); Ψ_δ is the potential at the location where the first layer of hydrated ions is located. The zeta plane represents the start of the region known as the diffuse double layer, which extends to the central plane where, if Ψ_d equals Ψ_o/e (e is the electron charge). This is approximately the thickness of water associated with the mineral surfaces and does not take part in normal advective water movement. Regions beyond this point between adjacent particles can be assumed to behave as bulk water.

Figure 5-18: Distribution of Layer Charges in a Clay Electrolyte System (Bag 2011)

5.5.2 Swelling Pressure in MX-80

The forces driving particles to separate are measured as swelling pressures on the walls of a rigid confinement. These same forces control water movement through the bentonite. The swelling pressure of a clay is therefore primarily a function of the strength of the surface charge on the clay platelets and the distance that these plates can separate. The controlling parameters are density (distance between clay particles) and pore fluid salinity (and composition), with a secondary influence of temperature.

The development of swelling pressure in MX-80 bentonite at densities relevant to the GFM and HCB has been studied by many laboratories. There are a number of methods available to generate swelling pressure values, rigid-wall constant-volume cells, triaxial consolidation tests and uniaxial consolidation cells. All have been used at various times and all provide a measure of bentonite swelling pressure at a known density. Although they should all provide the same value for swelling pressure for a given dry density, they unfortunately have some limitations with their comparability and speed with which testing can be accomplished. The most commonly used method to measure swelling pressure is use of the rigid-wall constant-volume cell and has the least complicated measuring system, requiring only a load measuring device to determine swelling pressure. Other methods allow for potentially substantial changes in specimen volume to occur before pressure-volume equilibrium is achieved and this may result in challenges in defining the density and swelling pressure associated with the specimen.

5.5.2.1 Role of Density and Pore Fluid Salinity

As with many other properties of bentonite materials, the swelling pressure developed is a function of the montmorillonite content, the density to which the montmorillonite is compacted,

and the chemical composition of the water associated with it. These parameters have been well characterised in many laboratory testing programs (examples are provided in Figure 5-19) and the results are combined in Figure 5-20. The data presented in Figure 5-19 is for MX-80 bentonite-only and was sourced from numerous papers including those by Bag 2011; Barone et al. 2014; Bucher et al. 1986; Dixon et al. 2018; Karnland 1998, Karnland et al. 2007; Ouyang & Daemen 1992; Pusch 1980a; Stroes-Gascoyne et al. 2006, 2010a; Dixon and Miller 1995; Dixon et al. 1986, 1996a,b, 2018. This allows for evaluation of the behaviour of MX-80 and the degree of scatter in the swelling pressure data obtained through use of similar testing methods.

An extensive body of data has been developed regarding the swelling pressure – specimen density relationship for MX-80 bentonite. Additionally, there is a large volume of data available on other high montmorillonite-content bentonites. The behaviour of these other bentonite materials can be combined with that of MX-80 through use of a normalizing parameter that accounts for differences in the swelling clay (montmorillonite) content between the materials. This parameter is the Effective Montmorillonite Dry Density (EMDD) discussed in Section 5.3.2 with respect to water activity and bacterial viability. However, for the purposes of this report, the focus will be on MX-80 and so dry density is used when discussing swelling pressure.

The swelling pressure in MX-80 can be described using exponential relationships that show a clear pattern of decreasing swelling pressure with increasing pore-fluid salinity for a given dry density (as is presented in Figure 5-20). However, when the literature data is combined, the pattern of reducing swelling pressure with TDS is still present but considerable overlap in data is evident at high (>1400 kg/m^3) density and modest (<~100 g/L) TDS.

Although there is still limited data available for MX-80 bentonite at high density and high salinity, there appears to be a limit to the TDS that affects swelling pressure. Figure 5-20 presents the swelling pressure – dry density in two ways, one plotted as dry density versus swelling pressure with swelling pressure shown on log scale and secondly as a linear – linear plot. Given the exponential nature of swelling pressure with regards to dry density, the log-linear scale allows for clearer presentation of data at very low salinity. Plotting of the data in a linear manner allows for swelling pressure behaviour over the range of density of interest to NWMO (1400-1700 kg/m^3) to be more clearly visualized with respect to the effect of pore fluid salinity. It would also appear that at very high density the effects of salinity become less evident. This can be attributed to the very close proximity of the clay particles to one-another and the strengthening of the interaction of the interlay charges due to this spacing.

The presence of even a modest TDS in the pore fluid (5-10 g/L) results in a notable decrease in the swelling pressure observed, particularly at lower density. This pattern of decreasing swelling pressure with increasing TDS is evident over the entire range of bentonite density of interest for a DGR. Of note is that it would appear that for specimens having TDS > 223 g/L (SR-L) salinity increase does not seem to result in decrease in the swelling pressure developed. This is of particular interest to the NWMO DGR option for sedimentary rock, where TDS could be in the 200-350 g/L range. This lack of influence of very high TDS on swelling pressure is attributable to the interaction of the pore fluid with the montmorillonite surfaces under these high TDS conditions. At such high TDS levels, the potential for additional interaction with the mineral surfaces is minimal as all possible cation-mineral interaction for a given dry density is already accomplished. The nature of the volume available for development of diffuse-double-layer volumes and hence influence of TDS at various dry densities is discussed in more detail by Dixon (1995); Karnland (1998) and Bag (2011). Equations describing the best-fit lines and prediction bands for MX-80 bentonite under several pore fluid salinity conditions at room temperature are provided in Appendix E and are summarized in Table 5-5. These equations are

the exponential equations that provide the best-fit lines for the 95% confidence limits and their associated prediction bands. The range in the prediction bands are very large, reflecting both data scatter and also the limited number of measurements available, particularly for high-TDS systems.

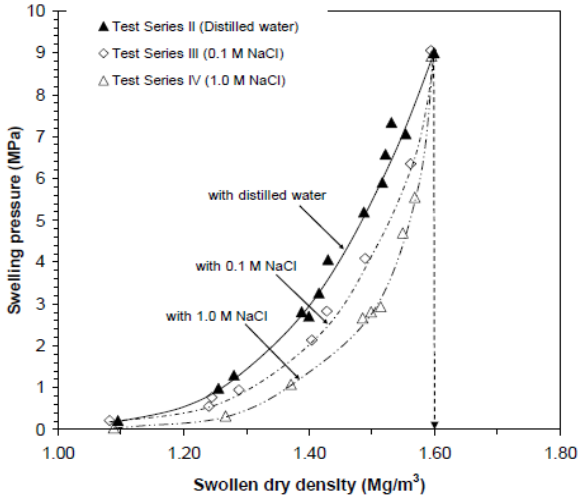

(Bag 2011)

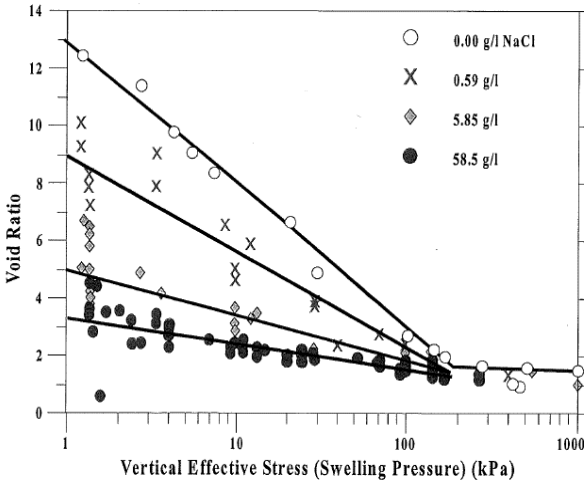

(Studds et al. 1998)

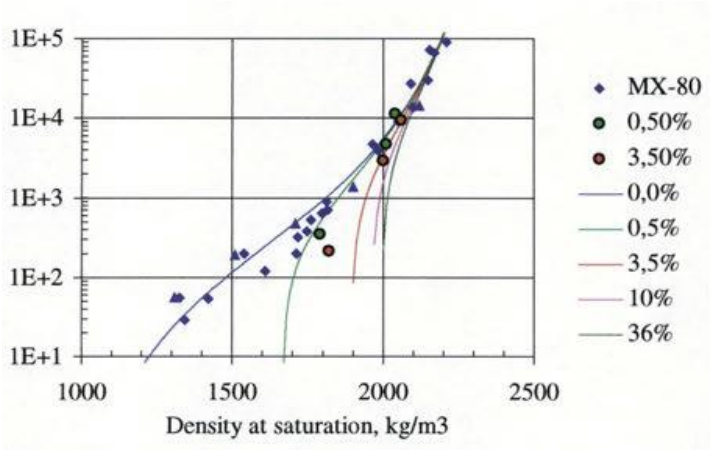

(Karnland 1998)

Figure 5-19: Examples of Studies on the Influence of TDS on Swelling Pressure.

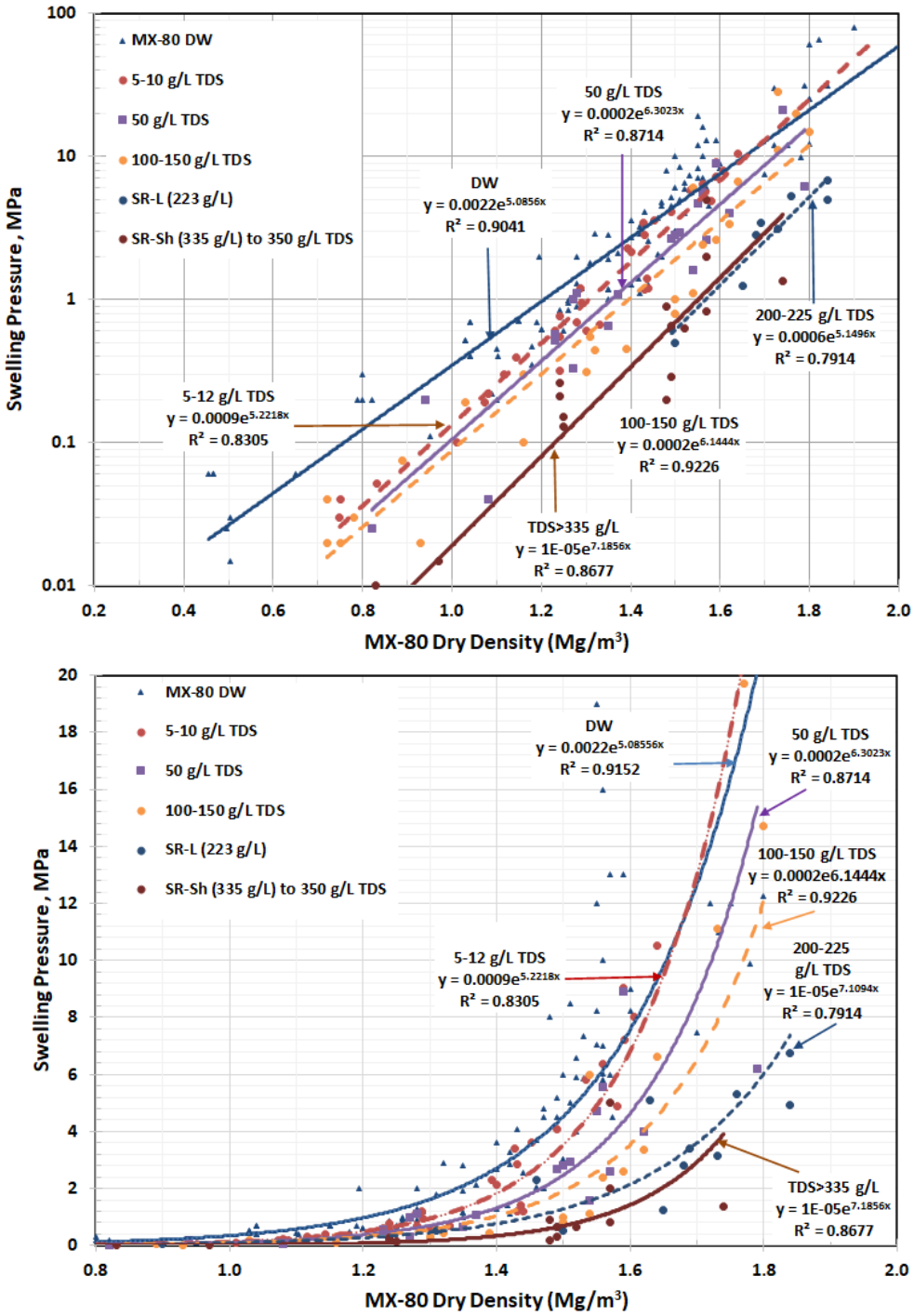

Figure 5-20: Influence of Density and Pore Fluid Salinity on Swelling Pressure of MX-80

Table 5-5: MX-80 Swelling Pressure @ 25°C for Various Pore Fluid Salinities

Solution TDS (g/L)	Equation	# of data points (n)	Ps @ 1400 kg/m^3 (MPa)	Ps @ 1600 kg/m^3 (MPa)	Ps @ 1700 kg/m^3 (MPa)
0	Ps = 0.0022e$^{5.0856DD}$ Prediction interval*	109	2.76 0.82 - 9.41	7.52 2.29 – 26.2	12.51 3.83 – 43.8
5-12	Ps = 0.0009e$^{5.2218DD}$ Prediction interval*	40	1.35 0.32 – 6.22	3.83 0.96 - 18.83	6.45 1.63 - 31.5
50	PS = 0.0002e$^{6.3023DD}$ Prediction interval*	21	1.36 0.26 - 7.94	4.79 0.96 – 27.0	9.0 1.83 - 49.8
100-150	Ps = 0.0002e$^{6.1444DD}$ Prediction interval*	25	1.09 0.18– 5.56	3.72 0.61 – 18.82	6.87 1.13 – 34.61
200-225 (SR-L)	Ps = 0.0006e$^{5.1496DD}$ Prediction interval*	14	0.81 0.09 – 7.4	2.27 0.28 – 18.5	3.80 0.50 – 29.2
>335 (SR-Sh)	Ps = 0.00001e$^{7.1856DD}$ Prediction interval*	16	0.23 0.03 – 3.62	0.98 0.13 – 14.7	2.02 0.28 – 29.6

Where Ps is swelling pressure (MPa) and DD is dry density (Mg/m^3). Data used and Equations generated are provided in Appendix E.
* PI is envelope within which 95% of data is predicted to be found.

5.5.2.2 Statistical Evaluation of Swelling Pressure Data

The data swelling pressure data presented in Section 5.5.2.1 and whose best-fit equations are provided in Table 5-5 were statistically analysed in order to determine their confidence and prediction bands. The analyses were undertaken using the methodology outlined in Section 5.2.2.3. The results of these statistical analyses are summarized in Appendix E. The statistical evaluations provided in Table 5-5 show the very wide ranges associated with the 95% prediction bands. The reasons for this variability in the results are similar to those described for hydraulic conductivity and are likely associated with material variability (including mineralogical and TDS uncertainties) and testing method (e.g. is density determined as-placed or as-measured at end of test). The measurement of swelling pressure, like hydraulic conductivity is complicated by the need to be able to identify equipment malfunctions (e.g. water leakage), which can be a challenge when testing at the pressures and low water flow conditions present when testing this type of material.

5.5.2.3 Influence of Temperature on Swelling Pressure

The majority of the swelling pressure data for bentonite materials has been collected at room temperature. The HCB and GFM installed in the DGR will however be exposed to considerably elevated temperatures as well as temperature gradients.

The effects of temperature on the swelling of bentonite has been examined by numerous researchers (Bag 2011; Komine and Ogata 1998; Lee et al. 2010a; Cho et al. 2000; Oscarson and Dixon 1990; Dixon et al. (1997); Pusch 1980a; Romero et al. 2001; Tang et al. 2007, 2008a,b; Tang and Cui 2009, 2010; Villar and Lloret 2004; Villar et al. 2002, 2010), Figure 5-21. The results of these studies were inconsistent, with substantial reduction in swelling pressure observed as the result of increased temperature in some studies (e.g. Lee et al. 2010a). In other studies, there was no discernible change or in some cases an increase in swelling pressure was reported. It is important to understand the conditions the tests were done under, in some cases the specimens were heated and then tested while still under elevated temperature and in others the specimens were exposed to elevated temperature and then cooled before testing. Each researcher used different methods to obtain their measurements

and in some cases the methodologies used are poorly documented or contain technical uncertainties making comparison of results difficult.

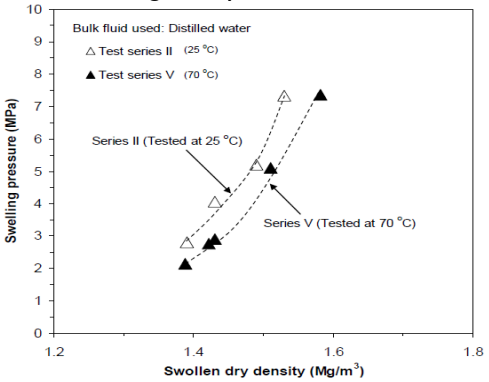

Bag (2011)

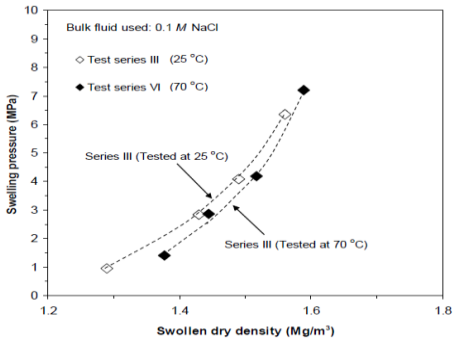

Bag (2011)

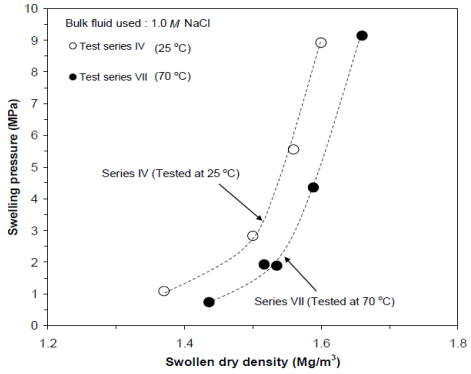

Bag (2011)

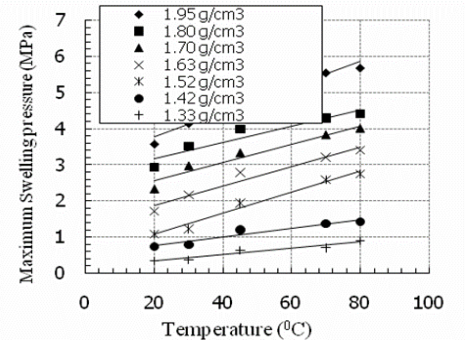

Shirazi et al. (2010)

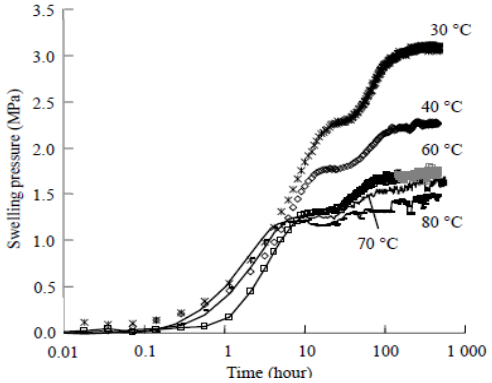

Villar et al. (2010)

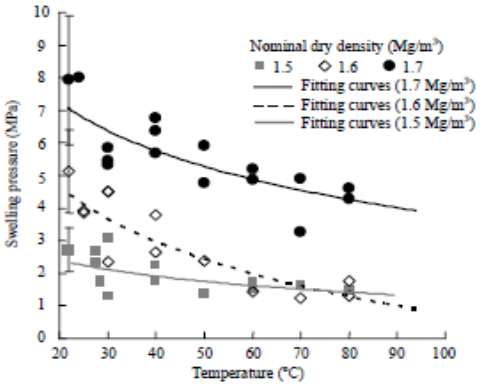

Villar et al. (2010)

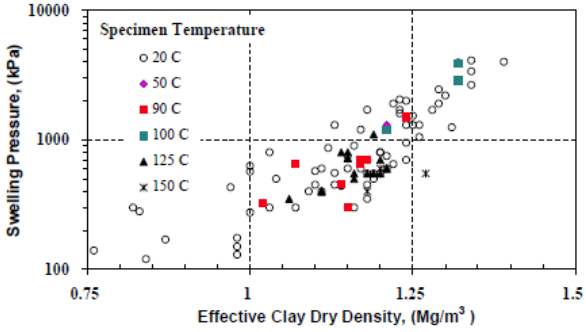

Dixon et al. (1997)

Figure 5-21: Effect of Temperature on Swelling Pressure Developed by MX-80 Bentonite

Observations related to the effects of temperature on swelling pressure include:

- Pusch (1980a) examined the swelling pressure of saturated MX-80 bentonite having dry density of approximately 1200 and 1850 kg/m^3 at temperatures of 20 and 90^{o}C as well as under different TDS conditions. Salinities examined ranged from freshwater to approximately 35 g/L TDS. It was observed that the swelling pressure reduced approximately 50% when temperature was increased from 20 to 90^{o}C.
- Bag (2011) examined the effect of elevated temperature on swelling pressure of MX-80 bentonite in freshwater and also pore fluids having approximately 6 and 58 g/L TDS. He reported that the swelling pressures measured at 70 °C were lower than those measured at ambient temperature (see Figure 5-21).
- Villar and Lloret (2004), Villar (2002), Villar et al. (2010) as shown in Figure 5-21, and Lee et al. (2010) also reported substantial decrease in swelling pressures for various bentonites when comparing results at room temperature to those obtained from testing at 80^{o}C.
- In contrast Shirazi et al. (2010) and Lee et al. (2010a) reported substantial increase in swelling pressure with increasing temperature as shown in Figure 5-21.
- Oscarson and Dixon (1989; 1990) examined the behaviour of bentonite-sand specimens that were heated to 90 to 150^{o}C under unsaturated conditions and then tested at elevated temperature or following cooling. They observed that there was no significant effect of temperature or heating on swelling pressure or hydraulic conductivity of saturated or unsaturated materials (Dixon et al. 1997).

The results provided above can be compared to the theoretical relationships outlined by Mitchell (1993) where it was determined that an increase in temperature results in an increase in the diffuse double layer thickness between clay platelets, decreases the surface potential and the dielectric constant of pore fluid. When taken together, these would predict a slight decrease in the swelling pressure of MX-80 bentonite with increase in temperature (Bag 2011). As noted above, there is however limited and conflicting data available with which to develop numerical estimates for the exact amount of swelling pressure change with temperature increase.

5.5.3 Bentonite homogenization

In a freshwater environment swelling pressure is at its maximum. There is typically a very rapid initial pressure development as water is drawn into the interlayer spaces between the bentonite particles and the clay attempts to expand and accommodate this. As hydration progresses water uptake generally slows as new water must move through already hydrated material where water is strongly adsorbed and not readily available for transfer. This can also be described as a reduction in the osmotic gradient between the free pore water and the water associated with the diffuse double layer. Additionally, the suction-induced hydraulic gradient between the region supplying the water and the montmorillonite further from the source decreases rapidly as water enters the unsaturated clay.

During the period of incomplete saturation there will be swelling-induced forces acting across the bentonite-filled regions, with hydrated regions applying compressive swelling pressures on unsaturated regions. The result is a complex process of clay swelling in the hydrated regions, consolidation of the unsaturated volume and then a counter consolidation as the densified formerly unsaturated regions hydrate and swell, consolidating materials that had previously compressed it as well as regions that are not yet saturated. This can be a very slow process in dense bentonites, where water supply from the outer surface of the bentonite is slow or large volumes of bentonite are involved but has been observed as density differences or gradients in

large-scale sealing tests (Dixon and Chandler 2000; Dixon et al. 1997; Martino et al. 2008). Non-uniform development of swelling pressure over relatively short time-scales has also been documented in laboratory tests where unlimited supply of water was provided on one end of a rigidly confined specimen (Pusch 1980a, Dixon et al. 1996 and Lee et al. 2010b) (Figure 5-22).

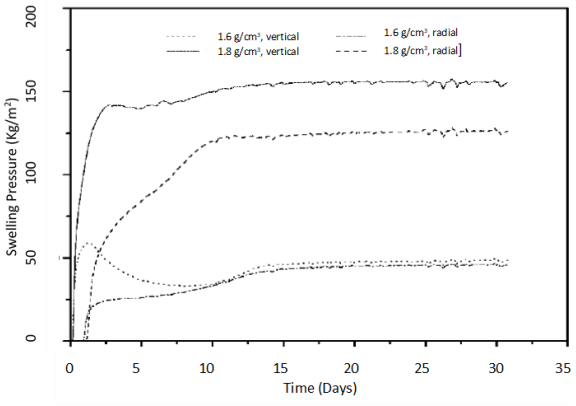

(Lee et al. 2010b)

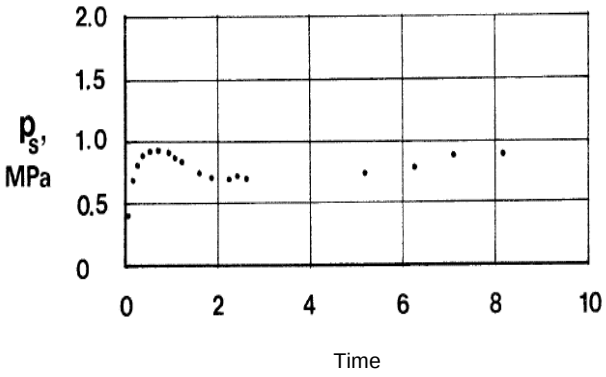

(Pusch 1980a)

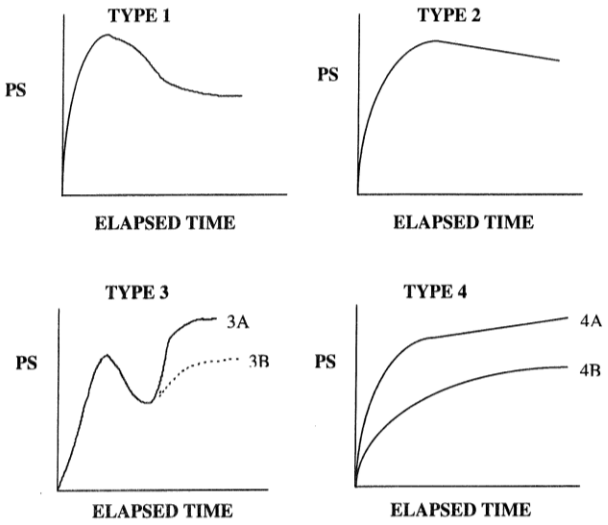

(Dixon et al. 1996)

Figure 5-22: Observed Patterns of Swelling Pressure Development in Bentonite

The degree to which density homogeneity will ultimately develop in fully-saturated bentonite systems is also an important consideration. As noted above, the water uptake process is going to be relatively slow and density equilibration will be even slower as bentonite swells and applies swelling pressure-induced consolidation or develops expansive forces within the placement room fill and its confinement. The issue of density homogenization has been examined and it can be concluded that some degree of density anisotropy may persist over the very long term within the bentonite-filled volumes in a DGR.

5.5.4 Secondary Process Effects: Cementation, Mineral Dissolution and Microbes

The processes resulting in removal or precipitation (cementation) on the hydraulic behaviour of bentonite materials was discussed in Section 5.4. There is limited evidence for cementation or dissolution of smectite that is substantial enough to alter the swelling pressure or hydraulic

behaviour of bentonite over the near-term. As summarized in Section 5.4, the development of cementation that could substantially reduce the swelling pressure of bentonite is likely to be limited to a narrow region immediately adjacent to concrete structures or massive sources of iron. Regions further removed from these features are expected to retain their unaltered swelling performance and thereby provide for enough swelling pressure to accommodate any volume strain requirements that might arise provided that the system remains confined.

Dissolution of smectite as the result of unfavourable geochemical conditions is likely to be limited to those regions where high pH persists. In those regions, other minerals and amorphous silica and alumina materials naturally present in the bentonite are likely to be more susceptible to alteration and would react before the bentonite. The result would be a highly localized zone of limited smectite mineral dissolution, with adjacent unaltered materials still providing the swelling capacity required of the HCB-GFM region.

The presence of a viable or active bacteria population in the HCB or density-equilibrated HCB-GFM system is unlikely for the reasons outlined in Section 5.4. If bacterial activity is present, it is likely to be confined to interface regions between the bentonite and the surrounding host rock (or concrete structures), where there may be sufficient occluded porosity or inadequately consolidated bentonite for bacteria to be active if porewater and temperature conditions are tolerable. These limited regions are insufficient to result in any bacterially-induced change in swelling pressure of the bentonite further removed from these areas. As noted previously, high temperature and high salinity conditions will also result in a severely limited bacteria population and activity.

5.5.5 Summary

Swelling pressure within water-saturated bentonite materials is primarily affected by smectite content, clay density and the salinity of the permeating fluid. There are additional environmental factors such a temperature, precipitate deposition, interaction with UFC corrosion products, interaction with highly alkaline pore fluids and bacteria activity that have been identified as potential materials and processes that could affect swelling pressure. In particular, the effects of temperature on swelling pressure need to be better understood and demonstrated. Generally, the other processes described above have been concluded to be of secondary importance or localized importance in terms of swelling pressure development, particularly in dense systems.

5.6 GAS TRANSPORT THROUGH HCB AND GFM

5.6.1 Gas Transport Process

Knowing the manner in which gas (and air) moves through the HCB and GFM components in the placement room is important for a number of reasons, including:

- Immediately following HCB and GFM installation in a wet environment (water entering placement room during installation which is a possibility in the granitic geosphere option), the air present in the pore spaces of the HCB and the GFM will begin to be compressed if it is not able to escape. This may result in compression of the air and then rapid decompression as the result of gas breakthrough to unfilled and unpressurized portions of the placement room. Additionally, trapped air in a dry placement room can represent a substantial portion of the porosity and ultimately this air needs to be able to escape from the placement room, either by dissolution into the surrounding groundwater or by migration. Otherwise it will be compressed to hydrostatic pressures (~1 MPa/100 m of water head in a freshwater environment, and as much as

~1.2 MPa/100m in a brine environment), as groundwater enters the sealed placement room.

- During initial system heating and pore fluid redistribution, not only the fluid component will be required to move but also the gas component, rising temperature in the placement room will also result in expansion of the trapped air and hence if prevented from escaping, gas pressure will increase.
- During gradual water uptake from the rock mass, the air/gas component will be compressed and/or forced to move to regions of lower fluid/gas pressure.
- Over the long-term, internal repository processes including water radiolysis, UFC corrosion and bacteria activity will all result in the generation of gas (mostly hydrogen) within the placement room, mostly in the region adjacent to the UFCs. This gas must either move into and through the bentonite-filled volume or else considerable gas pressures may develop, ultimately this might result in mechanical fracturing of the buffer material and rapid movement of gas from one location within the repository to another or even into fracture features that intersect the repository.

Movement of gas into and through the bentonite sealing materials is primarily controlled by the degree of water saturation as air/gas will move through the clay pores. There are also environmental conditions that will change the manner in which gas moves through bentonite. These include the pore fluid composition (water viscosity and reduced soil suction), ambient temperature, pore-size distribution in the clay, microbial activity, and gas composition. Dixon et al. (2018) fit air permeability curves generated from laboratory tests on MX-80 at 1500 kg/m^3 dry density using the van Genuchten-Mualem-Luckner model (Van Genuchten 1980). The curves provided in Figure 5-22 can be described by the following relationships:

$$k_{rg} = (1 - S_{ek})^{1/3} (1 - S_{ek}^{1/m})^{2m} \qquad \textbf{5-8}$$

$$S_{ek} = (S_l - S_{lr}) / (1 - S_{lr} - S_{gr}) \qquad \textbf{5-9}$$

where: k_{rg} = gas phase relative permeability (ratio);
k_g = gas phase permeability (m^2);
S_{ek} = effective saturation (volume ratio);
S_l = liquid saturation (volume ratio);
S_{lr} = residual liquid saturation (volume ratio);
S_{gr} = residual gas saturation (volume ratio); and
m = van Genuchten fitting parameter (unitless).

The gas permeability (k_g) can be calculated by multiplication of the liquid permeability (k) by the relative permeability (k_{rg}):

$$k_g = k_{rg} * k \qquad \textbf{5-10}$$

A summary of the parameters used in the gas (air) conductivity fitting functions that generated Figure 5-23 is shown in Table 5-6. In the case of Figure 5-23 and Table 5-6, the gas examined was air, hence the terms K_a and k_a are used to describe behaviour rather than K_g and k_g.

Figure 5-23 presents the data from Barone et al. (2014) for dense MX-80 for several pore fluid compositions (0 to 270 g/L TDS). These data show the same trends as observed for the 1500 kg/m^3 MX-80 from Dixon et al. (2018), excepting that the air conductivity for the denser materials was substantially lower, particularly at degrees of water saturation that exceed approximately 80%. This is to be expected since the volume of voids is substantially larger at lower density and so at the same degree of fluid saturation the volume of air (gas) - conductive

voids would be larger. Beyond approximately 80% saturation, the voids become disconnected and so ease of gas movement through them decreases rapidly.

Table 5-6. Curve-Fitting Functions for Air Conductivity and Air Permeability Curves.

	m	K_a* (m^2)	k_a* (m/s)	S_{gr}	S_{ir}
Barone et al. (2014), MX-80 @ ~1750-1800 kg/m^3					
DW	1.19	1.8E-13	1.0E-7	0.01	0
CR-10, 11 g/L	1.30	2.5E-13	1.4E-07	0.02	0
SR-160, 160 g/L	1.08	9.0E-14	5.0E-08	0.10	0
SR-270, 270 g/L	0.90	5.4E-14	3.0E-08	0.10	0
Dixon et al. (2018), MX-80 @ ~1500 kg/m^3					
DW	1.24	3.2E-12	1.759E-06	0.11	0
SR-L, 223 g/L	1.34	2.7E-12	1.513E-06	0.06	0
SR-Sh, 335 g/L	1.02	8.8E-13	4.872E-07	0.16	0

* value at 0% water saturation. To convert coefficient of air permeability (m^2) to air (gas) conductivity (m/s), air permeability is multiplied by 5.6E-05.

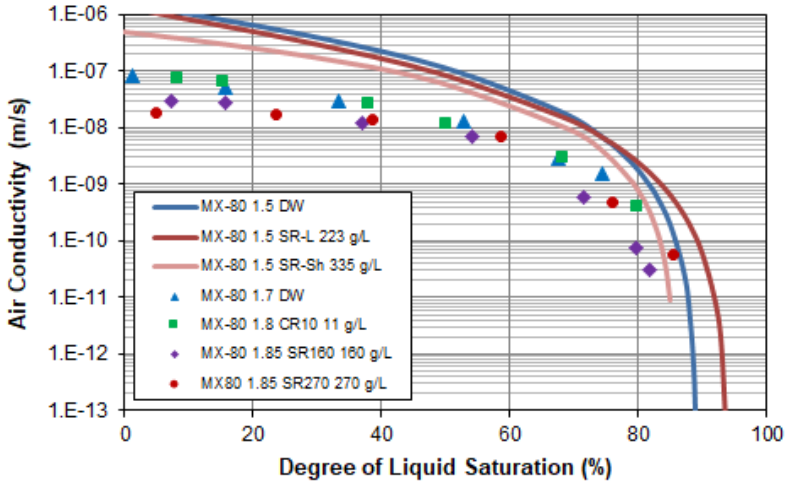

Figure 5-23: Effect of Density and Degree of Saturation on Air Conductivity (k_a)
(after Dixon et al. 2018, Barone et al. 2014)

The data and observations of Barone et al. (2014) and Dixon et al. (2018) are consistent with those of Gutiérrez-Rodrigo et al. (2014) who examined gas movement in MX-80 and FEBEX bentonites having dry densities in the range of 1500 to 1800 kg/m^3. They observed that gas permeability was dominated by the dry density with a 3 order-of-magnitude reduction when density was increased from 1500 to 1800 kg/m^3 at the same water content. Increasing water content also resulted in a decrease in gas permeability. They concluded that gas permeability was primarily related to accessible porosity for gas movement. A further effect of the granularity of the source material for specimen compaction was also noted with finer-grained bentonite (MX-80) having a lower gas permeability than for the coarser-grained FEBEX material.

5.6.2 Identification of Potential Influences on Gas Transport

There are several factors that can affect gas movement within the bentonite and through the placement room.

- The first potential influence on gas transport is not necessarily associated with the bentonite or engineered barrier system, it is the ability of the geosphere and in particular, the excavation damaged zone (EDZ) in the rock located immediately next to the bentonite. This zone of rock can potentially act as a short-cut for gas movement through the repository unless it is physically interrupted. In a repository environment where there is bentonite saturation of less than approximately 70-80%, gas will move relatively easily within the placement room and in a situation where considerable gas is being generated, this gas will migrate outwards to the EDZ and the surrounding geosphere. Depending on the nature of gas and the geosphere, should the gas contain radiological components, this could compromise barrier effectiveness. In contrast, in a highly saturated system, should gas be generated through processes such as iron corrosion in a UFC where the copper coating has been breached, gas migration away from the UFC will be resisted by the water-filled voids. This could in theory result in a situation where gas pressures rise to a point where it equals (or exceeds) the hydrostatic head at the repository location and ultimately gas may induce buffer fracture (or desaturation) allowing gas to move outwards to the rock-bentonite contact where movement via the EDZ is easier.
- Another factor that could influence gas transport would be cementation of the pore volume by precipitation of no-longer soluble minerals in the pore water in the macro voids. This will result in a localized reduction in the soil porosity as well as a disproportionate reduction of macro-voids where gas and fluid transport is less restricted. It has not however been demonstrated that soil cementation can actually occur at sufficient levels or uniformly enough to discernibly affect gas or water movement through bentonite. Of more concern would be the development of a more brittle soil structure and a tendency for the bentonite to be less able to re-seal should gas pressures induce fracturing of the bentonite. Again, this process has not be demonstrated to be particularly relevant in the DGR environment.
- A further potential influence on gas movement (and generation) within the bentonite-filled regions is that of bacterial activity. Microbes have the potential to (a) intrude into pores as they grow, (b) generate corrosion-inducing compounds that could influence UFC corrosion and hence gas generation, and (c) generate gas as the result of their metabolic processes. As discussed previously, there is little evidence that conditions within a DGR will be conducive to bacterial activity at levels that would result in any of these processes becoming a concern. The high suction of the bentonite and saline groundwater conditions are extremely unfavourable for bacterial activity and under conditions of extreme temperature and partial saturation that could be encountered adjacent to the UFCs, it is even less likely that bacterial activity will be of relevance to gas generation and movement.
- The presence of interfaces or joints between sealing materials (e.g. between HCB blocks, between HCB and GFM or contact with the surrounding rock mass) has the potential to provide preferential gas transport pathways that will negate the effectiveness of the bulk sealing materials. These interfaces will be present in the period following construction and may persist for a considerable period after water saturation is achieved and density equilibration is ongoing. In a study reported by Dixon et al. (1993, 2003) and Dixon and Kohle (2003), it was observed that these interfaces will tend to close and present resistance to flow (water) similar to that of an intact mass. This provides

evidence that such preferential pathways for gas migration may also disappear as the system saturates.

5.6.3 Summary

The movement of gas through bentonite materials is primarily determined by its density, the degree of water saturation and to a lesser extent the nature of the pore fluid. It has been observed that:

- gas permeability decreases with clay density,
- gas permeability decreases with increasing degree of water saturation
- gas permeability decreases slightly with increasing pore fluid salinity

It might also be expected that gas permeability will increase with increasing temperature as a result of decreased viscosity of the fluid and gas phases, although this may in part be offset by the slightly reduced porosity induced by thermally-induced expansion of the mineral components.

5.7 SUCTION - MOISTURE CHARACTERISTICS OF HCB, GFM AND EQUILIBRATED SEALING SYSTEM

5.7.1 Drying Shrinkage of HCB and Gap Fill Material

Shrinkage of the HCB and GFM components is a phenomenon that occurs as the result of moisture loss from the bentonite due to either thermally- or suction-induced drying. As the HCB components will be installed at the same density and moisture content throughout the placement room, there is certain to be a redistribution of the moisture within it as the temperature adjacent to the UFCs increases. Moisture will migrate from the regions closest to the UFC towards the cooler perimeter where the bentonite GFM is in contact with the rock. This process is well demonstrated by field tests (e.g. Buffer/Container Experiment (Dixon et al. 1997); SKB Temperature Buffer Test (Hökmark 2003) and Febex (Gens et al. 2009)).

Basic shrinkage tests on MX-80 were done by Dixon et al. (2018) and Barone et al. (2014) and involved specimens compacted to a known initial dry density and moisture content that were then exposed to the laboratory environment (~20 °C and ambient humidity conditions). Water was allowed to evaporate (or sorb) naturally with the mass and volume of each specimen measured at least once per day. On reaching mass and volume steady-state, they were oven dried at 50 ˚C until mass and volume equilibrium was once again achieved. A final oven-drying step at 110 °C was completed and the final mass and volume was determined for each specimen. Drying at 110 ˚C was done in order to consistently remove the non-structural water and to confirm that volume change was essentially complete.

As noted by Dixon et al. (2018), the presence of brine pore fluid is a complicating factor regarding interpretation of system behaviour. In a high humidity environment, the brine may absorb water from the atmosphere as the result of the high suction generated by the salt solution. Additionally, or alternatively, when drying of a saline system occurs, the fluid loss will be slowed by the suction caused by the saline fluid and as fluid weight loss occurs only the water component is lost, salts remain behind. This means that as drying progresses the salinity of the remaining pore fluid is steadily increasing, which will affect subsequent shrinkage behaviour and complicate interpretation (e.g. changing density of the pore fluid and hence fluid saturation) is difficult to assess. Salinity also affects the suction present within the specimen (the greater the salinity the greater the suction applied to the air adjacent to the specimen and

the tighter it will hold onto water associated with salt). Ultimately, when dried at 105°C there will be a considerable quantity of salts (mostly as solids), present in the specimen's pores and some water will remain associated with these salts. The presence of brine pore fluid means that when using the standard method for water content determination (drying at 110°C), the calculated gravimetric water content determined for freshwater systems will be discernibly higher than for a brine system and determination of actual dry density will be complicated by a need to account for residual salt and its associated water.

The drying shrinkage of MX-80 bentonite at approximately 1500 kg/m^3 and 1700 kg/m^3 initial density was determined by Dixon et al. (2018) and Abootalebi (2016, 2017), respectively. Clear differences were observed in the behavior of materials having freshwater as a pore fluid versus a brine solution (Figure 5-24):

- At 1500 kg/m^3 initial dry density, the freshwater specimens shrank approximately 23% while the brine systems shrank only 18%. In a freshwater-saturated material having initial dry densities of 1500 kg/m^3 this corresponds to fully-desiccated dry density of approximately 1950 kg/m^3 as shown in Figure 5-24. A brine-saturated specimen exhibited a density increase to only approximately 1800 kg/m^3. The reduced change in volume will be a result of the combined effects of suction reduction and precipitation of salt crystals from the porefluid and hence reduced ability of the material to shrink.
- At 1700 kg/m^3 initial dry density, and freshwater as the pore fluid, complete drying resulted in a material that also reached approximately 1.95 kg/m^3 density. Similarly, the presence of a brine pore fluid resulted in a final dry density in the order of 1800 kg/m^3.
- Brine solutions having TDS > 223 g/L TDS (SR-L) showed little influence of increasing salinity on the shrinkage behavior.
- Differences in shrinkage is attributable to reduced suction by the minerals caused by presence of salts and the formation of salt crystals or salt-slurry in the pore spaces that prevent further shrinkage.
- The drying shrinkage of a bentonite material having saline porefluid is also reported by Abootalebi (2016) to be strongly affected by the texture of the source material with fine-grained (e.g. 200 mesh) materials exhibiting almost twice the shrinkage as observed for the coarser-textured MX80 (80 mesh).

Barone et al. (2014) summarized influences on shrinkage behavior as follows:

"The rate-and-magnitude of drying shrinkage is primarily influenced by the key parameters of:

- *Density to which the sample is compacted: This will define the porosity of the sample and hence the volume that is potentially available to be involved in any volume change. In most soils there is a porosity below which further drying will not result in further shrinkage.*
- *Surface area available for evaporation/condensation: This will determine the rate and manner in which water can be lost from the block, larger blocks will lose moisture more slowly due to the distance required for moisture to move to the surface and subsequently evaporate. This will also affect the shrinkage magnitude since other macro-processes such as cracking may be more evident in larger blocks than small ones.*
- *Relative humidity of the surrounding atmosphere: The surrounding atmospheric conditions will strongly affect the drying and shrinkage behavior. The presence of low-humidity atmospheric conditions will tend to accelerate drying, give the blocks less opportunity to adjust to moisture loss without inducing cracks or substantial volume change. In contrast, where the atmosphere is very humid, there may actually be a water uptake (and swelling) by the backfill in response to the higher suction present in the soil pore space.*
- *Salinity of the water present in the pores: This parameter has several important influences on the volume and moisture evolution of the shaft backfill. Under low salinity*

conditions the processes listed above in bullets 1 through 3 above will dominate the samples drying behavior. At high porewater salinity (e.g. SR160 and SR270), the salts will play a very important role in defining how the volume of compacted materials will change. Both of these solutions contain very high TDS contents, which mean they have a very high suction present in the internal pores and will also influence their immediate surroundings. These materials will tend to lose moisture much more slowly than low salinity materials. "

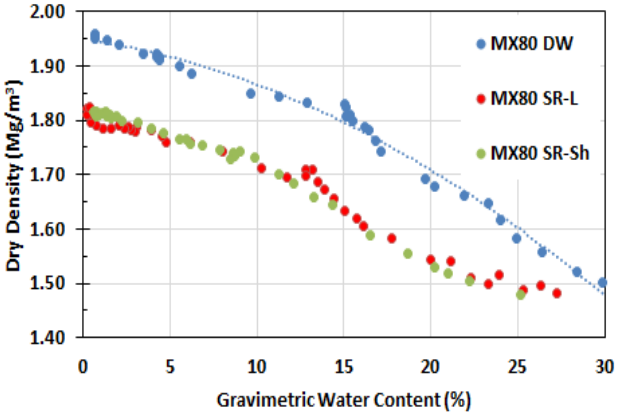

1500 kg/m^3 Dixon et al. (2018)

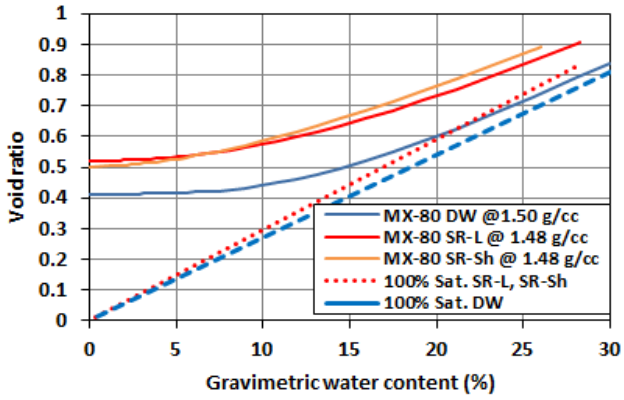

1500 kg/m^3 (Dixon et al. 2018)

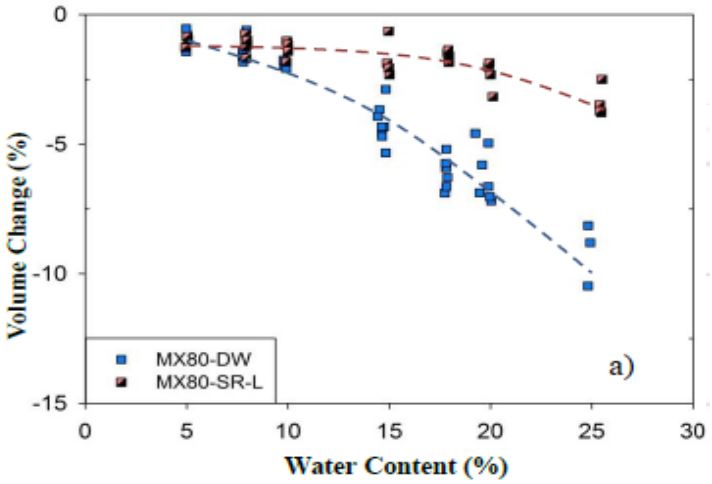

1700 kg/m^3 Abootalebi (2016)

Figure 5-24: Drying Shrinkage of MX-80 Bentonite @ 1500 and 1700 kg/m^3 Dry Density (Dixon et al. 2018; Abootalebi 2016)

The equation and fitting parameters used to generate the drying shrinkage best-fit lines were developed by Fredlund et al. (2002) using the equation below and are provided in Table 5-7

$$e = a_{sh} * (w^{csh}/b_{sh}^{csh}+1)^{(1/csh)} \qquad 5\text{-}11$$

where e =void ratio, w = gravimetric water content (%), a_{sh}, b_{sh} and c_{sh} are fitting parameters provided in Table 5-7, where a_{sh} is the minimum void ratio, b_{sh} is the slope of the line of tangency, and c_{sh} is the curvature of the shrinkage curve.

It should be noted that the drying shrinkage information provided in Figure 5-23 is for compacted bentonite that starts off at very high degree of saturation and remains intact. The drying shrinkage behaviour shown in Figure 5-24 is for a high-degree of saturation GFM or HCB that is density homogeneous and cohesive. Materials such as dry GFM or fissured HCB would not show the same behaviour as described above and might show smaller net shrinkage for a given moisture content due to the presence of fissures and cracks. Development of cracks and fissures will also change the T-H-M response of the buffer and GFM system as the result of the air-filled volumes associated with them.

Table 5-7: Fitting Parameter Values Used to Estimate Shrinkage in MX-80 (Dixon et al. 2018)

	a_{sh}	b_{sh}	c_{sh}
MX-80 DW	0.4129	0.1518	3.3804
MX-80 SR-L (223 g/L TDS)	0.5211	0.1916	2.1701
MX-80-SR-Sh (335 g/L TDS)	0.5024	0.1847	1.8341

5.7.2 Soil Water Characteristic Curves (SWCC)

The soil-water characteristic curve (SWCC), also referred to as the water retention curve, presents the relationship between the quantity of water in a soil and the negative pore water pressure, or soil suction that is holding this water in place for a continuously drying (or wetting) specimen. These suction tests provide a measure of the resistance to desaturation, water uptake and storage capacity of the bentonite materials. During wetting or drying, the change in water present is typically accompanied with change in specimen volume (void ratio) as described in Section 5.6.1 as well as changes in the size and size distribution of the individual pores. When drying occurs as the result of increasing external suction, water loss is first associated with the removal of weakly held “free” water from the macro-pores or clay surfaces. This is followed by the loss of water from continuous pores and water held loosely by the particle surfaces. The final drying phase involves loss of residual (or strongly bonded) water from the discontinuous water phase and a portion of the electrochemically-associated surface water. The strongly held water component associated with the montmorillonite surfaces as described in Figure 5-18 may remain depending on the drying conditions. This may mean that although there is a change in water content, the specimen will remain nearly fully saturated for a considerable range of suction simply by undergoing volumetric shrinkage to accommodate moisture loss.

The stepwise change in the strength with which water is held by bentonite materials is illustrated conceptually in Figure 5-25. Figure 5-25 also shows that hysteresis in the wetting and drying cycle for soils should also be observed in bentonite materials. The movement of water into and out of bentonite will therefore be determined by local conditions and changes in the pore structure of the bentonite as the result of local moisture conditions.

The SWCC is typically presented in terms of degree of fluid saturation, gravimetric or volumetric water content versus capillary pressure (suction). The SWCC behaviour of bentonite can be determined using several methods (Bag 2011; Barone et al. 2014; Dixon et al. 2018; Seiphoori 2015; Villar et al. 2005). Due to the high suctions generated by bentonite, the SWCC is usually generated using a combined data set that is generated by tests that are suited to specific ranges of suction. Work by Bag (2011); Barone et al. (2014); Dixon et al. (2018); Seiphoori

(2015) and Villar and Gomez-Espina (2008) Villar et al. (2005) determined the SWCC for MX-80 by combining the results obtained using the same approach and methods. Firstly, a pressure-plate device was used to measure the lower portion of the SWCC (suctions from 200 to 1500 kPa). Next, a chilled mirror device such as a WP4 measured the upper portion of the SWCC, from about 20,000 to 300,000 kPa (ASTM D 6836-02). Data was then combined to generate the complete SWCC. There are other methods that can also be used to determine the SWCC characteristic curve (Barone et al. 2014; Dixon et al. 2018; and Seiphoori 2015), including use of relative humidity (suction) sensors as described by Villar et al. (2005) and Bag (2011).

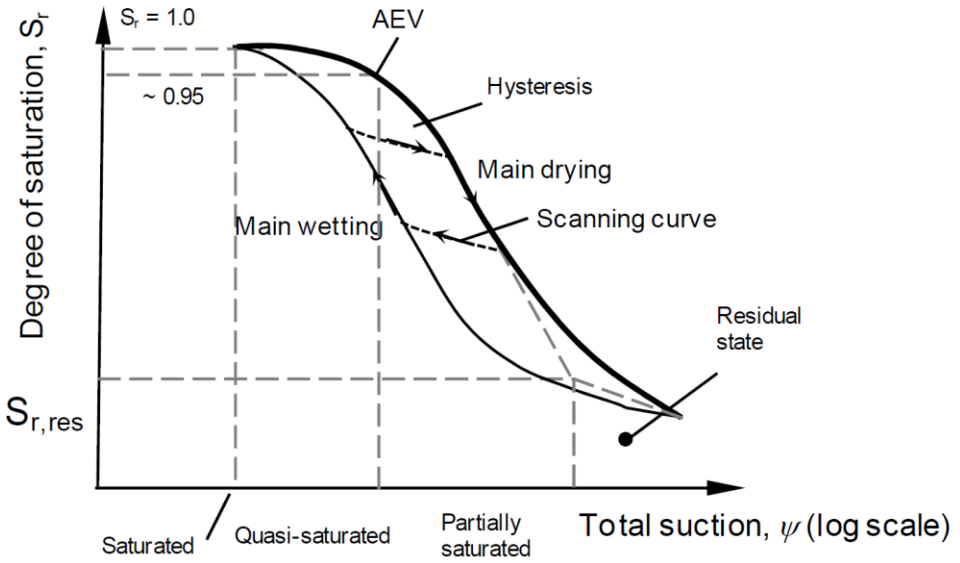

Figure 5-25: Stepwise Change in Water Content as the Result of Suction (Seiphoori 2015)

Using the methodology described by Bag (2011), Barone et al. (2014), Dixon et al. (2018), Tripathy et al. (2014); and Seiphoori (2015) the SWCC behaviour of the clay is based on the assumption that the capillary pressure (resistance of soil capillaries to desaturation (suction)) is equal to the air pressure used to induce desaturation. This means that the chilled mirror device and the relative humidity in the air immediately above the specimens provide a measure of the total suction in the specimen itself. The measured SWCC and shrinkage curve described in Section 5.7.1 and the specific gravity of the material are then combined to determine the relationship between degree of saturation and suction.

$$\textbf{Total suction } (\psi) = (-\rho_w RT/M_w)/\ln(RH) \qquad \textbf{5-12}$$

where R is the universal gas constant (i.e. 8.3143 J/mol K), ρ_w is water density, M_w is the molecular mass of water, RH is the relative humidity and T is the absolute temperature (K) of the sample. The suction-moisture (saturation) curves are typically described using the fitted SWCC curves generated using the van Genuchten model. These curves can be given the equation below and parameter values associated with the SWCC are provided in Table 5-8. Capillary pressure (suction) is derived as follows (Dixon et al. 2018):

$$P_c = -(1/\alpha)(S_{ec}^{-1/m} - 1)^{1/n} \qquad \textbf{5-13}$$

$$S_{ec} = (S_l - S_{lr}) / (1 - S_{lr}) \qquad \textbf{5-14}$$

where: P_c = capillary pressure (Pa), S_{ec} = effective saturation (volume ratio), S_l = liquid saturation (volume ratio), S_{lr} = residual liquid saturation (volume ratio), α = van Genuchten fitting parameter (1/Pa), m = van Genuchten fitting parameter (unitless), and n = van Genuchten fitting parameter (unitless).

The data presented in Figure 5-26 clearly illustrates the sensitivity of the SWCC to water content over the dry density range of 1500 to 1800 kg/m^3. Suction is clearly determined by the mass of water present. Using the data shown in Figure 5-25 and determining the suction associated with 95% saturation, the air-entry value (AEV) can be determined (see Figure 5-25). The change of AEV with void ratio is illustrated in Figure 5-27 and shows the changes in SWCC and AEV with the direction the specimen is moving (wetting or drying), although the hysteresis in the behaviour appears to be reversible.

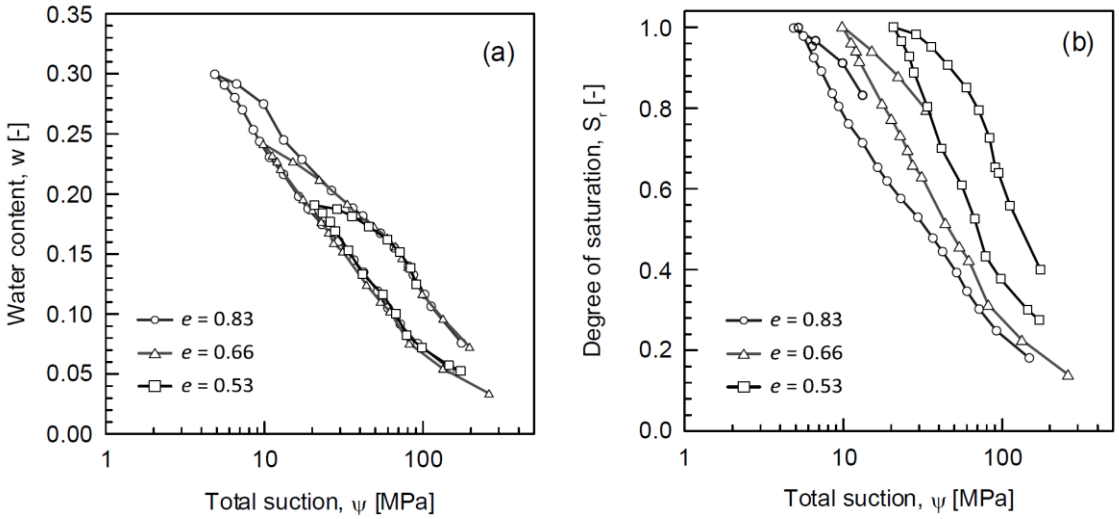

Figure 5-26: SWCC Curves of Wetting and Drying of MX-80 Bentonite (Seiphoori 2015)
(*e=0.53, 0.66 and 0.83 correspond to dry densities of 1800, 1650 and 1500 kg/m^3 respectively*)

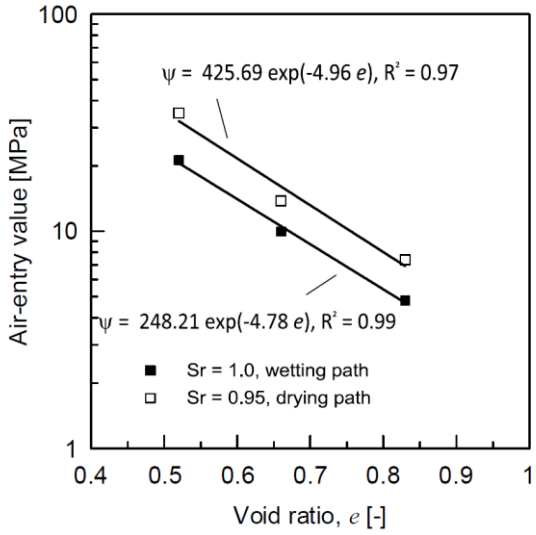

Figure 5-27: Air-Entry Values for MX-80 Bentonite (Seiphoori 2015)
(e=0.53, 0.66 and 0.83 correspond to dry densities of 1800, 1650 and 1500 kg/m^3 respectively)

The data of Bag (2011), Barone et al. (2014) and Dixon et al. (2018) are combined in Figure 5-28 and show slight offsets in their curves but they clearly follow the same trend of increasing suction with decreasing saturation (water content). The relative insensitivity of the SWCC to the density of the clay is also shown in Figure 5-27 and this is consistent with observations made by Jacinto et al. (2007, 2009), Villar and Lloret (2004); Tang and Cui (2010) and Bag (2011). Jacinto et al. (2009) concluded that beyond the 30 MPa suction the effect of dry density change in compacted bentonites will not be significant. This is of significance as this would relate to a degree of saturation of <70% in MX-80 materials. The equation associated with the data from Dixon et al. (2018) is provided below and the parameter values are provided in Table 5-8. These SWCC curves are defined as follows:

$$P_c = (1 / \alpha) (S_{ec}^{-1/m} - 1)^{1/n} \qquad 5\text{-}15$$

$$S_{ec} = (S_l - S_{lr}) / (1 - S_{lr}) \qquad 5\text{-}16$$

where: P_c = capillary pressure (Pa), S_{ec} = effective saturation (volume ratio), S_l = liquid saturation (volume ratio), S_{lr} = residual liquid saturation (volume ratio), α = van Genuchten fitting parameter (1/Pa), m = van Genuchten fitting parameter (unitless), and n = van Genuchten fitting parameter (unitless).

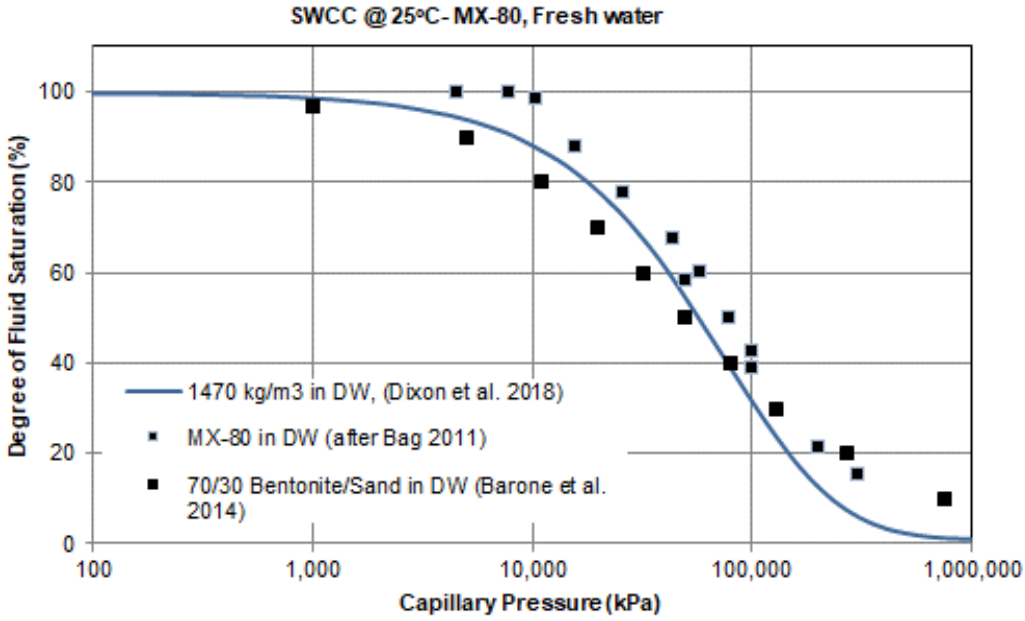

Figure 5-28: SWCC for MX-80 Under Freshwater Conditions

5.7.3 Influence of Temperature on Suction in MX-80

There is limited information available regarding the influence of temperature on the suction – moisture relationship for bentonite. As summarized by Bag (2011), Seiphoori (2015) and Villar and Lloret (2004), the water retention capacity of unsaturated soil at elevated temperature reduces slightly between the temperature of 22 and 40°C (Figure 5-29) due to change in the soil fabric and the surface tension of water (Romero et al. 2000; Villar and Lloret 2004; Tang and Cui 2005).

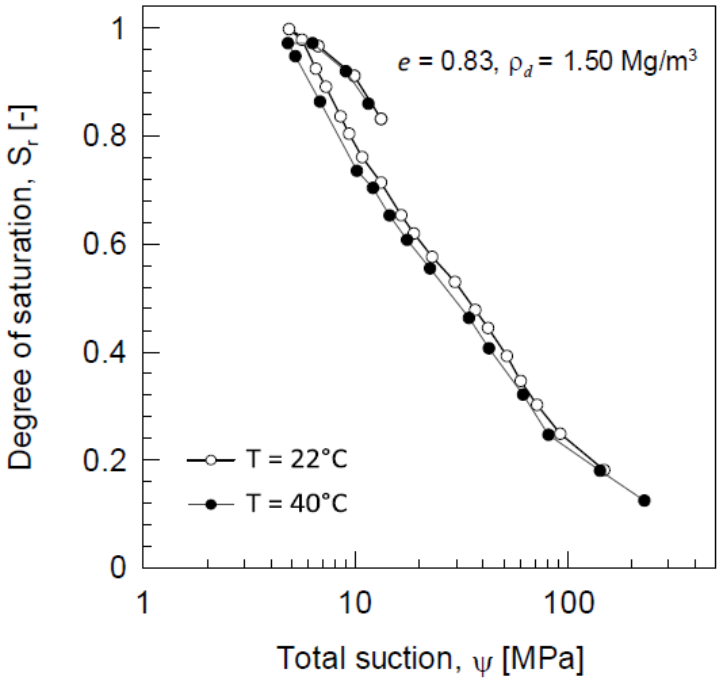

Figure 5-29: Effect of Small Increase in Temperature on Suction of MX-80
(Villar and Lloret 2004; Seiphoori 2015)

Klute (1986) observed that an increase in temperature leads to a reduction in water content of the soil at a given matric suction but the effect of temperature on suction-water content relationship is not very large. This is consistent with the observations of Jacinto et al. (2009), who reported that at higher suctions (low degree of saturation), an increase in the dry density or temperature will not have a significant influence on the SWCC behavior of compacted bentonite. A replot of the data from Villar and Gomez-Espina (2008) shown in Figure 5-30, indicates a substantial effect of high temperature on SWCC behaviour, with suction decreasing with temperature increase at a given degree of water saturation as well as decreasing with lowering of the specimen density. The decrease in suction is attributed to change in degree of water saturation as the result of thermal expansion and transfer of water from the tightly-bonded interlayer sites where its dry density is >1000 kg/m^3 (Villar and Gomez-Espina, 2008) to the larger pore spaces where its dry density is closer to 1000 kg/m^3. As a result, although the mass of water has not changed, the volume it occupies has increased, with resultant increase in degree of saturation and reduction in soil suction.

It should be noted that the data available on the effects of temperature on the SWCC is very limited for systems having high water content (near saturation) or at very low water content (<5%) and the relatively linear sections of the SWCC curves shown in Figures 5-29 and 5-30 will not be continued in the very low and very high suction regions since suction will trend towards 0 as degree of saturation approaches 100% as can be seen in Figure 5-28.

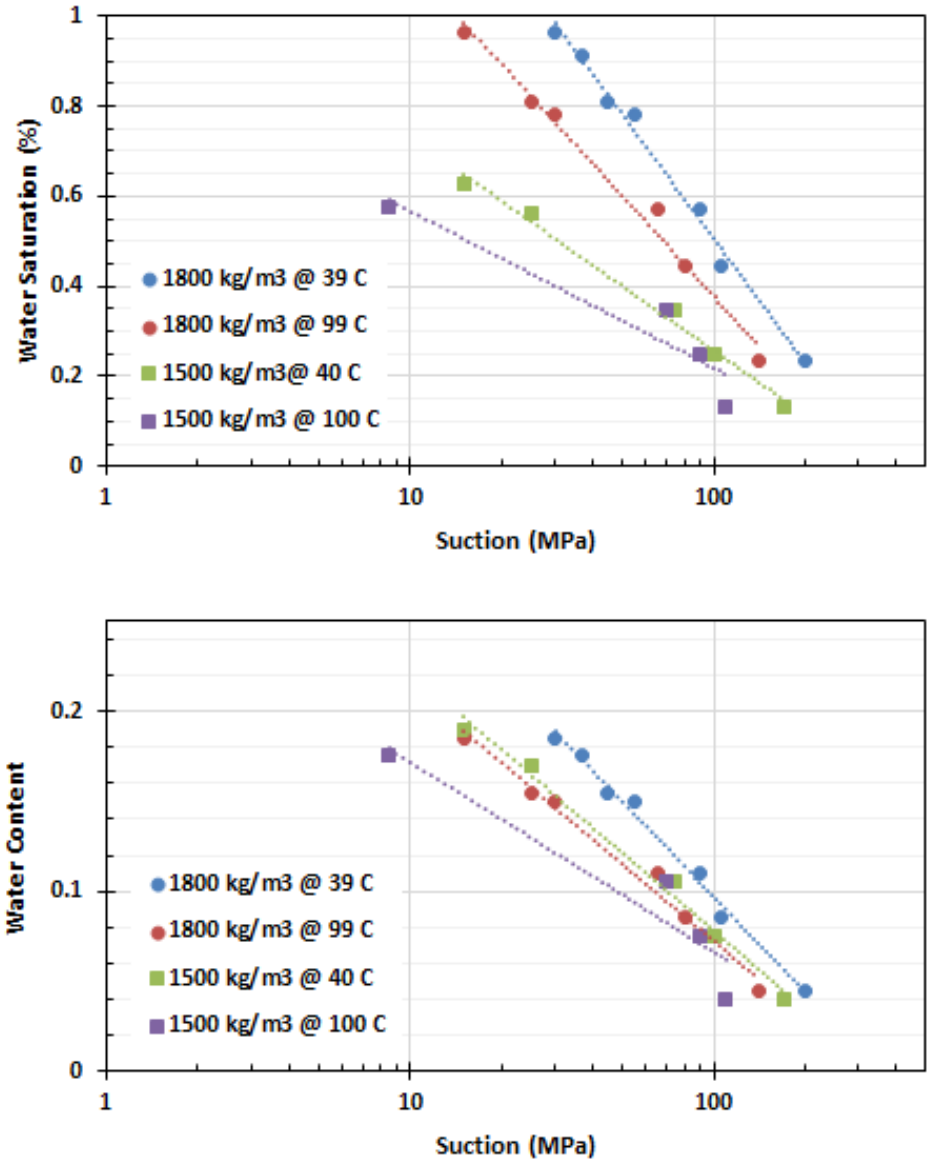

Figure 5-30: Effect of Density and Substantial Temperature Rise on Suction in MX-80
(after Villar and Gomez-Espina 2008, Villar et al. 2008)

5.7.4 Effect of Pore Fluid Salinity on Suction in MX-80

SWCC measurements have been completed by Barone et al. (2014) for MX-80 systems having freshwater and brine water associated with the clay. The results of previously unpublished tests commissioned by NWMO that examined the suction-moisture behaviour in the presence of the reference groundwater compositions are shown in Figure 5-31. The plot shows the substantial effect of pore water salinity on the suction -moisture behaviour of bentonite at densities relevant to the GFM. The suction required to desaturate (or saturate) the MX-80 increases for a given degree of saturation as the pore fluid salinity increases. The effect of salinity on suction seems to become less important when salinity exceeds that of the SR-L solution (223 g/L TDS). The shift in the suction-moisture curves can be attributed to the need for the atmospheric suction to

exceed that of the pore solution in order for moisture transfer to occur. Hence the extended suction range before desaturation occurs. Additionally, when the degree of saturation is less than approximately 20% there is little discernible effect of TDS on the suction measured. At this low level of water saturation, the majority of the remaining water is tightly held by the particle surfaces as well as precipitated salts in the pore spaces of the bentonite, so its removal is difficult.

The data for highly saline materials (SR-L and SR-Sh with 223 and 335 g/L TDS) from Dixon et al. (2018) and shown in Figure 5-30 were generated using the GCTS and WP4 devices and are combined to generate a plot of saturation versus suction and fitted using the van Genuchten (VG) curve fitting method to generate SWCC curves using the fitting parameters in Table 5-8.

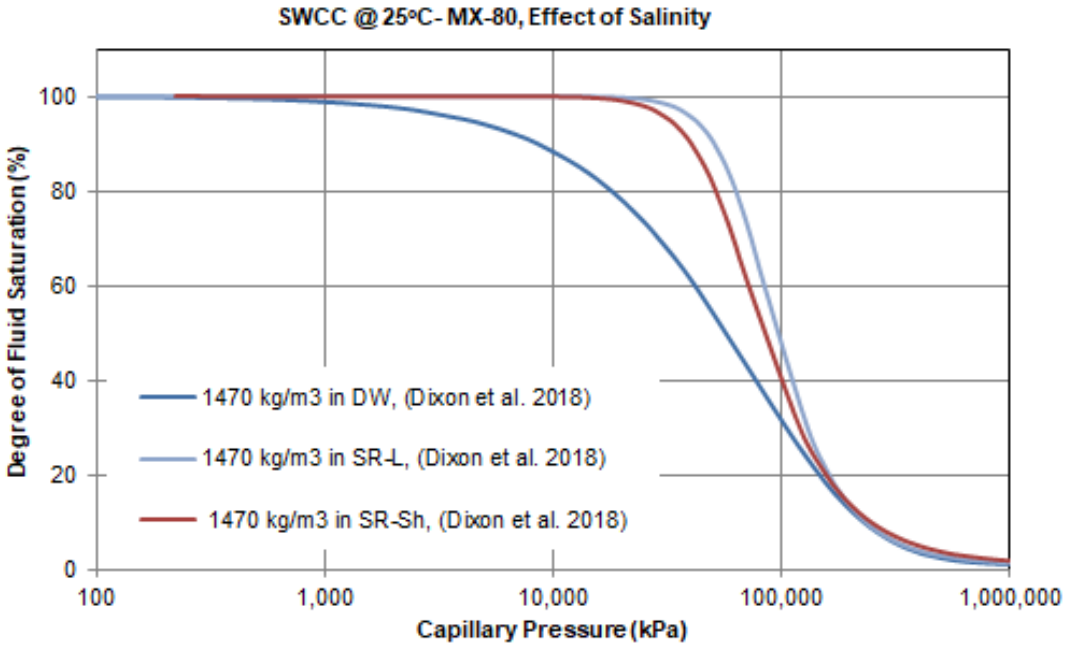

Figure 5-31: Influence of Pore Fluid Salinity on SWCC

Table 5-8: Equations Describing the SWCC Curves for MX-80 @ 25°C and Various TDS Conditions

	m	n	α (Pa^{-1})	S_{ir}
Dixon et al. (2018) for MX-80 @ 1470 kg/m^3				
DW	4.66	1.02	2.91E-09	0.01
SR-L	0.47	3.57	1.68E-08	0.01
SR-Sh	0.52	3.99	1.35E-08	0.01
Barone et al. (2014) for 70/30 MX80/Sand mix				
DI water	0.84	0.95	2.5E-08	0.01
CR10	0.80	1.10	2.0E-08	0.01
SR160	0.83	1.10	1.7E-08	0.01
SR270	1.00	1.40	1.2E-08	0.01

5.8 MECHANICAL PROPERTIES OF HCB AND GFM

5.8.1 Key Parameters associated with Mechanical behaviour

Knowledge of the mechanical behaviour of the HCB and GFM are critical in establishing the physical stability of the UFC in its as-placed position as well as load transfer within and across the backfilled placement rooms. These properties and environmental effects on them will determine how the sealing system components interact with one another as well as with the surrounding geological medium.

Amongst the more important mechanical properties processes and parameters that will affect the mechanical behaviour of the HCB and GFM are:

- Consolidation characteristics under both saturated and unsaturated conditions;
- Mechanical strength, tensile and compressive;
- Non-failure elasto-plastic deformation parameters; and
- Failure behaviour of saturated and unsaturated HCB materials.

5.8.2 Uniaxial (1-Dimensional) Consolidation Behaviour

The consolidation behaviour of HCB needs to be known as part of developing confidence in the ability to understand and predict the movement of a UFC within the placement room. The HCB that makes up the buffer box surrounding the UFC as well as the spacer blocks installed between them will experience a degree of movement as the result of the load induced by the UFC as well as interaction between fully-hydrated regions and those that are not yet fully saturated.

One-dimensional (1-D) consolidation tests are useful as they provide supplemental data regarding the elastic and hardening parameters determined from the triaxial tests. The 1D tests provide values for deformation indices including the coefficient of consolidation (Cv), coefficient of volume compressibility (m_v), preconsolidation pressure (Pc), coefficients of compressibility (C_c) and swelling (C_s or C_r), which are needed in some mechanical models for soil deformation. For the purposes of this study the symbol C_s is used to describe the swelling index. How these parameters are extracted from the test data for conventional materials is shown in Figure 5-31 and described in Lambe and Whitman (1979), Mitchell (1993) and other conventional soil mechanics textbooks. The Cs, Cs and Pc parameters are obtained using ASTM D2435M-11 “Standards for oedometer tests”, or similar standards, whereby loads and load increments resist and overcome substantial initial strain due to clay swelling, and induce sufficient consolidation to allow for determination of the required parameters. Figure 5-32 also shows how these deformation parameters relate to deformation parameters κ and λ normally derived from triaxial tests (see Section 5.8.5).

Figure 5-33 shows the type of consolidation frames typically used in the conduct of these tests. Other designs of equipment are also available, but all accomplish the same goal of measuring vertical deformation as the result of application of a known load. Although an apparently simple test, there are considerable challenges to conduct tests on HCB, including: high swelling pressure development in freshwater conditions. These high swelling pressures make maintaining confinement of the bentonite in the sample ring problematic and considerable volume changes can occur. Considerable care must therefore be taken to ensure that the test has been successfully accomplished and that the results obtained are representative.

As the result of technical challenges in adequately confining and then consolidating specimens of HCB, there is limited data available on the 1-D consolidation behaviour of MX80 bentonite at densities of interest to NWMO's DGR. The 1-D behaviour of MX-80 bentonite under a range of groundwater salinity conditions have been presented by Baumgartner et al. (2008); Priyanto et al. (2008a, b); and Man and Martino (2009). When combined these data and recently obtained NWMO unpublished data show the behavioural patterns shown in Figure 5-34.

The dry density for MX80 consolidation tests presented in Figure 5-34 are in the order of those of interest in NWMO's Mark II geometry (1400 to 1700 kg/m^3) and show little or no influence of dry density on the Compression Index (Cc), Swelling Index (Cs) or Coefficient of Compressibility (Cv) parameters.

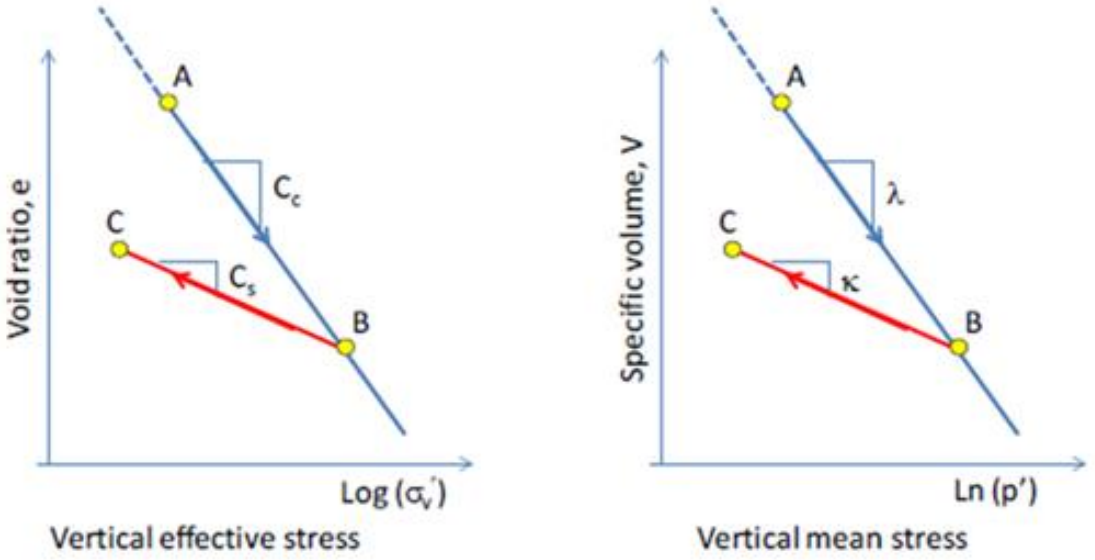

Figure 5-32: Derivation of the Parameters Cc, Cs in the 1-D Test (Priyanto et al. (2013)

Figure 5-33: Lever-Arm Oedometers Used in 1-D Consolidation Testing (Dixon et al. 2018)

Compression Index, Cc values show considerable scatter and average approximately 0.27 MPa^{-1} (with a range of approximately 0.10 to 0.43 for the majority of the data available), with no clear effect of density or TDS on the parameter value (Figure 5-34). The swelling index Cs isderived from the swelling of bentonite under reduced confining load. It is lower than the Cc and also shows considerable data scatter. Cs shows a slightly stronger apparent influence of density on the parameter value but the relationship between increasing density and decreasing Cs is weak. There is also an apparent decrease in the Cs value with increase in pore fluid TDS with an offset in values. The freshwater systems seem to show a trend of increasing Cs value with decreasing density, but the data is very limited. The observed behaviour is consistent with the effects of high cation concentration in reducing the swelling capacity of the bentonite. There is perhaps a weak trend for decreasing Cc with increasing porewater TDS but this is not certain given the degree of scatter in the data. As a result, it is reasonable to use the average values of Cc and Cs when considering the density range of interest (1400 to 1800 kg/m^3).

Coefficient of Consolidation (Cv) data shown in Figure 5-34, shows an apparent lack of influence of density on parameter value but shows a trend of slightly increasing value with increasing TDS. For the density range of interest (1400 to 1800 kg/m^3) it is reasonable to assume constant Cv values of 6.1×10^{-9} m^2/s and 7.9×10^{-9} m^2/s for freshwater and saline systems, respectively.

Preconsolidation Pressure, (Pc) is substantial for bentonite when compared to most conventional soils, this is a function of the strong electrical repulsive forces associated with the surfaces of the montmorillonite particles. The Pc is dominated by the swelling pressure at the density and salinity conditions present. Figure 5-34 shows the clear effect of pore fluid TDS on the swelling (and hence consolidation) behaviour of MX80. The Pc represents the load that will be necessary in order to initiate substantial consolidation of the MX80. Under freshwater conditions and as placed densities of approximately 1600 kg/m^3, the Pc is > 3.5 MPa and at elevated salinity this decreases to 0.35 to 0.4 MPa.

The Coefficient of Volume Change (m_v) presented in Figure 5-34, shows a clear separation of the data for freshwater and saline systems, with high TDS systems showing a discernibly higher value. Although the freshwater data is less abundant, there would seem to be no effect of density change over the range of densities examined (~1500 to 1800 kg/m^3). The observed higher m_v values for saline systems are consistent with the effects of reduced repulsive forces between adjacent bentonite particles. The m_v parameter value for freshwater conditions could be expected to be in the 10^{-6} to 10^{-5} m^2/kN. Under saline conditions the m_v increases to approximately 5×10^{-5} m^2/KN.

The observations above for consolidation tests on MX80 are consistent with those make by Castellanos et al. (2006) for a calcium bentonite, where salt concentrations in the pore fluid were observed to have a large effect on specimen consolidation but the salt-solution cations (e.g., Na+ and Ca2+) have little effect. Similarly, Dutta and Misra (2016) observed that bentonites consolidate faster in the presence of salt solution in comparison to water, Cc, m_v and t_{90} (t_{90} is the time required for completion of 90% of the consolidation resulting from a load increment during testing), of the bentonites decreased whereas Cv increased with the increase in salt concentration. Dutta and Misra (2016) also observed that bentonite with higher liquid limit and swelling capacity (e.g. higher montmorillonite content), exhibited higher values of t_{90}, m_v and Cc.

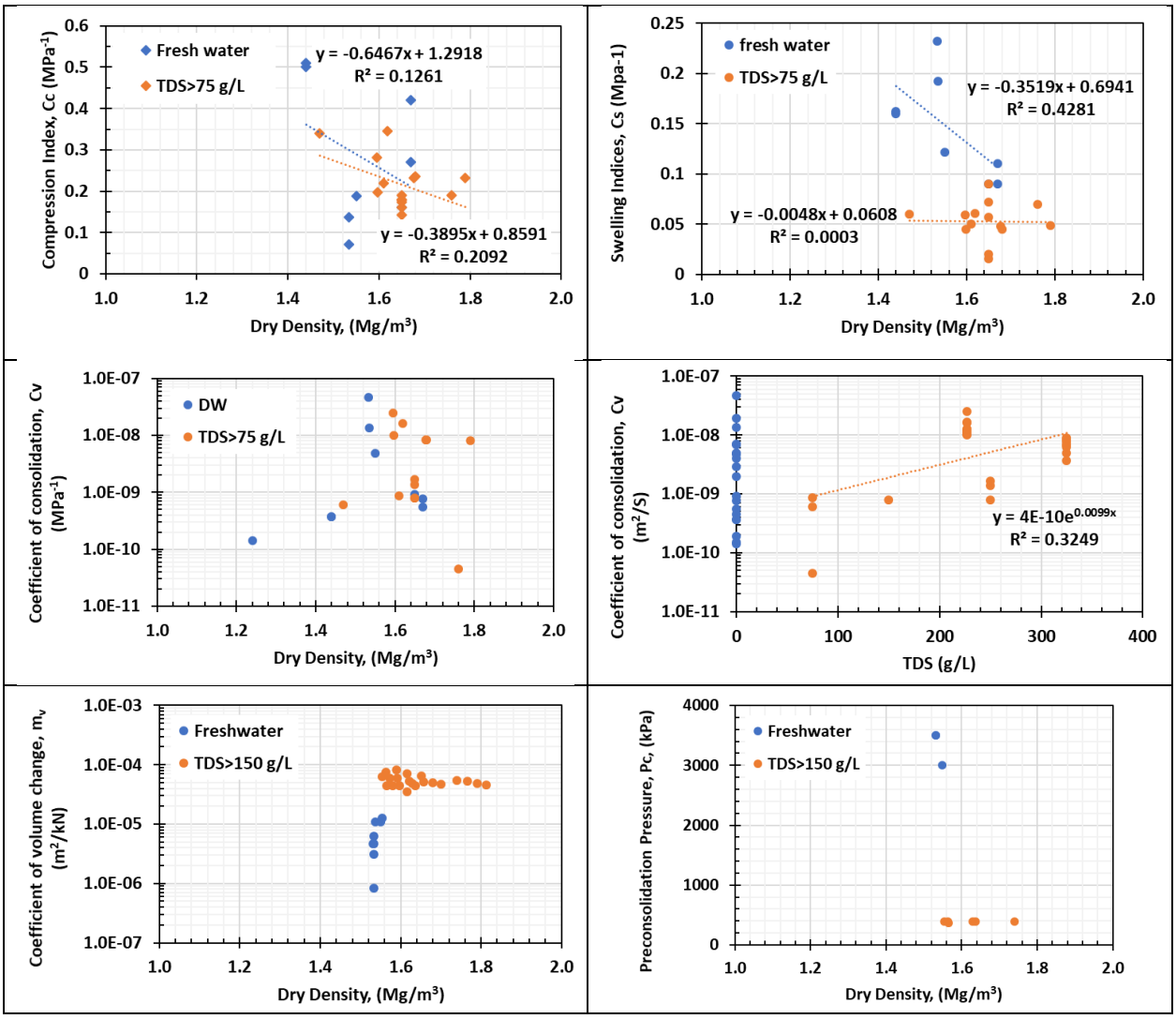

Figure 5-34: 1-D Consolidation Parameters for MX80 Bentonite

5.8.3 Tensile Strength

Under most anticipated conditions in NWMO's in-room placement geometry, the buffer will be under compression. However, it is possible that the system could experience brief periods where tensile forces are present (e.g. during buffer box or spacer-block handling and installation). Tensile forces may also come into play when there is a gap between the top section of the highly compacted block composing the upper portion of the buffer box and the UFC. Additionally, should there be an unanticipated gap between buffer-boxes and the spacer blocks, small regions within the buffer blocks, close to the location of the gap might also experience tension. In order to be able to properly model and assess such situations it is important to know the tensile behaviour of HCB.

Tensile strength and behaviour of HCB (MX80 or similar Wyoming bentonite), has been examined by Dixon et al. (2006), Pusch (2002), Kalbanter and Johnsson (2000), Johanesson et al. (2000) and Ritola and Pyy (2011). None of these studies used exactly the same method to determine tensile strength, providing some indication of the method-influence on measured tensile behaviour. The devices used are presented in Figure 5-35 through Figure 5-37.

- Dixon et al. (2006) determined tensile strength through use of pull-tests on compacted 50 mm-diameter by 100 mm length cylinders of HCB, utilizing the method described by Tang and Graham (2000) for testing bentonite-sand materials. In these tests, the specimens were compacted, glued lengthwise into a partial sleeve that left a substantial portion of the specimen unbonded and the specimen was then placed under tension through application of a fixed, slow rate of strain (0.030 mm/min extension) until the specimen split (as shown in Figure 5-35).
- Kalbanter and Johannesson (2000) used two testing techniques to examine the influence of procedure on the results obtained. The first was a three-load point tensile test on a prismatic sample of bentonite (Figure 5-36), and the second was a four-load point beam-bending test on the same type of cut prismatic sample.
- Pusch (2002) and Johannesson (1999) used a three-point measurement method that was similar to that of Kalbanter and Johannesson (2000).
- Ritola and Pyy (2011) undertook tensile tests using 75 mm radial diameter slices of HCB that were compressed in a splitting tensile strength test using the device shown in Figure 5-37.

Figure 5-35: Pull-Test, Tensile Strength Measurement of HCB (Dixon et al. 2006)

Figure 5-36: 3-Point Tensile Strength Test Setup (Eriksson 2016)

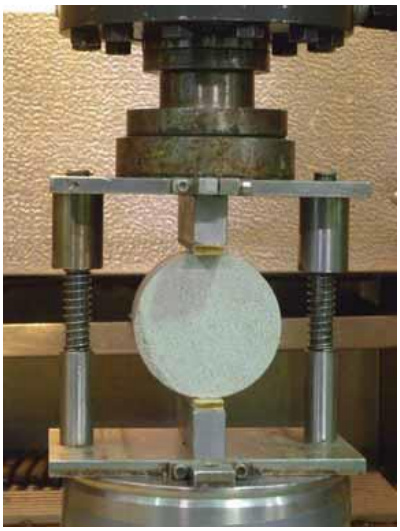

Figure 5-37: Tensile Strength Testing Device Used by Ritola and Pyy (2011).

The results of tensile strength testing of HCB materials are presented in Figure 5-38 and Figure 5-39. The data shows behaviour that is consistent with a soil material having considerable cohesive and tensile strength. HCB fails in a brittle manner with a sudden and complete mechanical rupture at peak tensile stress. The beam bending tests of Johannesson et al. (2000), Pusch (2002) and Kalbanter and Johannesson (2000), have the advantages of allowing a high degree of freedom as to where failure occurs but do not work well for soft or ductile materials. The methods of Dixon et al. (2006) and Ritola and Pyy (2011) are less sensitive to ductile material behaviour but force failure to occur through a relatively narrowly defined plane.

The HCB tests conducted by Johannesson et al. (2000), Kalbanter and Johannesson (2000), Ritola and Pyy (2011) and Pusch (2002) provide measurements of tensile strength at densities somewhat higher than those considered by NWMO but provide a check with regards to the comparability of the various techniques reported. The database available also only considers specimens where degree of saturation exceeds approximately 70%, and there is no information available for drier systems.

The data plotted in Figure 5-38 shows the influence of density and degree of saturation on the tensile strength behaviour of HCB. The tensile strength increases substantially with increasing dry density (and increasing porewater suction potential). It is however very clear that the techniques used to obtain these values result in very different tensile strength values. The methods of Dixon et al. (2006) and Ritola and Pyy (2011) seem to generate a consistent trendline of increasing tensile strength with increasing dry density. A second, equally consistent trendline showing a much higher tensile strength trendline for a given dry density is produced by the data from Pusch (2002) and Kalbanter and Johannesson (2000). The reason for such a difference in the trendlines may be attributable to the previously discussed differences in the manner in which failure occurs.

For the range of dry densities examined in all of these tests, there is perhaps a weak trend of increasing tensile strength with increasing degree of saturation (over range 70-100% saturation), as can be seen in Figure 5-39. The limited body of and scatter in available data makes it difficult to discern if there is a single strength-saturation trendline for systems having dry densities of 1600 to 1950 kg/m^3 dry density or there are actually a series of parallel lines.

Varying water content (saturation and suction potentials) of as-built HCB blocks could be expected to strongly influence the tensile strength of HCB since these forces act to pull the particles into contact and so must be overcome before tensile failure will occur. With this being the case, pore fluid composition should affect HCB tensile behaviour and strength. A reduction in the suction as the result of the presence of a saline pore fluid may result in a decrease in the tensile strength, however there was no literature located that addressed this aspect.

It should also be noted that none of the literature examined the effects of drying (and associated shrinkage and micro-cracking) on the tensile behaviour of HCB. These processes could be reasonably assumed to result in degradation of the tensile strength of HCB.

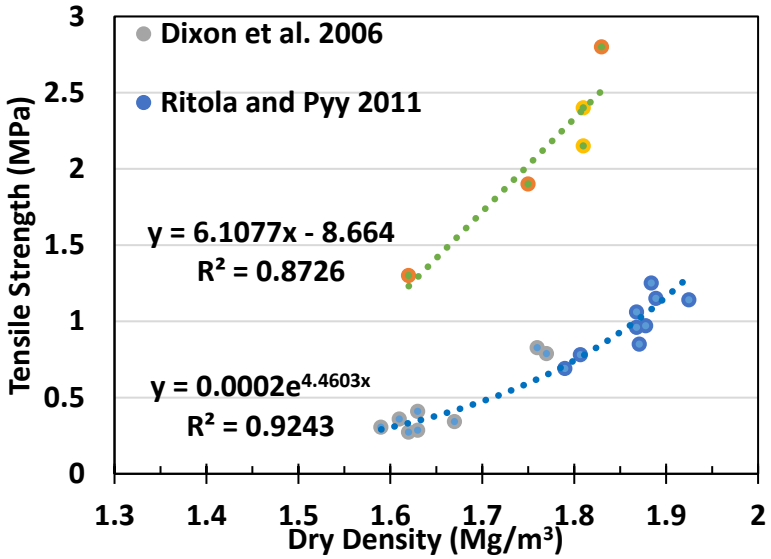

Figure 5-38: Effect of Dry Density on Tensile Strength with Degree of Saturation 75-85%

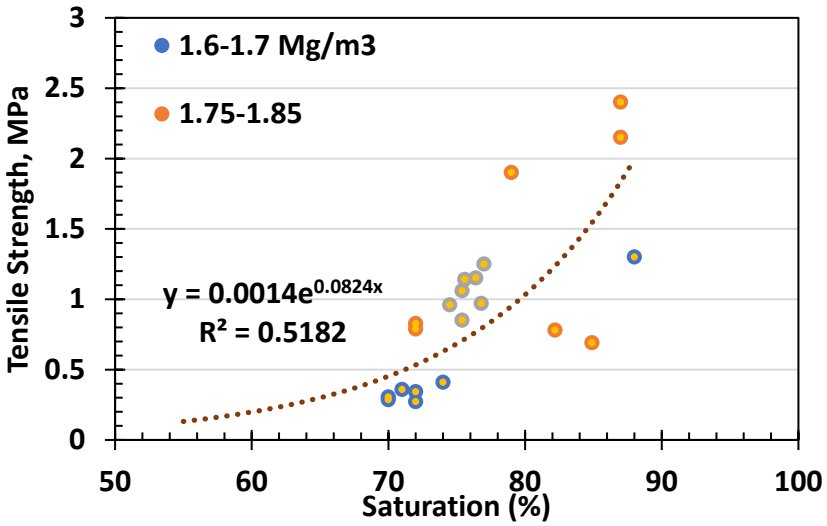

Figure 5-39: Effect of Degree of Saturation on Tensile Strength of HCB

The development of cementation bonds between clay particles would be expected to result in an increase in the tensile strength if it were uniformly distributed through the bentonite. In a heterogeneous distribution situation, it would have a much lesser influence since tensile failure could be expected to occur through the weakest region.

Based on the data presented in Figure 5-38 the tensile strength in HCB having a degree of saturation exceeding ~ 70% can be described in Equation 5-17a. Equation 5-17a is the more conservative of the two density-tensile strength relationships identified for freshwater systems. It would also appear that at degrees of water saturation less than approximately 70%, the as-built tensile strength of these materials is very low (estimated to be approximately 1/10th that of its compressive strength (Ritola and Pyy 2011), making it important to avoid situations where desiccated HCB is put into unsupported tension. In Equation 5-17b the more conservative (lower strength) data of Dixon et al. (2006) and Ritola and Pyy (2011) describing the relationship between specimen saturation and tensile strength is provided. The data used to generate this relationship shows great scatter and more information is required before this relationship can be used with confidence.

Tensile Strength = $0.0002e^{4.4603DD}$ **5-17a**

Or **Tensile Strength = $0.0014e^{0.0824S}$** **5-17b**

Where dry density (DD) is in Mg/m^3, VR is void ratio and strength is in MPa.

There was no data located that described the tensile properties or strengths of MX-80 under conditions of high pore fluid salinity. Based on shear strength information provided in Section 5.8.4 and 5.8.5 it might be expected that there will be a reduction in the tensile strength of MX-80 systems where the pore fluid is highly saline, but this needs to be confirmed through conduct of laboratory tests.

It was also noted by Ritola and Pyy (2011) that the tensile strength appears to be consistently approximately 1/10th of the compressive strength of highly compacted materials.

5.8.4 Compressive Strength

5.8.4.1 Background

The ability of the HCB to support the weight of the UFC without experiencing mechanical failure involving large movement of the failed material (and the UFC) within the placement room is a key behavioural requirement. The risk of undesirable movement due to mechanical failure of the HCB is greatest during its placement and in the period preceding installation of supporting gap fill materials. Once assembly is completed the HCB, and hence the UFC, has little room to move should mechanical failure occur. It is however important to understand what the mechanical loading limits are and how mechanical strength and deformation under load will change as the result of factors such as temperature, degree of saturation, density change and pore water salinity are considered.

The conduct of triaxial compression tests where the material being tested is first saturated in the triaxial cell (see Figure 5-40) and then sheared either allowing for water drainage from the specimen during shearing (drained) or sheared while not allowing water drainage (undrained) also provides strength data. Figure 5-40 shows the typical setup for a triaxial test presented by Börgesson et al. (1995). The methodology and equipment used has not changed substantially

in the 25 years since this early work on highly compacted bentonite. These tests provide compressive strength values as well as deformation parameters needed to evaluate the potential for long-term deformation of the bentonite under the mechanical load induced by the UFC. During these tests, the specimen is confined by a rubber membrane and a known water pressure is then applied to the exterior of the specimen with measurement of the pore pressure within the specimen also measured continuously. When the specimen comes into pressure/volume equilibrium and saturation is confirmed through conduct of a B-test, the specimen is sheared at a constant rate either with or without the drainage lines at the ends of the specimen being opened (drained and undrained tests).

The method commonly used to determine compressive strength in soil materials is use of unconfined triaxial testing (Figure 5-40) without use of a rubber membrane or confinement). This involves manufacturing cylindrical specimens that are then exposed to compressive forces through application of constant rate of strain and monitoring of their resistance to deformation. In these tests there is no lateral confinement provided and no addition or reduction in the as-built water content prior to testing. Unconfined compressive strength is therefore defined as occurring at the maximum load the specimen can support before undergoing excessive strain (plastic or brittle). Unconfined compressive tests do not produce other deformation parameters such as angle of friction, cohesion or elastic (Young's) modulus.

From confined triaxial tests a series of parameters are measured or calculated and these can then be used to generate important mechanical properties for use in prediction of system performance. Behaviour is based on the effective stress concept and was demonstrated to be valid for bentonite systems (Dixon et al. 1986 and Graham et al. 1992). The main parameters monitored are σ_1, σ_2 (cell (confining) pressure), σ_3 (vertical stress), ε (vertical strain) and u (pore pressure). From these measurements effective stresses and deformation properties are derived. The standard terminology used for these are as follows:

$$\sigma_1' = \sigma_1 - u \qquad \textbf{5-18}$$

$$\sigma_2' = \sigma_1' = \sigma_1 - u \qquad \textbf{5-19}$$

Deviator stress (q) and average effective stress (p') are derived as follows:

$$q = \sigma_3 - \sigma_1 \qquad \textbf{5-20}$$

$$p' = (\sigma_1' + \sigma_2' + \sigma_3')/3 \text{ or } p' = (\sigma_3' + 2\sigma_1')/3 \qquad \textbf{5-21}$$

Using the Mohr – Coulomb failure envelope the shear strength (τ_f) of the clay can be described using the following equation:

$$\tau_f = c' + \sigma_N \tan \Phi \qquad \textbf{5-22}$$

where c' is the cohesion intercept, σ_N' is the normal effective stress acting on the specimen ($\sigma_N' = \sigma_3 - u$) and Φ is the friction angle.

The failure behaviour of compression tests is often reported in literature in terms of the maximum deviator stress at the time of failure (either as an effective stress or a total stress). As these data often do not include the cohesion intercept or the friction angle, their use in determining shear strength is problematic. The data provided in Appendix B illustrates the limited body of literature information but does provide some bounding values.

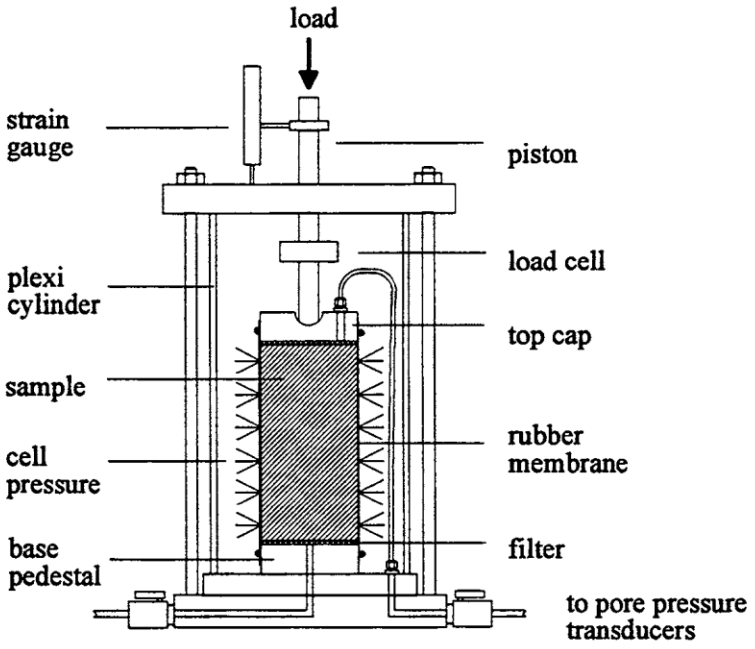

Figure 5-40: Schematic Showing Triaxial Cell and Specimen (Börgesson et al. 1995).

5.8.4.2 Compressive Strength Testing

The results of unconfined compression tests on MX80 have been reported by numerous authors (Börgesson et al. (1988, 1995, 2010); Dixon et al. (2006, 2018); Dueck 2010; Eloranta 2012; Pusch 1983; Rittola and Pyy, 2011; Tisata and Morelli, 2013; Hancilova and Hokr, 2016). These literature data have been compiled and their data recalculated so that the same assumptions regarding specific density of solids are used (2750 kg/m^3), this results in slight changes in the void ratio values and degrees of water saturation from those reported in the original literature but does not change the trends observed and ensures that consistent assumptions are used when determining parameters such as void ratio.

The available data exhibits considerable scatter in their results for stress-strain testing. This can in part be attributed to factors such as method of specimen preparation, potential slight differences in the material composition and granularity, and also the manner of testing. For example, the rate that the specimens were sheared varied for each study. Shear rates varied from 0.0042 mm/s (0.25% / minute), (Börgesson et al. (1988) to 0.001 mm/s (Dixon et al. (2006). Dueck et al. (2010) examined the effects of shear rate on results and observed little change in maximum strength for shear rates of 0.1 and 0.003 mm/s. Higher shear rates did result in higher strength being measured, however very low shear rates were not examined in that study and might result in slightly lower apparent shear strengths. Dixon et al. (2006) also examined the effects of shear rate (0.00017, 0.0005 and 0.001 mm/s) and also concluded that these shear rates did not affect the peak strength or the mode of failure.

Compilation of literature data into a single coherent database is complicated by gaps in the information provided in the various reports and papers examined. The reports collected tend to provide only processed data and often fail to provide some of the parameters associated with the results presented (see Appendix B). The information in literature presents differing deformation parameters (e.g. G but not E, B but not E or G, friction angle or no friction angle,

cohesion). In some reports, density is simply provided as bulk density and the reader is left to assume (or not) that this is a saturated bulk density, making estimation of specimen saturation difficult to evaluate without access to the original laboratory data. As a result, there are considerable uncertainties and a very limited body of data available to describe the triaxial deformation behaviour of HCB. The shear and triaxial deformation data collected are provided in Appendix B. Figures 5-41 and 5-42 show the effects of density, pore fluid composition and degree of saturation on the unconfined compressive strength and strain that occurs before failure occurs.

The plots in Figures 5-41 and 5-42 show the following:

- Increasing strength with increasing dry density (or decreasing e).
- Increase in strength when saturation is in range of 60-75%; This is accompanied with development of brittle failure characteristics at this lower saturation level (Dixon et al. 2006).
- Little effect of degree of saturation on strength when saturation exceeds approximately 75%.
- Little effect of pore fluid salinity on compressive strength in saturated systems having density 1350 -1500 kg/m^3. The effects at higher density have not been determined.
- Substantially higher pre-failure strain when degree of saturation exceeds approximately 80%) (Figure 5-42).
- A more extended period of plastic deformation is evident in materials having high degree of saturation, in some cases with no physical failure being observed, particularly for specimens of lower density and high degree of fluid saturation (Dixon et al. 2006).
- Drier materials (<80% saturation) tend to fail in an abrupt, brittle manner (Dixon et al. 2006).

Friction Angle Φ, in a saturated (>90% saturation) specimen shows little influence of dry density over the range of interest in placement room backfilling. There does however seem to be a substantial effect of pore fluid TDS on this parameter with friction angle increasing with increasing TDS (Figure 5-43) as follows;

- In freshwater conditions the friction angle is approximately 9.8^o,
- In a 35 g/L TDS environment the friction angle increases to approximately12.9^o, and
- In a brine environment (TDS>223 g/L) friction angle increases to approximately 25.5^o.

As noted previously, there is very limited data available related to the deformation parameters and particularly the effects of salinity, so the results provided here should be used for guidance purposes only. It should also be noted that the limited data for S>90% at high density (low e) results in flatter regression curves in Figure 5-41 and so may not accurately represent behaviour under those conditions.

The cohesion (c) determined for the saturated bentonite materials is provided in Appendix B. The value of c for the saturated bentonite materials is in the order of 40 to 87 kPa while the cohesion in specimens having 35 g/L TDS were slightly higher at 106 kPa.

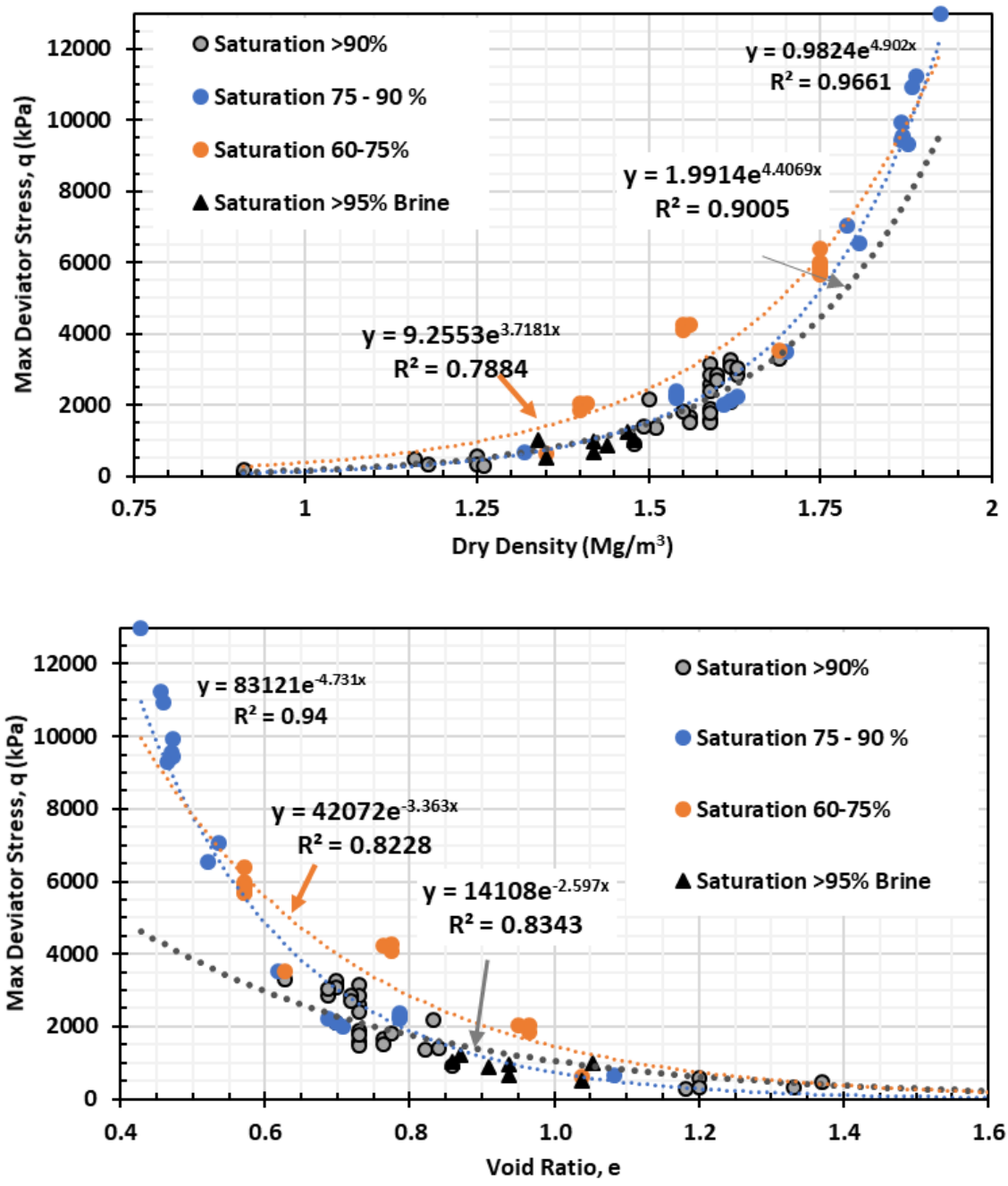

Figure 5-41: Effects of Density, Saturation and Salinity on Shear Strength of MX80

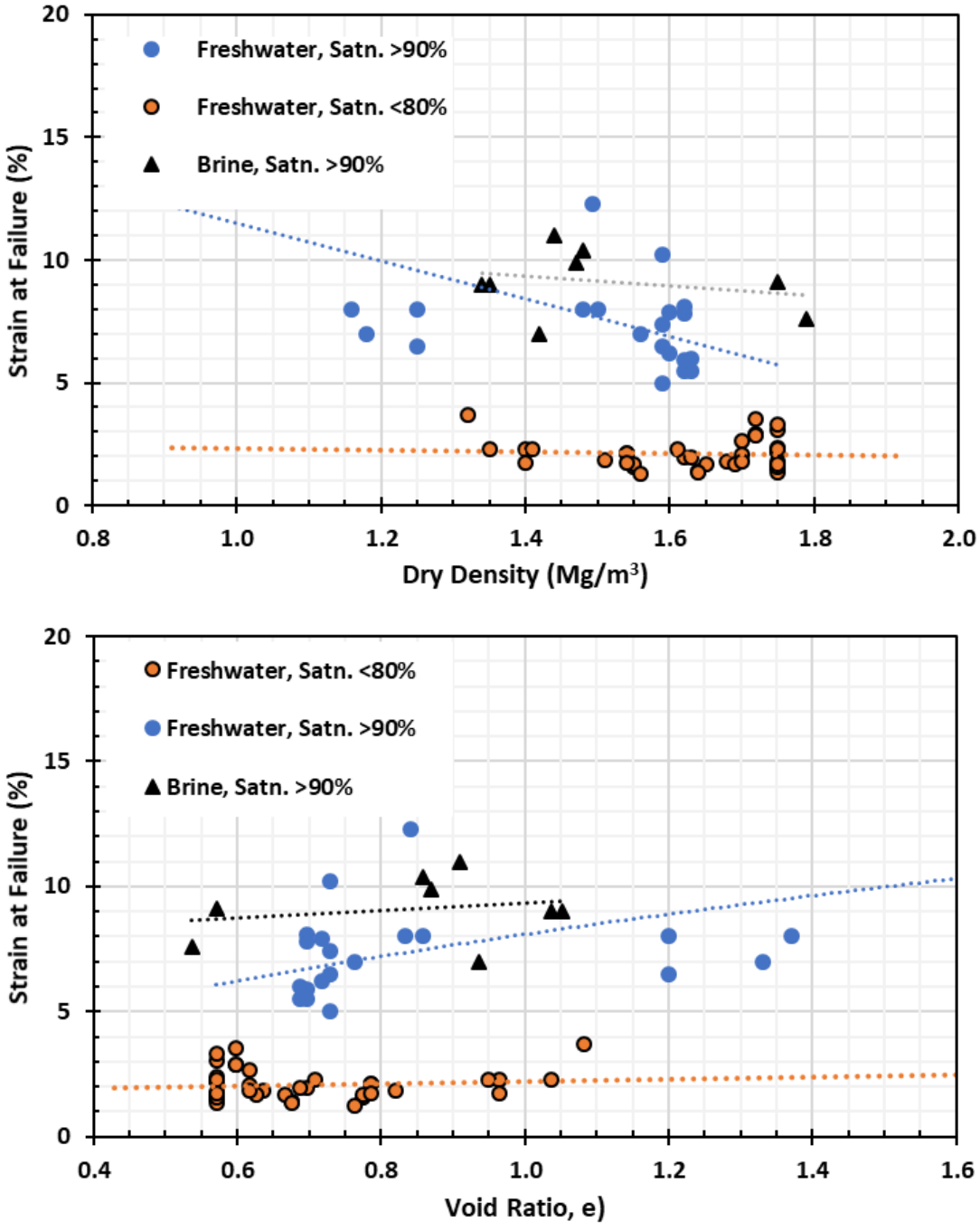

Figure 5-42: Effects of Density, Saturation and Salinity on Strain at Failure of MX-80.

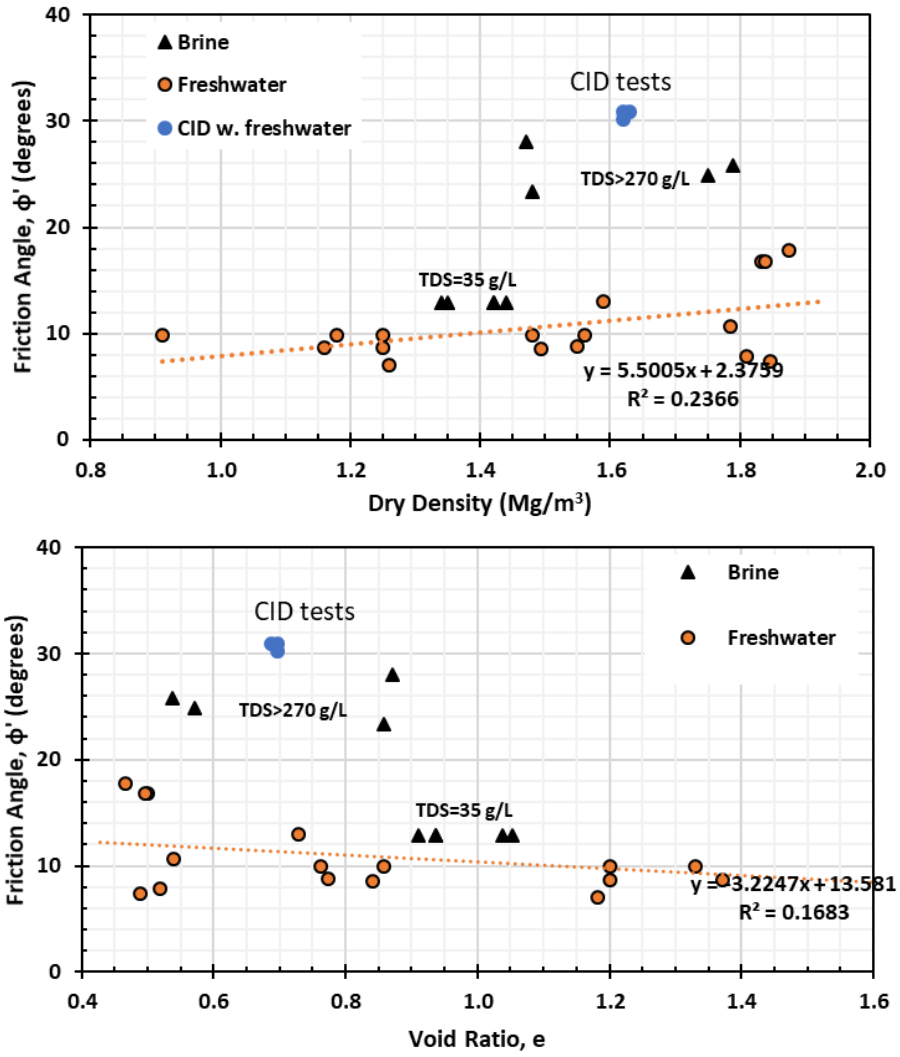

Figure 5-43: Effects of Density and Salinity on Friction Angle of MX-80 at Satn. >90%

5.8.4.3 Environmental Effects on Compressive Strength

It might be expected that the salinity of the water associated with the clay particles will have an influence on the strength of compacted bentonite since salinity controls the suction characteristics of the material. The presence of a saline pore fluid has however only been observed to result in a small change in the shear strength (perhaps a slight decrease) as shown in Figure 5-41. Saline pore fluid also results in a higher strain before failure as can be seen in Figure 5-42 as well as in Figure 5-43 where friction angle increases. Increase in TDS was reported to result in higher friction angle and higher cohesion by Börgesson et al. (1995) and so the literature is not consistent with respect to the effect on strength. It should be noted that these observations are based on a very limited body of data, and before effects can be properly quantified further materials testing will be necessary.

The effects of elevated temperature on unconfined compressive strength of HCB is a little-studied effect. In work by Lingnau et al. (1996), consolidated undrained triaxial and drained constant p' tests on 50:50 bentonite:sand materials observed lower maximum deviator stresses

before failure occurred, but it was also observed that although compressibility, stiffness and strength were affected by temperature up to 100 C, none of these changes were substantial. This is consistent with the results for 100% HCB reported by Börgesson et al. (1995) and Börgesson and Hernelind (1999) and presented as Figure 5-44 and Figure 5-45 where little effect of temperature (60 – 90^{o} C) or salinity (35 g/L) was observed. Börgesson et al. (1988) also reported that temperature increase from 20 to 60^{o}C had little effect on shear strength, particularly at high density. Dueck (2010) examined the effects of heating water-saturated MX-80 of 1700 kg/m^{3} dry density to temperatures >150 ^{o}C (followed by cooling before testing). In those tests the specimens exhibited more brittle behaviour. Similar behaviour was observed for specimens having degrees of saturation <90%. In both of these conditions the strain at failure was less than for other materials and conditions. This was attributed to cementation although it is not clear if this cementation was induced by cooling of the specimens. The temperatures examined were also much higher than will be experienced in NWMO's DGR.

Cementation of the soil matrix could result from precipitation of soluble materials relocated from elsewhere in the barrier system or from localized dissolution and then reprecipitated as a cementitious material. The movement of soluble materials from one region to another in the bentonite-filled region will be driven by the thermally-induced convective movement of gas and water. It has been reported that extended high pH conditions (e.g. 11.5-13.9) can result in silica dissolution and then subsequent reprecipitation occurs when pH conditions drop again. This topic was investigated by Laine and Karttunen (2010), who concluded that minor alterations of the region of the buffer closest to the source of alkaline water might occur if pH of 9.7 persists for a period of 5900 years. The substantial distance of the UFC in the Mark II geometry from concrete materials should ensure that this process does not adversely affect bentonite in the immediate vicinity of the UFC. Should cementation occur in the bentonite, it is expected that there would be a discernible increase in its compressive strength and mechanical failure would be brittle rather than ductile in nature as observed in a natural bentonite that had experienced silica cementation (Pusch et al. 1987,1998; Laine and Karttunen 2010).

There have been no studies identified that examined the effects of microbes on the deformation behaviour or strength of bentonite at densities of interest to DGR application.

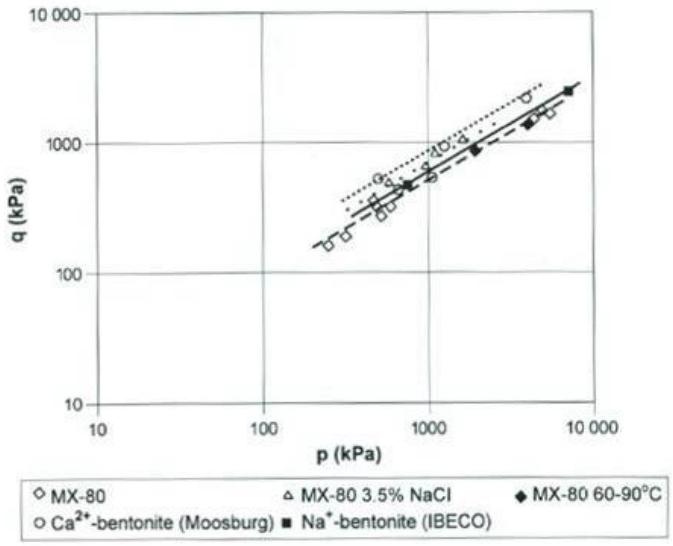

Figure 5-44: Triaxial Tests on MX-80 Bentonite (after Börgesson and Hernelind 1999).
(q = shear stress, p = average effective normal stress).

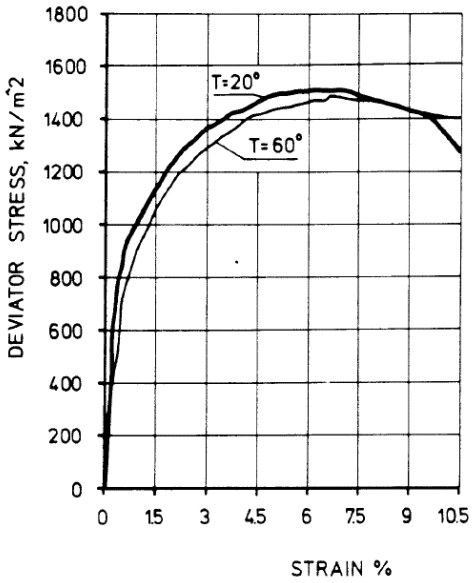

Figure 5-45: Effect of Temperature on Deformation of MX-80 (Börgesson et al. 1988)

5.8.5 Deformation Moduli

Key parameters in modelling deformation behaviour of the HCB-GFM system are the Shear (G), Bulk (B) and Elastic or Young's (E) moduli as well as the friction angle (Φ). These are based on elastic stresses and strains in the (x, y) horizontal, z (vertical) directions and are defined as follows (Lambe and Whitman 1979):

$$\mathbf{E = \sigma_z / \varepsilon_z} \qquad \mathbf{5\text{-}23}$$

where $\varepsilon_x = \varepsilon_y = - \mu \varepsilon_z$ **5-24**

When shear stresses τ_{zx} are applied to an elastic material, there will be a shear distortion Υ_{zx} such that:

$$\mathbf{\Upsilon_{zx} = \tau_{zx} / G} \qquad \mathbf{5\text{-}25}$$

And $G = E / (2(1+ \mu))$ **5-26**

Where μ is Poisson's ratio (normally between 0.25 and 0.5 for soils). The volumetric strain $\Delta V/V = \varepsilon_x + \varepsilon_y + \varepsilon_z$

The parameter known as the Bulk Modulus (B) is defined as:

$$\mathbf{B = \sigma_0 / \Delta V/V = E / (3(1-2 \mu))} \qquad \mathbf{5\text{-}27}$$

From these parameter definitions it is possible to calculate E, G or B provided that μ is known as well as one of the three parameter values, resulting in the following relationships:

$$\mathbf{G = E / (2(1+ \mu)) = E / (2 + 2 \mu)} \qquad \mathbf{5\text{-}28}$$

$$\mathbf{E = G (2(1+ \mu)) = G (2 + 2 \mu)} \qquad \mathbf{5\text{-}29}$$

$$\mathbf{B = E / (3(1-2 \mu)) = E / (3 - 6 \mu)} \qquad \mathbf{5\text{-}30}$$

As there is only a limited body of data available on the deformation moduli for densely compacted MX-80 bentonite, it is difficult to confidently define the deformation parameters. Differences in the manner in which tests have been undertaken (e.g. confining pressures, saturation processes and shear rates) also complicate comparison of the results available. There is very limited data related to the deformation behaviour of HCB under conditions of high pore fluid salinity or elevated temperature and there was none located for conditions combining high salinity and elevated temperature. As a result, quantification of these effects is problematic. There does however exist information on the effects of temperature on the deformation characteristics of 50% bentonite : 50% sand materials (Lingnau et al. 1996). This study provides an indication of the possible effects of temperature on deformation behaviour of HCB since at high bentonite:sand ratios, the bentonite:sand blend's behaviour is dominated by the bentonite component. Lingnau et al. (1996) reported that at elevated temperatures (60-100^{o}C) and pressures (up to 9 MPa effective stress) that an increase in temperature resulted in a slightly decreased maximum deviator stress (q_f) but to temperatures up to 100^{o}C this was only about a 10% decrease in strength. There was also a slight increase strain-softening behaviour with increasing temperature. It was also concluded that the 50:50 bentonite:sand mixture behaves as a normally-consolidated clay at temperatures up to 100^{o}C.

It was also reported by Börgesson et al. (1988) that during undrained testing the stress path does not affect stress-strain-strength behaviour, making comparison of tests conducted using differing conditions easier.

The collected information regarding the deformation moduli and parameters associated with the behaviour of HCB is summarized in Appendix B. These data are presented in Figure 5-46 through Figure 5-48 where Elastic, Shear and Bulk-Moduli are examined with respect to the density, saturation conditions and pore fluid salinity.

The Bulk Modulus (B) is evaluated using the data shown in Figure 5-46. The data for this parameter is limited but it appears that the B value for a saturated (>90% saturation), material in a freshwater environment increases with increasing density (decreasing e) and where low degree of saturation exists (<~75%) the B values are very much higher. Tisata and Morelli (2013) reported that specimens of approximately 1630 to 1740 kg/m^3 dry density, B increased with increasing confining pressure when tested at constant temperature (20^{o}C). The effect of pore fluid salinity is not well documented but based on two previously unpublished values obtained by NWMO, high TDS results in an apparent decrease in the B-values.

In a freshwater environment at densities of interest to the Mark II geometry (1400 to 1700 kg/m^3), B at 20^{o}C can be described using Equation 5-31. Tisato and Morelli (2013) reported a slight increase in the B-value with temperature increase from 30^{o}C to 80^{o}C and also that B increased as density increased (as shown in Figure 5-46). There is insufficient data available to quantify the B values under brine conditions.

Bulk Modulus	$\mathbf{B = 0.0087e^{7.4088DD}}$	**5-31**
Bulk Modulus	$\mathbf{B = 127763e^{-6.461VR}}$	**5-32**

Where DD is the dry density in Mg/m^3, VR is the void ratio of the bentonite under freshwater conditions and B is in GPa.

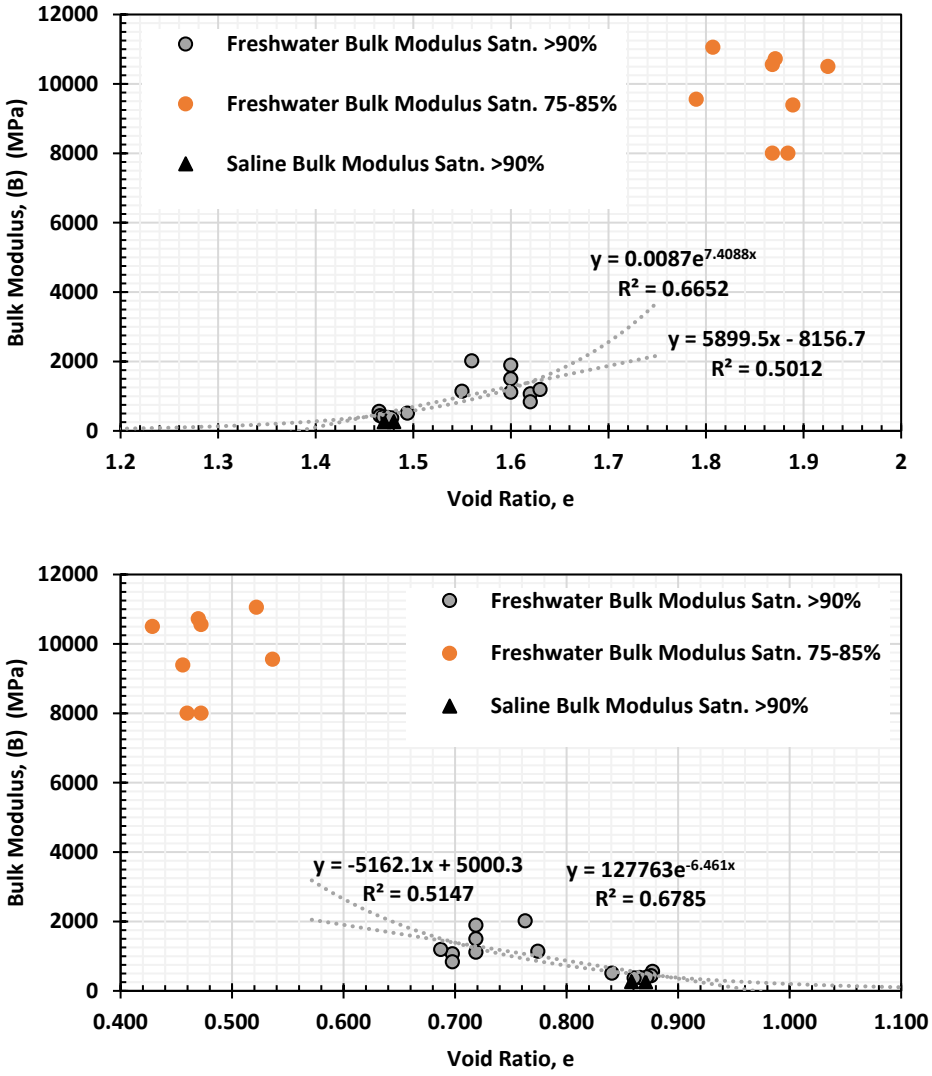

Figure 5-46: Effects of Density and Salinity on Bulk Modulus of MX-80

The Shear Modulus (G) is examined in Figure 5-47 using data sourced from Börgesson et al. (2010), Pusch (1983), Eloranta (2012) and Kiviranta et al. (2016). The limited data and lack of overlap in the densities examined for saturated and unsaturated specimens makes determination of the behavioural trends difficult. The G-value shows a trend for slightly increasing value with increasing density (decreasing e) and for the range of density of interest for placement room use (1400 to 1700 kg/m^3) there is sufficient data to provide estimates for a saturated material. There is no information available on the effect of lower degree of saturation. There are only two tests examining the effect of brine on G and they indicate that high TDS will result in a decrease in the G-value. The effect of temperature, confining pressure and density on G was studied by Tisato and Marelli (2013) who observed that as temperature increased from 30 to 80^{o}C, the shear modulus decreased slightly. G also increased with increased confining pressure. They also observed that as density decreased so did G for a given temperature.

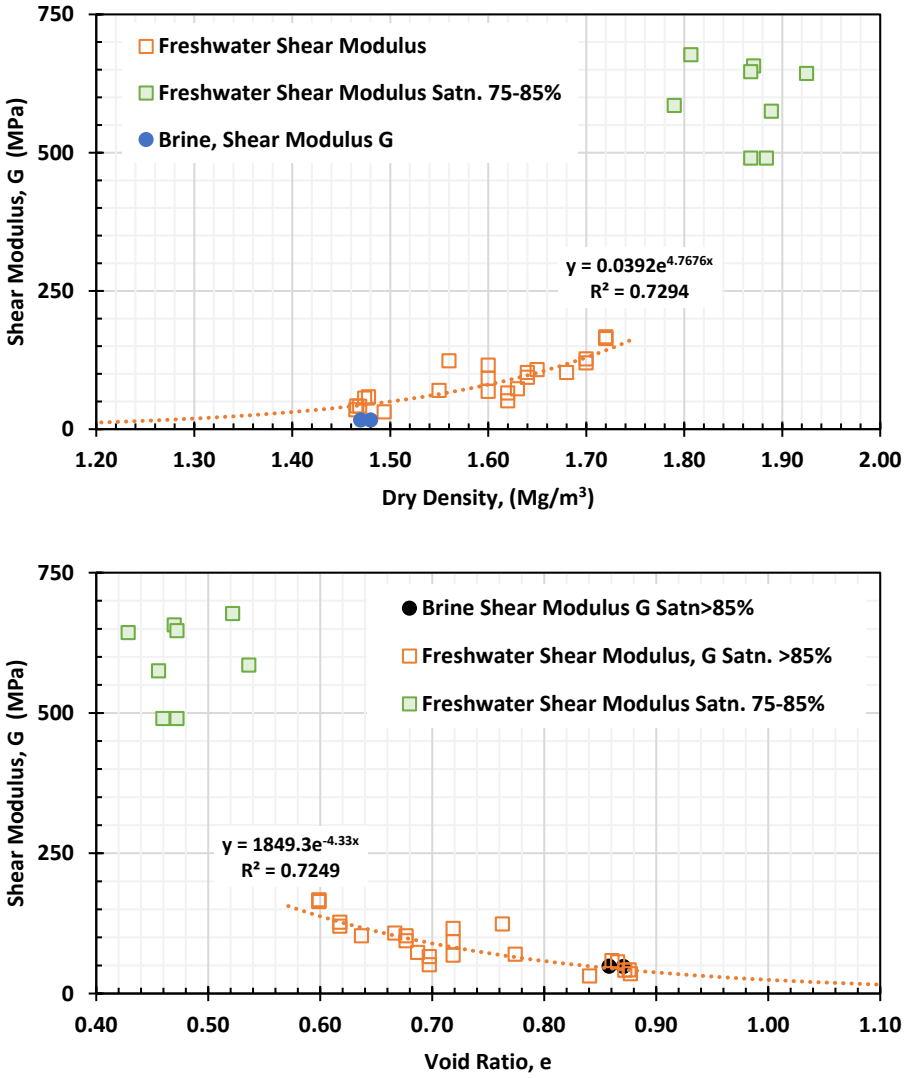

Figure 5-47: Effects of Density and Salinity on Shear Modulus

The relationship between void ratio for saturated bentonite and shear modulus for bentonite at approximately 20°C is described by the following equations.

Shear Modulus	$G = 1849.3e^{-4.33VR}$	**5-33**
Or Shear Modulus	$G = 0.0392e^{4.7676DD}$	**5-34**

Where VR is the void ratio and DD is the dry density in Mg/m^3 of the bentonite under freshwater conditions and G is in MPa.
The data for Elastic (Young's) modulus E, presented in Figure 5-48 includes tests conducted at saturation levels of 75-95% and densities of interest with respect to the HCB and GF components. These data are sourced from Borgesson et al. (2010), Eloranta (2012), Hancilova & Hokr (2016), Kiviranta et al. (2016), Pusch (1983) and Dixon et al. (2018). These data indicate

a much higher E for unsaturated and high-density materials than is present for the saturated and lower density material. This is consistent with the observations of Pusch (1983) who reported that E decreases with increasing degree of saturation.

The data indicates that E tends to increase with increasing dry density (decreasing e) under freshwater conditions. There are only 2 tests that have measured the E of bentonite under high (223 g/L) TDS conditions and these indicate a substantially lower E for a given dry density. It is not however possible to quantify E for high TDS conditions with the available information, further testing will be needed if this parameter is required although it should be possible to use the relationship established for freshwater as a conservative bounding condition.

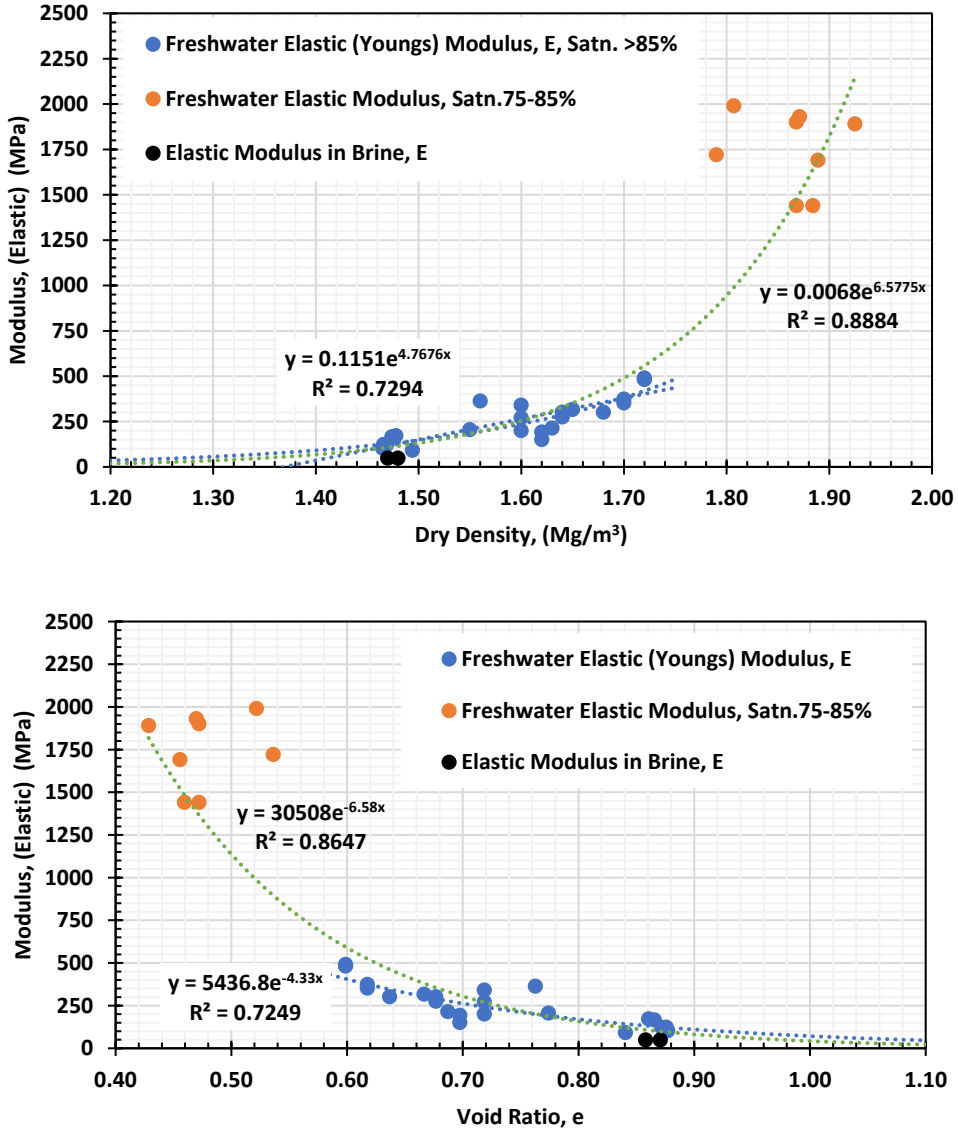

Figure 5-48: Effects of Density and Salinity on Elastic (Young's) Modulus

The relationship between void ratio and Elastic Modulus for a freshwater-saturated bentonite in the density range of interest in the Mark II geometry the following relationship can be used.

Elastic (Young's Modulus)	**$E = 0.0068e^{6.5775DD}$**	**5-35**
Elastic (Young's Modulus)	**$E = 30508e^{6.58VR}$**	**5-36**

Where DD is the dry density in Mg/m^3, VR is the void ratio of the bentonite under freshwater conditions and E is in MPa.

5.9 ANTICIPATED SYSTEM EVOLUTION AND T-H-M PARAMETERS FOR HCB AND GFM

5.9.1 Anticipated Dry Density Evolution of HCB and GFM and Effects on T-H-M Properties

The parameters and properties described in the preceding sections provide some of the basic information required to understand and predict the evolution of the thermal, hydraulic and mechanical behaviour of MX-80 materials proposed for use in NWMO's Mark II placement geometry.

The data show a good understanding has been developed for the thermal, hydraulic and swelling properties of bentonite materials under a wide range of temperature and pore fluid compositions. The mechanical behaviour is less-well established, particularly under conditions of elevated temperature and high pore fluid TDS conditions.

The bentonite materials installed in the placement room in NWMO's current Mark II placement geometry have a well-defined as-placed condition. This placement room fill consists of densely compacted (1700 kg/m^3 dry density) MX-80 bentonite that will be installed at degree of saturation likely in excess of 80% and pelletized or granulated bentonite material that will be installed to fill the spaces (gaps) not filled by the highly compacted bentonite and UFCs. This gap fill will be installed to a dry density of no less than 1400 kg/m^3 but will have a substantially lower as-placed degree of fluid saturation than the HCB. From this as-placed state, the combination of thermally-driven moisture redistribution and uptake of water from the surrounding rock mass is expected to result in a system that undergoes simultaneous desiccation and shrinkage (near the UFCs) and water uptake and swelling (close to the contact with the rock) during the period immediately following its installation. These mechanisms will result in localized changes in the T-H-M behaviour of the bentonite materials.

With reduction over time, in the thermal gradients present in the bentonite materials and with water influx from the surrounding geosphere, it is anticipated that the bentonite-filled volume will move towards density equilibrium and water saturation. Sections 3.3 and 3.4 discuss this and indicate that a reduction in the density of the HCB component and a densification of the GFM will occur, although it is as-yet uncertain to what degree density anisotropy will remain in the equilibrated system. This will depend on the stress or strain equilibrium achieved in the clay-filled volume.

Through evaluation of the bounding, as-placed behaviour of the bentonite component and the anticipated T-H-M behaviour of the system a general evolutionary description can be generated as follows:

1. As Placed bentonite/UFC system
    a. HCB 1700 kg/m^3 and >80% water saturation
    b. GFM ~ 1400 kg/m^3 and <50% water saturation

   c. No restrictions with respect to gas movement (open joints between blocks)
2. Initial thermally-induced water redistribution
   a. HCB close to UFC dries, shrinks slightly, becomes mechanically stronger and exhibits brittle behaviour. Thermal conductivity decreases with drying of HCB.
   b. HCB closest to GFM may swell slightly (depending on local conditions), becoming slightly weaker and more ductile with regards to its deformation behaviour.
   c. High temperatures, high bentonite density and low water contents will prevent bacterial activity in the region immediately adjacent to the UFC.
   d. GFM will take on water, swell and apply confinement to the HCB, but the GFM will not compress the HCB.

3. Period of extended exposure to elevated temperature and unsaturated conditions
   a. HCB will gradually hydrate as water becomes available and transfers inwards from the geosphere. During this time the compressive strength of the HCB will decrease as saturation increases but the material will be confined, meaning that the bentonite has nowhere to fail into if its compressive strength is exceeded provided that substantial volumetric drying shrinkage has not occurred.
   b. The GFM component will be consolidated by the hydrating HCB, resulting in continued slow decrease in the density of the HCB and increase in the density of the GFM,
   c. The pore fluid in the GFM and HCB will gradually increase as saline groundwater percolates into these materials. The result will be a decrease in the swelling pressure and increase in the hydraulic conductivity of the bentonite materials although literature has established that these properties will remain below the required threshold values. The deformation properties will change slightly also as salinity and saturation increase with the materials becoming more ductile.
   d. If processes leading to cementation of bentonite particles are present there may be a gradually-developed, likely localized region where the bentonite becomes more brittle, potentially stronger and also potentially less permeable than was originally the case.
   e. Gas migration will be restricted by the development of a saturated clay envelope. A balance between gas pressure development as new gas is generated and gas dissolution into the surrounding pore fluid and geosphere will need to develop or else there may be an influence on rate of system saturation. In an unbalanced system, gas pressure increase could ultimately result in clay desaturation and/or gas breaching the bentonite barrier.
4. Gradually decreasing thermal conditions and ongoing water inflow.
   a. With decreasing temperature (and thermal gradient) the movement of water into any remaining unsaturated regions will be less restricted and degree of saturation will increase (if the system had not already reached saturation).
   b. With saturation, the bentonite components will become more ductile and any stress-induced deformation will be more plastic in nature.
   c. The HCB-GFM system will approach a density-equilibrium.
   d. The T-H-M properties will be those of a system intermediate to that of the original materials, exhibit behaviour consistent with a material having high TDS pore fluid.
   e. If local conditions are conducive, there may be re-establishment of a viable bacterial population, particularly in the cooler regions closest to the GFM-rock contact where density conditions are anticipated to be lowest. There are at present no confirmed effects of bacterial activity on the T-H-M behaviour of the

HCB/GFM system although bacterially-induced corrosion of the UFC may be a consideration. Literature indicates that movement of corrosion products any distance is not likely and so would have minimal effects on the bentonite component's H-M behaviour.

5. Long-term, low-thermal gradient conditions
    a. The system will have come into density equilibrium.
    b. There will be a very low thermal gradient across the bentonite.
    c. The processes associated with this phase will have minimal effects on the T-H-M properties of the bentonite as it was at the end of Phase 4. Behaviour will be characterised as those observed for fluid-saturated materials having a high TDS pore fluid.

From this basic system evolutionary framework, the development and performance of the placement room bentonite can be modelled and evaluated. The materials parameter values described in this document and summarized in Section 5.9.2 provide some of the inputs needed in development of these numerical models.

5.9.2 Summary: T-H-M Parameter Values for HCB, GFM and Equilibrated System

The effects of density, pore fluid salinity, temperature, microbes, corrosion and dissolution processes and radiation on the thermal-hydraulic-mechanical behaviour of the MX-80 HCB and GFM components proposed for use in NWMO's Mark II repository concept have been examined through conduct of a literature survey.

The literature makes it clear that the dominating factors in determining the T-H-M performance of the HCB-GFM system are the dry density, degree of saturation and pore fluid salinity of the components installed. The temperature conditions will also affect the behaviour to a quantifiable amount (for systems having temperatures <90^{o}C), particularly in the period before fluid saturation is achieved. Processes associated with radiation, microbes, UFC corrosion and mineral dissolution or precipitation are secondary or tertiary in nature and although potentially of note under specific conditions are not likely to substantially alter the behaviour of the system in the geological environment and placement conditions specified by NWMO in its Mark II geometry.

A summation of the key T-H-M parameters under conditions of interest to NWMO's repository concept are provided below in Table 5-9. Where appropriate standard deviation or prediction interval values are also provided for the parameters listed. The nature of the PI is such that they provide very conservative banding values for the parameter being considered. Details regarding statistical evaluation of the various parameters can be found in the locations referenced in this table.

Table 5-9. Summary of T-H-M Parameter Values for MX-80 HCB and GFM at Approximately 20ºC (unless otherwise noted)

Parameter	Pore Fluid	GFM @ Dry Density (1400 kg/m^3)	HCB @ Dry Density (1700 kg/m^3)	Equilibrated HCB-GFM (1600 kg/m^3)	Reference Section
Free Swell Volume (cm^3/2g)	FW	31±5	31±5	31±5	6.1.2
	Brine	4			
Drying Shrinkage (%)$^{++}$	FW	~28*	~10	No data	6.1.2
	Brine	~15*	~4		
Thermal Conductivity (W/mºK)	Saturated FW, 25ºC	1.11±0.13	1.37±0.17	1.22±0.12	Table 5-2
	Saturated Brine*	1.16 - 1.20	1.25 -1.30	1.29 - 1.30	
	As-Placed in FW^{+++}	0.31±0.13 (S<10%)***	0.85±0.17 (S=45%)***		Table 5-2
	Saturated FW @ 80C^{++}	~105 -110%	~101-105%		Fig. 5-7
Water Activity, (a_w)	FW saturated	0.98	0.90	0.945	Fig. 5-10
	Brine saturated	<0.95	<0.95	0.945	
Hydraulic Conductivity (m/s)	FW saturated	2.3x10^{-13}	8.6x10^{-14}	1.1x10^{-13}	Table 5-4
	FW saturated PI	3.4E-14 / 2.6E-12	1.1E-14 / 8.5E-13	1.6E-14 / 1.2E-12	
	100 g/L TDS	1.5x10^{-11}	3.5x10^{-12}	5.5x10^{-12}	
	100 g/L TDS PI	4.2E-12 / 2.2E-8	6.8E-14 / 2.6E-8	1.3E-13 / 2.4E-8	
	>200 g/L TDS	1.7x10^{-11}	1.1x10^{-12}	2.5x10^{-12}	
	>200 g/L TDS PI	3.1E-13 / 2.6E-9	9.6E-15 / 8.4E-11	3.1E-14 / 2.6E-10	
	FW @ 80ºC	~3x10^{-13}	~10^{-13}	~10^{-13}	Fig. 5-15
Swelling Pressure (kPa)	FW saturated	2,760	12,510	7,520	Table 5-5
	FW saturated PI	820-9,410	3,830-43,800	2,290-26,200	
	100 g/L TDS	1,090	6,870	3,720	
	100 g/L TDS PI	180-5,560	1,130-34,610	610-18,820	
	>200 g/L TDS	810	3,800	2,270	
	>200 g/L TDS PI	90-7,400	500-29,200	280-18,500	
	FW @ 80ºC	~1,700**	~8,000**	4,600**	Fig. 5-20
Air Conductivity (m/s)	FW saturated	<3x10^{-12}	<2x10^{-13}	<1x10^{-13}	Table 5-6
	100 g/L saturated	<3x10^{-12}	<9x10^{-14}	<2x10^{-13}	
	>200 g/L saturated	<8x10^{-13}	<5x10^{-14}	<1x10^{-13}	
Tensile Strength (kPa)$^{+}$	FW >75% satn.	108	251	393	Fig. 5-37
	FW 60% satn.	<<100	<<250	<<390	Fig. 5-38
Compression Index, Cc (MPa^{-1})	FW saturated	No data	0.271±0.165	0.271±0.165	Fig 5-33
	Saline saturated	No data	0.192±0.058	0.192±0.058	
Swelling Index,	FW saturated	0.145±0.055	0.144±0.055	0.144±0.055	Fig. 5-33

Parameter	Pore Fluid	GFM @ Dry Density (1400 kg/m^3)	HCB @ Dry Density (1700 kg/m^3)	Equilibrated HCB-GFM (1600 kg/m^3)	Reference Section
Cs (MPa^{-1})	Saline saturated	0.053±0.023	0.053±0.023	0.053±0.023	
Coeff. of Consolidation, cv (m^2/KN)	FW saturated	6.1±10.9 x10^{-9}	6.1±10.9 x10^{-9}	6.1±10.9 x10^{-9}	Fig. 5-33
	Saline saturated	7.9±5.6 x10^{-9}	7.9±5.6 x10^{-9}	7.9±5.6 x10^{-9}	
Coeff. of Volume Change, mv (m^2/KN)	FW saturated	No data	4.19±2.37 x10^{-5}	4.19±2.37 x10^{-5}	Fig. 5-33
	Saline saturated	No data	5.37±1.10 x10^{-5}	5.37±1.10 x10^{-5}	
Max Deviator Stress (kPa)	FW >75% satn.	940	4090	2500	Fig. 5-40
	FW<75% satn.	1685	5145	3550	
	Brine 95% satn.	<950	<3570	<2300	
	Temperature <80^{o}C	Little effect	Little effect	Little effect	Fig. 5-44
Strain @ Failure (%)	FW saturated	7.9	7.9	7.9	Fig 5-41
	Brine saturated	9.1	9.1	9.1	
	FW <80% satn.	2.0	2.0	2.0	
	Brine <80% satn.*	<5	<5	<5	
Friction Angle (^{o})	FW	9.7	11.7	11.2	Fig. 5-42
	35 g/L TDS	12.9	No data (~14)	No data (~14.5)	
	Brine >200 g/L TDS	~25.5	~25.5	~25.5	
Bulk Modulus, B (GPa)	FW >90% satn.	0.299	1.224	2.567	Fig. 5-45
	Brine > 90% satn.	<0.2*	<1*	<2.5*	
	Temperature to 80^{o}C	Small increase*	Small increase*	Small increase*	5.8.5
Shear Modulus, G (MPa)	FW >90% satn.	32.6	80.6	129.8	Fig. 5-46
	Brine >90% satn.	<30*	<75*	<125*	
	Temperature to 80^{o}C	Small increase*	Small increase*	Small increase*	6.8.5
Elastic Modulus, E (MPa)	FW >90% satn.	72.5	252.9	488.3	Fig. 5-47
	Brine >90% satn.	<40*	<250*	<450*	

FW=Freshwater; Brine is TDS>100 g/L unless otherwise specified
PI = Prediction Interval;
± standard-deviation of a data set, or confidence interval, see referenced section for details.
* Estimated, see text for details;
** Estimated, literature is inconsistent, a 40% reduction is assumed for T rise from 20 to 80^{o}C,
*** for GFM placed at ~3% and HCB placed at ~ 10% gravimetric moisture content. TC will change with changes in saturation.
$^+$ For density < ~1600 kg/m^3 and/or saturation < approximately 60% the tensile strength is very low.
++ Shrinkage estimated from initially saturated condition. It will be lower if initial saturation is <100%. Drier initial condition also results in less potential for desiccation cracking.
+++ estimated as-placed gravimetric water contend of GFM=3%; HCB=10%.

6. INFLUENCE OF LOCAL GEOSPHERE ON REPOSITORY EVOLUTION

The anticipated conditions present in the placement rooms of NWMO's DGR concept for sedimentary and crystalline rock have been briefly described previously and parameter values provided in Table 5-9. Basic T-H-M behaviour of the bentonite is controlled by the material density and its degree of fluid saturation. The dominating environmental considerations of relevance to the bentonite component of the engineered barriers systems are associated with the heat emitted by the UFCs and the salinity of the surrounding groundwater. Under the conditions expected, the bentonite sealing materials are expected to exhibit the properties described in Section 5.

There are some potential upset scenarios related to the local geosphere that have been identified in some studies associated with repository evolution. These include the following:

- Localized high groundwater inflow rate,
- Erosion of bentonite during placement room backfilling or following placement room closure,
- Shearing of the bentonite as the result of sudden rock movement.
- Failure to completely close the DGR before it is abandoned.

The first two scenarios are primarily associated with the crystalline (granitic) geosphere environment where water-bearing features (fractures) will certainly be present in some of the rock volume utilized for UFC placement. The sedimentary environment also being considered by NWMO is expected to be extremely tight, with little in the way of free-water inflow during the period of UFC installation. As a result, the risk of large-inflow conditions developing in the placement rooms of a DGR in sedimentary rock is very low and this is not of active concern, although it will need to be reconsidered once site selection has occurred and detailed characterization begins. In the third case above, there would be a large, sudden movement of the rock adjacent to the placement room, resulting in application of high-energy shear forces to the buffer and UFC(s) in the region immediately adjacent to the rock movement. The fourth scenario is not technically a geosphere condition, but the geosphere would play a role in the evolution of the incompletely closed repository, potentially resulting in local loss of bentonite and associated loss of density in the region surrounding the UFC's in any unsealed regions. Although mentioned for completeness of consideration, this situation is not considered to be relevant as the repository will be entirely backfilled and sealed as part of its closure.

6.1 Localized High Water Inflow Rate

Localized high rates of water inflow results when the placement room intersects hydraulic features that are able to supply (individually or collectively) large enough volumes of water to the opening that the adjacent bentonite's ability to take it into its matrix is exceeded. Statistical evaluations of the number of placement rooms having water inflow rates of concern to a crystalline rock geosphere were presented by Hartley et al. (2012a,b,c) for the Olkiluoto site in Finland and the methodology allows for avoiding locations where highly unsuitable conditions exist. This will therefore allow for limiting the number of placement rooms that will potentially require remedial water handling. From these studies and the development of statistical estimations of the water inflow rates of the placement rooms and subsequently development of methods to remediate placement rooms having high water inflow rates have been developed. Although such statistical methods have limited tunnel-specific value, they do however provide an indication of how many placement rooms might be encountered that will require special consideration regarding water control or may prove to be unsuitable for placement operations. They may also provide for estimation of where water control efforts may be needed.

There are three basic options for placement room remediation or avoidance of unsuitable rock:

- Grouting (pre- or post-excavation) of the region(s) where water inflow is greatest so as to limit inflow during UFC, HCB and GFM placement,
- Installation of specialized water collection and removal devices that will allow for placement operations to continue without risks associated with free water movement in a tunnel being backfilled (Sandén and Börgesson 2014; Sandén 2016).
- Abandonment of a placement room, or not excavating it if issues are identified during pre-excavation characterisation of the rock.

The methods identified above are intended to have minimal impact on the sealing system once the placement room is closed and sealed. Grouting is a conventional technology (although specialized grout formulations will be required to minimize geochemical interactions) and would provide localized restriction of water inflow for the period of placement operations and perhaps for a period afterwards but is not relied on for any type of longer-term function. Once placement room closure is achieved, inflowing water is still restricted by the grouting and so water would ideally first move into and through the unsaturated gap fill bentonite in the region between then HCB and rock and then be taken up more gradually by the HCB. That the placement room is already closed should mean that any relocation of bentonite by the inflowing water is limited. The gradual degradation of the effectiveness of the grout might result in the system achieving water saturation more rapidly than for placement rooms having a lower water inflow rate but ideally would have no other effects on system evolution provided that the bentonite remains within the placement room. It should be noted that grouting is a technology that cannot guarantee entire cutting off of water inflow and needs to be carefully evaluated with respect to its likely effectiveness for each feature to be remediated. Studies of options for grouting and grout materials in a DGR located in crystalline rock are provided by Bodén and Sievänen (2005); Grandia et al. (2010); Hollmén et al. (2012); Sievänen et al. (2004; 2005).

The presence of high water inflow features will depend on site-specific conditions and the threshold at which inflow becomes an issue will depend on numerous factors. These include the nature of the pellet fill (its volume, porosity, density, fines content), the nature of the groundwater entering (salinity), as well as the area over which inflow occurs and the rate at which the placement room is filled. It was noted in several studies (e.g. Dixon et al. 2008a,b; Martikainen and Schatz 2016; Sandén and Borgesson 2014; Sanden and Jensen 2016); that water movement through pellet material (e.g. Gap fill) is not notably restricted at higher water inflow rates and that water movement into and distribution in the pellet component is dependent on factors such as pellet size, shape, method of manufacture, fines content and even the bentonite used in their manufacture.

Methods to handle the impact of very localized water-bearing features without (or in conjunction with) grouting of water-supplying features has been developed by Posiva and SKB (Sandén et al. 2018). This involves installation of water collection and diversion devices in the region where inflow is occurring and then moving this water off to a location where it can be removed to the surface without having interacted substantially with the placement room fill. In this method, the water diversion system would have a very limited extent and once installation of placement room fill has progressed far enough away from the source of water inflow, the drainage pipes would be removed. The water uptake and redistribution properties of the GFM and HCB blocks would then be relied on for the remaining time during which placement activities are ongoing prior to installation of the placement room end plug. A detailed review of options for handling of inflowing water has been undertaken and is provided in the report by Sandén et al. (2018).

Minimizing the impact of high water inflow is focussed on avoiding situations where water entering the open placement room forms a disruptive feature that can result in erosive processes. The best approach is one that is recognized in the basic concept for placement room location, that is avoiding regions identified as having severely adverse hydraulic conditions before UFC placement begins. This is accomplished through drilling and evaluation of a test boreholes / pilot holes along the length proposed for each placement room. This will identify most locations where the water supply could be problematic, allowing such locations to be avoided.

6.2 Physical Erosion of Bentonite

Physical erosion of bentonite within a placement room is a situation that might be encountered in a placement room where water inflow rates are very high and localized. If water inflow rates are high and not addressed during the period prior to UFC installation, there is the potential for inflowing water to first interact with the gap fill component and initially move preferentially into the GFM, potentially forming discrete flow channels through the bentonite and also carrying bentonite with the water as it moves. These features have been described in studies by Börgesson et al. (2015); Dixon et al. (2008) a,b; Riikonen (2008); Sandén et al. (2008) and have the potential to cause considerable disruption to the GFM regions and also to ongoing placement activities in the placement room. This process is best avoided through:

- selection of locations for placement rooms that avoid high inflow structures,
- pre-treatment of the water-supplying features to restrict water inflow during placement operations, and
- installation of water collection and redistribution devices to control water movement for the period prior to placement room closure.

Erosion of bentonite within a closed placement room may be of concern if the water entering the placement room moves through the backfilled volume via discrete flow paths and carries bentonite with it. There is also an increased risk if the groundwater is saline as opposed to fresh as salinity will restrict the ability of the bentonite to form erosion-resistant gels. This requires several conditions before it might prove to be a substantial issue, firstly there needs to be development of a flow channel, and secondly it must be able to relocate enough bentonite within the closed placement room to be of concern. In a closed placement room, water might initially move preferentially through the GFM, carrying with it small quantities of bentonite, however there is no large unfilled volume for the water to continue flowing into when the placement room is closed. The water movement along any flow channels would slow and channels would close as water was taken up by the surrounding clay and swelling occurred. The erosive disruption of bentonite pellet and block tunnel mock-ups is described by Dixon et al. (2008a,b) and Riikonen (2008). All of these simulated situations involved free-drainage of water from the downstream face of the installation, a situation that would not exist in a closed placement room.

In the full-scale Tunnel Sealing Experiment (TSX) undertaken by AECL at their Underground Research Laboratory, a large-volume leakage developed with water moving from a flooded and pressurized tunnel section through a 3 m-thick bentonite-based block and granulate GFM bulkhead to an open section of tunnel. Flow occurred as the result of incomplete saturation and a very high pressure gradient across the installation with development of flow channels through the GFM and along the contacts between the bentonite blocks. Large quantities of water escaped from the tunnel during these leakage events but there was minimal loss of material and once depressurized, the system resealed and performed well under a 4.2 MPa pressure

gradient across the seal (Martino et al. 2008). In this construction, the downstream face of the seal was provided with a solid face that prevented physical disruption of the seal and so allowed for recovery of the system as the bentonite hydrated and swelled to seal the flow path. This is a situation similar to that described by Sandén et al. (2018) as a temporary plug to prevent material disruption. Based on these conclusions/observations, substantive redistribution of bentonite within a closed tunnel is unlikely to be an ongoing process with proper planning for tunnel closure. Additionally, a margin built into the minimum as-placed densities required for the equilibrated system would provide for any localized loss of material.

Sandén et al. (2018) reviewed the options and issues associated with water handling and bentonite erosion in tunnel backfilling. Although this work was related to backfilling of tunnels where in-floor placement of very large UFCs occurred, the tunnel fill consists of an assembly of HCB blocks and bentonite GFM pellets which is directly applicable to NWMO's Mark II placement concept. The key conclusions associated with this work were as follows and are based on the rate of backfill placement specified for the SKB and Posiva placement rooms:

1. Although bentonite pellets are to be used to fill the gaps between HCB blocks, the inflow rates at Forsmark (Sweden) and Olkiluoto (Finland) are such that the pellets can only accommodate localized inflow rates of <0.5 L/min and placement room inflow total of between 0.5 and 1.0 L/min for a tunnel of approximately 350 m length. Where a number of smaller inflows (<0.25 L/min each) exist, total tunnel inflows of 1 to 5 L/min may be able to be handled by GFM alone.
2. Geotextile-based inflow collection from localized seepage areas can improve the ability of the system to handle water inflow where point-inflow rate is 0.25 to 1.0 L/min.
3. Geotextile collection regions will include isolating materials (wet GFM) immediately downstream from the geotextile so as to constrain water movement and direct it into drainage pipes (recommended for inflow conditions of 0.5 to 1.0 L/min).
4. Where excessive inflow is occurring (5 to 10 L/min) it will likely be necessary to install drainage lines that direct water to an adjacent (still open) tunnel until backfilling operations are completed and then seal the drainage borehole.

Sandén et al. (2018) also note the potential to use localized freezing to provide temporary restriction to water inflow to a placement room, however this has not been demonstrated as being practical or feasible and may induce additional rock damage.

A mathematical model that can be used to estimate the time available before the inflowing water reaches the working face of a still-open placement room for specific deposition tunnel geometries and for specific water inflow situations was also referenced by Sandén et al. (2018)

6.3 Localized Shearing

Shear forces resulting from sudden and substantial rock movement has the potential to induce unexpected localized loads on the bentonite and UFC. The occurrence of an earthquake-related shearing activation of the faults, fracture-zones and other features around a DGR is deemed to be of greatest likelihood in the period immediately following the next glaciation when unloading of the rock begins. The modelling of such tectonic activity at the Olkiloto site in Finland was completed by Fälth and Hökmark (2012, 2015) who observed that the higher the shear velocity the stiffer would be the response of the HCB buffer in a placement borehole of the KBS-3V geometry. A stiffer material will transfer shear forces more effectively to the UFC and increase the risk of damage to it. This situation was also reviewed for SKB by Read (2011) with regards to evaluation of the impact of rock shearing on the placement borehole proposed for use in the KBS-3V geometry and a program of testing was proposed. A study by Fälth et al. (2008) also examined the effects of earthquakes on a KBS-3 repository.

It should be noted that in the KBS-3V geometry there is only a thin layer of pellets and blocks between the UFC and the surrounding rock, a situation that is much more sensitive to shear forces than the NWMO Mark II placement geometry with much larger volumes of pellets and HCB between the UFC and the surrounding rock. The stiffness and deformation properties assumed for the HCB/GFM components will also greatly affect the results obtained in modelling exercises.

Evaluation of the effect of rock displacement on the engineered barriers system was evaluated by JNC (2003) and in the abstract for this report it was noted that the buffer material diminished the shear stress acting of the UFC. It was concluded that rock displacement as much as 80% of the buffer thickness didn't affect the UFC if the velocity of the fault movement was under 0.01 m/s. A similar conclusion regarding buffer thickness and density was reached by Börgesson and Hernelind (2003; 2006; 2010); Dillstrom and Bolinder (2010), and Hernelind (2010) as increased density is associated with increased bentonite stiffness and hence increased stress transfer to the UFC.

Börgesson and Hernelind (2006) examined the influence of buffer density, shear plane location, shear rate and magnitude of the shear displacement. It was determined that the bentonite density had a controlling effect on shear transfer to the UFC, but the angle of the shearing process also had a substantive effect on UFC deformation. For example, at a saturated density of 2100 kg/m^3 and a shear displacement of the borehole of 20 cm, the internal cast iron element of the SKB UFC deformed 19%. In comparison, for a saturated density of 2000 kg/m^3 and a borehole shear displacement of 10%, the plastic deformation of the UFC was 1.6%. This would seem to indicate that at more moderate densities, the impact of shear displacement on the UFC in the KBS-3 in-floor borehole placement geometry would be substantially reduced.

The studies referenced above indicate the potentially adverse effects of increasing stiffness of HCB by increasing its as-placed density, as density increased so did stress transfer to a UFC and the greater the potential effect on the integrity of the UFC. These studies only examined the situation where there is a relatively small thickness of HCB in a vertical borehole of the type proposed for use in the KBS-3V placement geometry. The models also did not take into account the presence of any lower-density GFM (or lower density HCB that resulted from density equilibration of the HCB and GFM components). Hence it is difficult to estimate the manner in which the Mark II geometry would respond to large rock shear events, excepting that average density may be lower than for the SKB/Posiva systems and hence stress transfer to a UFC may be lower. The Mark II geometry also has a substantially larger volume of buffer between it and the surrounding rock mass, potentially a further mitigating factor should rock shearing occur. A study of this process in the NWMO-relevant geometry would be of value.

7. SUMMARY

The Mark II DGR concept developed by NWMO includes extensive use of bentonite-based materials, particularly as part of the engineered barriers system installed in the placement room. Highly compacted bentonite will be used to surround the UFCs and provide the desired spacing between the containers. Lower density Gap Fill materials will be used to fill any voids not occupied by the UFCs and HCB. As a closed placement room experiences water redistribution as the result of thermal gradients induced by the heat-generating UFCs and potentially simultaneously takes on water from the surrounding rock mass, there will be a complex process of T-H-M-C interactions. These interactions will primarily be associated with the changing

density of the HCB (swelling and decreasing in density) and the GFM (hydrating, swelling and then being densified by the swelling of the adjacent HCB).

The current density specifications for the HCB (1700 kg/m^3 dry density), GFM (1400 kg/m^3 dry density) and volume occupied by the UFCs in placement rooms meeting the geometric specifications set by NWMO will result in an average system dry density for the bentonite-filled component of between 1615 and 1636 kg/m^3. Slight improvements demonstrated to be achievable for the HCB blocks and GFM will increase the averaged dry density to as much as 1676 kg/m^3. These values do not however consider voids associated with interface gaps between HCB blocks or associated with construction of tunnel end plugs that will result in some reduction in the average density. Additionally, these values are based on full density equilibration of the HCB-GFM components, a situation that does not seem certain. While localized densities of more than 1400 kg/m^3 and less than 1600 kg/m^3 are not likely to be of importance with respect to the equilibrated T-H-M properties of the water-saturated sealing system, the currently set density value for the bentonite system is a minimum average dry density of 1600 kg/m^3. This value is based on the conservatively estimated density at which bacterial activity is supressed. Based on the results of bacterial studies completed, it may be possible to relax the minimum density requirements somewhat, but this is a subject that will require further careful consideration. Slight improvement in the average (and hence local minimum) dry density of the bentonite can also be achieved through increasing the as-placed dry density of the HCB and/or GFM components. Improvements will however be small and use of higher density components may result in technological challenges associated with block manufacture and GFM placement. Higher density systems are also apparently more sensitive to transfer of stresses from the surrounding rock to the UFC during rock shear and so increase in the sealing material density needs to be considered with respect to any additional risks.

Literature is not always in complete agreement with respect to the absolute values associated with the various T-H-M parameters and in particular the role of chemical (C) and Biological (B) process. There will be some quantifiable effects of chemical processes on bentonite and the sealing system over the longer-term but it has not been demonstrated that they will be substantive enough to result in the sealing material not being able to fulfil its role in physically supporting and isolating the UFC from the surrounding geosphere during the period of interest.

With respect to the effects of groundwater and physical-chemical processes, the HCB/GFM system is robust. The thermal, hydraulic, chemical conditions or biological processes thus far identified as being potentially active in the vicinity of the UFC in the Mark II geometry under saturated conditions do not seem to result in loss of ability of the bentonite to provide isolation to the UFCs. The effects of T-H-M-C (B) processes on non-bentonite components is not considered in this document.

Further evaluation of the combined effects of elevated temperature and high pore fluid salinity on the deformation properties of the sealing materials would be of value with respect to generating more accurate stress-strain predictions for the system.

8. REFERENCES

Abootalebi, P. 2016. Characterization and thermal-hydraulic modeling of engineered barriers for a Canadian Deep Geological Repository for used nuclear fuel. MASc thesis, Queens University. Kingston, Canada.

Abootalebi, P. and G. Siemens. 2017. Thermal properties of engineered barriers for a Canadian deep geological repository. Can. Geotech. J. 55, 759-776.

Åkesson M., L. Borgesson and O. Kristensson. 2010a SR-Site data report. THM modelling of buffer backfill and other system components. Updated 2013-12, Swedish Nuclear Fuel and Waste Management Company Report SKB TR-10-44. Stockholm, Sweden

Åkesson, M., O. Kristensson, L. Börgesson, A.Dueck, and J. Hernelind. 2010b. THM modelling of buffer, backfill and other system components. Critical processes and scenarios. Updated 2015-08, Swedish Nuclear Fuel and Waste Management Company Report SKB TR-10-11. Stockholm, Sweden

Åkesson, M., T. Sandén and L. Börgesson. 2016. Water handling during backfill installation - Conceptual and mathematical models of water storage and spreading. Swedish Nuclear Fuel and Waste Management Company Report SKB R-16-12. Stockholm, Sweden.

Al, T., I.D. Clark, L. Kennell, M. Jensen and K.G. Raven. 2015. Geochemical evolution and residence time of porewater in low-permeability rocks of the Michigan Basin, Southwest Ontario. Chemical Geology 404, 1–17.

Allard, T. and G. Calas. 2009. Radiation effects on clay mineral properties. Applied Clay Science 43, 143-149.

Allard, T., E. Balan and G. Calas. 2013. Chapter 4 – Radiation effects on clay minerals, in Handbook of Clay Sci., Developments in Clay Science (Ed. F. Bergaya and G. Lagaly), Vol. 5, 2013, 127-138, Elsevier.

Allen, C.C. and M. I. Wood. 1988. Bentonite in nuclear waste disposal: A review of research in support of the Basalt Waste Isolation Project, Applied Clay Sci. 3, 11-30.

Alonso, E.E. and A. Ledesma. 2003. Advances in understanding engineered clay barriers. Proc. Intl. Symp. on Large-Scale Field Tests in Granite, Nov. 2003. Sitges, Barcelona, Spain.

Anton-Paar 2011. Effect of Temperature on Freshwater Density and Viscosity, https://wiki.anton-paar.com/en/water/

Arthur, R. and W. Zhou. 2005. Reactive-Transport model of buffer cementation. Swedish Nuclear Power Inspectorate (SKI) Report 2005:59. Stockholm, Sweden.

Arvidsson, A., P. Josefsson, P. Eriksson, T. Sandén and M. Ojala. 2014. System design of backfill: Project results. Swedish Nuclear Fuel and Waste Management Company Technical Report SKB TR-14-20. Stockholm, Sweden.

ASTM C837-09. 2014. Standard test method for Methylene Blue index of clay. Am. Soc. Testing Materials. West Conshohocken, Pennsylvania, USA.

ASTM D2435M-11. 2014. Standard test methods for one-dimensional consolidation properties of soils using incremental loading. Am. Soc. Testing Materials. West Conshohocken, Pennsylvania, USA.

ASTM D5890–11. 2011. Standard test method for swell index of clay mineral component of geosynthetic clay liners. Am. Soc. Testing Materials. West Conshohocken, Pennsylvania, USA.

ASTM D6836-02. 2002. Standard test methods for determination of the soil water characteristic curve for desorption using hanging column, pressure extractor, chilled mirror hygrometer, or centrifuge. Am. Soc. Testing Materials. West Conshohocken, Pennsylvania, USA.

Bag, R. 2011. Coupled thermo-hydro-mechanical-chemical behaviour of MX80 bentonite in geotechnical applications. Ph. D Thesis, Cardiff University, School of Engineering. Cardiff, UK.

Barone, F., J. Stone and A. Man. 2014. Geotechnical properties of candidate shaft backfill. Nuclear Waste Management Organization Report NWMO-TR-2014-12. Toronto, Canada.

Baumgartner, P. 2006. Generic thermal-mechanical-hydraulic (THM) data for sealing materials: Volume 1: soil-water relationships. Ontario Power Generation Report 06819-REP-01300-10122-R00. Toronto, Canada.

Baumgartner, P., D. Priyanto, J.R. Baldwin, J.A. Blatz, B.H. Kjartanson and H. Batenipour. 2008. Preliminary results of one-dimensional consolidation testing on bentonite clay-based sealing components subjected to two pore-fluid chemistry conditions. Nuclear Waste Management Organization Report NWMO-TR-2008-04. Toronto, Canada.

Bengtsson, A., J. Edlund, B. Hallbeck, C. Heed, and K. Pedersen. 2015. Microbial sulphide-producing activity in MX-80 bentonite at 1750 and 2000 kg/m^3 wet density. Swedish Nuclear Fuel and Waste Management Company Report SKB R-15-05. Stockholm, Sweden.

Bengtsson, A., A. Blom, B. Hallbeck, C. Heed, L. Johansson, J. Stahlen and K. Pedersen. 2016. Microbial sulphide-producing activity in water-saturated MX-80, Asha and Calcigel bentonite at wet densities from 1500 and 2000 kg/m^3. Swedish Nuclear Fuel and Waste Management Company Technical Report SKB-TR-16-09. Stockholm, Sweden.

Bennett, C. 2014. An experimental study on the hydraulic conductivity of compacted bentonites in geoenvironmental applications. PhD Thesis, Cardiff University, School of Engineering. Cardiff, UK.

Beziat, A., M. Dardaine and V. Gabis. 1988. Effect of compaction pressure and water content on the thermal conductivity of some natural clays. Clays & Clay Minerals 36(5) 462-466.

Birch, K. and M. Mielcarek. 2017. Development of NWMO buffer program - from concept to full scale demonstrations. Apr. 09-12, IHLRWM 2017. Charlotte, USA.

Birgersson, M. and R. Goudarzi. 2015. Vapor transport and sealing capacity of buffer slots (“sauna” effects). Swedish Nuclear Fuel and Waste Management Company Technical Report SKB TR-15-09. Stockholm, Sweden.

Birgersson, M., L. Börgesson, M. Hedström, O. Karnland and U. Nilsson. 2009. Bentonite erosion final report. Swedish Nuclear Fuel and Waste Management Company Technical Report SKB TR-09-34. Stockholm, Sweden.

Boden, A. and U. Sievanen. 2005. Low-pH injection grout for deep repositories, Summary report from a co-operative project between NUMO (Japan), Posiva (Finland) and SKB (Sweden), Posiva Oy, Working Report 2005-24. Olkiluoto, Finland.

Börgesson, L. and J. Hernelind. 1999. Prototype Repository: Preliminary modelling of the watersaturation phase of the buffer and backfill materials, Swedish Nuclear Fuel and Waste Management Company, International Progress Report, IPR-00-11. Stockholm, Sweden.

Börgesson, L. and J. Hernelind. 2003. Earthquake induced rock shear through a deposition hole. Effect on the canister and the buffer. Swedish Nuclear Fuel and Waste Management Company Technical Report SKB TR-04-02. Stockholm, Sweden.

Börgesson, L. and J. Hernelind. 2006. Earthquake induced rock shear through a deposition hole. Influence of shear plane inclination and location as well as buffer properties on the damage caused to the canister. Swedish Nuclear Fuel and Waste Management Company Technical Report SKB TR-06-43. Stockholm, Sweden.

Börgesson, L. and J. Hernelind. 2010. Earthquake induced rock shear through a deposition hole: Modelling of three model tests scaled 1:10. Swedish Nuclear Fuel and Waste Management Company Technical Report SKB TR-10-33. Stockholm, Sweden.

Börgesson, L., H. Hökmark and O. Karnland. 1988. Rheological properties of sodium smectite clay. Swedish Nuclear Fuel and Waste Management Company Technical Report SKB TR 88-30. Stockholm, Sweden.

Börgesson, L., A. Fredrikson and L. E. Johannesson. 1994. Heat conductivity of buffer materials. Swedish Nuclear Fuel and Waste Management Company Technical Report SKB TR-94-29. Stockholm, Sweden.

Börgesson, L., L.E. Johannesson, T. Sandén and J. Hernelind. 1995. Modelling of the physical behaviour of water saturated clay barriers. Laboratory tests, material models and finite element application. Swedish Nuclear Fuel and Waste Management Company Technical Report SKB TR 95-20. Stockholm, Sweden.

Börgesson, L., A. Dueck and L.E. Johannesson. 2010. Material model for shear of the buffer. Evaluation of laboratory test results. Swedish Nuclear Fuel and Waste Management Company Technical Report SKB TR-10-31. Stockholm, Sweden.

Börgesson, L., T. Sandén, A. Dueck, L. Andersson, V.Jensen, U. Nilsson, S. Olsson, M. Åkesson, O. Kristensson and U. Svensson. 2015. Consequences of water inflow and early wwaer uptake in deposition holes. EVA-project. Swedish Nuclear Fuel and Waste Management Company Technical Report SKB TR-14-22. Stockholm, Sweden.

Bradbury, M.H., U. Berner, E. Curti, W. Hummel, G. Kosakowski and T. Thoenen. 2012. The long term geochemical evolution of the nearfield of the HWl repository. National Cooperative for the Disposal of Radioactive Waste (NAGRA) Technical Report TR-12-01. Wettingen, Switzerland.

Bradbury, M.H. and B. Baeyens. 2011. Physico-Chemical characterisation data and sorption measurements of Cs, Ni, Eu, Th, U, Cl, I and Se on MX-80 bentonite. Nuclear Energy

and Safety Research Department Laboratory for Waste Management, Paul Scherrer Institut, # 11-05. Villigen, Switzerland.

Bucher, F., P. Jedalhauser and P. A. Mayor. 1986. Quell-, Durchlassigkeits- und Schrumph-versuche an Quarzsand-Bentonit-Gemischen. National Cooperative for the Disposal of Radioactive Waste (NAGRA) Technical Report, 86-13. Wettingen, Switzerland.

Carlson, L. 2004. Bentonite Mineralogy; Part 1: Methods of investigation-a literature review; Part 2: Mineralogical research of selected bentonites. Posiva Oy Working Report 2004-02. Olkiluoto, Finland.

Carlson, L., O. Karnland, S. Olsson, N. Smart and A. Rance. 2006. Experimental studies on the interaction between anaerobically corroding iron and bentonite. Posiva Oy Working Report 2006-60. Olkiluoto, Finland.

Castellanos, E., A. Gens, A. Lloret and E. Romero. 2006. Influence of water chemistry on the swelling capacity of high-density bentonite. In Unsaturated Soils 2006, Proc. 4th. Int'l. Conf. of Unsaturated Soils, Apr. 2006, Carefree, Arizona, A.S.C.E. Reston, Virginia, USA.

Cho, W.J., J.O. Lee and K.S. Chun. 1999. The temperature effects on hydraulic conductivity of compacted bentonite. Applied Clay Science 14, 47-58.

Cho, W.J., J.O. Lee and K.S. Chun. 2000. Influence of temperature elevation on the sealing performance of a potential buffer material for a high-level radioactive waste repository. Ann. Nucl. Energy 2000, 27, 1271–1284.

Clark, I.D., T. Al, M. Jensen, L. Kennell, M. Mazurek R. Mohapatra and K.G. Raven. 2013. Paleozoic-aged brine and authigenic helium preserved in an Ordovician shale aquiclude. GEOLOGY, September 2013; v. 41; no. 9; p. 951–954.

Clark, I.D., D. Ilin, R.E. Jackson, M. Jensen, L. Kennell, H. Mohammadzadeh, A. Poulain, Y.P. Xing and K.G. Raven. 2015. Paleozoic-aged microbial methane in an Ordovician shale and carbonate aquiclude of the Michigan Basin, southwestern Ontario. Organic Geochemistry 83-84 (2015) 118–126.

Crowe, R., K. Birch, J. Freire-Canosa, J. Chen, D. Doyle, F. Garisto, P. Gierszewski, M. Gobien, C. Hatton, N. Hunt, S. Hirschorn, M. Hobbs, M. Jensen, P. Keech, L. KennellMorrison, E. Kremer, J. McKelvie, C. Medri, M. Mielcarek, A. Murchison, A. Parmenter, R. Ross, E. Sykes and T. Yang. 2016. Technical Program for Long-Term Management of Canada's Used Nuclear Fuel – Annual Report 2015. Nuclear Waste Management Organization Report NWMO-TR-2016-01. Toronto, Canada.

Cui, Y.J. 2017. On the hydro-mechanical behaviour of MX80 bentonite-based materials. Journal of Rock Mechanics and Geotechnical Engineering 9 (2017) pp. 565-574.

Daniels, K.A., J.F. Harrington, G. Zihms and A.C. Wiseall. 2017. Bentonite permeability at elevated temperature. Geosciences, 7, 3.

Davies, C.W., C.T. Davie, E.A. Charles and M.L. White. 2017. Physicochemical and geotechnical alterations to MX-80 bentonite at the waste canister interface in an engineered barrier system. Geosciences 2017, 7, 69.

Dillström, P. and T. Bolinder. 2010. Damage tolerance analysis of canister inserts for spent nuclear fuel in the case of an earthquake induced rock shear load. Swedish Nuclear

Fuel and Waste Management Company Technical Report SKB TR-10-29. Stockholm, Sweden.

Dixon, D.A. 1994. Sodium bentonites of Canada, the United States and Mexico: Sources, reserves and properties, in Engineering Materials for Waste Isolation, Canadian Society for Civil Engineering Special Publication.

Dixon, D.A., 1995. Towards an understanding of water structure and water movement through dense clays. Ph.D. Thesis, Dept. Civil and Geol. Engineering. University of Manitoba, Winnipeg, Canada.

Dixon, D.A. 2000. Porewater salinity and the development of swelling pressure in bentonite-based buffer and backfill materials. Posiva Oy Report 2000-04. Olkiluoto, Finland.

Dixon, D.A. and N.A. Chandler. 2000. Physical properties of materials recovered from the Isothermal Buffer-Rock-Concrete Plug Interaction Test conducted at the URL. Ontario Power Generation, Nuclear Waste Management Division, Report 06819-REP-01300-10003-R00. Toronto, Canada.

Dixon, D.A. and C.L. Kohle. 2003. Laboratory study to evaluate the influence of interfaces on the hydraulic performance of repository sealing materials. Ontario Power Generation, Nuclear Waste Management Division, Technical Report 06819-REP-01200-10096-R00. Toronto, Canada.

Dixon, D.A. and S.H. Miller. 1995. Comparison of the mineralogical composition, physical swelling and hydraulic properties of untreated sodium bentonites from Canada, the United States and Japan. Atomic Energy of Canada Report, AECL-11303, COG-95-156. Chalk River, Canada.

Dixon, D.A., M.N. Gray, P. Baumgartner and G.L. Rigby. 1986. Pressure acting on waste containers in bentonite-based materials. Proc. Canadian Nuclear Society 2nd Intl conf. on Radioactive Waste Management, pp 221-227. Winnipeg, Canada.

Dixon, D.A., S.C.H. Cheung, M.N. Gray and B.C. Davidson. 1987. The hydraulic conductivity of dense clay soils. in Proc. 40th Canadian Geotechnical Conference, Regina, 19-21 Oct. 1987.

Dixon, D.A., A.W-L. Wan, J. Graham and S.L. Campbell. 1993. Assessment of self-sealing and self-healing abilities of dense, high-bentonite-content sealing materials. In Proceedings of 1993 Joint CSCE-ASCE National Conference on Environmental Engineering, Montreal, PQ, July 12-14, 1993.

Dixon, D.A., M.N. Gray and J. Graham. 1996a. Swelling and hydraulic properties of bentonites from Japan, Canada and the USA. 2nd International Congress on Environmental Geotechnics, pp. 43-48, Osaka, Japan, Nov 1996.

Dixon, D.A. A.W-L. Wan, M.N. Gray and S.H. Miller. 1996b. Water uptake and stress development in bentonites and bentonite-sand buffer materials. Atomic Energy of Canada Limited Report, AECL-11591, COG-96-221. Chalk River, Canada.

Dixon, D.A., N.A. Chandler, N.A., A.W-L. Wan, S. Stroes-Gascoyne, J. Graham and D.W. Oscarson. 1997. Pre- and post-test properties of the buffer, backfill, sand and rock components of the Buffer/Container Experiment. Atomic Energy of Canada Limited, Report AECL-11786 (COG-97-287-I). Chalk River, Canada.

Dixon, D.A., J. Graham and M.N. Gray. 1999. Hydraulic conductivity of clays in confined tests under low hydraulic gradients. Can. Geotech. J. 36, 815-825.

Dixon, D.A., B.H. Kjartanson, P. Baumgartner and J.B. Martino. 2003. The role of interfaces and permeant salinity on the hydraulic behaviour of bentonite-based barriers, in Proceedings of 56th Canadian Geotechnical Society Conference, September 29-Oct 1, Winnipeg, Canada.

Dixon, D.A., S. Stroes-Gascoyne, B. Kjartanson and P. Baumgartner. 2005. Development of sealing materials for application as engineered barriers in a deep geologic repository for used fuel disposal: Filling the gaps. In Proc. Canadian Nuclear Society Waste Management, Decommissioning and Environmental Restoration for Canada's Nuclear Activities: Current and Future Needs, May 8-11, 2005, Ottawa, Canada.

Dixon D, S. Anttila, M. Viitanen, P. Keto. 2008a. Tests to determine water uptake behaviour of tunnel backfill. SKB R-08-134, Svensk Kärnbränslehantering AB, Stockholm, Sweden.

Dixon D, C. Lundin, E. Örtendahl, M. Hedin, G. Ramqvist. 2008b. Deep repository – engineered barrier system. Half scale tests to examine water uptake by bentonite pellets in a block – pellet backfill system. SKB R-08-132, Svensk Kärnbränslehantering AB, Stockholm, Sweden.

Dixon, D.A., C.L. Kohle, D. Drew and S.G. Keith. 2006. Tensile and unconfined compression properties of Highly Compacted Bentonite, Bentonite-Sand Buffer, Dense and Light Backfill. Ontario Power Generation, Nuclear Waste Management Division, 06819-REP-01300-10118-R00. Toronto, Canada.

Dixon, D.A., A. Man, J. Stone, S. Rimal, G. Siemens, P. Abootalebi and K. Birch. 2016. Backfilling and sealing materials for a deep geological repository, 3rd Canadian Conference on Nuclear Waste Management, Decommissioning and Environmental Restoration, Ottawa, Canada.

Dixon, D.A., A. Man, S. Rimal, J. Stone and G. Siemens. 2018. Bentonite seal properties in saline water. Nuclear Waste Management Organization Report NWMO-TR-2018-20. Toronto, Canada.

Dueck, A. 2010. Thermo-mechanical cementation effects in bentonite investigated by unconfined compression tests. Swedish Nuclear Fuel and Waste Management Company Technical Report SKB TR-10-31. Stockholm, Sweden.

Dueck, A. 2014. Laboratory studies on stress-strain behaviour, Deliverable D2.2-12. Long-term Performance of Engineered Barrier Systems PEBS, European Commission 7th Euratom Framework Programme for Nuclear Research & Training Activities (2007-2011).

Dueck,A, R. Goudarazi and L. Borgesson. 2016. Buffer homogenisation. Status Report 3. Swedish Nuclear Fuel and Waste Management Company Technical Report, TR-16-04. Stockholm, Sweden.

Dueck A., L. Borgesson and L-E Johannesson. 2010. Stress-strain relation of bentonite at undrained shear: Laboratory tests to investigate the influence of material composition and test technique, Swedish Nuclear Fuel and Waste Management Company Report SKB R-10-32. Stockholm, Sweden.

Dueck A., L. Börgesson, O. Kristensson, D. Malmberg, M. Åkesson, J. Hernelind. 2019. Bentonite homogenisation: Laboratory study, model development and modelling of homogenisation processes, Swedish Nuclear Fuel and Waste Management Company Technical Report SKB TR-19-11. Stockholm, Sweden

Dutta, J. and A.K. Mishra. 2016. Consolidation behaviour of bentonites in the presence of salt solutions. Applied Clay Science, Vol. 120, pp 61-69.

Eloranta, A. 2012. Experimental methods for measuring elasto-plastic parameters of bentonite clay. Master Thesis, University of Jyväskylä, Finland.

ENRESA. 2006. FEBEX Project final report: Post-mortem bentonite analysis. Ed. M.V. Villar, Enresa Technical Publication 05-1/2006, Madrid, Spain.

Eriksson, P. 2016. Compaction properties of bentonite clay. Swedish Nuclear Fuel and Waste Management Company Technical Report SKB TR-16-16, Stockholm, Sweden.

Fälth, B. and H. Hökmark, 2012. Modelling end-glacial earthquates at Olkiluoto, Expansion of the 2010 study, Posiva Oy. Work Report WR-2012-08, Olkiluoto, Finland.

Fälth B. and H. Hökmark. 2015. Effects of hypothetical large earthquakes on repository host rock fractures, Posiva Oy. Work Report WR-2015-18, Olkiluoto, Finland

Fälth, B., H. Hökmark and R. Munier. 2008. Effects of large earthquakes on a KBS-3 repository. Evaluation of modelling results and their implications for layout and design. Swedish Nuclear Fuel and Waste Management Company, Technical Report SKB TR-08-11. Stockholm, Sweden.

Frape, S.K., P. Fritz, and R.H. McNutt. 1984. Water-rock interaction and chemistry of groundwaters from the Canadian Shield. Geochim. Cosmochim. Acta 48, 1617-1627.

Fourdin, C., T. Allard, I. Monnet, N. Menguy, M. Benedetti and G. Calas. 2010. Effect of radiation-induced amorphization on smectite dissolution. Environmental Science & Technology, 2509.

Fredlund, M.D., G.W. Wilson and D.G. Fredlund. 2002. Representation and estimation of the shrinkage curve. UNSAT 2002, Proceedings of the Third International Conference on Unsaturated Soils, Recife, Brazil, March 10-13, pp. 145-149.

Gascoyne, M., C.C. Davison, J.D. Ross and R. Pearson. 1987. Saline groundwaters and brines in plutons in the Canadian Shield. In, Saline water and gases in crystalline rocks, Ed. Fritz, P. and Frape, S.K., Geol. Assoc. of Canada, Special Paper 33, pp. 53-68.

Gens, A., M. Sanchez, L. Do, N. Guimaraes, E.E. Alonso, A. LLoret, S. Oliverlla, M.V. Villar nad F. Huertas. 2009. A full-scale in situ heating test for high-level nuclear waste disposal: observations, analysis and interpretation. Geotechnique, 59 (4) pp 377-399.

Gobien, M., F. Garisto, E. Kremer, and, C. Medri. 2018. Seventh Case Study: Reference data and codes. Nuclear Waste Management Organization Report NWMO-TR-2018-10. Toronto, Canada.

Gournis, D., A.E. Mantaka-Marketou, M.A. Karakassides and D. Petridis. 2000. Effect of γ-irradiation on clays and organoclays: a Mössbauer and XRD study. Physics and Chemistry of Minerals, Volume 27, Issue 7, pp 514–521.

Graham, J., J.M. Oswell and M.N. Gray. 1992. The effective stress concept in saturated sand-clay buffer. Canadian Geotechnical Journal, 29, 1033-1043.

Graham, J., N.A. Chandler, D.A. Dixon, P.J. Roach, T. To and A.W.L. Wan. 1997. The Buffer/Container Experiment: Results. Atomic Energy of Canada Ltd, TR-11746. Chalk River, Canada.

Grandia, F., J.M. Galindez, D. Arcos and J. Molinero. 2010. Quantitative modelling of the degradation processes of cement grout, Project CEMMOD. Swedish Nuclear Fuel and Waste Management Company Technical Report SKB TR-10-25. Stockholm, Sweden.

Grauer, R. 1986. Bentonite as a backfill material in the high-level waste repository: chemical aspects. National Cooperative for the Disposal of Radioactive Waste (NAGRA) Technical Report 86-12E. Baden, Switzerland.

Guo, R. 2018. Thermal response of a conceptual deep geological repository in sedimentary rock. Nuclear Waste Management Organization Report NWMO-TR-2018-09. Toronto, Canada.

Gutiérrez-Rodrigo, V., M. V. Villar, P.L. Martin and F.J. Romero. 2014. Gas transport properties of compacted bentonite. In Unsaturated Soils: Research & Applications, Khalili, Russell & Khoshghalb (eds). CRC Press, Taylor & Francis Grp. London, UK.

Haire, R.G. and G.W. Beall. 1979. Consequences of radiation from sorbed transplutonium elements on clays selected for waste isolation. In, Ed. R.F. Gould, Radioactive waste in geologic storage; ACS Symp. Series 100, Ch 16, pp 291-295, Miami Beach, 11-15 Sept 1978.

Hancilova I. and M. Hokr. 2016. Coupled hydro-mechanical model of bentonite hydration and swelling, Earth and Environmental Science 44 (2016).

Hansen, J. 2004. Planned use of cement in Onkalo, In a KBS-3V type and KBS-3H type repository in crystalline rock. Posiva Oy Working Report WR-2004-25. Olkiluoto, Finland.

Hartley L., P. Appleyard, S. Baxter, J. Hoek, D. Roberts and D. Swan. 2012a. Development of a Hydrogeological Discrete Fracture Network Model for the Olkiluoto Site Descriptive Model 2011, Volume I, Posiva Oy, Working Report, WR-2012-32, Olkiluoto, Finland.

Hartley, L., J. Hoek, D. Swan, P. Appleyard, S. Baxter, D. Roberts, & T. Simpson. 2012b. Hydrogeological Modelling for Assessment of Radionuclide Release Scenarios for the Repository System 2012, Posiva Oy, Working Report, WR-2012-42, Olkiluoto, Finland.

Hartley, L., J. Hoek, D. Swan, S. Baxter and H. Woollard. 2012c. Hydrogeological Discrete Fracture Modelling to Support Rock Suitability Classification, Posiva Oy, Working Report, WR-2012-48, Olkiluoto, Finland

Hatton, C. 2015. Development of the Canadian used fuel repository engineered barrier system. Proc. IHLRWM 2015, Charleston, South Carolina, USA, April 12-16, 2015.

Hedström, M., E.E. Hansen and U. Nilsson. 2015. Montmorillonite phase behavior: Relevance for buffer erosion in dilute groundwater. Swedish Nuclear Fuel and Waste Management Company Technical Report SKB TR-15-07. Stockholm, Sweden.

Hernelind, J. 2010. Modelling and analysis of canister and buffer for earthquake induced rock shear and glacier load. Swedish Nuclear Fuel and Waste Management Company Technical Report SKB TR-10-34. Stockholm, Sweden.

Hobbs M.Y., S.K. Frape, O. Shouakar-Stash and L.R. Kennell. 2011. Regional hydrogeochemistry – Southern Ontario, Nuclear Waste Management Organization Report, DGR-TR-2011-12. Toronto, Canada.

Holmboe, M., S. Wold and M. Jonsson. 2012. Porosity investigation of compacted bentonite using XRD profile modeling. J. Contam. Hydrol. V128 (1), pp 19-32.

Hökmark, H. 2003. Temperature Buffer Test – Comparison of modelling results/experimental findings: Causes of differences. In proc. Large Scale Field Tests in Granite – Barrier behaviour and T-H-M modelling, Stiges, Spain.

Hollmén, K., U. Sievänen, J. Funehag, N. Granberg, T. Lyytinen, P. Syrjänen and J. Säippä. 2012. Colloidal Silica–grouting in Demonstration Tunnel 2 in ONKALO, Posiva OY, Work Report 2012-84, Olkiluoto, Finland.

Huang, W-H. and W.C. Chen. 2004. Swelling behavior of a potential buffer material under simulated near field environment. Journal of Nuclear Science and Technology, Vol. 41, No. 12, p. 1271–1279.

Idiart, A. and M. Pekala. 2015. Models for diffusion in compacted bentonite. Swedish Nuclear Fuel and Waste Management Company Technical Report SKB TR-15-06. Stockholm, Sweden.

Jacinto, A.C., M.V. Villar, R. Gomez-Espina and A. Ledesma. 2009. Adaptation of the van Genuchten expression to the effects of temperature and density for compacted bentonites. Applied Clay Science, (42), 575–582.

Jacinto, A., R. Gomez-Espina, M.V. Villar and A. Ledesma. 2007. Effect of temperature on the retention capacity of compacted bentonite: An experimental and numerical investigation. In Proceedings of the International Meeting on Clays in Natural & Engineered Barriers for Radioactive Waste Confinement, Lille, France, 17–20 September 2007.

JNC. 2003. Assessment on mechanical effect of engineering barrier system to fault movement. JNC TN8400 2003-009 (provided as appendix by Read 2011). Japan.

Johannesson, L. E. 1999. Compaction of full size blocks of bentonite for the KBS-3 concept: Initial tests for evaluation the technique. Swedish Nuclear Fuel and Waste Management Company Report SKB R-99-66. Stockholm, Sweden.

Johannesson, L.E., S. Nord, R. Pusch and R. Sjoblom. 2000. Isostatic compaction of beaker shaped bentonite blocks on the scale 1:4, Swedish Nuclear Fuel and Waste Management Company Report SKB TR-00-14. Stockholm, Sweden.

Johannesson, L. E. and L. Börgesson. 2002. Laboratory tests on Friedland Clay - Friedland Clay as backfill material. Results of laboratory tests and swelling/compression calculations. Swedish Nuclear Fuel and Waste Management Company International Progress Report IPR-02-50. Stockholm, Sweden.

Johannesson, L. E, A. Dueck L. Andersson and V. Jensen. 2015. Investigations of hydraulic and mechanical processes of the barriers embedding the silo in SFR Laboratory tests. Swedish Nuclear Fuel and Waste Management Company Technical Report SKB TR-15-05. Stockholm, Sweden.

Johnson, L.H. and F. King. 2002. Canister options for the disposal of spent fuel. National Cooperative for the Disposal of Radioactive Waste (NAGRA) Technical Report 02-11. Wettingen, Switzerland.

Johnsson, A. and T. Sandén. 2013. System design of backfill: Pellet optimization. Swedish Nuclear Fuel and Waste Management Company Report SKB R-13-47. Stockholm, Sweden.

Jonsson, M. 2012. Radiation effects on materials used in geological repositories for spent nuclear fuel. Review Article, International Scholarly Research Network ISRN Materials Science, Volume 2012, Article ID 639520, 13 pages, doi:10.5402/2012/639520.

Kalbanter, P. and L.E. Johannesson. 2000. Hallfasthetsberakningar for en bentonitebuffert bestaende av enaxlight kmopakterade bentonitkropar. Swedish Nuclear Fuel and Waste Management Company Report SKB R-00-42. Stockholm, Sweden. (in Swedish).

Karnland, O. 1997. Bentonite swelling pressure in strong NaCl solutions: Correlation of model calculations to experimentally determined data. Swedish Nuclear Fuel and Waste Management Company Technical Report SKB TR-97-31. Stockholm, Sweden.

Karnland, O. 1998. Bentonite swelling pressure in strong NaCl solutions: Correlation of model calculations to experimentally determined data. Posiva Oy Report Posiva 98-01. Olkiluoto, Finland.

Karnland, O., S. Olsson and U. Nilsson. 2006. Mineralogy and sealing properties of various bentonites and smectite-rich clay materials. Swedish Nuclear Fuel and Waste Management Company Technical Report SKB TR-06-30. Stockholm, Sweden.

Karnland, O., S. Olsson, U. Nilsson and P. Sellin. 2007. Experimentally determined swelling pressures and geochemical interactions of compacted Wyoming bentonite with highly alkaline solutions. Physics and Chemistry of the Earth, 32, 275-286.

Karnland, O. 2010. Chemical and mineralogical; characterization of the bentonite buffer for the acceptance control procedure in a KBS-3 repository. Swedish Nuclear Fuel and Waste Management Company Technical Report SKB TR-10-60. Stockholm, Sweden.

Keto P., D. Dixon, E. Jonsson, D. Gunnarsson, L. Börgesson and J. and Hansen. 2009. Assessment of backfill design for KBS-3V repository. Swedish Nuclear Fuel and Waste Management Company Technical Report SKB-R-09-52. Stockholm, Sweden.

Khan, M.I. 2013. Hydraulic conductivity of moderate and highly dense expansive clays. PhD. Thesis, Faculty of Civil and Environ. Engrg. Ruhr-Universität Bochum, Germany.

Kim, C.S. and D.P. Priyanto. 2011. Two-Component swelling tests operated for three, nine and twenty seven months, NWMO TR-2011-15, Toronto, Canada.

Kim, C.S., A. Man, D. Dixon, E. Holt and A. Fritzell. 2012. Clay-based pellets for use in tunnel backfill and as gap fill in a deep geological repository: characterisation of thermal-mechanical properties. Nuclear Waste Management Organization Report NWMO-TR-2012-05. Toronto, Canada.

Kim, J-S. S. Kwon, J-W. Choi and G-C. Cho. 2011. Properties of low-pH cement grout as a sealing material for the geological disposal of radioactive waste. Nuclear Engineering and Technology, V43(5) pp 459-468. http://dx.doi.org/10.5516/NET.2011.43.5.459

Kiviranta L. and S. Kumpulainen. 2011. Quality control and characterization of bentonite materials. Posiva Oy Working Report WR-2011-84. Eurajoki, Finland.

Kiviranta, L., S. Kumpulainen, X. Pintado and P. Schatz, T. 2016, Characterization of bentonite and clay materials 2012-2015, Posiva Oy Working Report WR-2016-05, Olkiluoto, Finland.

Kleinbaum, D.G. and L.L. Kupper. 1978. Applied regression analysis and other multivariable methods. Duxbury Press. North Scituate, Massachusetts, USA.

Klute, A. 1986. Water retention: Laboratory Methods. Methods of Soil Analysis Part 1: Physical and Mineralogical Methods, ed. Klute A. Madison, WI: American Society of Agronomy and Soil Science Society of America, 635-662.

Knutsson, S. 1983. On the thermal conductivity and thermal diffusivity of highly compacted bentonite. Swedish Nuclear Fuel and Waste Management Company Technical Report KBS-83-72. Stockholm, Sweden.

Kobayashi, I., K. Suzuki, H. Asano, P. Sellin, C. Svemar and M. Holmqvist. 2014. Mechanical interpretations of the homogeneous nature of bentonite due to swelling. In Clays in Natural and Engineered Barriers for Radioactive Waste Confinement, (eds. Norris, Bruno, Cathelineau, Delage, Fairhurst, Gaucher, Holn, Kalinichev, Lalieux and Sellin). Geol. Soc. London Special Publ. Vol. 400.

Kochmanova, N. and H. Tanaka. 2011. Microstructure formation in bentonite, Proceedings of the 17th International Conference on Soil Mechanics and Geotechnical Engineering. M. Hamza et al. (Eds.)

Komine, H. and N. Ogata. 1998. Thermal influence on compacted bentonite for nuclear waste disposal. In Proceedings of the 3rd International Congress on Environmental Geotechnics, volume 1, pages 34–39.

Koskinen V. and T. Sandén. 2014. System design of backfill. Distribution of inflowing water by using geotextile. Swedish Nuclear Fuel and Waste Management Company Technical Report SKB R-14-10. Stockholm, Sweden.

Koskinen, V. 2015. State-of-the-art, November 2014 – Water handling during backfill installation. Swedish Nuclear Fuel and Waste Management Company Report SKB R-15-18. Stockholm, Sweden.

Laine, H. and P. Karttunen. 2010. Long-term stability of Bentonite – A literature review. Posiva Oy Working Report WR-2010-53. Olkiluoto, Finland.

Lambe, T.W. and R. V. Whitman. 1979. Soil Mechanics: SI Version. J. Wiley and Sons. 553 pgs. Toronto, Canada.

Lee, J-H, M-S. Lee, H-J Choi and J-W. Choi. 2010a, Temperature effect on the swelling pressure of a domestic compacted bentonite buffer. J. of Nuclear Fuel Cycle and Waste Technology, Korean Radioactive Waste Soc., V8 (3) pp 207-213.

Lee, J.O., W.J. Cho, C.H. Kang and K.S. Chun. 2010b. Swelling and hydraulic properties of Ca-Bentonite for the buffer of a waste repository. IAEA-SM-357/68, Vienna, Austria.

Lee, J.O., H. Choi and J.Y. Lee. 2016. Thermal conductivity of compacted bentonite as a buffer material for a high-level radioactive waste repository. Annals of Nuclear Energy. 94: 848-855.

Lehikoinen J. 2009. Bentonite-cement interaction – Preliminary results from model calculations, Posiva Oy Working Report, WR-2009-37, Olkiluoto, Finland.

Leupin, O.X., M. Birgersson, O. Karnland, P. Korkeakoski, P. Sellin, U. Mader and P. Wersin. 2014. Montmorillonite stability under near-field conditions. National Cooperative for the Disposal of Radioactive Waste (NAGRA) Technical Report 14-12, Wettingen, Switzerland.

Lingnau, B., J. Graham, D. Yarechewski, N. Tanaka and M.N. Gray. 1996. Effects of temperature on strength and compressibility of sand-bentonite buffer. Engrg. Geol. 41(1) 103-115.

LLoret, A., M.V. Villar, M. Sanchez, A. Gens, X. Pintado and E. Alonso. 2003. Mechanical behaviour of heavily compacted bentonite under high suction changes. Geotechnique, 53 (1), pp 27-40.

Lofman, J., A. Poteri and P. Pitkanen. 2010. Modelling of salt water upconing in Olkiluoto. Posiva Oy Working Report, WR-2010-25. Olkiluoto, Finland.

Madsen, F. T. 1998. Clay mineralogical investigations related to nuclear waste disposal. Clay Minerals, 33(1), pp. 109-129.

Man, A. and J. Martino. 2009. Thermal, Hydraulic and Mechanical properties of sealing materials. Nuclear Waste Management Organization Report NWMO-TR-2009-20. Toronto, Canada.

Man, A., J. Martino, C.S. Kim and D. Priyanto. 2011. Characterization and improving the thermal conductivity of engineered clay barriers for sealing a deep geological repository. Waste Management, Decommissioning and Environmental Restoration for Canada's Nuclear Activities. Toronto, Canada.

Martikainen J. and T. Schatz. 2011. Laboratory tests to determine the effect of Olkiluoto bounding brine water on buffer performance, Posiva Oy, Working Report WR-2011-68. Eurajoki, Finland.

Martikainen J. and T. Schatz 2016. Initial Buffer and Backfill Wetting: Pellet-filling component, Posiva Oy, Working Report WR-2016-53 – Section 6-1. Eurajoki, Finland.

Marshall, M.H.M. and M.J. Simpson. 2014. Characterization of natural organic matter in bentonite clays. Nuclear Waste Management Organization Report NWMO-TR-2014-10. Toronto, Canada.

Martino, J., D. Dixon, S. Stroes-Gascoyne, R. Guo, E.T. Kozak, M. Gascoyne, T. Fujita, B. Vignal, Y. Sugita, K. Masumoto, T. Saskura, X. Bourbon, A. Gingras-Genois and D. Collins. 2008. The Tunnel Sealing Experiment: 10 Year Summary Report. Atomic Energy of Canada Limited, Tunnel Sealing Experiment Report URL-121550-REPT-001 R0. Chalk River, Canada.

Meunier, A., B. Velde and L. Griffault. 1998. The reactivity of bentonites: a review. An application to clay barrier stability for nuclear waste storage. Clay Minerals, 187-196.

Mielcarek, M. and K. Birch. 2016a. Demonstration of gap fill material delivery technology to backfill placement room voids. In: 3rd Canadian Conference on Nuclear Waste Management, Decommissioning and Environmental Restoration, Ottawa, Canada.

Mielcarek, M. and K. Birch. 2016b, The Use of isostatic compression to produce full-scale highly compacted bentonite blocks. In: 3rd Canadian Conference on Nuclear Waste Management, Decommissioning and Environmental Restoration, Ottawa, Canada.

Mitchell, J. K. 1993. Fundamentals of Soil Behavior. 2nd Edition. John Wiley & Sons, Inc. New York, USA. 422 pgs.

Montes, H, G., J. Duplay, L. Martinez, Y. Geraud and B. Rousset-Tournier. 2003. Influence of interlayer cations on the water sorption and swelling–shrinkage of MX80 bentonite. Applied Clay Science, 23(2003), 309-321.

Morco, R.P., J. M. Joseph, D.S. Hall, C. Medri, D.W. Shoesmith and J.C. Wren. 2017. Modelling of radiolytic production of HNO_3 relevant to corrosion of a used fuel container in deep geologic repository environments. Corrosion Engineering, Science and technology, 2017, VOL. 52, NO. S1, 141–147. https://doi.org/10.1080/1478422X.2017.1340227

Motamedi, M. 1999. The survival and activity of bacteria in compacted bentonite clay in conditions relevant to high level radioactive waste (HLW) repositories. PhD thesis. Göteborg University, Göteborg, Sweden.

Müller, H.R., B. Garitte, T. Vogt, S. Köhler, T. Sakaki, H. Weber, T. Spillmann, M. Hertrich, J.K. Becker, N. Giroud, V. Cloet, N. Diomidis and T. Vietor. 2017. Implementation of the full-scale emplacement (FE) experiment at the Mont Terri rock laboratory. Paper #14, Mont Terri Special Issue of Swiss J. Geosci.

Muurinen, A. 2009. Studies on the chemical conditions and microstructure in the reference bentonites of Alternative Buffer Materials Project (ABM) in Äspö. Posiva Oy Working Report WR-2009-42. Olkiluoto, Finland.

Muurinen, A. and T. Carlsson. 2013. Bentonite pore structure based on SAXS, chloride exclusion and NMR studies. Posiva Oy Working Report WR-2013-53. Olkiluoto, Finland.

Nasseri, M.H.B. and R.P. Young. 2014. Thermo-Hydro-Mechanical properties of Cobourg limestone. Nuclear Waste Management Organization Report NWMO-TR-2014-26. Toronto, Canada.

Negron, A., S. Ramos, A.L. Blumenfeld, G. Pacheco and J.J. Fripiat. 2002. On the structural stability of montmorillonite submitted to heavy γ-irradiation. Clays and Clay Minerals, vol. 50, no. 1, pp. 35–37.

Noronha, J. 2016. Deep geological repository conceptual design report: Crystalline / sedimentary rock environment. Nuclear Waste Management Organization Report NWMO-APM-REP-00440-0015 R001. Toronto, Canada.

NWMO. 2011a. Geoscientific verification plan. Nuclear Waste Management Organization Report DGR-TR-2011-38. Toronto, Canada.

NWMO. 2011b. Geosynthesis. Nuclear Waste Management Organization Report, NWMO-DGR-TR-2011-11. Toronto, Canada.

NWMO. 2017. Postclosure safety assessment of a used fuel repository in crystalline rock. Nuclear Waste Management Organization Report NWMO-TR-2017-02. Toronto, Canada.

NWMO. 2018. Postclosure safety assessment of a used fuel repository in sedimentary rock. Nuclear Waste Management Organization Report NWMO-TR-2018-08. Toronto, Canada.

Onofrei, M. and M.N. Gray. 1990. Laboratory studies on the longevity of cement grouts. Nuclear Energy Agency of the OECD (NEA): Organization for Economic Co-operation and Development. Paris, France.

Oscarson, D.W. and D.A. Dixon. 1989. The effect of steam on montmorillonite. Appl. Clay Sci., 4, 279-292.

Oscarson, D.W. and D.A. Dixon. 1990. Effect of heating unsaturated bentonite on the swelling and hydraulic properties of subsequently saturated clay. Can. Soc. Civil Engrg., 1990 Annual Conference, Vol II-1, pp II-312-322, Hamilton, Canada.

Oscarson, D.W., D.A. Dixon and M. Onofrei. 1996a. Preliminary study of clay/concrete interactions. Atomic Energy of Canada Limited, TR-753, COG-96-316, Chalk River, Canada.

Oscarson, D.W., D.A. Dixon and H.B. Hume. 1996b. Mass transport and swelling properties of defected bentonite plugs. 49th Cdn. Geotech. Conf. 23-25 Sept. 1996, St. Johns, Canada.

Ould-Lahoucine, C., H. Sakashita and T. Kumada. 2002. Measurement of thermal conductivity of buffer materials and evaluation of existing correlations predicting it. Nuclear Engineering and Design Journal, 216(1), pp. 1-11.

Ouyang, S. and J.J.K. Daemen. 1992. Sealing performance of bentonite and bentonite/crushed rock borehole plugs. U.S. Nucl. Reg. Comm. (NUREG) Report, NUREG/CR-5685, Washington, DC, USA.

Ozbek, H., J.A. Fair and S.L. Phillips. 1977, Viscosity of aqueous sodium chloride solutions from 0 – 150°C. Lawrence Berkeley National Laboratory, LBL-5931. Berkeley, USA. http://escholarship.org/uc/item/3jp6n2bf.

Pastina, B. and P. Hellä. 2006. Expected evolution of a spent nuclear fuel repository at Olkiluoto. POSIVA Oy Working Report 2006-05. Olkiluoto, Finland.

Pedersen K., M. Motamedi O. Karnland and T. Sandén. 2000. Cultivability of microorganisms introduced into a compacted bentonite clay buffer under high-level radioactive waste repository conditions. Engineering Geology 58, 149–161.

Plotze, M., G. Kahr and R.H. Stengele. 2003. Alteration of clay minerals-gamma-irradiation effects on physicochemical properties. Applied Clay Science, vol. 23, no. 1-4, pp. 195–202.

Pramuditya, S. 2011. Water thermodynamic properties. ITB Physics Department – Technical Document. https://syeilendrapramuditya.wordpress.com/2011/08/20/water-thermodynamic-properties/

Priyanto, D.G., J. A. Blatz, G.A. Siemens, R. Offman, J.S. Boyle and D.A. Dixon. 2008a. The effects of initial conditions and liquid composition on the one-dimensional consolidation behaviour of clay-based sealing materials. Nuclear Waste Management Organization Report NWMO-TR-2008-06. Toronto, Canada.

Priyanto, D.G., J. A. Blatz, G.A. Siemens, R. Offman, J.S. Powell and D.A. Dixon. 2008b. The effects of fluid composition on the one-dimensional consolidation behaviour of clay-based sealing materials. Nuclear Waste Management Organization Report NWMO-TR-2008-20. Toronto, Canada.

Priyanto, D.G. 2012. Unpublished statistical analyses. Basic spreadsheet formulations used by permission (D.Priyanto pers comm. 02 Oct. 2018).

Priyanto, D.G., C.S. Kim and D.A. and Dixon. 2013. Geotechnical characterization of a potential shaft backfill material. Nuclear Waste Management Organization Report NWMO-TR-2013-03. Toronto, Canada.

Pusch R. 1977. Influence of cementation on the deformation properties of bentonite/Quartz buffer substance. Swedish Nuclear Fuel and Waste Management Company Technical Report SKB KBS-TR-14. Stockholm, Sweden.

Pusch, R. 1980a. Swelling pressure of highly compacted bentonite. Swedish Nuclear Fuel and Waste Management Company Technical Report SKB TR-80-13. Stockholm, Sweden.

Pusch, R. 1980b. Permeability of highly compacted bentonite. Swedish Nuclear Fuel and Waste Management Company Technical Report SKB KBS-80-16. Stockholm, Sweden.

Pusch R., 1983. Stress/strain/time properties of highly compacted bentonite. SKBF/KBS Technical Report 83-47, Swedish Nuclear Fuel and Waste Management Company, Stockholm

Pusch, R. 1993. Waste disposal in rock. Developments in Geotechnical Engineering, 76, Elsevier.

Pusch, R. 2001. The microstructure of M-80 clay with respect to its bulk physical properties under different environmental conditions, Swedish Nuclear Fuel and Waste Management Company SKB, Technical Report TR-01-08. Stockholm, Sweden.

Pusch, R. 2002. The Buffer and Backfill Handbook Part 2: Materials and techniques. Swedish Nuclear Fuel and Waste Management Company Technical Report SKB TR-02-12. Stockholm, Sweden.

Pusch, R., O. Karland and H. Hökmark. 1990. GMM – A general microstructural model for qualitative and quantitative studies of smectite clays. Swedish Nuclear Fuel and Waste Management Company Technical Report SKB TR-90-43. Stockholm, Sweden.

Pusch, R., L. Börgesson and M. Erlström. 1987. Alteration of isolating properties of dense smectite clay repository environment as exemplified by seven prequaternary clays. Swedish Nuclear Fuel and Waste Management Company Technical Report SKB TR 87-29. Stockholm, Sweden.

Pusch, R., H. Takase, S. Benbow. 1998. Chemical processes causing cementation in heat-affected smectite – the Kinnekulle bentonite, Swedish Nuclear Fuel and Waste Management Company TR-98-25, Stockholm, Sweden.

Pusch, R., H. Takase and S. Benbow. 1998. Chemical processes causing cementation in heat-affected smectite – the Kinnekulle bentonite. Swedish Nuclear Fuel and Waste Management Company Technical Report SKB TR-98-25. Stockholm, Sweden.

Radakovic-Guzina, Z., A. Riahi and B. Damjanac. 2015. Long-Term stability analysis of APM conceptual repository design in sedimentary and crystalline rock settings. Nuclear Waste Management Organization Report NWMO-TR-2015-27. Toronto, Canada.

Radhakrishna, H. S., H.T. Chan A. Crawford and K.C. Lau. 1989. Thermal and physical properties of candidate buffer-backfill materials for a nuclear fuel waste disposal vault. Canadian Geotechnical Journal, 26(4), pp. 629-639.

Rautioaho, E. and L. Korkiala-Tanttu. 2009. Bentomap: Survey of bentonite and tunnel backfill knowledge State-of-the-art. VTT Working Papers 133, Helsinki, Finland.

Read, R.S. 2011. Effects of earthquake induced rock shear on containment system integrity: Laboratory testing plan development. Swedish Nuclear Fuel and Waste Management Company Report SKB R-11-21. Stockholm, Sweden.

Reed, D.T., S.D. Donar and M.F. Weiner. 1987. Gamma and alpha radiation levels in a basalt high-level waste repository: potential impact on container corrosion and packing properties. In: ed. Tsang C-F, Coupled Processes Associated with Nuclear Waste Repositories. Academic Press Inc. Toronto, Canada.

Riikonen E. 2008. Flow-through and wetting tests of pre-compacted backfill blocks in a quarter-scale test tunnel. Posiva Oy Working Report, WR-2008-89. Olkiluoto, Finland.

Ritola, J. and E. Pyy. 2011. Isostatic compression of buffer blocks – Middle scale. Posiva Oy Working Report, WR-2011-62. Olkiluoto, Finland.

Robinson, R.A. and R.H. Stokes 1959. Electrolyte solutions, 2nd ed., London, Butterworths, 559p.

Romero, E., A. Gens and A. Lloret. 2000. Temperature effects on water retention and water permeability of an unsaturated clay. Proceeding of Unsaturated Soils for Asia, (Eds. Rahardjo, Toll and Leong), Balkema, 433-438.

Romero, E., A. Gens and A. Lloret. 2001. Temperature effects on the hydraulic behaviour of an unsaturated clay. Geotechnical and Geological Engineering, 19(3):311–332.

Romero, E. and P.H. Simms. 2008. Microstructure investigation in unsaturated soils: A review with special attention to contribution of mercury intrusion porosymetry and environmental scanning electron microscopy. Geotechnical and Geological Engineering, 26, 705-727.

Safi, I. 2017. Radiation effects on KBS-3 Barriers, SKB's work so far. KTH Royal Institute of Technology, School of Chemical Science and Engineering. Stockholm, Sweden.

Sandén, T. 2016. Geotextile and temporary drainage, Design of methods KBP1011: Water handling during backfill installation. Swedish Nuclear Fuel and Waste Management Company Report SKB P-16-15. Stockholm, Sweden.

Sandén, T. and L. Börgesson. 2014. System design of backfill: Methods for water handling Swedish Nuclear Fuel and Waste Management Company Report, SKB R-14-09. Stockholm, Sweden.

Sandén, T. and V. Jensen. 2016. Pellet optimization – influence of fine material KBP1011 Water handling during backfill installation. Swedish Nuclear Fuel and Waste Management Company Report SKB R-16-15. Stockholm, Sweden.

Sandén, T., L. Börgesson, A. Dueck, R.Goudarzi and M. Lönnqvist. 2008. Deep repository-engineered barrier system; erosion and sealing processes in tunnel backfill materials investigated in laboratory. Swedish Nuclear Fuel and Waste Management Company Technical Report SKB R-08-135. Stockholm, Sweden.

Sandén, T., U. Nilsson and L. Andersson. 2016. Investigation of parameters influencing bentonite block quality. Swedish Nuclear Fuel and Waste Management Company Report SKB P-16-06. Stockholm, Sweden.

Sandén , T., Marjavaara, P. and Fritzell, A. 2018. Water handling during backfilling: Development Report, Posiva SKB Report 5, Olkiluoto, Finland.

Savage, D. 2013. An assessment of the impact of the long-term evolution of engineered structures on the safety-relevant functions of the bentonite buffer in a HLW repository, Nagra Technical Report, 13-02, Wettingen, Switzerland.

Seiphoori, A. 2015. Thermo-hydro-mechanical characterisation and modelling of Wyoming granular bentonite. National Cooperative for the Disposal of Radioactive Waste (NAGRA) Technical Report NTB-15-05. Wettingen, Switzerland.

Shirazi, S.M., H. Kazama, J. Kuwano and M.M. Rashid. 2010. The influence of temperature on swelling characteristics of compacted bentonite for waste disposal. Environment Asia, 3(1) 60-64. www.tshe.org/EA.

Siemens, G., J.A. Blatz, and D. Ruth. 2007. A capillary-tube model for two-phase transient flow through bentonite materials. Can. Geotech. J., 44 (12), pp 1446-1461.

Sievänen, U., P. Syrjänen and S. Rantaaho. 2004. Injection grout for deep repositories – low-pH cementitious grout for larger fractures. Field testing in Finland, Pilot Tests. Posiva Oy Working Report WR-2004, Olkiluoto, Finland.

Sievänen, U. and A. Bodén. 2005. Low-pH injection grout for deep repositories. Summary report from a co-operative project between NUMO (Japan), Posiva (Finland) and SKB (Sweden). Swedish Nuclear Fuel and Waste Management Company Report R-05-40. Stockholm, Sweden.

SKB, 2006. Buffer and Backfill process report for the Safety Assessment SR-Can, Swedish Nuclear Fuel and Waste Management Company Technical Report SKB R-08-135. Stockholm, Sweden.

Sorieul, S. 2003. Radiation damage study in montmorillonites. Application to the high-level nuclear waste disposal in France. PhD. Thesis, University of Paris. Paris, France.

Sorieul, S., T. Allard, L.M. Wang, L.M. Grambin-Lapeyre‖, J. Lian, G. Calas and R.C. Ewing. 2008. Radiation-stability of smectite. Environ. Sci. Technol., 2008, 42 (22), pp 8407–8411.

Stone, W., O. Kroukamp, J. McKelvie, D.R. Korber and G.M. Walfaardt. 2016. Microbial metabolism in bentonite clay: Saturation, desiccation and relative humidity. Applied Clay Sci. 129, pp54-64.

Stroes-Gascoyne, S. 2005. A review of international experience with microbial activity in bentonite-based sealing materials and argillaceous host rocks. Ontario Power Generation Report 06819-REP-01300-10109-R00. Toronto, Canada.

Stroes-Gascoyne, S. and C.J. Hamon. 2008. The effect of intermediate dry densities (1.1-1.5 g/cm^3) and intermediate porewater salinities (60-90 g NaCl/L) on the culturability of heterotrophic aerobic bacteria in compacted 100% bentonite. Nuclear Waste Management Organization Report NWMO-TR-2008-11. Toronto, Canada.

Stroes-Gascoyne, S. and C.J. Hamon. 2010. The effects of elevated temperatures on the viability and culturability of bacteria indigenous to Wyoming MX-80 bentonite. Nuclear Waste Management Organization Report NWMO-TR-2010-08. Toronto, Canada.

Stroes-Gascoyne, S., C.J. Hamon, D.A. Dixon and B. Kjartanson. 2005. Factors affecting microbial activity in compacted clay-based sealing materials proposed for use in a deep geologic repository for used nuclear fuel. In Proc. Canadian Nuclear Society conference "Waste Management, Decommissioning and Environmental Restoration for Canada's Nuclear Activities: Current Practices and Future Needs". 2005 May 8-11, Ottawa, Canada.

Stroes-Gascoyne, S., C.J. Hamon, C. Kohle and D.A. Dixon. 2006. The effects of dry density and porewater salinity on the physical and microbiological characteristics of highly compacted bentonite. Ontario Power Generation Report 06819-REP-01200-10016-R00. Toronto, Canada.

Stroes-Gascoyne, S., P. Maak, C.J. Hamon and C. Kohle. 2007a. Potential implications of microbes and salinity on the design of repository sealing system components. Nuclear Waste Management Organization Report NWMO-TR-2007-10. Toronto, Canada.

Stroes-Gascoyne S., C.J. Hamon D.A. Dixon C.L. Kohle and P. Maak. 2007b. The effects of dry density and pore-water salinity on the physical and microbiological characteristics of compacted 100% bentonite. In: Proceedings of the symposium on Scientific Basis for Nuclear Waste Management, Sheffield, UK.

Stroes-Gascoyne, S., P. Maak, C.J. Hamon and C. Kohle. 2010a. Potential implications of microbes and salinity on the design of repository sealing system components. Nuclear Waste Management Organization Report NWMO-TR-2007-10. Toronto, Canada.

Stroes-Gascoyne, S., C.J. Hamon, P. Maak and S. Russell. 2010b. The effects of the physical properties of highly compacted smectitic clay (bentonite) on the culturability of indigenous microorganisms. Applied Clay Science 47, 155-162.

Stroes-Gascoyne S., C.J. Hamon, D.A. Dixon and D. Priyanto. 2010c. The effect of $CaCl_2$ porewater salinity (50-100 g/L) on the culturability of heteroptrophic aerobic bacteria in compacted 100% bentonite with dry densities of 0.8 and 1.3 g/cm^3. Nuclear Waste Management Organization Report NWMO-TR-2010- 06. Toronto, Canada.

Studds, P.G. D.I. Stewart and T.W. Cousens. 1998. The effects of salt solutions on the properties of bentonite-sand mixtures. Clay Minerals, Vol 33, pp 651-660.

Suzuki, H., M. Shibata, J. Yamagata, I. Hirose and K. Terakado. 1992. Physical and mechanical properties of bentonite (I). PNC TN1410 92–52 (in Japanese). Japan.

Suzuki, S., H. Sato, T. Ishidera and N. Fujii. 2004. Study on anisotropy of effective diffusion coefficient and activation energy for deuterated water in compacted sodium bentonite. Journal of Contaminant Hydrology, 68(1-2): 23-37.

Swartzendruber, D. 1962. Non-Darcy flow behaviour in liquid-saturated porous media. J. Geeophys. Res. 67, 5205-5213.

Tang, A.M. and Y.J. Cui. 2005. Controlling suction by the vapour equilibrium technique at different temperatures and its application in determining the water retention properties of MX80 clay. Canadian Geotechnical Journal, 42 (1): 287-296.

Tang, A.M. and Y.J. Cui. 2009. Modelling the thermo-mechanical behaviour of compacted expansive clays. Géotechnique, 59 (3): 185-195.

Tang, A.M. and Y.J. Cui. 2010. Effects of mineralogy on thermo-hydro-mechanical parameters of MX 80 bentonite. Journal of Rock Mechanics and Geotechnical Engineering. 2(1): 91–96.

Tang, G.X. and J. Graham. 2000. A method for testing tensile strength in unsaturated soils. ASTM Geotechnical Testing Journal, 23 (3). West Conshohocken, Pennsylvania, USA.

Tang, A.M., Y.J. Cui and N. Barnel. 2007. A new isotropic cell for studying the thermo-mechanical behavior of unsaturated expansive soil. Geotechnical Testing Journal, 30 (5): 341 – 348.

Tang, A. M., Y.J. Cui and T.T. Le. 2008a. A study on the thermal conductivity of compacted bentonites. Applied Clay Science, 41(3), pp. 181-189.

Tang, A.M., Y.J. Cui and N. Barnel. 2008b. Thermo-mechanical behaviour of a compacted swelling clay. Géotechnique, 58 (1): 45-54.

Tripathy, S., M.Y.M. Tadza and H.R. Thomas. 2014. Soil-Water characteristic curves of clays. Can. Geotech. J. 51(8) 869-883.

Tisata, N., and S. Marelli. 2013. Laboratory measurements of the longitudinal and transverse wave velocities of compacted bentonite as a function of water content, temperature and confining pressure. J. Geophys. Res. Solid Earth V118, (3380-3393).

Van Genuchten, M.T. 1980. A closed-form equation for predicting the hydraulic conductivity of unsaturated soils. Soils Science Society of America Journal. 44, pp. 892-898.

Vieillard, P., L. Tajeddine, H. Gailhanou, P.Blanc and A. Lassin. 2016. Thermo-Analytical techniques on MX-80 montmorillonite: A way to know the behavior of water and its thermodynamic properties during hydration – dehydration processes. Pharm. Anal. Acta 7:462. doi: 10.4172/2153-2435.1000462.

Villar, M.V. 2002. Thermo-hydro-mechanical characterisation of a bentonite from Cabo de Gata: A study applied to the use of bentonite as sealing material in high level radioactive waste repositories. ENRESA technical publication 04-2002. Madrid, Spain.

Villar, M.V. and A. Lloret. 2004. Influence of temperature on the hydro-mechanical behaviour of a compacted bentonite. Applied Clay Science, 26(1-4):337 – 350.

Villar, M.V. and R. Gomez-Espina. 2008. Effect of temperature on the water retention capacity of FEBEX and MX-8- bentonites. In Toll et al., Unsat Soils: Advances in Geo-Engineering, Taylor & Francis group, (ISBN 978-0-415-47692-8). London, UK.

Villar, M.V., P.L. Martin and A. Lloret. 2005. Determination of water retention curves of two bentonites at high temperature. In: Advanced Experimental Unsaturated Soil Mechanics, ed Tarantino, Romero and Cui. Taylor & Frances, ISBN 0 415 38337 4. London, UK.

Villar, M.V., R. Gomez-Espina and A. Lloret. 2010. Experimental investigation into temperature effect on hydro-mechanical behaviours of bentonite. J Rock Mech and Geotechnical Engineering, 2 pp 71-78.

Wang, Q., A.M. Tang, Y.J. Cui, P. Delage and B. Gatmiri. 2012. Experimental study on the swelling behaviour of bentonite/claystone mixture. Engineering Geology, 124, pp.59-66.

Westsik, J.H., F.N. Hodges, W.L. Kuhn and E.J. Wheelwright. 1982. Permeability, swelling and radionuclide retardation properties of candidate backfill materials. Pacific Northwest Laboratories, Richland, USA.

Wersin, P. 2003. Geochemical modelling of bentonite porewater in high-level waste repositories. J. Contam. Hydr., 61, 405-422.

Wersin, P., L. Johnson and I. McKinley. 2007. Performance of the bentonite barrier at temperatures beyond 100ºC: A critical review. Physics and Chemistry of the Earth 32, 780-788.

Wersin, P., M. Birgersson, S. Olsson, O. Karnland and M. Snellman. 2008. Impact of corrosion-derived iron on the bentonite buffer within the KBS-3H disposal concept, The Olkiluoto site as case study. Swedish Nuclear Fuel and Waste Management Company Report SKB-R-08-34. Stockholm, Sweden.

Wimelius, H. and R. Pusch. 2008. Backfilling of KBS-3V deposition tunnels – possibilities and limitations. Swedish Nuclear Fuel and Waste Management Company Report SKB-R-08-59. Stockholm, Sweden.

Wilson, J. D. Savage, A. Bond, S. Watson, R. Pusch and D. Bennett. 2011. Bentonite – A review of key properties, processes and issues for consideration in the UK context. Quintessa Ltd., Henley-on-Thames, UK.

Wood M.I., G.D. Aden and D.L. Lane. 1983. Evaluation of sodium bentonite and crushed basalt as waste package backfill materials, US DOE Report RHO-BW-ST-21 P, NTIS, Springfield Virginia USA.

Xie, M.L., R. Miehe, J. Kasbohm, H-J. Herbert, L. Meyer and U. Ziesche. 2012. Bentonite barriers – New experiments and state of the art bentonite as barrier material for the sealing of underground disposal sites: Final Report. Gesellschaft für Anlagen- und Reaktorsicherheit (GRS), Report GRS-300, ISBN 978-3-939355-79-3. Germany.

Yong, R.N. and B.P. Warkentin. 1975. Soil properties and behaviour. Developments in Geotechnical Engineering 5, Elsevier. New York, USA.

Zihms, S.G. and J.F. Harrington. 2015. Thermal cycling: impact on bentonite permeability. Mineral. Mag. 2015, 79, 1543–1550.

APPENDICES

APPENDIX A. 1-D CONSOLIDATION DATA SUMMARY

Table A-1: Summary of 1-D Consolidation Test Data for HCB

Test Number	TDS g/L	Dry Density Mg/m^3	Avg Density (Mg/m^3)	EMDD (Mg/m^3)	Void Ratio e	Avg e	cv. m^2/s	Avg. Cv (m^2/s)	mv m^2/kN	Avg mv m^2/kN	Cc MPa^{-1}	Cr Cs MPa^{-1}	Pc (kPa)	e at Pc	Reference
MX80 DW (1)	0	1.532	1.533	1.387	0.853	0.852	4.71E-08	2.45E-08	3.13E-06	2.88E-06	0.071	0.232	>4000	<0.85	Dixon et al. 2018
	0	1.533			0.852		1.95E-08		8.22E-07						Dixon et al. 2018
	0	1.534			0.850		6.76E-09		4.70E-06						Dixon et al. 2018
MX80 DW (2)	0	1.531	1.534	1.388	0.855	0.851	1.36E-08	8.51E-09	4.72E-06	7.34E-06	0.138	0.192	>4000	<0.84	Dixon et al. 2018
	0	1.534			0.852		7.15E-09		6.29E-06						Dixon et al. 2018
	0	1.538			0.847		4.76E-09		1.10E-05						Dixon et al. 2018
MX80 DW (3)	0	1.548	1.551	1.406	0.835	0.829	4.90E-09	4.19E-09		1.18E-05	0.189	0.122	>3500	<0.83	Dixon et al. 2018
	0	1.550			0.830		4.78E-09		1.10E-05						Dixon et al. 2018
	0	1.555			0.824		2.89E-09		1.26E-05						Dixon et al. 2018
MX80 DW HCB1	0	1.670	1.670	1.529	0.647	0.647	7.60E-10				0.420	0.110			Priyanto et al. 2008
MX80 DW HCB2	0	1.670	1.670	1.529	0.647	0.647	5.50E-10				0.270	0.090			Priyanto et al. 2008
MX80 DW HCB5	0	1.440	1.440	1.293	0.910	0.910	3.67E-10				0.500	0.160			Priyanto et al. 2008
MX80 DW HCB5	0	1.440	1.440	1.293	0.910	0.910	3.67E-10				0.510	0.162			Priyanto et al. 2008
MX80 DW HCB9	0	1.650	1.650	1.508	0.667	0.667	9.17E-10				0.160	0.090			Priyanto et al. 2008
MX80 DW	0										0.179	0.149			Man 2009
MX80-75g/L HCB3	75	1.610	1.610	1.466	0.708	0.708	8.60E-10				0.220	0.050			Priyanto 2008
MX80-75g/L HCB4	75	1.760	1.760	1.624	0.563	0.563	4.50E-11				0.190	0.070			Priyanto 2008
MX80-75g/L HCB6	75	1.470	1.470	1.323	0.871	0.871	6.00E-10				0.340	0.060			Priyanto 2008
MX80-75g/L	75										0.219	0.103			Man 2009
MX80-150g/L HCB11	150	1.650	1.650	1.508	0.667	0.667					0.180	0.016			Man 2009
MX80-150g/L	150	1.650	1.650	1.508	0.667	0.667	8.00E-10				0.180	0.020			Priyanto 2008
MX80-250g/L HCB7	250	1.650	1.650	1.508	0.667	0.667	7.83E-10				0.160	0.090			Priyanto 2008
MX80-250g/L HCB8	250	1.650	1.650	1.508	0.667	0.667	1.37E-09				0.180				Priyanto 2008
MX80-250g/L HCB10	250	1.650	1.650	1.508	0.667	0.667	1.67E-09				0.190				Priyanto 2008
MX80-250g/L CaCl2	250	1.650	1.650	1.508	0.667	0.667					0.173	0.072			Man 2009
MX80-250g/L NaCl	250	1.650	1.650	1.508	0.667	0.667					0.143	0.057			Man 2009
MX80 SR-L (1)	227	1.554	1.596	1.452	0.757	0.711	2.50E-08	1.32E-08	6.32E-05	5.71E-05	0.282	0.059	646	0.785	Dixon et al. 2018
	227	1.573			0.735		1.06E-08		6.00E-05						Dixon et al. 2018
	227	1.592			0.714		1.25E-08		5.88E-05						Dixon et al. 2018
	227	1.622			0.683		1.64E-08		5.24E-05						Dixon et al. 2018
MX80 SR-L (2)	227	1.564	1.619	1.476	0.746	0.687	1.60E-08	1.11E-08	7.55E-05	7.20E-05	0.346	0.061	648	0.775	Dixon et al. 2018
	227	1.590			0.717		1.12E-08		8.10E-05						Dixon et al. 2018
	227	1.615			0.691		1.19E-08		7.01E-05						Dixon et al. 2018
	227	1.652			0.652		1.02E-08		6.49E-05						Dixon et al. 2018
MX80 SR-L (3)	227	1.566	1.597	1.453	0.743	0.719	1.01E-08	1.17E-08	4.42E-05	4.11E-05	0.198	0.045	659	0.760	Dixon et al. 2018
	227	1.580			0.728		1.18E-08		4.40E-05						Dixon et al. 2018
	227	1.597			0.709		1.27E-08		4.41E-05						Dixon et al. 2018
	227	1.615					1.05E-08		3.53E-05						Dixon et al. 2018
MX80 SR-Sh (1)	325	1.740	1.789	1.655	0.514	0.471	8.13E-09	6.51E-09	5.48E-05	4.90E-05	0.232	0.049	764	0.516	Dixon et al. 2018
	325	1.765			0.489		6.82E-09		5.26E-05						Dixon et al. 2018
	325	1.790			0.473		7.80E-09		4.82E-05						Dixon et al. 2018
	325	1.813			0.450		4.91E-09		4.62E-05						Dixon et al. 2018
MX80 SR-Sh (2)	325	1.637	1.679	1.538	0.611	0.567	8.37E-09	8.17E-09	4.42E-05	4.95E-05	0.236	0.045	778	0.613	Dixon et al. 2018
	325	1.658			0.586		8.73E-09		5.14E-05						Dixon et al. 2018
	325	1.680			0.569		8.96E-09		5.06E-05						Dixon et al. 2018
	325	1.701			0.547		6.81E-09		4.64E-05						Dixon et al. 2018
MX80 SR-Sh (3)	325	1.629	1.677	1.536	0.627	0.580	8.34E-09	6.20E-09	4.88786E-05	5.06E-05	0.232	0.048	732	0.630	Dixon et al. 2018
	325	1.658			0.599		8.75E-09		5.75954E-05						Dixon et al. 2018
	325	1.674			0.583		6.18E-09		4.86686E-05						Dixon et al. 2018
	325	1.699			0.560		3.67E-09		4.54794E-05						Dixon et al. 2018

APPENDIX B: EXAMPLES OF UNCONFINED COMPRESSIVE SHEAR BEHAVIOUR OF MX80 BENTONITE AND COMPILATION OF LITERATURE DATA

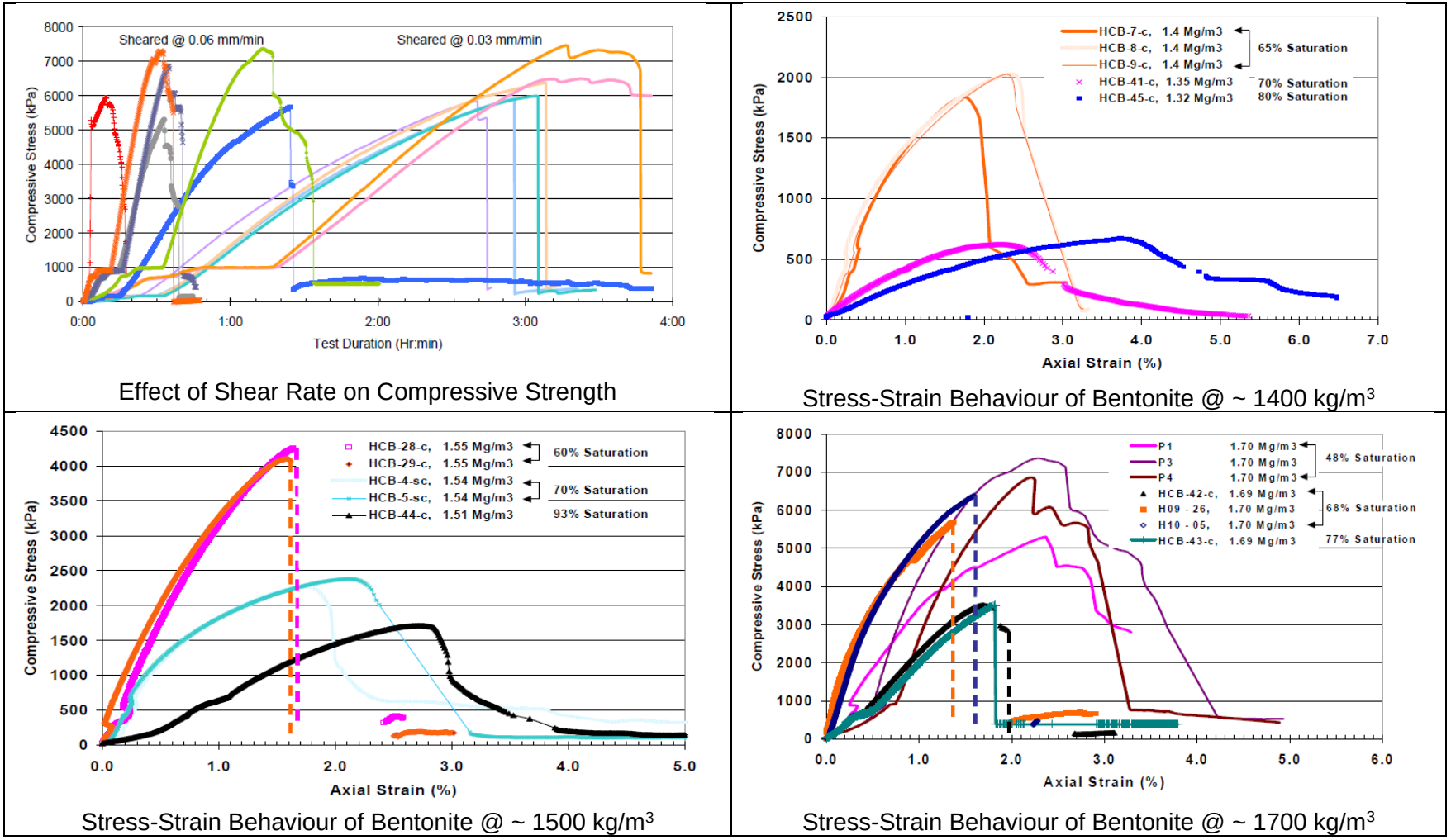

Figure B-1: Unconfined Compressive Behaviour of MX80 Bentonite (from Dixon et al. 2006)

Table B-1: Summary of Triaxial Test Data for MX-80

note: values in red italics are calculated based on relationships below using the provided modulus value (black)

G = E / (2(1+ μ)) = E / (2 + 2 **μ**),

E = G (2(1+ μ)) = G (2 + 2 **μ**), **and**

B = E / (3(1-2 μ)) = E / (3 - 6 **μ**)

μ = 0.47 0.47

Sample	estimated dry density Mg/m3	Water Content %	Saturation @2.75 Gs	e	Bulk Modulus B MPa	K MPa	Shear Modulus G MPa	Elastic Modulus E MPa	M	Effective Friction Angle ϕ'	Effective Friction Angle ϕ'	max σ1 - σ3 kPa	Failure strain <90% satn.	Failure strain >90% satn. (%)	notes
Dixon et al. 2006	1.35	25.98	0.70	1.037								621	2.29		plastic ?
Dixon et al. 2006	1.32	31.36	0.80	1.083								670	3.72		plastic ?
Borgesson etal 1995	1.16		0.98	1.371							8.7	470		8	
Borgesson etal 1995	1.25		0.98	1.200							8.7	572		8	
Borgesson etal 1995	0.91		0.99	2.022							9.9	158		17	
Borgesson etal 1995	1.18		0.99	1.331							9.9	326		7	
Borgesson etal 1995	1.25		0.99	1.200							9.9	311		6.5	
Borgesson et al 1998	1.26	43.2	1	1.183							7	288			
Pusch 1983	1.60		0.5	0.719								8000			
Dixon et al. 2006	1.55	16.6	0.60	0.774								4099	1.59		brittle
Dixon et al. 2006	1.55	16.6	0.60	0.774								4257	1.66		brittle
Dixon et al. 2006	1.56	16.4	0.60	0.763								4250	1.27		brittle
Dixon et al. 2006	1.4	22.4	0.65	0.964								1840	1.74		brittle
Dixon et al. 2006	1.4	22.5	0.65	0.964								2025	2.31		brittle
Dixon et al. 2006	1.41	22.4	0.66	0.950								2025	2.3		brittle
Dixon et al. 2006	1.54	21.8	0.77	0.786								2204	2.11		brittle
Dixon et al. 2006	1.54	22	0.78	0.786								2382	2.11		brittle
Dixon et al. 2006	1.54	22	0.78	0.786								2272	1.73		brittle
Dixon et al. 2006	1.51	23.4	0.93	0.821								1352	1.84		brittle
Dueck etal 2010	1.59	25.2	0.96	0.730								3150		5	
ISO-BENT100-DW	1.49	27.7	0.97	0.841	*506.3*	53.8	31.0	*91.1*	0.31		8.5	1385		12.3	
Borgesson etal 1995	1.56		0.98	0.763							9.9	1664		7	
Borgesson etal 1995	1.48		0.99	0.858							9.9	906		8	
Dueck etal 2010	1.60	25.8	0.99	0.719											
Dueck etal 2010	1.50		1	0.833								2170		8	
Borgesson et al 1998	1.55	27.7	1	0.774							8.8	1800			
Borgesson et al. 2010	1.56		1	0.763	*2016.7*		*123.5*	363.0							
Borgesson et al 1998	1.56	28.8	1	0.763								1520			
Borgesson et al 1998	1.59	30.5	1	0.730							13	1600			
Borgesson et al 1998	1.59	28.5	1	0.730								1880			
Borgesson et al 1998	1.59	28.3	1	0.730								1490			60 C test
Borgesson et al 1998	1.59	28.1	1	0.730								1777			
Dueck etal 2010	1.59	27.7	1	0.730								2580		6.5	
Dueck etal 2010	1.59	27.7	1	0.730								2400		7.4	
Dueck etal 2010	1.59		1	0.730								2835		10.2	
Pusch 1983	1.60		1	0.719	*1888.9*		*115.6*	340.0							
Pusch 1983	1.60		1	0.719	*1500.0*		*91.8*	270.0							
Pusch 1983	1.60		1	0.719	*1111.1*		*68.0*	200.0							
Dueck etal 2010	1.60	26.9	1	0.719								2850		6.2	
Dueck etal 2010	1.60		1	0.719								2704		7.9	
Eloranta 2017	1.47		*1*	0.877	557.0		34.9	*102.6*							
Eloranta 2017	1.47		*1*	0.876	435.0		41.9	*123.2*							
Eloranta 2017	1.47		*1*	0.872	395.0		41.1	*120.8*							
Eloranta 2017	1.47		*1*	0.866	381.0		56.1	*164.9*							
Eloranta 2017	1.48		*1*	0.861	370.0		58.3	*171.4*							
Hancilova and Hokr 2016	1.55		*1*	0.774	*1138.9*		*69.7*	205.0							

Sample	estimated dry density Mg/m3	Water Content %	Saturation @2.75 Gs	e	Bulk Modulus B MPa	K MPa	Shear Modulus G MPa	Elastic Modulus E MPa	M	Effective Friction Angle ϕ'	Effective Friction Angle ϕ'	max σ1 - σ3 kPa	Failure strain <90% satn.	Failure strain >90% satn. (%)	notes
Tisata and Morelli 2013	1.66	10	0.42	0.657											
Dixon et al. 2006	1.75	10.5	0.52	0.571								5304	2.37		brittle
Dixon et al. 2006	1.75	10.5	0.52	0.571								5951	3.07		
Dixon et al. 2006	1.75	10.5	0.52	0.571								6860	2.21		brittle
Dixon et al. 2006	1.75	10.5	0.52	0.571								6495	2.25		
Dixon et al. 2006	1.75	10.5	0.52	0.571								7462	1.79		
Dixon et al. 2006	1.75	10.5	0.52	0.571								7294	2.21		brittle
Dixon et al. 2006	1.75	10.5	0.52	0.571								10087	3.31		brittle
Dixon et al. 2006	1.75	10.9	0.53	0.571								7366	2.29		brittle
Dixon et al. 2006	1.69	14.59	0.65	0.627								3510	1.68		Brittle
Dixon et al. 2006	1.75	15	0.74	0.571								5902	1.57		brittle
Dixon et al. 2006	1.75	15	0.74	0.571								5700	1.6		brittle
Dixon et al. 2006	1.75	15	0.74	0.571								5842	1.51		brittle
Dixon et al. 2006	1.75	15	0.74	0.571								5680	1.37		brittle
Dixon et al. 2006	1.75	15	0.74	0.571								6378	1.59		brittle
Dixon et al. 2006	1.75	15	0.74	0.571								5993	1.71		brittle
Dixon et al. 2006	1.7	17.18	0.77	0.618								3507	1.82		brittle
Dixon et al. 2006	1.62	19.7	0.79	0.698								2106	1.96		brittle
Dixon et al. 2006	1.61	20.2	0.80	0.708								1992	2.31		brittle
Dixon et al. 2006	1.63	19.9	0.81	0.687								2217	1.98		brittle
Tisata & Morelli 2013	1.66	20	0.84	0.657											
CID-HCB-DW2	1.62	24.2	0.95	0.698	*1066.7*		*65.3*	192.0	1.23	30.9		3150		8.1	
Dueck etal 2010	1.62	24.7	0.95	0.698								3250		5.5	
CID-HCB-DW3	1.62	24.8	0.98	0.698	*833.3*		*51.0*	150.0	1.21	30.2		3077		7.8	
Dueck etal 2010	1.62	28.8	0.98	0.698								2098		5.9	
Dueck etal 2010	1.63	27	0.99	0.687								2860		5.5	
CID-HCB-DW1	1.63	24.9	1	0.687	*1188.9*		*72.8*	214.0	1.24	30.9		3042		6	
Borgesson et al 1998	1.69	24.8	1	0.627								3300			
CIU-HCB-DW															
Ritola and Pyy 2011	1.884	12.8	0.77	0.460	*8000.0*		*489.8*	1440.0				10930			
Ritola and Pyy 2011	1.889	12.6	0.764	0.456	*9388.9*		*574.8*	1690.0				11230			
Ritola and Pyy 2011	1.925	11.8	0.756	0.429	*10500.0*		*642.9*	1890.0				13000			
Ritola and Pyy 2011	1.868	12.9	0.754	0.472	*8000.0*		*489.8*	1440.0				9930			
Ritola and Pyy 2011	1.871	12.9	0.754	0.470	*10722.2*		*656.5*	1930.0				9540			
Ritola and Pyy 2011	1.868	12.8	0.745	0.472	*10555.6*		*646.3*	1900.0				9440			
Ritola and Pyy 2011	1.790	16.5	0.849	0.536	*9555.6*		*585.0*	1720.0				7050			
Ritola and Pyy 2011	1.878	12.9	0.768	0.464								9310			
Ritola and Pyy 2011	1.807	15.6	0.822	0.522	*11055.6*		*676.9*	1990.0				6540			

Sample	estimated dry density Mg/m3	Water Content %	Saturation @2.75 Gs	e	Bulk Modulus B MPa	K MPa	Shear Modulus G MPa	Elastic Modulus E MPa	M	Effective Friction Angle ϕ'	Effective Friction Angle ϕ'	max σ1 - σ3 kPa	Failure strain <90% satn.	Failure strain >90% satn. (%)	notes
Borgesson etal 1995	1.42		0.98	0.937							12.9	957		7	3.5% TDS
Borgesson etal 1995	1.44		1	0.910							12.9	873		11	3.5% TDS
Borgesson etal 1995	1.35		0.98	1.037							12.9	515		9	3.5% TDS
Borgesson etal 1995	1.34		0.99	1.052							12.9	996		9	3.5% TDS
Borgesson etal 1995	1.42		1	0.937							12.9	669			3.5% TDS
ISO-BSM7030-SR-L	1.79	18.3	0.94	0.537	*310.3*	44.6	19.0	*55.9*	1.02		25.8			7.6	brine
ISO-BSM7030-SR-Sh	1.75	17.2	0.91	0.571	*401.8*	34.4	24.6	*72.3*	0.98		24.9			9.1	brine
ISO-BENT100-SR-L	1.48	28.3	1.04	0.858	*267.9*	26	16.4	*48.2*	0.91		23.3	1014		10.4	brine
ISO-BENT100-SR-Sh	1.47	29.9	0.94	0.871	*264.6*	14.9	16.2	*47.6*	1.11		28	1228		9.9	brine

Note: Values in red are calculated rather than having been measured or reported in original test data

APPENDIX C. STATISTICAL ANALYSES OF THERMAL DATA

C1. Statistical Evaluation of Thermal Data – Thermal Conductivity

Thermal conductivity 1.4 Mg/m^3 dry density

Date:
Spreadsheet Author: D. Priyanto 2012
data UPDATED and spreadsheet Modified by:
D.Dixon 2018 Oct 02
All Data for Wyoming Bentonite

Derived values			
Slope, m	m	0.875	SLOPE(y,x)
Intercept, b	b	0.230	INTERCEPT(y,x)
Observations, n	n	43.0	COUNT(x)
Std error in estimate, S_{yx}	SYX	0.055	STEYX(y,x)
Average x	XAVG	0.464	AVERAGE(x)
SSX	SSX	4.184	DEVSQ(x)
t(a/2,df)	t	2.327	TINV(a/2,df)
Degree of confidence (%)		95	
	a	0.05	
	df	41	n-2

Experimental data					Regression line	Confidence interval				Prediction interval		
		k	saturation	TC								
Number of data points	saturation %	Thermal conducivity W/mK	x	y	Saturation x	TC y	CI	y+CI	y-CI	PI	y+PI	y-PI
1	5.90	0.30	0.06	0.30	0.01	0.24	0.03	0.27	0.20	0.13	0.37	0.11
2	5.50	0.30	0.06	0.30	0.06	0.28	0.03	0.31	0.25	0.13	0.41	0.15
3	5.60	0.30	0.06	0.30	0.11	0.33	0.03	0.36	0.30	0.13	0.46	0.20
4	19.00	0.40	0.19	0.40	0.16	0.37	0.03	0.40	0.34	0.13	0.50	0.24
5	18.80	0.40	0.19	0.40	0.21	0.41	0.03	0.44	0.39	0.13	0.54	0.28
6	19.30	0.40	0.19	0.40	0.26	0.46	0.02	0.48	0.43	0.13	0.59	0.33
7	32.40	0.50	0.32	0.50	0.31	0.50	0.02	0.52	0.48	0.13	0.63	0.37
8	34.00	0.50	0.34	0.50	0.36	0.55	0.02	0.57	0.52	0.13	0.67	0.42
9	33.10	0.50	0.33	0.50	0.41	0.59	0.02	0.61	0.57	0.13	0.72	0.46
10	50.80	0.70	0.51	0.70	0.46	0.63	0.02	0.65	0.61	0.13	0.76	0.50
11	50.50	0.70	0.51	0.70	0.51	0.68	0.02	0.70	0.66	0.13	0.81	0.55
12	50.70	0.70	0.51	0.70	0.56	0.72	0.02	0.74	0.70	0.13	0.85	0.59
13	68.90	0.90	0.69	0.90	0.61	0.76	0.02	0.79	0.74	0.13	0.89	0.63
14	69.20	0.90	0.69	0.90	0.66	0.81	0.02	0.83	0.78	0.13	0.94	0.68
15	69.00	0.90	0.69	0.90	0.71	0.85	0.02	0.88	0.83	0.13	0.98	0.72
16	87.70	1.10	0.88	1.10	0.76	0.90	0.03	0.92	0.87	0.13	1.03	0.76
17	87.00	1.10	0.87	1.10	0.81	0.94	0.03	0.97	0.91	0.13	1.07	0.81
18	86.10	1.10	0.86	1.10	0.86	0.98	0.03	1.01	0.95	0.13	1.11	0.85
19	0.00	0.30	0.00	0.30	0.91	1.03	0.03	1.06	0.99	0.13	1.16	0.89
20	5.00	0.31	0.05	0.31	0.96	1.07	0.04	1.11	1.03	0.13	1.20	0.94
21	10.00	0.32	0.10	0.32	1.01	1.11	0.04	1.15	1.07	0.13	1.25	0.98
22	20.00	0.35	0.20	0.35								
23	30.00	0.40	0.30	0.40								
24	40.00	0.50	0.40	0.50								
25	50.00	0.60	0.50	0.60								
26	60.00	0.70	0.60	0.70								
27	70.00	0.75	0.70	0.75								
28	80.00	0.87	0.80	0.87								
29	90.00	0.95	0.90	0.95								
30	95.00	1.00	0.95	1.00								
31	100.00	1.05	1.00	1.05								
32	0.00	0.30	0.00	0.30								
33	5.00	0.30	0.05	0.30								
34	10.00	0.33	0.10	0.33								
35	20.00	0.36	0.20	0.36								
36	30.00	0.45	0.30	0.45								
37	40.00	0.53	0.40	0.53								
38	50.00	0.63	0.50	0.63								
39	60.00	0.73	0.60	0.73								
40	70.00	0.85	0.70	0.85								
41	80.00	0.95	0.80	0.95								
42	90.00	1.03	0.90	1.03								
43	95.00	1.08	0.95	1.08								

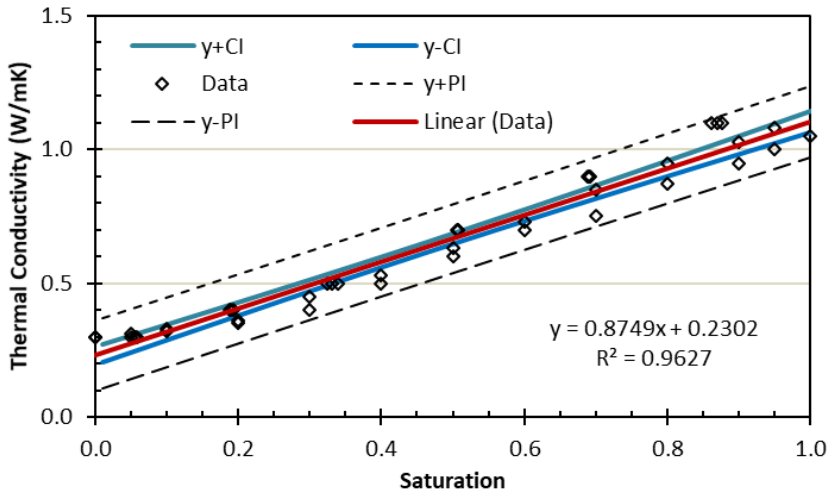

Thermal conductivity 1.5 Mg/m^3 dry density

Date:

Spreadsheet Author: D. Priyanto 2012

data UPDATED and spreadsheet Modified by: D.Dixon 2018 Oct 02

All Data for Wyoming Bentonite

Derived values			
Slope, m	m	0.884	SLOPE(y,x)
Intercept, b	b	0.400	INTERCEPT(y,x)
Observations, n	n	34.0	COUNT(x)
Std error in estimate, S_{yx}	SYX	0.071	STEYX(y,x)
Average x	XAVG	0.369	AVERAGE(x)
SSX	SSX	3.051	DEVSQ(x)
t(a/2,df)	t	2.352	TINV(a/2,df)
Degree of confidence (%)		95	
	a	0.05	
	df	32	n-2

Experimental data						Regression line		Confidence interval			Prediction interval		
Number of data points	Dry Density (Mg/m3)	Satn. %	Thermal conducivity W/mK	Satn. x	TC y	x	y	CI	y+CI	y-CI	PI	y+PI	y-PI
1	1.50	0.00	0.48	0.00	0.48	0.01	0.41	0.04	0.45	0.36	0.17	0.58	0.24
2	1.52	0.00	0.48	0.00	0.48	0.06	0.45	0.04	0.49	0.41	0.17	0.62	0.28
3	1.51	0.00	0.51	0.00	0.51	0.11	0.50	0.04	0.53	0.46	0.17	0.67	0.33
4	1.51	0.07	0.46	0.07	0.46	0.16	0.54	0.03	0.58	0.51	0.17	0.71	0.37
5	1.50	0.07	0.44	0.07	0.44	0.21	0.59	0.03	0.62	0.55	0.17	0.75	0.42
6	1.52	0.06	0.47	0.06	0.47	0.26	0.63	0.03	0.66	0.60	0.17	0.80	0.46
7	1.48	0.11	0.46	0.11	0.46	0.31	0.67	0.03	0.70	0.64	0.17	0.84	0.50
8	1.51	0.11	0.47	0.11	0.47	0.36	0.72	0.03	0.75	0.69	0.17	0.89	0.55
9	1.49	0.09	0.44	0.09	0.44	0.41	0.76	0.03	0.79	0.73	0.17	0.93	0.59
10	1.50	0.16	0.52	0.16	0.52	0.46	0.81	0.03	0.84	0.78	0.17	0.98	0.64
11	1.52	0.16	0.54	0.16	0.54	0.51	0.85	0.03	0.88	0.82	0.17	1.02	0.68
12	1.50	0.17	0.52	0.17	0.52	0.56	0.89	0.03	0.93	0.86	0.17	1.06	0.72
13	1.55	0.20	0.42	0.20	0.42	0.61	0.94	0.04	0.98	0.90	0.17	1.11	0.77
14	1.51	0.21	0.57	0.21	0.57	0.66	0.98	0.04	1.02	0.94	0.17	1.15	0.81
15	1.50	0.21	0.54	0.21	0.54	0.71	1.03	0.04	1.07	0.98	0.17	1.20	0.85
16	1.51	0.21	0.52	0.21	0.52	0.76	1.07	0.05	1.12	1.02	0.17	1.24	0.90
17	1.51	0.29	0.67	0.29	0.67	0.81	1.12	0.05	1.17	1.06	0.17	1.29	0.94
18	1.51	0.35	0.74	0.35	0.74	0.86	1.16	0.05	1.21	1.10	0.18	1.33	0.98
19	1.49	0.34	0.80	0.34	0.80	0.91	1.20	0.06	1.26	1.14	0.18	1.38	1.03
20	1.52	0.39	0.67	0.39	0.67	0.96	1.25	0.06	1.31	1.18	0.18	1.43	1.07
21	1.53	0.37	0.70	0.37	0.70	1.01	1.29	0.07	1.36	1.22	0.18	1.47	1.11
22	1.53	0.36	0.69	0.36	0.69	1.06	1.34	0.07	1.41	1.26	0.18	1.52	1.15
23	1.55	0.48	0.85	0.48	0.85	1.11	1.38	0.08	1.46	1.30	0.18	1.56	1.20
24	1.53	0.46	0.82	0.46	0.82	1.16	1.42	0.08	1.51	1.34	0.19	1.61	1.24
25	1.52	0.45	0.80	0.45	0.80	1.21	1.47	0.09	1.55	1.38	0.19	1.66	1.28
26	1.57	0.61	0.90	0.61	0.90								
27	1.57	0.61	0.99	0.61	0.99								
28	1.57	0.62	1.09	0.62	1.09								
29	1.51	0.87	1.27	0.87	1.27								
30	1.46	0.80	1.15	0.80	1.15								
31	1.43	0.84	0.94	0.84	0.94								
32	1.41	0.97	1.26	0.97	1.26								
33	1.44	0.95	1.20	0.95	1.20								
34	1.45	0.96	1.30	0.96	1.30								

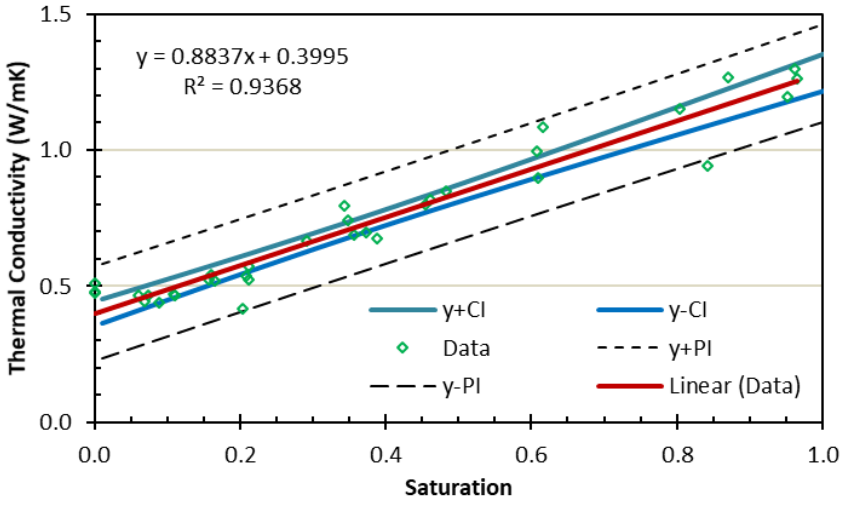

Thermal conductivity 1.6 Mg/m^3 dry density

Date:

Spreadsheet Author: D. Priyanto

data UPDATED and spreadsheet Modified by: D.Dixon 2018 Oct 02

All Data for MX80 Bentonite

Derived values			
Slope, m	m	0.852	SLOPE(y,x)
Intercept, b	b	0.368	INTERCEPT(y,x)
Observations, n	n	24.0	COUNT(x)
Std error in estimate, S_{yx}	SYX	0.048	STEYX(y,x)
Average x	XAVG	0.395	AVERAGE(x)
SSX	SSX	1.583	DEVSQ(x)
t(a/2,df)	t	2.405	TINV(a/2,df)
Degree of confidence (%)		95	
	a	0.05	
	df	22	n-2

Experimental data

			k	satn.	TC	Regression line		Confidence interval			Prediction interval		
Number of data points	Dry Density (Mg/m3)	Satn.	Thermal conducivity W/mK	x	y	x	y	CI	y+CI	y-CI	PI	y+PI	y-PI
1	1.50	5.51	0.43	0.06	0.43	0.01	0.38	0.04	0.42	0.33	0.12	0.50	0.25
2	1.52	4.81	0.43	0.05	0.43	0.06	0.42	0.04	0.46	0.38	0.12	0.54	0.30
3	1.51	5.06	0.43	0.05	0.43	0.11	0.46	0.04	0.50	0.43	0.12	0.58	0.34
4	1.51	17.84	0.53	0.18	0.53	0.16	0.50	0.03	0.54	0.47	0.12	0.62	0.38
5	1.50	16.66	0.50	0.17	0.50	0.21	0.55	0.03	0.58	0.52	0.12	0.67	0.43
6	1.52	16.12	0.48	0.16	0.48	0.26	0.59	0.03	0.62	0.56	0.12	0.71	0.47
7	1.48	30.88	0.55	0.31	0.55	0.31	0.63	0.02	0.66	0.61	0.12	0.75	0.51
8	1.51	30.32	0.57	0.30	0.57	0.36	0.67	0.02	0.70	0.65	0.12	0.79	0.56
9	1.49	30.50	0.60	0.31	0.60	0.41	0.72	0.02	0.74	0.69	0.12	0.84	0.60
10	1.50	47.25	0.70	0.47	0.70	0.46	0.76	0.02	0.78	0.74	0.12	0.88	0.64
11	1.52	46.11	0.69	0.46	0.69	0.51	0.80	0.03	0.83	0.78	0.12	0.92	0.68
12	1.50	44.70	0.70	0.45	0.70	0.56	0.85	0.03	0.87	0.82	0.12	0.96	0.73
13	1.55	64.15	0.87	0.64	0.87	0.61	0.89	0.03	0.92	0.86	0.12	1.01	0.77
14	1.51	63.03	0.88	0.63	0.88	0.66	0.93	0.03	0.96	0.90	0.12	1.05	0.81
15	1.50	63.09	0.88	0.63	0.88	0.71	0.97	0.04	1.01	0.94	0.12	1.09	0.85
16	1.51	83.04	1.09	0.83	1.09	0.76	1.02	0.04	1.06	0.97	0.12	1.14	0.89
17	1.51	82.83	1.10	0.83	1.10	0.81	1.06	0.04	1.10	1.01	0.12	1.18	0.93
18	1.51	82.65	1.10	0.83	1.10	0.86	1.10	0.05	1.15	1.05	0.13	1.23	0.98
19	1.49	7.00	0.48	0.07	0.48	0.91	1.14	0.05	1.20	1.09	0.13	1.27	1.02
20	1.52	16.00	0.53	0.16	0.53	0.96	1.19	0.06	1.24	1.13	0.13	1.31	1.06
21	1.53	25.00	0.64	0.25	0.64	1.01	1.23	0.06	1.29	1.17	0.13	1.36	1.10
22	1.53	41.00	0.76	0.41	0.76								
23	1.55	54.00	0.91	0.54	0.91								
24	1.53	71.00	1.06	0.71	1.06								

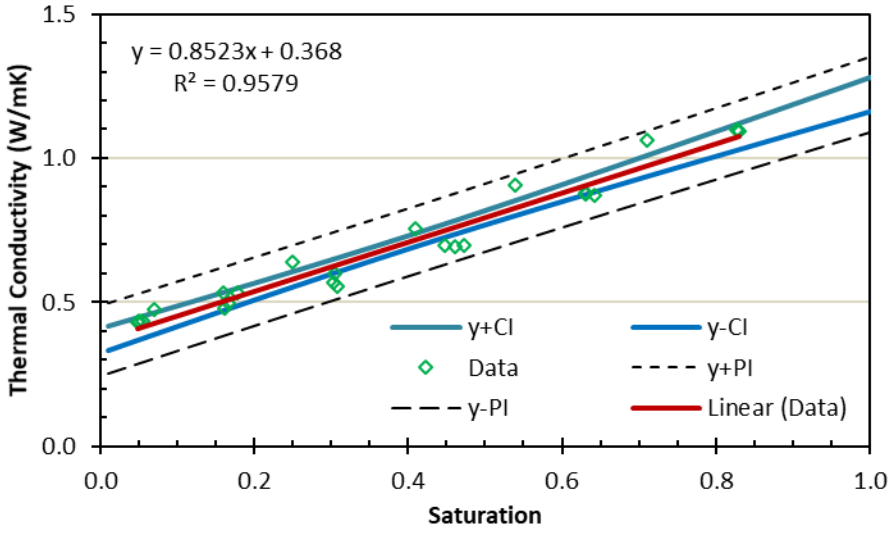

Thermal conductivity 1.7 Mg/m^3 dry density

Date:
Spreadsheet Author: D. Priyanto 2012
data UPDATED and spreadsheet Modified by:
D.Dixon 2018 Oct 02
All Data for Wyoming Bentonite

Derived values			
Slope, m	m	0.861	SLOPE(y,x)
Intercept, b	b	0.506	INTERCEPT(y,x)
Observations, n	n	39.0	COUNT(x)
Std error in estimate, S_{yx}	SYX	0.072	STEYX(y,x)
Average x	XAVG	0.410	AVERAGE(x)
SSX	SSX	3.556	DEVSQ(x)
t(a/2,df)	t	2.336	TINV(a/2,df)
Degree of confidence (%)		95	
	a	0.05	
	df	37	n-2

Experimental data						Regression line		Confidence interval			Prediction interval		
			k	satn.	TC								
Number of data points	Dry Density (Mg/m3)	Saturation	Thermal conducivity W/mK	x	y	x	y	CI	y+CI	y-CI	PI	y+PI	y-PI
1	1.70	0.00	0.57	0.00	0.57	0.01	0.51	0.04	0.56	0.47	0.17	0.69	0.34
2	1.71	0.00	0.53	0.00	0.53	0.06	0.56	0.04	0.60	0.52	0.17	0.73	0.38
3	1.72	0.00	0.55	0.00	0.55	0.11	0.60	0.04	0.64	0.56	0.17	0.77	0.43
4	1.70	0.06	0.57	0.06	0.57	0.16	0.64	0.03	0.68	0.61	0.17	0.81	0.47
5	1.68	0.05	0.56	0.05	0.56	0.21	0.69	0.03	0.72	0.65	0.17	0.86	0.52
6	1.72	0.06	0.57	0.06	0.57	0.26	0.73	0.03	0.76	0.70	0.17	0.90	0.56
7	1.69	0.11	0.55	0.11	0.55	0.31	0.77	0.03	0.80	0.74	0.17	0.94	0.60
8	1.67	0.11	0.56	0.11	0.56	0.36	0.82	0.03	0.84	0.79	0.17	0.99	0.65
9	1.68	0.10	0.62	0.10	0.62	0.41	0.86	0.03	0.89	0.83	0.17	1.03	0.69
10	1.69	0.15	0.59	0.15	0.59	0.46	0.90	0.03	0.93	0.87	0.17	1.07	0.73
11	1.69	0.15	0.58	0.15	0.58	0.51	0.94	0.03	0.97	0.92	0.17	1.11	0.77
12	1.70	0.15	0.62	0.15	0.62	0.56	0.99	0.03	1.02	0.96	0.17	1.16	0.82
13	1.68	0.19	0.64	0.19	0.64	0.61	1.03	0.03	1.06	1.00	0.17	1.20	0.86
14	1.71	0.19	0.67	0.19	0.67	0.66	1.07	0.03	1.11	1.04	0.17	1.25	0.90
15	1.71	0.19	0.70	0.19	0.70	0.71	1.12	0.04	1.15	1.08	0.17	1.29	0.95
16	1.70	0.25	0.61	0.25	0.61	0.76	1.16	0.04	1.20	1.12	0.17	1.33	0.99
17	1.76	0.25	0.68	0.25	0.68	0.81	1.20	0.04	1.25	1.16	0.17	1.38	1.03
18	1.70	0.24	0.70	0.24	0.70	0.86	1.25	0.05	1.29	1.20	0.17	1.42	1.07
19	1.72	0.39	0.88	0.39	0.88	0.91	1.29	0.05	1.34	1.24	0.18	1.46	1.11
20	1.73	0.40	0.83	0.40	0.83	0.96	1.33	0.06	1.39	1.28	0.18	1.51	1.16
21	1.71	0.38	0.85	0.38	0.85	1.01	1.38	0.06	1.43	1.32	0.18	1.55	1.20
22	1.64	0.43	0.92	0.43	0.92	1.06	1.42	0.06	1.48	1.35	0.18	1.60	1.24
23	1.63	0.44	0.86	0.44	0.86	1.11	1.46	0.07	1.53	1.39	0.18	1.64	1.28
24	1.65	0.46	0.94	0.46	0.94	1.16	1.50	0.07	1.58	1.43	0.18	1.69	1.32
25	1.69	0.58	1.08	0.58	1.08	1.21	1.55	0.08	1.62	1.47	0.18	1.73	1.36
26	1.66	0.56	0.98	0.56	0.98								
27	1.62	0.52	0.86	0.52	0.86								
28	1.67	0.74	1.25	0.74	1.25								
29	1.66	0.74	1.16	0.74	1.16								
30	1.66	0.68	1.32	0.68	1.32								
31	1.76	0.71	1.05	0.71	1.05								
32	1.70	0.66	1.09	0.66	1.09								
33	1.71	0.66	1.13	0.66	1.13								
34	1.66	0.92	1.32	0.92	1.32								
35	1.64	0.89	1.35	0.89	1.35								
36	1.625	0.87	1.34	0.87	1.34								
37	1.655	0.92	1.15	0.92	1.15								
38	1.64	0.89	1.14	0.89	1.14								
39	1.625	0.87	1.14	0.87	1.14								

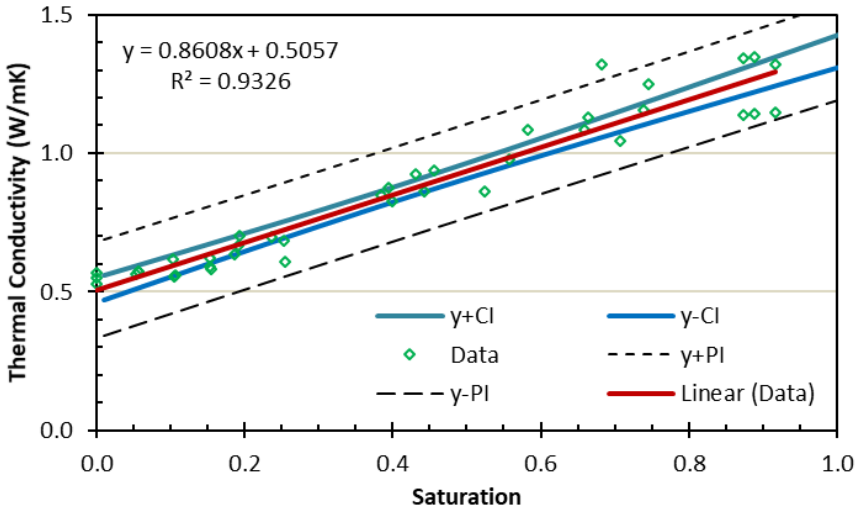

C2. Statistical Evaluation of Thermal Data – Thermal Diffusivity

Thermal diffusivity 1.5 Mg/m^3 dry density

Date:
Spreadsheet Author: D. Priyanto 2012
data UPDATED and spreadsheet Modified by:
D.Dixon 2018 Oct 02
All Data for Wyoming Bentonite
Man & Martino 2010; 200 mesh wyom bentonite
Dixon et al. 2018; MX80 bentonite

Derived values			
Slope, m	m	0.150	SLOPE(y,x)
Intercept, b	b	0.290	INTERCEPT(y,x)
Observations, n	n	52.0	COUNT(x)
Std error in estimate, S_{yx}	SYX	0.070	STEYX(y,x)
Average x	XAVG	0.383	AVERAGE(x)
SSX	SSX	4.346	DEVSQ(x)
t(a/2,df)	t	2.311	TINV(a/2,df)
Degree of confidence (%)		95	
	a	0.05	
	df	50	n-2

Experimental data				saturation	TD	Regression line		Confidence interval			Prediction interval		
Number of data points	Dry Density (Mg/m3)	Satn.	Thermal diffusivity mm2/s	satn. x	TD y	Saturation x	TD y	CI	y+CI	y-CI	PI	y+PI	y-PI
1	1.50	0.00	0.38	0.00	0.38	0.01	0.29	0.04	0.33	0.25	0.17	0.46	0.12
2	1.52	0.00	0.38	0.00	0.38	0.06	0.30	0.03	0.33	0.27	0.17	0.47	0.13
3	1.51	0.00	0.40	0.00	0.40	0.11	0.31	0.03	0.34	0.28	0.17	0.47	0.14
4	1.51	0.07	0.28	0.07	0.28	0.16	0.31	0.03	0.34	0.29	0.17	0.48	0.15
5	1.50	0.07	0.26	0.07	0.26	0.21	0.32	0.03	0.35	0.30	0.16	0.49	0.16
6	1.52	0.06	0.30	0.06	0.30	0.26	0.33	0.02	0.35	0.30	0.16	0.49	0.16
7	1.48	0.11	0.27	0.11	0.27	0.31	0.34	0.02	0.36	0.31	0.16	0.50	0.17
8	1.51	0.11	0.23	0.11	0.23	0.36	0.34	0.02	0.37	0.32	0.16	0.51	0.18
9	1.49	0.09	0.21	0.09	0.21	0.41	0.35	0.02	0.37	0.33	0.16	0.52	0.19
10	1.50	0.16	0.28	0.16	0.28	0.46	0.36	0.02	0.38	0.34	0.16	0.52	0.19
11	1.52	0.16	0.29	0.16	0.29	0.51	0.37	0.02	0.39	0.34	0.16	0.53	0.20
12	1.50	0.17	0.23	0.17	0.23	0.56	0.37	0.03	0.40	0.35	0.16	0.54	0.21
13	1.55	0.20	0.21	0.20	0.21	0.61	0.38	0.03	0.41	0.35	0.17	0.55	0.22
14	1.51	0.21	0.24	0.21	0.24	0.66	0.39	0.03	0.42	0.36	0.17	0.55	0.22
15	1.50	0.21	0.22	0.21	0.22	0.71	0.40	0.03	0.43	0.36	0.17	0.56	0.23
16	1.51	0.21	0.21	0.21	0.21	0.76	0.40	0.04	0.44	0.37	0.17	0.57	0.24
17	1.51	0.29	0.31	0.29	0.31	0.81	0.41	0.04	0.45	0.37	0.17	0.58	0.24
18	1.51	0.35	0.31	0.35	0.31	0.86	0.42	0.04	0.46	0.38	0.17	0.59	0.25
19	1.49	0.34	0.32	0.34	0.32	0.91	0.43	0.05	0.47	0.38	0.17	0.60	0.26
20	1.52	0.39	0.22	0.39	0.22	0.96	0.43	0.05	0.48	0.38	0.17	0.60	0.26
21	1.53	0.37	0.29	0.37	0.29	1.01	0.44	0.05	0.50	0.39	0.17	0.61	0.27
22	1.53	0.36	0.29	0.36	0.29	1.06	0.45	0.06	0.51	0.39	0.17	0.62	0.28
23	1.55	0.48	0.32	0.48	0.32	1.11	0.46	0.06	0.52	0.40	0.17	0.63	0.28
24	1.53	0.46	0.29	0.46	0.29	1.16	0.46	0.06	0.53	0.40	0.18	0.64	0.29
25	1.52	0.45	0.33	0.45	0.33	1.21	0.47	0.07	0.54	0.40	0.18	0.65	0.29
26	1.57	0.61	0.36	0.61	0.36								
27	1.57	0.61	0.34	0.61	0.34								
28	1.57	0.62	0.38	0.62	0.38								
29	1.51	0.87	0.48	0.87	0.48								
30	1.46	0.80	0.34	0.80	0.34								
31	1.43	0.84	0.39	0.84	0.39								
32	1.41	0.97	0.49	0.97	0.49								
33	1.44	0.95	0.33	0.95	0.33								
34	1.45	0.96	0.43	0.96	0.43								
35	1.53	0.06	0.38	0.06	0.38								
36	1.52	0.05	0.41	0.05	0.41								
37	1.54	0.05	0.43	0.05	0.43								
38	1.56	0.18	0.38	0.18	0.38								
39	1.54	0.17	0.41	0.17	0.41								
40	1.53	0.16	0.40	0.16	0.40								
41	1.46	0.31	0.34	0.31	0.34								
42	1.46	0.30	0.36	0.30	0.36								
43	1.48	0.31	0.38	0.31	0.38								
44	1.48	0.47	0.39	0.47	0.39								
45	1.48	0.46	0.37	0.46	0.37								
46	1.48	0.45	0.40	0.45	0.40								
47	1.5	0.64	0.43	0.64	0.43								
48	1.5	0.63	0.45	0.63	0.45								
49	1.5	0.63	0.43	0.63	0.43								
50	1.51	0.83	0.49	0.83	0.49								
51	1.52	0.83	0.50	0.83	0.50								
52	1.52	0.83	0.52	0.83	0.52								

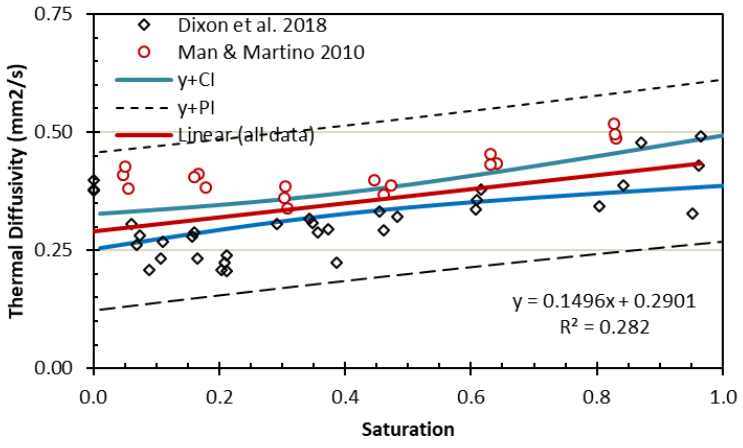

Thermal Diffusivity 1.7 Mg/m^3 dry density

Date:
Spreadsheet Author: D. Priyanto 2012
data UPDATED and spreadsheet Modified by:
D.Dixon 2018 Oct 02
All Data for MX80 Bentonite

Derived values			
Slope, m	m	0.161	SLOPE(y,x)
Intercept, b	b	0.295	INTERCEPT(y,x)
Observations, n	n	39.0	COUNT(x)
Std error in estimate, S_{yx}	SYX	0.045	STEYX(y,x)
Average x	XAVG	0.410	AVERAGE(x)
SSX	SSX	3.556	DEVSQ(x)
t(a/2,df)	t	2.336	TINV(a/2,df)
Degree of confidence (%)		95	
	a	0.05	
	df	37	n-2

Experimental data						Regression line		Confidence interval			Prediction interval		
Number of data points	Dry Density (Mg/m3)	satn. %	Thermal diffusivity mm2/s	satn. x	TD y	x	y	CI	y+CI	y-CI	PI	y+PI	y-PI
1.00	1.70	0.00	0.39	0.00	0.39	0.010	0.297	0.028	0.325	0.269	0.108	0.405	0.189
2.00	1.71	0.00	0.36	0.00	0.36	0.060	0.305	0.026	0.330	0.279	0.107	0.412	0.197
3.00	1.72	0.00	0.32	0.00	0.32	0.110	0.313	0.024	0.336	0.289	0.107	0.420	0.206
4.00	1.70	0.06	0.31	0.06	0.31	0.160	0.321	0.022	0.343	0.299	0.107	0.428	0.214
5.00	1.68	0.05	0.31	0.05	0.31	0.210	0.329	0.020	0.349	0.309	0.106	0.435	0.223
6.00	1.72	0.06	0.33	0.06	0.33	0.260	0.337	0.019	0.356	0.318	0.106	0.443	0.231
7.00	1.69	0.11	0.25	0.11	0.25	0.310	0.345	0.018	0.363	0.327	0.106	0.451	0.239
8.00	1.67	0.11	0.26	0.11	0.26	0.360	0.353	0.017	0.370	0.336	0.106	0.459	0.247
9.00	1.68	0.10	0.32	0.10	0.32	0.410	0.361	0.017	0.378	0.344	0.106	0.467	0.255
10.00	1.69	0.15	0.26	0.15	0.26	0.460	0.369	0.017	0.386	0.352	0.106	0.475	0.263
11.00	1.69	0.15	0.27	0.15	0.27	0.510	0.377	0.018	0.395	0.360	0.106	0.483	0.271
12.00	1.70	0.15	0.28	0.15	0.28	0.560	0.385	0.019	0.404	0.367	0.106	0.491	0.279
13.00	1.68	0.19	0.34	0.19	0.34	0.610	0.393	0.020	0.413	0.373	0.106	0.500	0.287
14.00	1.71	0.19	0.37	0.19	0.37	0.660	0.401	0.022	0.423	0.380	0.107	0.508	0.295
15.00	1.71	0.19	0.35	0.19	0.35	0.710	0.409	0.024	0.433	0.386	0.107	0.516	0.302
16.00	1.70	0.25	0.30	0.25	0.30	0.760	0.417	0.026	0.443	0.392	0.107	0.525	0.310
17.00	1.76	0.25	0.38	0.25	0.38	0.810	0.425	0.028	0.453	0.398	0.108	0.533	0.317
18.00	1.70	0.24	0.38	0.24	0.38	0.860	0.433	0.030	0.463	0.403	0.109	0.542	0.325
19.00	1.72	0.39	0.36	0.39	0.36	0.910	0.441	0.032	0.474	0.409	0.109	0.551	0.332
20.00	1.73	0.40	0.35	0.40	0.35	0.960	0.449	0.035	0.484	0.415	0.110	0.559	0.339
21.00	1.71	0.38	0.37	0.38	0.37	1.010	0.457	0.037	0.495	0.420	0.111	0.568	0.347
22.00	1.64	0.43	0.32	0.43	0.32	1.060	0.466	0.040	0.505	0.426	0.112	0.577	0.354
23.00	1.63	0.44	0.28	0.44	0.28	1.110	0.474	0.042	0.516	0.431	0.113	0.586	0.361
24.00	1.65	0.46	0.33	0.46	0.33	1.160	0.482	0.045	0.526	0.437	0.114	0.595	0.368
25.00	1.69	0.58	0.42	0.58	0.42	1.210	0.490	0.047	0.537	0.442	0.115	0.604	0.375
26.00	1.66	0.56	0.39	0.56	0.39								
27.00	1.62	0.52	0.36	0.52	0.36								
28.00	1.67	0.74	0.45	0.74	0.45								
29.00	1.66	0.74	0.40	0.74	0.40								
30.00	1.66	0.68	0.50	0.68	0.50								
31.00	1.76	0.71	0.38	0.71	0.38								
32.00	1.70	0.66	0.31	0.66	0.31								
33.00	1.71	0.66	0.37	0.66	0.37								
34.00	1.66	0.92	0.47	0.92	0.47								
35.00	1.64	0.89	0.43	0.89	0.43								
36.00	1.63	0.87	0.46	0.87	0.46								
37.00	1.66	0.92	0.45	0.92	0.45								
38.00	1.64	0.89	0.44	0.89	0.44								
39.00	1.63	0.87	0.50	0.87	0.50								

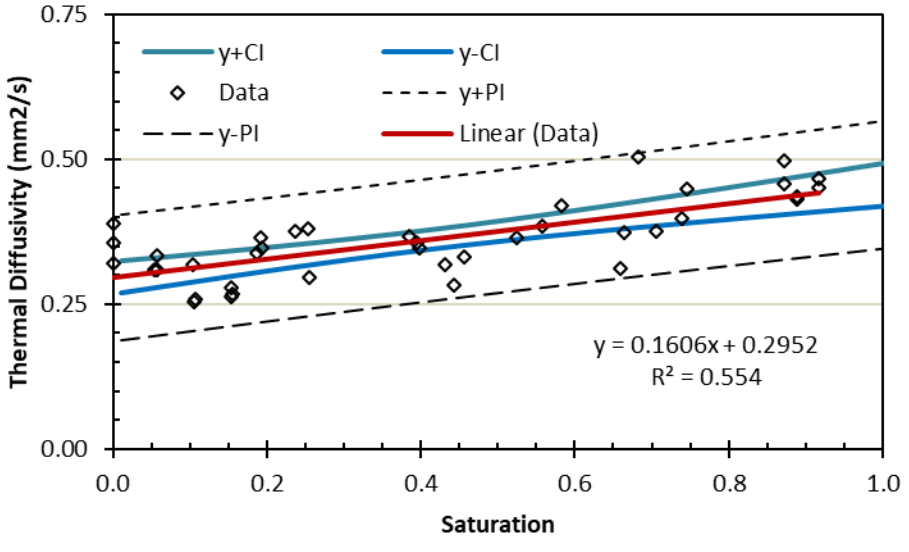

C3. Statistical Evaluation of Thermal Data – Specific Heat

Specific Heat 1.4 Mg/m^3 dry density

Date:
Author: D. Priyanto 2012
data UPDATED and spreadsheet Modified by:
D.Dixon 2018 Oct 02
All Data for MX80 Bentonite

Derived values			
Slope, m	m	2.464	SLOPE(y,x)
Intercept, b	b	0.998	INTERCEPT(y,x)
Observations, n	n	25.0	COUNT(x)
Std error in estimate, S_{yx}	SYX	0.160	STEYX(y,x)
Average x	XAVG	0.480	AVERAGE(x)
SSX	SSX	2.750	DEVSQ(x)
t(a/2,df)	t	2.398	TINV(a/2,df)
Degree of confidence (%)		95	
	a	0.05	
	df	23	n-2

erimental data

				Satn.	SH	Regression line	Confidence interval				Prediction interval		
Number of data points	Dry Density (Mg/m3)	Satn.	Specific Heat	x	y	Saturation x	SH y	CI	y+CI	y-CI	PI	y+PI	y-PI
1	1.40	0.00	0.82	0.00	0.82	0.01	1.02	0.13	1.16	0.89	0.41	1.43	0.62
2	1.40	0.05	0.98	0.05	0.98	0.06	1.15	0.12	1.27	1.02	0.40	1.55	0.74
3	1.40	0.10	1.1	0.10	1.10	0.11	1.27	0.11	1.38	1.15	0.40	1.67	0.87
4	1.40	0.20	1.4	0.20	1.40	0.16	1.39	0.11	1.50	1.29	0.40	1.79	0.99
5	1.40	0.30	1.7	0.30	1.70	0.21	1.52	0.10	1.61	1.42	0.40	1.91	1.12
6	1.40	0.40	2.1	0.40	2.10	0.26	1.64	0.09	1.73	1.55	0.39	2.03	1.24
7	1.40	0.50	2.55	0.50	2.55	0.31	1.76	0.09	1.85	1.68	0.39	2.15	1.37
8	1.40	0.60	2.65	0.60	2.65	0.36	1.89	0.08	1.97	1.80	0.39	2.28	1.49
9	1.40	0.70	2.98	0.70	2.98	0.41	2.01	0.08	2.09	1.93	0.39	2.40	1.62
10	1.40	0.80	3.1	0.80	3.10	0.46	2.13	0.08	2.21	2.05	0.39	2.52	1.74
11	1.40	0.90	3.25	0.90	3.25	0.51	2.25	0.08	2.33	2.18	0.39	2.65	1.86
12	1.40	0.95	3.25	0.95	3.25	0.56	2.38	0.08	2.46	2.30	0.39	2.77	1.99
13	1.40	1.00	3.25	1.00	3.25	0.61	2.50	0.08	2.58	2.42	0.39	2.89	2.11
14	1.40	0.00	0.89	0.00	0.89	0.66	2.62	0.09	2.71	2.54	0.39	3.02	2.23
15	1.40	0.05	1.05	0.05	1.05	0.71	2.75	0.09	2.84	2.65	0.39	3.14	2.35
16	1.40	0.10	1.25	0.10	1.25	0.76	2.87	0.10	2.97	2.77	0.40	3.27	2.47
17	1.40	0.20	1.55	0.20	1.55	0.81	2.99	0.11	3.10	2.89	0.40	3.39	2.60
18	1.40	0.30	1.95	0.30	1.95	0.86	3.12	0.12	3.23	3.00	0.40	3.52	2.72
19	1.40	0.40	2.15	0.40	2.15	0.91	3.24	0.13	3.37	3.11	0.40	3.64	2.84
20	1.40	0.50	2.3	0.50	2.30	0.96	3.36	0.13	3.50	3.23	0.41	3.77	2.96
21	1.40	0.60	2.55	0.60	2.55	1.01	3.49	0.14	3.63	3.34	0.41	3.90	3.08
22	1.40	0.70	2.75	0.70	2.75	1.06	3.61	0.15	3.76	3.46	0.41	4.02	3.20
23	1.40	0.80	2.85	0.80	2.85	1.11	3.73	0.16	3.90	3.57	0.42	4.15	3.32
24	1.40	0.90	3	0.90	3.00	1.16	3.86	0.17	4.03	3.68	0.42	4.28	3.43
25	1.40	0.95	3.1	0.95	3.10	1.21	3.98	0.19	4.16	3.79	0.43	4.41	3.55

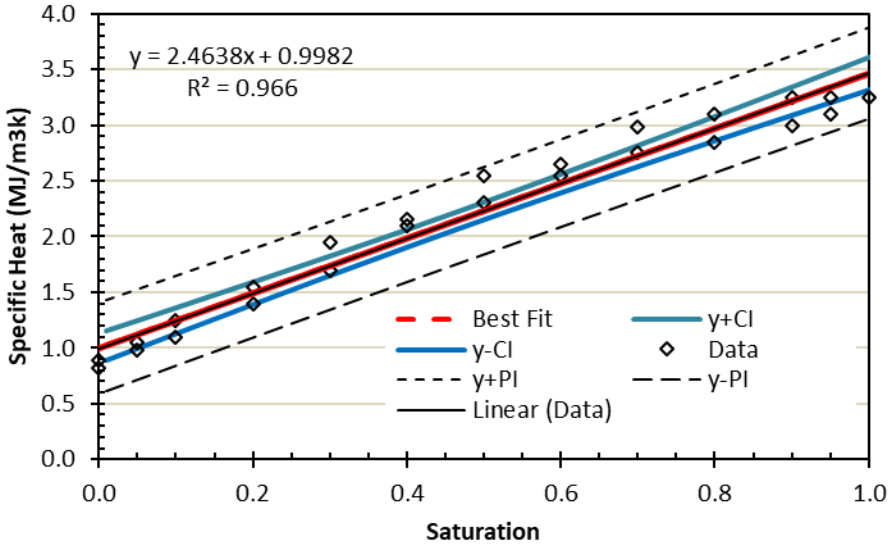

Specific heat 1.5 Mg/m^3 dry density

Date:
Author: D. Priyanto
data UPDATED and spreadsheet Modified by:
D.Dixon 2018 Oct 02
All Data for Wyoming Bentonite
Man & Martino 2010; 200 mesh Wyoming bentonite
Dixon et al. 2018; MX80 bentonite

Derived values			
Slope, m	m	1.445	SLOPE(y,x)
Intercept, b	b	1.534	INTERCEPT(y,x)
Observations, n	n	52.0	COUNT(x)
Std error in estimate, S_{yx}	SYX	0.444	STEYX(y,x)
Average x	XAVG	0.383	AVERAGE(x)
SSX	SSX	4.346	DEVSQ(x)
t(a/2,df)	t	2.311	TINV(a/2,df)
Degree of confidence (%)		95	
	a	0.05	
	df	50	n-2

Experimental data

						Regression line	Confidence interval				Prediction interval		
Number of data points	Dry Density (Mg/m3)	Satn.	Specific Heat	Satn. x	SH y	Saturation x	SH y	CI	y+CI	y-CI	PI	y+PI	y-PI
1	1.50	0.00	1.27	0.00	1.27	0.01	1.55	0.23	1.78	1.32	1.05	2.60	0.50
2	1.52	0.00	1.26	0.00	1.26	0.06	1.62	0.21	1.83	1.41	1.05	2.67	0.57
3	1.51	0.00	1.29	0.00	1.29	0.11	1.69	0.20	1.89	1.50	1.04	2.74	0.65
4	1.51	0.07	1.65	0.07	1.65	0.16	1.76	0.18	1.94	1.59	1.04	2.81	0.72
5	1.50	0.07	1.71	0.07	1.71	0.21	1.84	0.17	2.00	1.67	1.04	2.88	0.80
6	1.52	0.06	1.53	0.06	1.53	0.26	1.91	0.15	2.06	1.75	1.04	2.95	0.87
7	1.48	0.11	1.73	0.11	1.73	0.31	1.98	0.15	2.13	1.83	1.04	3.02	0.95
8	1.51	0.11	2.03	0.11	2.03	0.36	2.05	0.14	2.20	1.91	1.04	3.09	1.02
9	1.49	0.09	2.10	0.09	2.10	0.41	2.13	0.14	2.27	1.98	1.04	3.16	1.09
10	1.50	0.16	1.88	0.16	1.88	0.46	2.20	0.15	2.35	2.05	1.04	3.23	1.16
11	1.52	0.16	1.88	0.16	1.88	0.51	2.27	0.16	2.43	2.11	1.04	3.31	1.23
12	1.50	0.17	2.24	0.17	2.24	0.56	2.34	0.17	2.51	2.18	1.04	3.38	1.30
13	1.55	0.20	2.01	0.20	2.01	0.61	2.41	0.18	2.60	2.23	1.04	3.46	1.37
14	1.51	0.21	2.40	0.21	2.40	0.66	2.49	0.20	2.68	2.29	1.04	3.53	1.44
15	1.50	0.21	2.42	0.21	2.42	0.71	2.56	0.21	2.77	2.34	1.05	3.61	1.51
16	1.51	0.21	2.54	0.21	2.54	0.76	2.63	0.23	2.87	2.40	1.05	3.68	1.58
17	1.51	0.29	2.19	0.29	2.19	0.81	2.70	0.25	2.96	2.45	1.06	3.76	1.65
18	1.51	0.35	2.42	0.35	2.42	0.86	2.78	0.27	3.05	2.50	1.06	3.84	1.71
19	1.49	0.34	2.51	0.34	2.51	0.91	2.85	0.30	3.14	2.55	1.07	3.92	1.78
20	1.52	0.39	3.01	0.39	3.01	0.96	2.92	0.32	3.24	2.60	1.07	3.99	1.85
21	1.53	0.37	2.38	0.37	2.38	1.01	2.99	0.34	3.33	2.65	1.08	4.07	1.91
22	1.53	0.36	2.39	0.36	2.39	1.06	3.06	0.36	3.43	2.70	1.09	4.15	1.98
23	1.55	0.48	2.64	0.48	2.64	1.11	3.14	0.38	3.52	2.75	1.10	4.23	2.04
24	1.53	0.46	2.80	0.46	2.80	1.16	3.21	0.41	3.62	2.80	1.10	4.31	2.11
25	1.52	0.45	2.41	0.45	2.41	1.21	3.28	0.43	3.71	2.85	1.11	4.39	2.17
26	1.57	0.61	2.52	0.61	2.52								
27	1.57	0.61	2.95	0.61	2.95								
28	1.57	0.62	2.87	0.62	2.87								
29	1.51	0.87	2.65	0.87	2.65								
30	1.46	0.80	3.36	0.80	3.36								
31	1.43	0.84	2.43	0.84	2.43								
32	1.41	0.97	2.57	0.97	2.57								
33	1.44	0.95	3.65	0.95	3.65								
34	1.45	0.96	3.02	0.96	3.02								
35	1.53	0.06	1.143	0.06	1.14								
36	1.52	0.05	1.054	0.05	1.05								
37	1.54	0.05	1.018	0.05	1.02								
38	1.56	0.18	1.388	0.18	1.39								
39	1.54	0.17	1.209	0.17	1.21								
40	1.53	0.16	1.19	0.16	1.19								
41	1.46	0.31	1.632	0.31	1.63								
42	1.46	0.30	1.577	0.30	1.58								
43	1.48	0.31	1.563	0.31	1.56								
44	1.48	0.47	1.805	0.47	1.81								
45	1.48	0.46	1.89	0.46	1.89								
46	1.48	0.45	1.758	0.45	1.76								
47	1.5	0.64	2.014	0.64	2.01								
48	1.5	0.63	1.931	0.63	1.93								
49	1.5	0.63	2.039	0.63	2.04								
50	1.51	0.83	2.247	0.83	2.25								
51	1.52	0.83	2.216	0.83	2.22								
52	1.52	0.83	2.12	0.83	2.12								

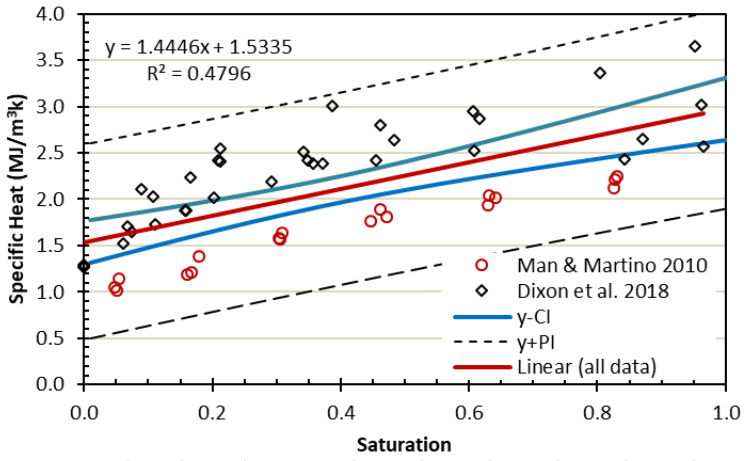

Specific heat 1.6 Mg/m^3 dry density

Date:
Author: D. Priyanto 2012
data UPDATED and spreadsheet Modified by:
D.Dixon 2018 Oct 02
All Data for MX80 Bentonite

Derived values			
Slope, m	m	0.901	SLOPE(y,x)
Intercept, b	b	1.092	INTERCEPT(y,x)
Observations, n	n	18.0	COUNT(x)
Std error in estimate, S_{yx}	SYX	0.183	STEYX(y,x)
Average x	XAVG	0.357	AVERAGE(x)
SSX	SSX	0.880	DEVSQ(x)
t(a/2,df)	t	2.473	TINV(a/2,df)
Degree of confidence (%)		95	
	a	0.05	
	df	16	n-2

Experimental data

				Satn.	SH	Regression line		Confidence interval			Prediction interval		
Number of data points	Dry Density (Mg/m3)	saturation	Specific Heat	x	y	Saturation x	SH y	CI	y+CI	y-CI	PI	y+PI	y-PI
1	1.66	0.06	0.75	0.06	0.75	0.01	1.10	0.20	1.30	0.90	0.49	1.59	0.61
2	1.61	0.07	1.14	0.07	1.14	0.06	1.15	0.18	1.32	0.97	0.49	1.63	0.66
3	1.72	0.07	0.88	0.07	0.88	0.11	1.19	0.16	1.35	1.03	0.48	1.67	0.71
4	1.64	0.17	1.28	0.17	1.28	0.16	1.24	0.14	1.38	1.09	0.47	1.71	0.76
5	1.65	0.17	1.32	0.17	1.32	0.21	1.28	0.13	1.41	1.15	0.47	1.75	0.81
6	1.62	0.16	1.33	0.16	1.33	0.26	1.33	0.12	1.44	1.21	0.47	1.79	0.86
7	1.58	0.27	1.43	0.27	1.43	0.31	1.37	0.11	1.48	1.26	0.46	1.84	0.91
8	1.59	0.25	1.43	0.25	1.43	0.36	1.42	0.11	1.52	1.31	0.46	1.88	0.95
9	1.58	0.24	1.43	0.24	1.43	0.41	1.46	0.11	1.57	1.35	0.46	1.93	1.00
10	1.59	0.41	1.77	0.41	1.77	0.46	1.51	0.12	1.62	1.39	0.47	1.97	1.04
11	1.60	0.40	1.56	0.40	1.56	0.51	1.55	0.13	1.68	1.42	0.47	2.02	1.08
12	1.60	0.41	1.64	0.41	1.64	0.56	1.60	0.14	1.74	1.45	0.47	2.07	1.12
13	1.59	0.53	1.52	0.53	1.52	0.61	1.64	0.16	1.80	1.48	0.48	2.12	1.16
14	1.61	0.56	1.50	0.56	1.50	0.66	1.69	0.18	1.87	1.51	0.49	2.17	1.20
15	1.61	0.54	1.74	0.54	1.74	0.71	1.73	0.20	1.93	1.53	0.49	2.23	1.24
16	1.62	0.73	1.58	0.73	1.58	0.76	1.78	0.22	2.00	1.56	0.50	2.28	1.27
17	1.60	0.70	1.53	0.70	1.53	0.81	1.82	0.24	2.06	1.58	0.51	2.33	1.31
18	1.63	0.70	1.64	0.70	1.64	0.86	1.87	0.26	2.13	1.60	0.52	2.39	1.34
						0.91	1.91	0.29	2.20	1.63	0.53	2.45	1.38
						0.96	1.96	0.31	2.27	1.65	0.55	2.50	1.41

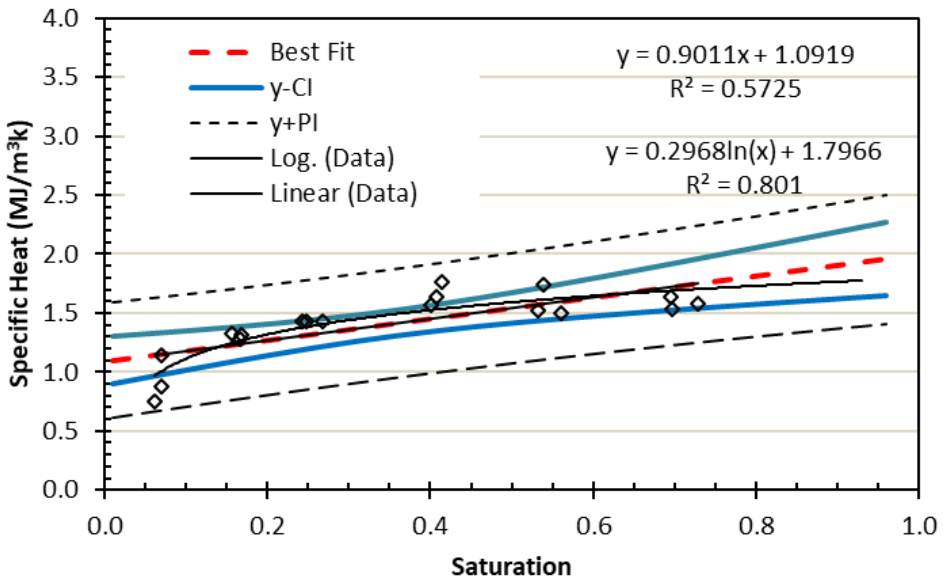

Specific heat 1.7 Mg/m^3 dry density

Date:

Author: D. Priyanto 2012

data UPDATED and spreadsheet Modified by:

D.Dixon 2018 Oct 02

All Data for MX80 Bentonite

Derived values			
Slope, m	m	1.296	SLOPE(y,x)
Intercept, b	b	1.821	INTERCEPT(y,x)
Observations, n	n	39.0	COUNT(x)
Std error in estimate, S_{yx}	SYX	0.302	STEYX(y,x)
Average x	XAVG	0.410	AVERAGE(x)
SSX	SSX	3.556	DEVSQ(x)
t(a/2,df)	t	2.336	TINV(a/2,df)
Degree of confidence (%)		95	
	a	0.05	
	df	37	n-2

Experimental data						Regression line		Confidence interval			Prediction interval		
Number of data points	Dry Density (Mg/m^3)	Satn.	Specific Heat	satn. x	SH y	Saturation x	SH y	CI	y+CI	y-CI	PI	y+PI	y-PI
1	1.70	0.00	1.46	0.00	1.46	0.01	1.83	0.19	2.02	1.65	0.73	2.56	1.11
2	1.71	0.00	1.49	0.00	1.49	0.06	1.90	0.17	2.07	1.73	0.73	2.63	1.17
3	1.72	0.00	1.72	0.00	1.72	0.11	1.96	0.16	2.12	1.80	0.72	2.69	1.24
4	1.70	0.06	1.85	0.06	1.85	0.16	2.03	0.15	2.18	1.88	0.72	2.75	1.31
5	1.68	0.05	1.83	0.05	1.83	0.21	2.09	0.14	2.23	1.96	0.72	2.81	1.38
6	1.72	0.06	1.71	0.06	1.71	0.26	2.16	0.13	2.28	2.03	0.72	2.87	1.44
7	1.69	0.11	2.18	0.11	2.18	0.31	2.22	0.12	2.34	2.10	0.71	2.94	1.51
8	1.67	0.11	2.15	0.11	2.15	0.36	2.29	0.11	2.40	2.17	0.71	3.00	1.57
9	1.68	0.10	1.94	0.10	1.94	0.41	2.35	0.11	2.47	2.24	0.71	3.07	1.64
10	1.69	0.15	2.23	0.15	2.23	0.46	2.42	0.11	2.53	2.30	0.71	3.13	1.70
11	1.69	0.15	2.18	0.15	2.18	0.51	2.48	0.12	2.60	2.36	0.71	3.20	1.77
12	1.70	0.15	2.22	0.15	2.22	0.56	2.55	0.13	2.67	2.42	0.72	3.26	1.83
13	1.68	0.19	1.88	0.19	1.88	0.61	2.61	0.14	2.75	2.48	0.72	3.33	1.89
14	1.71	0.19	1.83	0.19	1.83	0.66	2.68	0.15	2.82	2.53	0.72	3.40	1.96
15	1.71	0.19	2.02	0.19	2.02	0.71	2.74	0.16	2.90	2.58	0.72	3.46	2.02
16	1.70	0.25	2.05	0.25	2.05	0.76	2.81	0.17	2.98	2.63	0.73	3.53	2.08
17	1.76	0.25	1.79	0.25	1.79	0.81	2.87	0.19	3.06	2.68	0.73	3.60	2.14
18	1.70	0.24	1.86	0.24	1.86	0.86	2.94	0.20	3.14	2.73	0.73	3.67	2.20
19	1.72	0.39	2.47	0.39	2.47	0.91	3.00	0.22	3.22	2.78	0.74	3.74	2.26
20	1.73	0.40	2.38	0.40	2.38	0.96	3.07	0.23	3.30	2.83	0.74	3.81	2.32
21	1.71	0.38	2.32	0.38	2.32								
22	1.64	0.43	2.90	0.43	2.90								
23	1.63	0.44	3.06	0.44	3.06								
24	1.65	0.46	2.82	0.46	2.82								
25	1.69	0.58	2.58	0.58	2.58								
26	1.66	0.56	2.53	0.56	2.53								
27	1.62	0.52	2.37	0.52	2.37								
28	1.67	0.74	2.79	0.74	2.79								
29	1.66	0.74	2.91	0.74	2.91								
30	1.66	0.68	2.62	0.68	2.62								
31	1.76	0.71	2.78	0.71	2.78								
32	1.70	0.66	3.49	0.66	3.49								
33	1.71	0.66	3.03	0.66	3.03								
34	1.66	0.92	2.83	0.92	2.83								
35	1.64	0.89	3.12	0.89	3.12								
36	1.625	0.87	2.94	0.87	2.94								
37	1.655	0.92	2.54	0.92	2.54								
38	1.64	0.89	2.62	0.89	2.62								
39	1.625	0.87	2.28	0.87	2.28								

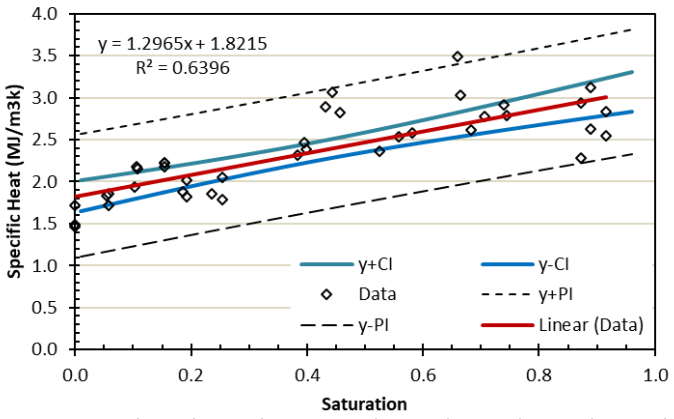

APPENDIX D. STATISTICAL ANALYSES OF HYDRAULIC CONDUCTIVITY DATA: EXPONENTIAL AND POWER FITS

D1. Hydraulic Conductivity Statistical Analyses to Determine Confidence and Prediction Intervals, Exponential Analyses

Freshwater

Derived values			
Slope, m	m	-3.694	SLOPE(y,x)
Intercept, b	b	-23.676	INTERCEPT(y,x)
Observations, n	n	105	COUNT(x)
Std error in estimate, S_{yx}	SYX	0.946	STEYX(y,x)
Average x	XAVG	1.496	AVERAGE(x)
SSX	SSX	16.470	DEVSQ(x)
t(a/2,df)	t	2.275	TINV(a/2,df)
Degree of confidence (%)		95	
	a	0.05	
	df	103	n-2

Regression line		Confidence interval			Prediction interval			Invers X & Y		upper CL	Lower CL	Upper PB	Lower PB
x	y	CI	y+CI	y-CI	PI	y+PI	y-PI	Dry Density Mg/m3	Best Fit m/s	Conf. Band m/s	Conf. Band m/s	Pred. Band m/s	Pred. Band m/s
0	-23.676	0.820	-22.856	-24.496	2.302	-21.374	-25.978	0	5.22E-11	1.19E-10	2.30E-11	5.22E-10	5.22E-12
0.1	-24.045	0.769	-23.276	-24.814	2.284	-21.761	-26.330	0.1	3.61E-11	7.78E-11	1.67E-11	3.54E-10	3.67E-12
0.2	-24.415	0.718	-23.697	-25.133	2.268	-22.147	-26.683	0.2	2.49E-11	5.11E-11	1.22E-11	2.41E-10	2.58E-12
0.3	-24.784	0.668	-24.117	-25.452	2.252	-22.532	-27.037	0.3	1.72E-11	3.36E-11	8.84E-12	1.64E-10	1.81E-12
0.4	-25.154	0.617	-24.536	-25.771	2.238	-22.915	-27.392	0.4	1.19E-11	2.21E-11	6.42E-12	1.12E-10	1.27E-12
0.5	-25.523	0.568	-24.955	-26.091	2.225	-23.298	-27.748	0.5	8.23E-12	1.45E-11	4.67E-12	7.62E-11	8.90E-13
0.6	-25.892	0.519	-25.373	-26.411	2.213	-23.679	-28.105	0.6	5.69E-12	9.56E-12	3.39E-12	5.20E-11	6.22E-13
0.7	-26.262	0.471	-25.791	-26.733	2.202	-24.060	-28.464	0.7	3.93E-12	6.30E-12	2.46E-12	3.56E-11	4.35E-13
0.8	-26.631	0.424	-26.207	-27.055	2.193	-24.439	-28.824	0.8	2.72E-12	4.15E-12	1.78E-12	2.43E-11	3.03E-13
0.9	-27.001	0.379	-26.622	-27.380	2.184	-24.816	-29.185	0.9	1.88E-12	2.74E-12	1.29E-12	1.67E-11	2.11E-13
1	-27.370	0.336	-27.034	-27.706	2.177	-25.193	-29.547	1	1.30E-12	1.82E-12	9.27E-13	1.15E-11	1.47E-13
1.1	-27.740	0.297	-27.443	-28.036	2.172	-25.568	-29.911	1.1	8.97E-13	1.21E-12	6.67E-13	7.87E-12	1.02E-13
1.2	-28.109	0.262	-27.847	-28.371	2.167	-25.942	-30.276	1.2	6.20E-13	8.06E-13	4.77E-13	5.41E-12	7.10E-14
1.3	-28.478	0.234	-28.244	-28.712	2.164	-26.314	-30.642	1.3	4.29E-13	5.42E-13	3.39E-13	3.73E-12	4.92E-14
1.4	-28.848	0.216	-28.632	-29.064	2.162	-26.686	-31.010	1.4	2.96E-13	3.68E-13	2.39E-13	2.57E-12	3.41E-14
1.5	-29.217	0.210	-29.007	-29.427	2.161	-27.056	-31.379	1.5	2.05E-13	2.53E-13	1.66E-13	1.78E-12	2.36E-14
1.6	-29.587	0.217	-29.370	-29.804	2.162	-27.425	-31.749	1.6	1.41E-13	1.76E-13	1.14E-13	1.23E-12	1.63E-14
1.7	-29.956	0.236	-29.720	-30.192	2.164	-27.792	-32.120	1.7	9.78E-14	1.24E-13	7.72E-14	8.51E-13	1.12E-14
1.8	-30.326	0.265	-30.061	-30.590	2.167	-28.158	-32.493	1.8	6.76E-14	8.81E-14	5.19E-14	5.90E-13	7.74E-15
1.9	-30.695	0.300	-30.395	-30.995	2.172	-28.523	-32.867	1.9	4.67E-14	6.30E-14	3.46E-14	4.10E-13	5.32E-15
2	-31.064	0.340	-30.724	-31.404	2.178	-28.886	-33.242	2	3.23E-14	4.53E-14	2.30E-14	2.85E-13	3.66E-15
2.1	-31.434	0.383	-31.051	-31.817	2.185	-29.249	-33.619	2.1	2.23E-14	3.27E-14	1.52E-14	1.98E-13	2.51E-15
2.2	-31.803	0.428	-31.375	-32.232	2.193	-29.610	-33.997	2.2	1.54E-14	2.37E-14	1.00E-14	1.38E-13	1.72E-15
2.3	-32.173	0.475	-31.697	-32.648	2.203	-29.970	-34.376	2.3	1.07E-14	1.71E-14	6.62E-15	9.65E-14	1.18E-15
2.4	-32.542	0.523	-32.019	-33.065	2.214	-30.328	-34.756	2.4	7.36E-15	1.24E-14	4.36E-15	6.74E-14	8.05E-16

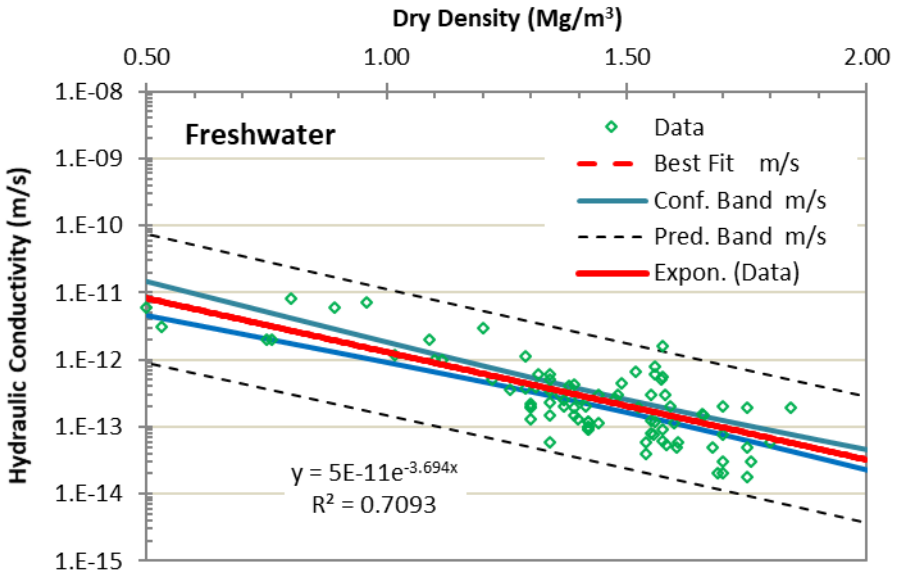

Figure D1. Exponential Best-Fit and Confidence Bands for Hydraulic Conductivity in Freshwater

5 to 15 g/L

Derived values			
Slope, m	m	-7.929	SLOPE(y,x)
Intercept, b	b	-17.096	INTERCEPT(y,x)
Observations, n	n	70	COUNT(x)
Std error in estimate, S_{yx}	SYX	1.279	STEYX(y,x)
Average x	XAVG	1.439	AVERAGE(x)
SSX	SSX	2.729	DEVSQ(x)
t(a/2,df)	t	2.292	TINV(a/2,df)
Degree of confidence (%)		95	
	a	0.05	
	df	68	n-2

Regression line		Confidence interval			Prediction interval			Invers X & Y		upper CL	Lower CL	Upper PB	Lower PB
x	y	CI	y+CI	y-CI	PI	y+PI	y-PI	Dry Density Mg/m3	Best Fit m/s	Conf. Band m/s	Conf. Band m/s	Pred. Band m/s	Pred. Band m/s
0	-17.1	2.578	-14.519	-19.674	3.904	-13.193	-21.000	0	3.76E-08	4.95E-07	2.85E-09	1.86E-06	7.58E-10
0.1	-17.89	2.402	-15.487	-20.291	3.790	-14.099	-21.680	0.1	1.70E-08	1.88E-07	1.54E-09	7.53E-07	3.84E-10
0.2	-18.68	2.227	-16.456	-20.909	3.682	-15.001	-22.364	0.2	7.70E-09	7.13E-08	8.31E-10	3.06E-07	1.94E-10
0.3	-19.48	2.052	-17.424	-21.527	3.578	-15.897	-23.054	0.3	3.48E-09	2.71E-08	4.48E-10	1.25E-07	9.73E-11
0.4	-20.27	1.877	-18.391	-22.145	3.481	-16.787	-23.749	0.4	1.58E-09	1.03E-08	2.41E-10	5.12E-08	4.85E-11
0.5	-21.06	1.703	-19.358	-22.764	3.391	-17.671	-24.452	0.5	7.13E-10	3.92E-09	1.30E-10	2.12E-08	2.40E-11
0.6	-21.85	1.530	-20.325	-23.384	3.307	-18.547	-25.161	0.6	3.23E-10	1.49E-09	6.99E-11	8.81E-09	1.18E-11
0.7	-22.65	1.357	-21.290	-24.005	3.231	-19.416	-25.878	0.7	1.46E-10	5.68E-10	3.76E-11	3.70E-09	5.77E-12
0.8	-23.44	1.187	-22.253	-24.627	3.163	-20.277	-26.603	0.8	6.61E-11	2.17E-10	2.02E-11	1.56E-09	2.80E-12
0.9	-24.23	1.019	-23.214	-25.252	3.104	-21.129	-27.337	0.9	2.99E-11	8.28E-11	1.08E-11	6.66E-10	1.34E-12
1	-25.03	0.854	-24.172	-25.880	3.054	-21.972	-28.080	1	1.35E-11	3.18E-11	5.76E-12	2.87E-10	6.38E-13
1.1	-25.82	0.696	-25.123	-26.515	3.013	-22.805	-28.832	1.1	6.12E-12	1.23E-11	3.05E-12	1.25E-10	3.01E-13
1.2	-26.61	0.550	-26.062	-27.162	2.983	-23.629	-29.595	1.2	2.77E-12	4.80E-12	1.60E-12	5.47E-11	1.40E-13
1.3	-27.4	0.428	-26.976	-27.833	2.963	-24.442	-30.368	1.3	1.25E-12	1.92E-12	8.17E-13	2.43E-11	6.48E-14
1.4	-28.2	0.357	-27.841	-28.555	2.954	-25.244	-31.151	1.4	5.67E-13	8.11E-13	3.97E-13	1.09E-11	2.96E-14
1.5	-28.99	0.367	-28.624	-29.357	2.955	-26.036	-31.945	1.5	2.57E-13	3.71E-13	1.78E-13	4.93E-12	1.34E-14
1.6	-29.78	0.452	-29.331	-30.236	2.967	-26.817	-32.750	1.6	1.16E-13	1.83E-13	7.39E-14	2.26E-12	5.98E-15
1.7	-30.58	0.581	-29.996	-31.157	2.989	-27.588	-33.565	1.7	5.26E-14	9.40E-14	2.94E-14	1.04E-12	2.65E-15
1.8	-31.37	0.730	-30.639	-32.100	3.021	-28.348	-34.391	1.8	2.38E-14	4.94E-14	1.15E-14	4.88E-13	1.16E-15
1.9	-32.16	0.890	-31.272	-33.053	3.064	-29.098	-35.226	1.9	1.08E-14	2.62E-14	4.42E-15	2.31E-13	5.03E-16
2	-32.96	1.056	-31.900	-34.011	3.116	-29.839	-36.071	2	4.87E-15	1.40E-14	1.70E-15	1.10E-13	2.16E-16
2.1	-33.75	1.224	-32.524	-34.973	3.177	-30.571	-36.926	2.1	2.20E-15	7.50E-15	6.48E-16	5.29E-14	9.19E-17
2.2	-34.54	1.395	-33.146	-35.937	3.247	-31.294	-37.788	2.2	9.98E-16	4.03E-15	2.47E-16	2.57E-14	3.88E-17
2.3	-35.33	1.568	-33.766	-36.902	3.325	-32.009	-38.659	2.3	4.51E-16	2.17E-15	9.41E-17	1.25E-14	1.62E-17
2.4	-36.13	1.741	-34.386	-37.868	3.410	-32.717	-39.537	2.4	2.04E-16	1.17E-15	3.58E-17	6.18E-15	6.75E-18

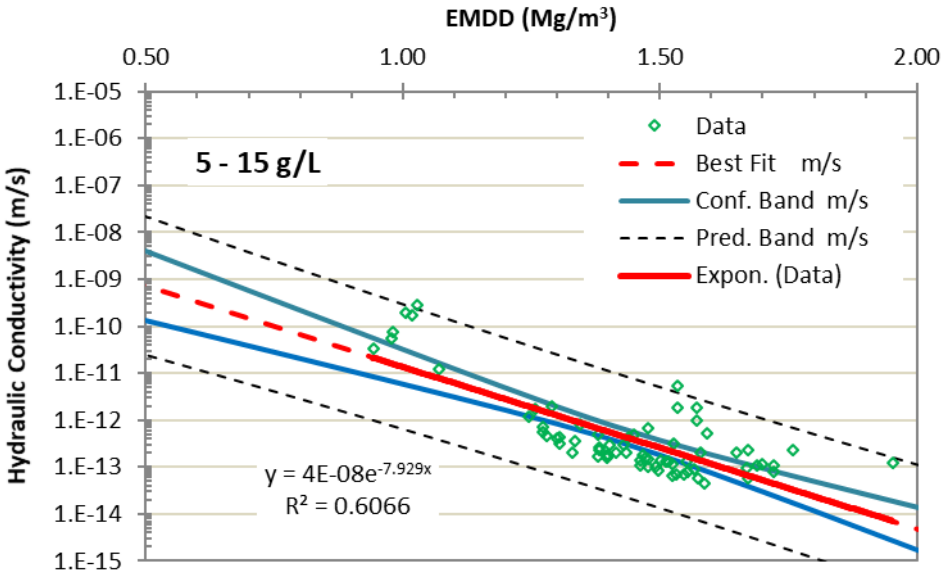

Figure D2. Exponential Best-Fit and Confidence Bands for k in 5-15 g/L TDS

50-70 g/L TDS

Derived values			
Slope, m	m	-17.219	SLOPE(y,x)
Intercept, b	b	-4.560	INTERCEPT(y,x)
Observations, n	n	22	COUNT(x)
Std error in estimate, S_{yx}	SYX	3.136	STEYX(y,x)
Average x	XAVG	0.880	AVERAGE(x)
SSX	SSX	0.895	DEVSQ(x)
t(a/2,df)	t	2.423	TINV(a/2,df)
Degree of confidence (%)		95	
	a	0.05	
	df	20	n-2

Regression line		Confidence interval			Prediction interval			Invers X & Y		upper CL	Lower CL	Upper PB	Lower PB
x	y	CI	y+CI	y-CI	PI	y+PI	y-PI	Dry Density Mg/m^3	Best Fit m/s	Conf. Band m/s	Conf. Band m/s	Pred. Band m/s	Pred. Band m/s
0	-4.560	7.252	2.692	-11.813	10.505	5.944	-15.065	0	1.05E-02	1.48E+01	7.41E-06	3.82E+02	2.87E-07
0.1	-6.282	6.472	0.190	-12.754	9.982	3.700	-16.264	0.1	1.87E-03	1.21E+00	2.89E-06	4.04E+01	8.64E-08
0.2	-8.004	5.698	-2.306	-13.702	9.498	1.494	-17.502	0.2	3.34E-04	9.96E-02	1.12E-06	4.46E+00	2.51E-08
0.3	-9.726	4.933	-4.793	-14.659	9.060	-0.666	-18.786	0.3	5.97E-05	8.29E-03	4.30E-07	5.14E-01	6.94E-09
0.4	-11.448	4.182	-7.265	-15.630	8.674	-2.773	-20.122	0.4	1.07E-05	6.99E-04	1.63E-07	6.24E-02	1.82E-09
0.5	-13.170	3.456	-9.714	-16.626	8.348	-4.821	-21.518	0.5	1.91E-06	6.04E-05	6.02E-08	8.06E-03	4.52E-10
0.6	-14.892	2.772	-12.120	-17.664	8.089	-6.802	-22.981	0.6	3.41E-07	5.45E-06	2.13E-08	1.11E-03	1.05E-10
0.7	-16.614	2.172	-14.442	-18.785	7.904	-8.710	-24.517	0.7	6.09E-08	5.34E-07	6.94E-09	1.65E-04	2.25E-11
0.8	-18.336	1.743	-16.593	-20.079	7.797	-10.539	-26.132	0.8	1.09E-08	6.22E-08	1.91E-09	2.65E-05	4.48E-12
0.9	-20.057	1.628	-18.429	-21.686	7.772	-12.285	-27.830	0.9	1.95E-09	9.91E-09	3.82E-10	4.62E-06	8.20E-13
1	-21.779	1.885	-19.894	-23.665	7.830	-13.949	-29.609	1	3.48E-10	2.29E-09	5.28E-11	8.75E-07	1.38E-13
1.1	-23.501	2.398	-21.104	-25.899	7.969	-15.533	-31.470	1.1	6.22E-11	6.84E-10	5.65E-12	1.80E-07	2.15E-14
1.2	-25.223	3.039	-22.185	-28.262	8.185	-17.039	-33.408	1.2	1.11E-11	2.32E-10	5.32E-13	3.98E-08	3.10E-15
1.3	-26.945	3.743	-23.202	-30.688	8.471	-18.474	-35.416	1.3	1.99E-12	8.38E-11	4.70E-14	9.48E-09	4.16E-16
1.4	-28.667	4.480	-24.187	-33.147	8.822	-19.845	-37.489	1.4	3.55E-13	3.13E-11	4.02E-15	2.41E-09	5.23E-17
1.5	-30.389	5.237	-25.152	-35.626	9.229	-21.159	-39.618	1.5	6.34E-14	1.19E-11	3.37E-16	6.46E-10	6.22E-18
1.6	-32.111	6.006	-26.104	-38.117	9.687	-22.424	-41.797	1.6	1.13E-14	4.60E-12	2.79E-17	1.82E-10	7.04E-19
1.7	-33.833	6.783	-27.049	-40.616	10.187	-23.646	-44.019	1.7	2.03E-15	1.79E-12	2.29E-18	5.38E-11	7.63E-20
1.8	-35.555	7.566	-27.989	-43.121	10.724	-24.831	-46.278	1.8	3.62E-16	6.99E-13	1.87E-19	1.64E-11	7.97E-21
1.9	-37.277	8.352	-28.924	-45.629	11.292	-25.984	-48.569	1.9	6.47E-17	2.74E-13	1.53E-20	5.19E-12	8.07E-22
2	-38.999	9.142	-29.857	-48.140	11.888	-27.111	-50.887	2	1.16E-17	1.08E-13	1.24E-21	1.68E-12	7.95E-23
2.1	-40.720	9.933	-30.787	-50.654	12.507	-28.214	-53.227	2.1	2.07E-18	4.26E-14	1.00E-22	5.59E-13	7.65E-24
2.2	-42.442	10.727	-31.716	-53.169	13.146	-29.297	-55.588	2.2	3.69E-19	1.68E-14	8.11E-24	1.89E-13	7.22E-25
2.3	-44.164	11.521	-32.643	-55.686	13.802	-30.362	-57.966	2.3	6.60E-20	6.66E-15	6.55E-25	6.51E-14	6.69E-26
2.4	-45.886	12.317	-33.569	-58.203	14.473	-31.413	-60.359	2.4	1.18E-20	2.64E-15	5.28E-26	2.28E-14	6.11E-27

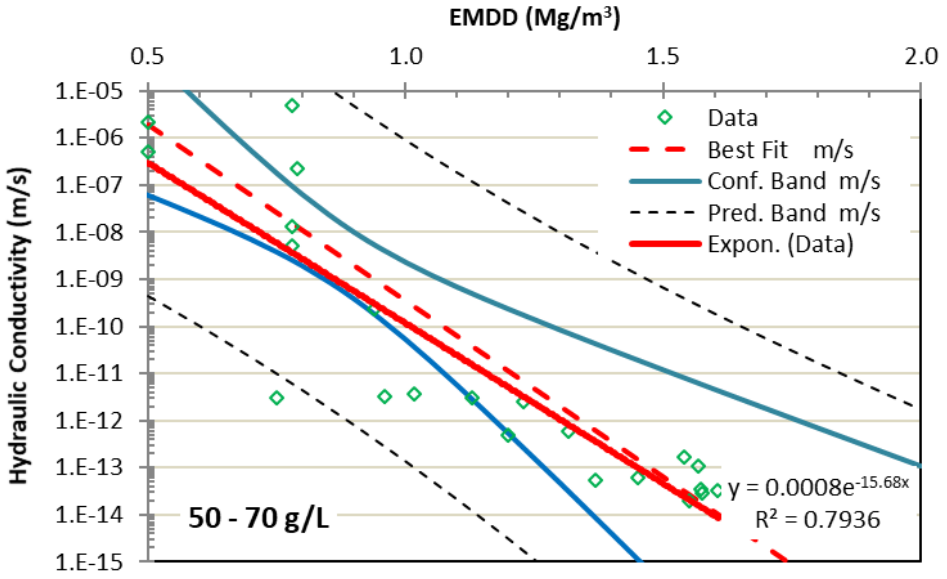

Figure D3. Exponential Best-Fit and Confidence Bands for k in 50-70 g/L TDS

100-160 g/L TDS

Derived values			
Slope, m	m	-2.761	SLOPE(y,x)
Intercept, b	b	-19.198	INTERCEPT(y,x)
Observations, n	n	6	COUNT(x)
Std error in estimate, S_{yx}	SYX	1.356	STEYX(y,x)
Average x	XAVG	1.125	AVERAGE(x)
SSX	SSX	0.489	DEVSQ(x)
t(a/2,df)	t	3.495	TINV(a/2,df)
Degree of confidence (%)		95	
	a	0.05	
	df	4	n-2

Regression line		Confidence interval			Prediction interval			Invers X & Y		upper CL	Lower CL	Upper PB	Lower PB
x	y	CI	y+CI	y-CI	PI	y+PI	y-PI	Dry Density Mg/m^3	Best Fit k (m/s)	Conf. Band	Conf. Band	Pred. Band	Pred. Band
0	-19.198	7.867	-11.330	-27.065	9.185	-10.013	-28.383	0	4.60E-09	1.20E-05	1.76E-12	4.48E-05	4.72E-13
0.1	-19.474	7.212	-12.262	-26.686	8.630	-10.844	-28.104	0.1	3.49E-09	4.73E-06	2.57E-12	1.95E-05	6.23E-13
0.2	-19.750	6.562	-13.188	-26.312	8.095	-11.655	-27.845	0.2	2.65E-09	1.87E-06	3.74E-12	8.67E-06	8.08E-13
0.3	-20.026	5.918	-14.109	-25.944	7.582	-12.444	-27.608	0.3	2.01E-09	7.46E-07	5.41E-12	3.94E-06	1.02E-12
0.4	-20.302	5.282	-15.021	-25.584	7.097	-13.206	-27.399	0.4	1.52E-09	3.00E-07	7.75E-12	1.84E-06	1.26E-12
0.5	-20.578	4.658	-15.921	-25.236	6.645	-13.933	-27.223	0.5	1.16E-09	1.22E-07	1.10E-11	8.89E-07	1.50E-12
0.6	-20.854	4.051	-16.804	-24.905	6.235	-14.619	-27.089	0.6	8.77E-10	5.04E-08	1.53E-11	4.48E-07	1.72E-12
0.7	-21.130	3.470	-17.660	-24.601	5.874	-15.256	-27.005	0.7	6.66E-10	2.14E-08	2.07E-11	2.37E-07	1.87E-12
0.8	-21.406	2.932	-18.474	-24.339	5.573	-15.833	-26.980	0.8	5.05E-10	9.48E-09	2.69E-11	1.33E-07	1.92E-12
0.9	-21.683	2.464	-19.219	-24.146	5.342	-16.341	-27.024	0.9	3.83E-10	4.50E-09	3.26E-11	8.01E-08	1.83E-12
1	-21.959	2.112	-19.846	-24.071	5.189	-16.769	-27.148	1	2.91E-10	2.40E-09	3.52E-11	5.21E-08	1.62E-12
1.1	-22.235	1.942	-20.292	-24.177	5.122	-17.112	-27.357	1.1	2.21E-10	1.54E-09	3.16E-11	3.70E-08	1.32E-12
1.2	-22.511	2.001	-20.510	-24.511	5.145	-17.366	-27.656	1.2	1.67E-10	1.24E-09	2.26E-11	2.87E-08	9.76E-13
1.3	-22.787	2.270	-20.517	-25.056	5.255	-17.532	-28.042	1.3	1.27E-10	1.23E-09	1.31E-11	2.43E-08	6.63E-13
1.4	-23.063	2.687	-20.376	-25.750	5.448	-17.614	-28.511	1.4	9.64E-11	1.42E-09	6.56E-12	2.24E-08	4.15E-13
1.5	-23.339	3.195	-20.144	-26.534	5.716	-17.623	-29.055	1.5	7.31E-11	1.78E-09	3.00E-12	2.22E-08	2.41E-13
1.6	-23.615	3.756	-19.859	-27.372	6.048	-17.567	-29.663	1.6	5.55E-11	2.37E-09	1.30E-12	2.35E-08	1.31E-13
1.7	-23.891	4.352	-19.540	-28.243	6.434	-17.457	-30.326	1.7	4.21E-11	3.27E-09	5.42E-13	2.62E-08	6.76E-14
1.8	-24.167	4.968	-19.199	-29.135	6.866	-17.301	-31.033	1.8	3.19E-11	4.59E-09	2.22E-13	3.06E-08	3.33E-14
1.9	-24.443	5.598	-18.845	-30.042	7.335	-17.108	-31.779	1.9	2.42E-11	6.54E-09	8.98E-14	3.72E-08	1.58E-14
2	-24.719	6.239	-18.480	-30.958	7.835	-16.884	-32.554	2	1.84E-11	9.42E-09	3.59E-14	4.65E-08	7.27E-15
2.1	-24.995	6.886	-18.109	-31.882	8.360	-16.635	-33.355	2.1	1.40E-11	1.37E-08	1.43E-14	5.96E-08	3.27E-15
2.2	-25.271	7.539	-17.732	-32.811	8.906	-16.366	-34.177	2.2	1.06E-11	1.99E-08	5.63E-15	7.80E-08	1.44E-15
2.3	-25.548	8.196	-17.351	-33.744	9.468	-16.079	-35.016	2.3	8.03E-12	2.91E-08	2.21E-15	1.04E-07	6.21E-16
2.4	-25.824	8.857	-16.967	-34.680	10.045	-15.779	-35.869	2.4	6.09E-12	4.28E-08	8.68E-16	1.40E-07	2.64E-16

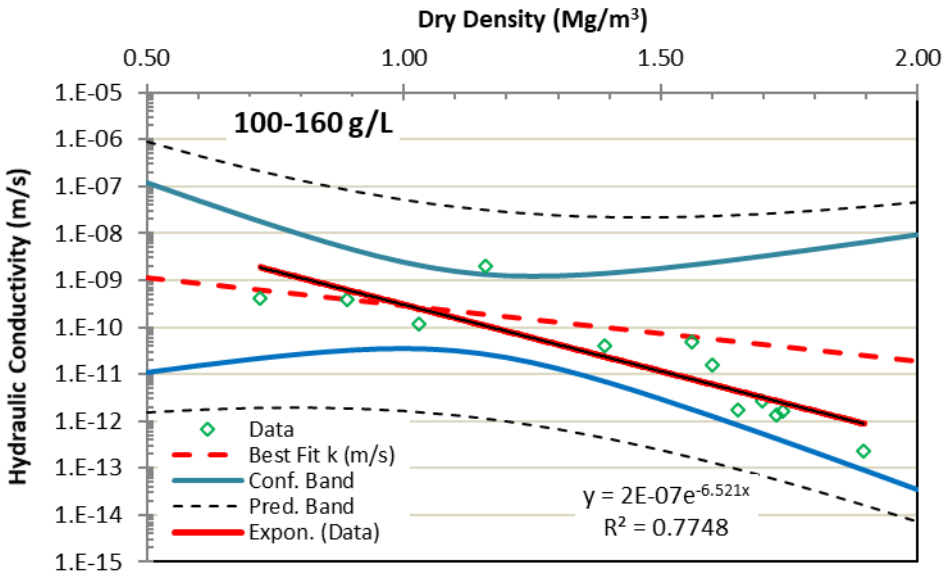

Figure D4. Exponential Best-Fit and Confidence Bands for k in 100-160 g/L TDS

>223 g/L TDS			
Derived values			
Slope, m	m	-11.549	SLOPE(y,x)
Intercept, b	b	-8.110	INTERCEPT(y,x)
Observations, n	n	43	COUNT(x)
Std error in estimate, S_{yx}	SYX	1.917	STEYX(y,x)
Average x	XAVG	1.472	AVERAGE(x)
SSX	SSX	4.760	DEVSQ(x)
t(a/2,df)	t	2.327	TINV(a/2,df)
Degree of confidence (%)		95	
	a	0.05	
	df	41	n-2

Regression line	Confidence interval			Prediction interval			Invers X & Y			upper	lower	upper	lower
x	y	CI	y+CI	y-CI	PI	y+PI	y-PI	EMDD	Best Fit	Conf. Band	Conf. Band	Pred. Band	Pred. Band
0	-8.110	3.086	-5.023	-11.196	5.424	-2.685	-13.534	0	3.01E-04	6.58E-03	1.37E-05	6.82E-02	1.33E-06
0.1	-9.264	2.887	-6.377	-12.152	5.314	-3.951	-14.578	0.1	9.47E-05	1.70E-03	5.28E-06	1.92E-02	4.66E-07
0.2	-10.419	2.689	-7.730	-13.108	5.209	-5.211	-15.628	0.2	2.99E-05	4.39E-04	2.03E-06	5.46E-03	1.63E-07
0.3	-11.574	2.492	-9.083	-14.066	5.110	-6.465	-16.684	0.3	9.41E-06	1.14E-04	7.79E-07	1.56E-03	5.68E-08
0.4	-12.729	2.296	-10.433	-15.025	5.017	-7.712	-17.746	0.4	2.96E-06	2.94E-05	2.98E-07	4.47E-04	1.96E-08
0.5	-13.884	2.101	-11.783	-15.985	4.931	-8.953	-18.815	0.5	9.34E-07	7.64E-06	1.14E-07	1.29E-04	6.74E-09
0.6	-15.039	1.909	-13.130	-16.948	4.852	-10.187	-19.891	0.6	2.94E-07	1.99E-06	4.36E-08	3.77E-05	2.30E-09
0.7	-16.194	1.719	-14.474	-17.913	4.781	-11.413	-20.974	0.7	9.27E-08	5.18E-07	1.66E-08	1.11E-05	7.78E-10
0.8	-17.348	1.534	-15.815	-18.882	4.717	-12.631	-22.066	0.8	2.92E-08	1.35E-07	6.30E-09	3.27E-06	2.61E-10
0.9	-18.503	1.354	-17.150	-19.857	4.662	-13.842	-23.165	0.9	9.21E-09	3.56E-08	2.38E-09	9.74E-07	8.70E-11
1	-19.658	1.181	-18.477	-20.839	4.615	-15.044	-24.273	1	2.90E-09	9.45E-09	8.90E-10	2.93E-07	2.87E-11
1.1	-20.813	1.021	-19.792	-21.834	4.576	-16.237	-25.389	1.1	9.14E-10	2.54E-09	3.29E-10	8.88E-08	9.41E-12
1.2	-21.968	0.879	-21.089	-22.847	4.547	-17.421	-26.515	1.2	2.88E-10	6.94E-10	1.20E-10	2.72E-08	3.05E-12
1.3	-23.123	0.766	-22.357	-23.889	4.526	-18.597	-27.649	1.3	9.08E-11	1.95E-10	4.22E-11	8.39E-09	9.82E-13
1.4	-24.278	0.696	-23.582	-24.974	4.515	-19.763	-28.793	1.4	2.86E-11	5.74E-11	1.43E-11	2.61E-09	3.13E-13
1.5	-25.433	0.683	-24.750	-26.115	4.513	-20.920	-29.945	1.5	9.01E-12	1.78E-11	4.55E-12	8.22E-10	9.88E-14
1.6	-26.587	0.729	-25.859	-27.316	4.520	-22.067	-31.108	1.6	2.84E-12	5.88E-12	1.37E-12	2.61E-10	3.09E-14
1.7	-27.742	0.824	-26.918	-28.567	4.536	-23.206	-32.279	1.7	8.95E-13	2.04E-12	3.92E-13	8.35E-11	9.58E-15
1.8	-28.897	0.955	-27.942	-29.852	4.562	-24.335	-33.459	1.8	2.82E-13	7.32E-13	1.08E-13	2.70E-11	2.94E-15
1.9	-30.052	1.108	-28.944	-31.160	4.596	-25.456	-34.649	1.9	8.88E-14	2.69E-13	2.93E-14	8.81E-12	8.96E-16
2	-31.207	1.276	-29.931	-32.482	4.640	-26.567	-35.847	2	2.80E-14	1.00E-13	7.82E-15	2.90E-12	2.70E-16
2.1	-32.362	1.453	-30.909	-33.814	4.691	-27.670	-37.053	2.1	8.82E-15	3.77E-14	2.06E-15	9.61E-13	8.09E-17
2.2	-33.517	1.636	-31.881	-35.153	4.751	-28.765	-38.268	2.2	2.78E-15	1.43E-14	5.41E-16	3.22E-13	2.40E-17
2.3	-34.672	1.824	-32.848	-36.496	4.819	-29.852	-39.491	2.3	8.76E-16	5.43E-15	1.41E-16	1.08E-13	7.07E-18
2.4	-35.826	2.015	-33.811	-37.842	4.895	-30.932	-40.721	2.4	2.76E-16	2.07E-15	3.68E-17	3.69E-14	2.06E-18

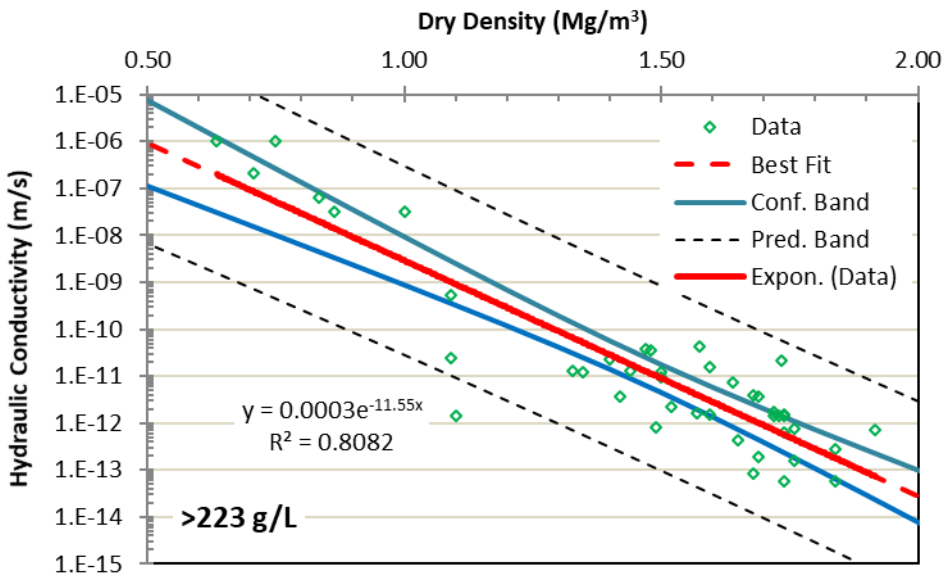

Figure D5. Exponential Best-Fit and Confidence Bands for k in >223 g/L TDS

>325 g/L TDS

Derived values			
Slope, m	m	-13.664	SLOPE(y,x)
Intercept, b	b	-4.300	INTERCEPT(y,x)
Observations, n	n	13	COUNT(x)
Std error in estimate, S_{yx}	SYX	1.031	STEYX(y,x)
Average x	XAVG	1.486	AVERAGE(x)
SSX	SSX	1.101	DEVSQ(x)
t(a/2,df)	t	2.593	TINV(a/2,df)
Degree of confidence (%)		95	
	a	0.05	
	df	11	n-2

Regression line		Confidence interval			Prediction interval			Invers X & Y					
x	y	CI	y+CI	y-CI	PI	y+PI	y-PI	EMDD	Best Fit	Conf. Band m/s	Conf. Band m/s	Pred. Band m/s	Pred. Band m/s
0	-4.300	3.860	-0.440	-8.159	4.696	0.396	-8.996	0	1.36E-02	6.44E-01	2.86E-04	1.49E+00	1.24E-04
0.1	-5.666	3.610	-2.056	-9.276	4.493	-1.173	-10.159	0.1	3.46E-03	1.28E-01	9.36E-05	3.09E-01	3.87E-05
0.2	-7.032	3.361	-3.671	-10.393	4.295	-2.737	-11.328	0.2	8.83E-04	2.54E-02	3.06E-05	6.48E-02	1.20E-05
0.3	-8.399	3.113	-5.286	-11.512	4.104	-4.295	-12.503	0.3	2.25E-04	5.06E-03	1.00E-05	1.36E-02	3.72E-06
0.4	-9.765	2.866	-6.899	-12.631	3.920	-5.845	-13.685	0.4	5.74E-05	1.01E-03	3.27E-06	2.89E-03	1.14E-06
0.5	-11.132	2.621	-8.511	-13.752	3.745	-7.387	-14.876	0.5	1.46E-05	2.01E-04	1.07E-06	6.19E-04	3.46E-07
0.6	-12.498	2.377	-10.121	-14.875	3.578	-8.920	-16.076	0.6	3.73E-06	4.02E-05	3.47E-07	1.34E-04	1.04E-07
0.7	-13.864	2.137	-11.728	-16.001	3.423	-10.441	-17.288	0.7	9.52E-07	8.07E-06	1.12E-07	2.92E-05	3.11E-08
0.8	-15.231	1.900	-13.331	-17.130	3.281	-11.950	-18.511	0.8	2.43E-07	1.62E-06	3.63E-08	6.46E-06	9.13E-09
0.9	-16.597	1.668	-14.929	-18.265	3.152	-13.445	-19.749	0.9	6.19E-08	3.28E-07	1.17E-08	1.45E-06	2.65E-09
1	-17.964	1.444	-16.519	-19.408	3.040	-14.924	-21.003	1	1.58E-08	6.69E-08	3.73E-09	3.30E-07	7.56E-10
1.1	-19.330	1.232	-18.097	-20.562	2.945	-16.385	-22.275	1.1	4.03E-09	1.38E-08	1.17E-09	7.66E-08	2.12E-10
1.2	-20.696	1.040	-19.656	-21.737	2.870	-17.827	-23.566	1.2	1.03E-09	2.91E-09	3.63E-10	1.81E-08	5.83E-11
1.3	-22.063	0.881	-21.182	-22.943	2.816	-19.247	-24.879	1.3	2.62E-10	6.32E-10	1.09E-10	4.38E-09	1.57E-11
1.4	-23.429	0.774	-22.656	-24.203	2.784	-20.645	-26.213	1.4	6.68E-11	1.45E-10	3.08E-11	1.08E-09	4.13E-12
1.5	-24.796	0.743	-24.053	-25.538	2.776	-22.020	-27.571	1.5	1.70E-11	3.58E-11	8.11E-12	2.73E-10	1.06E-12
1.6	-26.162	0.797	-25.365	-26.959	2.791	-23.371	-28.953	1.6	4.35E-12	9.64E-12	1.96E-12	7.08E-11	2.67E-13
1.7	-27.528	0.921	-26.608	-28.449	2.829	-24.700	-30.357	1.7	1.11E-12	2.78E-12	4.41E-13	1.87E-11	6.55E-14
1.8	-28.895	1.091	-27.804	-29.986	2.889	-26.006	-31.783	1.8	2.83E-13	8.41E-13	9.49E-14	5.08E-12	1.57E-14
1.9	-30.261	1.290	-28.972	-31.551	2.969	-27.292	-33.230	1.9	7.21E-14	2.62E-13	1.98E-14	1.40E-12	3.70E-15
2	-31.628	1.505	-30.122	-33.133	3.069	-28.559	-34.697	2	1.84E-14	8.28E-14	4.08E-15	3.96E-13	8.54E-16
2.1	-32.994	1.732	-31.262	-34.726	3.186	-29.808	-36.180	2.1	4.69E-15	2.65E-14	8.30E-16	1.13E-13	1.94E-16
2.2	-34.360	1.965	-32.396	-36.325	3.319	-31.042	-37.679	2.2	1.20E-15	8.53E-15	1.68E-16	3.30E-14	4.33E-17
2.3	-35.727	2.203	-33.524	-37.930	3.465	-32.262	-39.192	2.3	3.05E-16	2.76E-15	3.37E-17	9.75E-15	9.53E-18
2.4	-37.093	2.445	-34.649	-39.538	3.623	-33.470	-40.717	2.4	7.77E-17	8.96E-16	6.75E-18	2.91E-15	2.07E-18

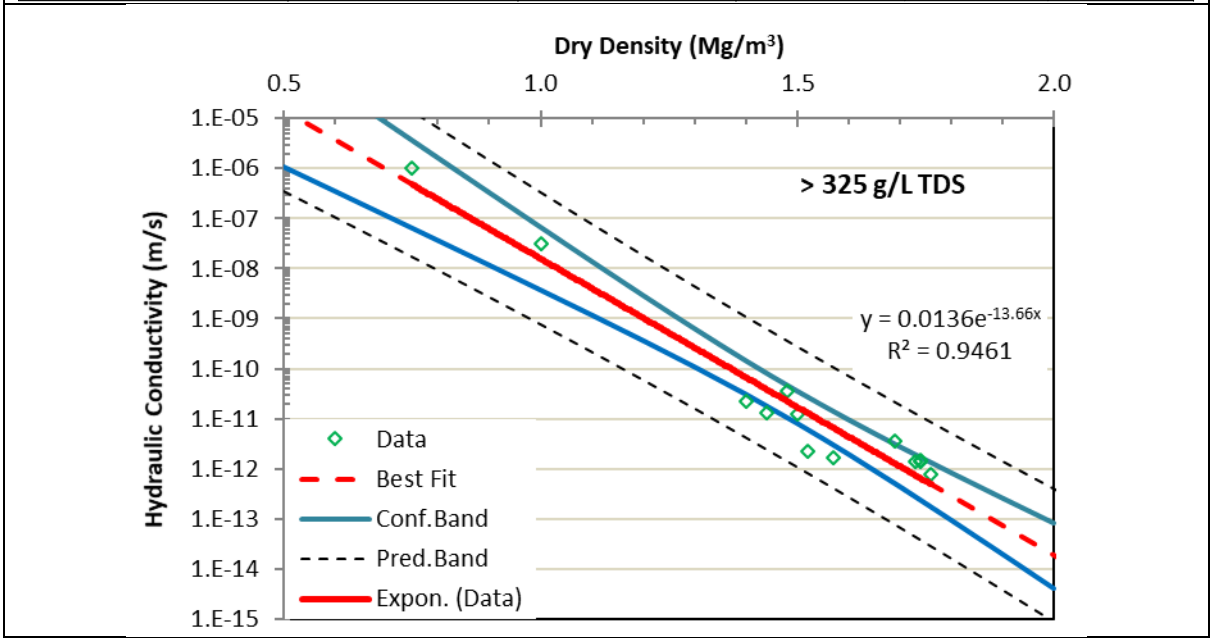

Figure D6. Exponential Best-Fit and Confidence Bands for k in >325 g/L TDS

D2. Hydraulic Conductivity Statistical Analyses to Determine Confidence and Prediction Intervals, Power-Fit

Freshwater

Derived values			
Slope, m	m	-4.620	SLOPE(y,x)
Intercept, b	b	-27.547	INTERCEPT(y,x)
Observations, n	n	105	COUNT(x)
Std error in estimate, S_{yx}	SYX	0.894	STEYX(y,x)
Average x	XAVG	0.358	AVERAGE(x)
SSX	SSX	10.993	DEVSQ(x)
t(a/2,df)	t	2.275	TINV(a/2,df)
Degree of confidence (%)		95	
	a	0.05	
	df	103	n-2

Regression line		Confidence interval			Prediction interval			Invers X & Y		upper	lower	upper	lower
x	y	CI	y+CI	y-CI	PI	y+PI	y-PI	Dry Density	Best Fit	Conf. Band	Conf. Band	Pred. Band	Pred. Band
-4.605	-6.273	3.050	-3.223	-9.323	3.666	-2.607	-9.938	0.01	1.89E-03	3.98E-02	8.94E-05	7.37E-02	4.83E-05
-2.207	-17.350	1.585	-15.765	-18.936	2.578	-14.772	-19.929	0.11	2.92E-08	1.42E-07	5.97E-09	3.84E-07	2.21E-09
-1.561	-20.338	1.193	-19.145	-21.531	2.357	-17.980	-22.695	0.21	1.47E-09	4.85E-09	4.46E-10	1.55E-08	1.39E-10
-1.171	-22.137	0.958	-21.178	-23.095	2.248	-19.889	-24.385	0.31	2.43E-10	6.34E-10	9.33E-11	2.30E-09	2.57E-11
-0.892	-23.429	0.791	-22.637	-24.220	2.182	-21.247	-25.610	0.41	6.69E-11	1.48E-10	3.03E-11	5.92E-10	7.54E-12
-0.673	-24.437	0.663	-23.774	-25.100	2.138	-22.298	-26.575	0.51	2.44E-11	4.73E-11	1.26E-11	2.07E-10	2.87E-12
-0.494	-25.264	0.559	-24.705	-25.823	2.109	-23.155	-27.373	0.61	1.07E-11	1.87E-11	6.10E-12	8.79E-11	1.29E-12
-0.342	-25.965	0.473	-25.492	-26.438	2.088	-23.878	-28.053	0.71	5.29E-12	8.49E-12	3.30E-12	4.27E-11	6.56E-13
-0.211	-26.574	0.401	-26.173	-26.975	2.072	-24.502	-28.646	0.81	2.88E-12	4.30E-12	1.93E-12	2.29E-11	3.62E-13
-0.094	-27.112	0.341	-26.771	-27.453	2.062	-25.050	-29.173	0.91	1.68E-12	2.36E-12	1.20E-12	1.32E-11	2.14E-13
0.010	-27.593	0.291	-27.302	-27.885	2.054	-25.539	-29.647	1.01	1.04E-12	1.39E-12	7.76E-13	8.10E-12	1.33E-13
0.104	-28.030	0.252	-27.777	-28.282	2.049	-25.981	-30.078	1.11	6.71E-13	8.64E-13	5.22E-13	5.21E-12	8.65E-14
0.191	-28.428	0.223	-28.205	-28.651	2.045	-26.383	-30.473	1.21	4.51E-13	5.63E-13	3.60E-13	3.48E-12	5.83E-14
0.270	-28.795	0.206	-28.589	-29.000	2.044	-26.751	-30.838	1.31	3.12E-13	3.84E-13	2.54E-13	2.41E-12	4.05E-14
0.344	-29.135	0.199	-28.936	-29.333	2.043	-27.092	-31.178	1.41	2.22E-13	2.71E-13	1.82E-13	1.71E-12	2.88E-14
0.412	-29.451	0.201	-29.250	-29.652	2.043	-27.408	-31.494	1.51	1.62E-13	1.98E-13	1.32E-13	1.25E-12	2.10E-14
0.476	-29.747	0.211	-29.536	-29.959	2.044	-27.703	-31.792	1.61	1.20E-13	1.49E-13	9.75E-14	9.30E-13	1.56E-14
0.536	-30.026	0.227	-29.799	-30.253	2.046	-27.980	-32.072	1.71	9.12E-14	1.14E-13	7.27E-14	7.05E-13	1.18E-14
0.593	-30.288	0.245	-30.043	-30.534	2.048	-28.240	-32.336	1.81	7.01E-14	8.96E-14	5.49E-14	5.44E-13	9.05E-15
0.647	-30.537	0.266	-30.271	-30.803	2.051	-28.486	-32.587	1.91	5.47E-14	7.14E-14	4.19E-14	4.25E-13	7.04E-15
0.698	-30.773	0.288	-30.485	-31.061	2.053	-28.719	-32.826	2.01	4.32E-14	5.76E-14	3.24E-14	3.37E-13	5.54E-15
0.747	-30.997	0.310	-30.687	-31.307	2.057	-28.940	-33.054	2.11	3.45E-14	4.71E-14	2.53E-14	2.70E-13	4.42E-15
0.793	-31.211	0.333	-30.878	-31.543	2.060	-29.151	-33.271	2.21	2.79E-14	3.89E-14	2.00E-14	2.19E-13	3.55E-15
0.837	-31.415	0.355	-31.061	-31.770	2.064	-29.351	-33.479	2.31	2.27E-14	3.24E-14	1.59E-14	1.79E-13	2.89E-15
0.880	-31.611	0.376	-31.235	-31.988	2.068	-29.543	-33.679	2.41	1.87E-14	2.72E-14	1.28E-14	1.48E-13	2.36E-15

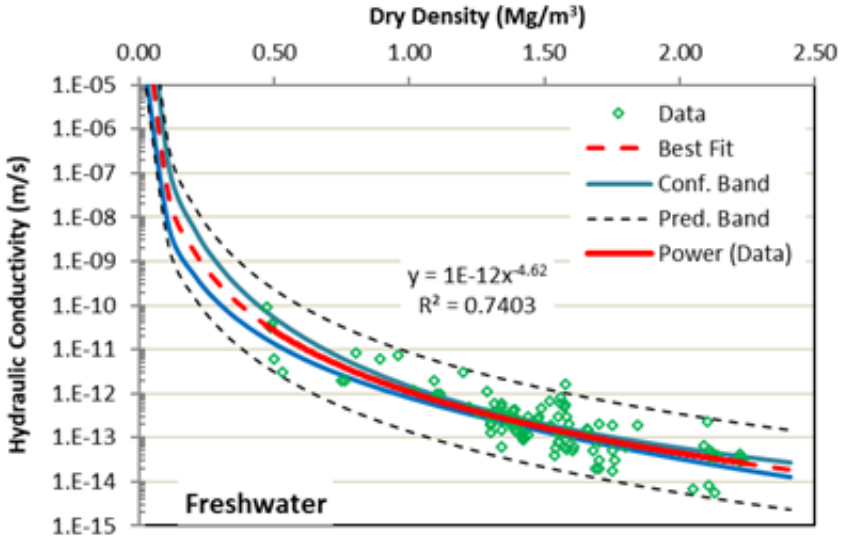

Figure D7. Power-Fit and Confidence Bands for Hydraulic Conductivity in Freshwater

5-15 g/L

Derived values			
Slope, m	m	-11.188	SLOPE(y,x)
Intercept, b	b	-24.550	INTERCEPT(y,x)
Observations, n	n	70.0	COUNT(x)
Std error in estimate, S_{yx}	SYX	1.170	STEYX(y,x)
Average x	XAVG	0.354	AVERAGE(x)
SSX	SSX	1.515	DEVSQ(x)
t(a/2,df)	t	2.292	TINV(a/2,df)
Degree of confidence (%)		95	
	a	0.05	
	df	68	n-2

Regression line		Confidence interval			Prediction interval			Invers X & Y		upper	lower	upper	lower
x	y	CI	y+CI	y-CI	PI	y+PI	y-PI	EMDD	Best Fit	Conf. Band m/s	Conf. Band m/s	Pred. Band m/s	Pred. Band m/s
-4.605	26.974	10.811	37.785	16.162	11.139	38.113	15.835	0.01	5.18E+11	2.57E+16	1.05E+07	3.57E+16	7.53E+06
-2.207	0.145	5.590	5.736	-5.445	6.200	6.346	-6.055	0.11	1.16E+00	3.10E+02	4.32E-03	5.70E+02	2.35E-03
-1.561	-7.089	4.184	-2.905	-11.273	4.970	-2.119	-12.059	0.21	8.34E-04	5.47E-02	1.27E-05	1.20E-01	5.79E-06
-1.171	-11.447	3.338	-8.108	-14.785	4.283	-7.164	-15.729	0.31	1.07E-05	3.01E-04	3.79E-07	7.74E-04	1.48E-07
-0.892	-14.575	2.733	-11.842	-17.307	3.829	-10.745	-18.404	0.41	4.68E-07	7.19E-06	3.04E-08	2.15E-05	1.02E-08
-0.673	-17.017	2.261	-14.756	-19.277	3.508	-13.508	-20.525	0.51	4.07E-08	3.91E-07	4.25E-09	1.36E-06	1.22E-09
-0.494	-19.020	1.875	-17.144	-20.895	3.273	-15.747	-22.293	0.61	5.49E-09	3.58E-08	8.42E-10	1.45E-07	2.08E-10
-0.342	-20.718	1.551	-19.168	-22.269	3.099	-17.620	-23.817	0.71	1.01E-09	4.74E-09	2.13E-10	2.23E-08	4.53E-11
-0.211	-22.193	1.271	-20.922	-23.463	2.969	-19.224	-25.161	0.81	2.30E-10	8.20E-10	6.46E-11	4.48E-09	1.18E-11
-0.094	-23.495	1.027	-22.467	-24.522	2.873	-20.622	-26.368	0.91	6.26E-11	1.75E-10	2.24E-11	1.11E-09	3.54E-12
0.010	-24.661	0.815	-23.847	-25.476	2.804	-21.858	-27.465	1.01	1.95E-11	4.40E-11	8.63E-12	3.22E-10	1.18E-12
0.104	-25.718	0.631	-25.087	-26.348	2.756	-22.962	-28.474	1.11	6.78E-12	1.27E-11	3.61E-12	1.07E-10	4.31E-13
0.191	-26.683	0.479	-26.204	-27.161	2.725	-23.958	-29.408	1.21	2.58E-12	4.16E-12	1.60E-12	3.94E-11	1.69E-13
0.270	-27.571	0.369	-27.202	-27.940	2.708	-24.863	-30.279	1.31	1.06E-12	1.54E-12	7.34E-13	1.59E-11	7.08E-14
0.344	-28.394	0.321	-28.073	-28.716	2.702	-25.692	-31.096	1.41	4.66E-13	6.43E-13	3.38E-13	6.95E-12	3.13E-14
0.412	-29.161	0.345	-28.816	-29.506	2.705	-26.456	-31.866	1.51	2.17E-13	3.06E-13	1.53E-13	3.24E-12	1.45E-14
0.476	-29.878	0.417	-29.461	-30.296	2.715	-27.163	-32.593	1.61	1.06E-13	1.60E-13	6.96E-14	1.60E-12	7.00E-15
0.536	-30.553	0.512	-30.041	-31.064	2.731	-27.822	-33.284	1.71	5.39E-14	8.98E-14	3.23E-14	8.27E-13	3.51E-15
0.593	-31.188	0.613	-30.575	-31.801	2.752	-28.437	-33.940	1.81	2.85E-14	5.26E-14	1.54E-14	4.47E-13	1.82E-15
0.647	-31.790	0.715	-31.075	-32.506	2.776	-29.014	-34.567	1.91	1.56E-14	3.19E-14	7.64E-15	2.51E-13	9.73E-16
0.698	-32.361	0.816	-31.545	-33.177	2.804	-29.557	-35.165	2.01	8.83E-15	2.00E-14	3.90E-15	1.46E-13	5.34E-16
0.747	-32.904	0.915	-31.990	-33.819	2.834	-30.070	-35.739	2.11	5.13E-15	1.28E-14	2.05E-15	8.73E-14	3.01E-16
0.793	-33.422	1.010	-32.413	-34.432	2.866	-30.556	-36.289	2.21	3.05E-15	8.38E-15	1.11E-15	5.37E-14	1.74E-16
0.837	-33.917	1.102	-32.816	-35.019	2.900	-31.017	-36.818	2.31	1.86E-15	5.60E-15	6.19E-16	3.38E-14	1.02E-16
0.880	-34.392	1.190	-33.201	-35.582	2.935	-31.457	-37.327	2.41	1.16E-15	3.81E-15	3.52E-16	2.18E-14	6.16E-17

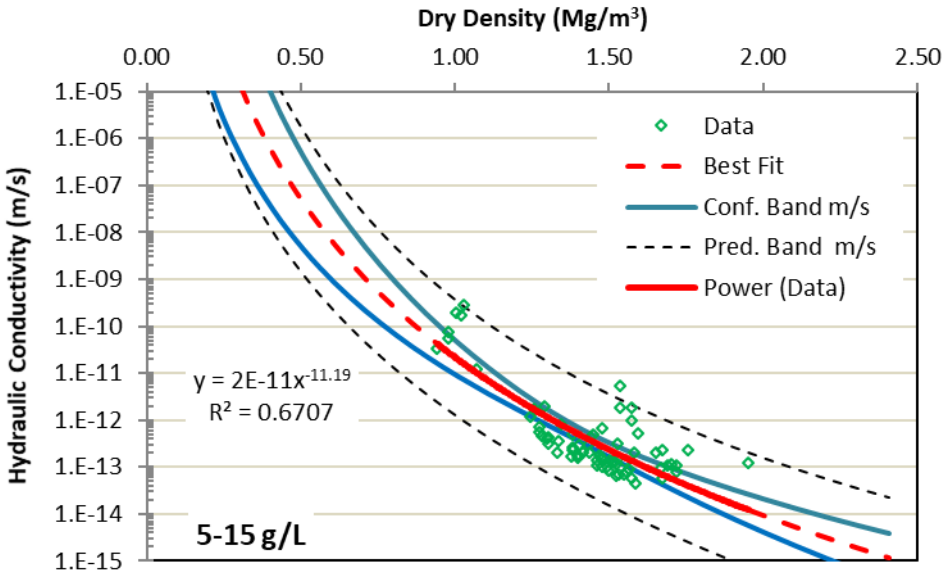

Figure D8. Power-Fit and Confidence Bands for k in 5-15 g/L TDS

50-70 g/L TDS

Derived values			
Slope, m	m	-16.004	SLOPE(y,x)
Intercept, b	b	-23.893	INTERCEPT(y,x)
Observations, n	n	22	COUNT(x)
Std error in estimate, S_{yx}	SYX	2.887	STEYX(y,x)
Average x	XAVG	0.065	AVERAGE(x)
SSX	SSX	2.819	DEVSQ(x)
t(a/2,df)	t	2.423	TINV(a/2,df)
Degree of confidence (%)		95	
	a	0.05	
	df	20	n-2

Regression line		Confidence interval			Prediction interval			Invers X & Y		upper	lower	upper	lower
x	y	CI	y+CI	y-CI	PI	y+PI	y-PI	Dry Density m/s	Best Fit k	Conf. Band	Conf. Band	Pred. Band	Pred. Band
-4.605	49.808	19.515	69.323	30.293	20.731	70.539	29.077	0.01	4.28E+21	1.28E+30	1.43E+13	4.31E+30	4.25E+12
-2.207	11.432	9.585	21.017	1.847	11.866	23.298	-0.434	0.11	9.22E+04	1.34E+09	6.34E+00	1.31E+10	6.48E-01
-1.561	1.083	6.936	8.020	-5.853	9.851	10.934	-8.768	0.21	2.95E+00	3.04E+03	2.87E-03	5.61E+04	1.56E-04
-1.171	-5.150	5.363	0.213	-10.512	8.814	3.665	-13.964	0.31	5.80E-03	1.24E+00	2.72E-05	3.90E+01	8.62E-07
-0.892	-9.624	4.256	-5.368	-13.880	8.188	-1.436	-17.813	0.41	6.61E-05	4.66E-03	9.37E-07	2.38E-01	1.84E-08
-0.673	-13.117	3.420	-9.697	-16.537	7.786	-5.331	-20.903	0.51	2.01E-06	6.14E-05	6.58E-08	4.84E-03	8.35E-10
-0.494	-15.983	2.768	-13.215	-18.750	7.523	-8.460	-23.505	0.61	1.15E-07	1.82E-06	7.19E-09	2.12E-04	6.19E-11
-0.342	-18.412	2.261	-16.151	-20.673	7.352	-11.061	-25.764	0.71	1.01E-08	9.67E-08	1.05E-09	1.57E-05	6.47E-12
-0.211	-20.521	1.883	-18.638	-22.404	7.244	-13.277	-27.765	0.81	1.22E-09	8.05E-09	1.86E-10	1.71E-06	8.74E-13
-0.094	-22.384	1.633	-20.751	-24.017	7.183	-15.201	-29.567	0.91	1.90E-10	9.73E-10	3.71E-11	2.50E-07	1.44E-13
0.010	-24.053	1.509	-22.543	-25.562	7.156	-16.896	-31.209	1.01	3.58E-11	1.62E-10	7.92E-12	4.59E-08	2.79E-14
0.104	-25.563	1.500	-24.063	-27.064	7.154	-18.409	-32.718	1.11	7.91E-12	3.54E-11	1.76E-12	1.01E-08	6.18E-15
0.191	-26.944	1.580	-25.364	-28.524	7.172	-19.772	-34.116	1.21	1.99E-12	9.65E-12	4.09E-13	2.59E-09	1.53E-15
0.270	-28.215	1.718	-26.497	-29.933	7.203	-21.012	-35.418	1.31	5.58E-13	3.11E-12	1.00E-13	7.50E-10	4.15E-16
0.344	-29.392	1.889	-27.503	-31.281	7.246	-22.146	-36.638	1.41	1.72E-13	1.14E-12	2.60E-14	2.41E-10	1.23E-16
0.412	-30.489	2.077	-28.412	-32.565	7.297	-23.192	-37.786	1.51	5.74E-14	4.58E-13	7.20E-15	8.47E-11	3.89E-17
0.476	-31.515	2.271	-29.244	-33.786	7.355	-24.160	-38.870	1.61	2.06E-14	1.99E-13	2.12E-15	3.22E-11	1.32E-17
0.536	-32.479	2.465	-30.014	-34.945	7.417	-25.062	-39.896	1.71	7.84E-15	9.23E-14	6.66E-16	1.30E-11	4.71E-18
0.593	-33.389	2.658	-30.731	-36.047	7.483	-25.906	-40.872	1.81	3.16E-15	4.50E-14	2.21E-16	5.61E-12	1.78E-18
0.647	-34.250	2.846	-31.403	-37.096	7.552	-26.697	-41.802	1.91	1.34E-15	2.30E-14	7.75E-17	2.54E-12	7.01E-19
0.698	-35.066	3.029	-32.037	-38.095	7.623	-27.443	-42.689	2.01	5.90E-16	1.22E-14	2.85E-17	1.21E-12	2.89E-19
0.747	-35.843	3.207	-32.636	-39.050	7.695	-28.148	-43.539	2.11	2.71E-16	6.70E-15	1.10E-17	5.96E-13	1.23E-19
0.793	-36.584	3.379	-33.206	-39.963	7.769	-28.816	-44.353	2.21	1.29E-16	3.79E-15	4.41E-18	3.06E-13	5.47E-20
0.837	-37.293	3.545	-33.747	-40.838	7.842	-29.450	-45.135	2.31	6.37E-17	2.21E-15	1.84E-18	1.62E-13	2.50E-20
0.880	-37.971	3.706	-34.265	-41.677	7.916	-30.054	-45.887	2.41	3.23E-17	1.32E-15	7.94E-19	8.86E-14	1.18E-20

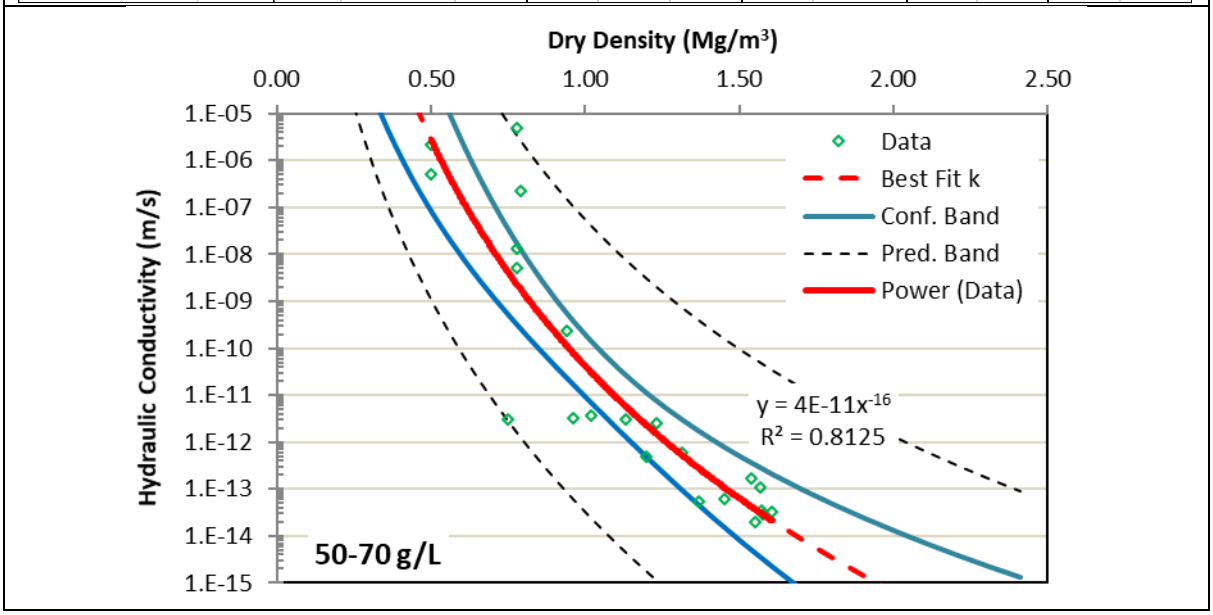

Figure D9. Power-Fit and Confidence Bands for k in 50-70 g/L TDS

100-160 g/L TDS

Derived values			
Slope, m	m	-7.623	SLOPE(y,x)
Intercept, b	b	-22.291	INTERCEPT(y,x)
Observations, n	n	12	COUNT(x)
Std error in estimate, S_{yx}	SYX	1.633	STEYX(y,x)
Average x	XAVG	0.312	AVERAGE(x)
SSX	SSX	1.046	DEVSQ(x)
t(a/2,df)	t	2.634	TINV(a/2,df)
Degree of confidence (%)		95	
	a	0.05	
	df	10	n-2

Regression line		Confidence interval			Prediction interval			Invers X & Y		upper	lower	upper	lower
x	y	CI	y+CI	y-CI	PI	y+PI	y-PI	EMDD	Best Fit	Conf. Band	Conf. Band	Pred. Band	Pred. Band
-4.605	12.816	20.724	33.540	-7.909	21.166	33.982	-8.350	0.01	3.68E+05	3.68E+14	3.68E-04	5.73E+14	2.36E-04
-2.207	-5.464	10.671	5.207	-16.136	11.506	6.042	-16.970	0.11	4.24E-03	1.83E+02	9.83E-08	4.21E+02	4.27E-08
-1.561	-10.394	7.976	-2.418	-18.369	9.062	-1.332	-19.455	0.21	3.06E-05	8.91E-02	1.05E-08	2.64E-01	3.55E-09
-1.171	-13.363	6.362	-7.000	-19.725	7.680	-5.682	-21.043	0.31	1.57E-06	9.12E-04	2.71E-09	3.41E-03	7.27E-10
-0.892	-15.494	5.214	-10.280	-20.708	6.759	-8.735	-22.253	0.41	1.87E-07	3.43E-05	1.02E-09	1.61E-04	2.17E-10
-0.673	-17.158	4.327	-12.830	-21.485	6.102	-11.056	-23.260	0.51	3.54E-08	2.68E-06	4.67E-10	1.58E-05	7.92E-11
-0.494	-18.523	3.612	-14.910	-22.135	5.617	-12.905	-24.140	0.61	9.03E-09	3.35E-07	2.44E-10	2.48E-06	3.28E-11
-0.342	-19.680	3.021	-16.659	-22.701	5.256	-14.424	-24.936	0.71	2.84E-09	5.82E-08	1.38E-10	5.44E-07	1.48E-11
-0.211	-20.685	2.526	-18.159	-23.210	4.988	-15.696	-25.673	0.81	1.04E-09	1.30E-08	8.32E-11	1.52E-07	7.09E-12
-0.094	-21.572	2.113	-19.459	-23.685	4.793	-16.779	-26.365	0.91	4.28E-10	3.54E-09	5.17E-11	5.16E-08	3.55E-12
0.010	-22.367	1.777	-20.590	-24.144	4.654	-17.712	-27.021	1.01	1.93E-10	1.14E-09	3.27E-11	2.03E-08	1.84E-12
0.104	-23.086	1.518	-21.568	-24.605	4.562	-18.525	-27.648	1.11	9.41E-11	4.30E-10	2.06E-11	9.01E-09	9.83E-13
0.191	-23.744	1.343	-22.401	-25.087	4.506	-19.238	-28.251	1.21	4.88E-11	1.87E-10	1.27E-11	4.42E-09	5.38E-13
0.270	-24.349	1.254	-23.095	-25.604	4.481	-19.868	-28.830	1.31	2.66E-11	9.33E-11	7.59E-12	2.35E-09	3.01E-13
0.344	-24.910	1.249	-23.661	-26.159	4.479	-20.431	-29.390	1.41	1.52E-11	5.30E-11	4.36E-12	1.34E-09	1.72E-13
0.412	-25.433	1.311	-24.121	-26.744	4.497	-20.935	-29.930	1.51	9.01E-12	3.34E-11	2.43E-12	8.09E-10	1.00E-13
0.476	-25.921	1.421	-24.500	-27.343	4.530	-21.391	-30.452	1.61	5.53E-12	2.29E-11	1.33E-12	5.13E-10	5.96E-14
0.536	-26.381	1.560	-24.821	-27.941	4.576	-21.805	-30.957	1.71	3.49E-12	1.66E-11	7.33E-13	3.39E-10	3.59E-14
0.593	-26.814	1.716	-25.099	-28.530	4.631	-22.183	-31.445	1.81	2.26E-12	1.26E-11	4.07E-13	2.32E-10	2.21E-14
0.647	-27.224	1.879	-25.345	-29.103	4.694	-22.530	-31.918	1.91	1.50E-12	9.83E-12	2.30E-13	1.64E-10	1.37E-14
0.698	-27.613	2.045	-25.568	-29.658	4.763	-22.850	-32.376	2.01	1.02E-12	7.87E-12	1.32E-13	1.19E-10	8.69E-15
0.747	-27.983	2.211	-25.773	-30.194	4.837	-23.147	-32.820	2.11	7.03E-13	6.41E-12	7.71E-14	8.86E-11	5.58E-15
0.793	-28.336	2.374	-25.962	-30.710	4.913	-23.423	-33.250	2.21	4.94E-13	5.31E-12	4.60E-14	6.72E-11	3.63E-15
0.837	-28.674	2.535	-26.139	-31.208	4.993	-23.680	-33.667	2.31	3.53E-13	4.45E-12	2.80E-14	5.20E-11	2.39E-15
0.880	-28.997	2.692	-26.305	-31.688	5.074	-23.922	-34.071	2.41	2.55E-13	3.77E-12	1.73E-14	4.08E-11	1.60E-15

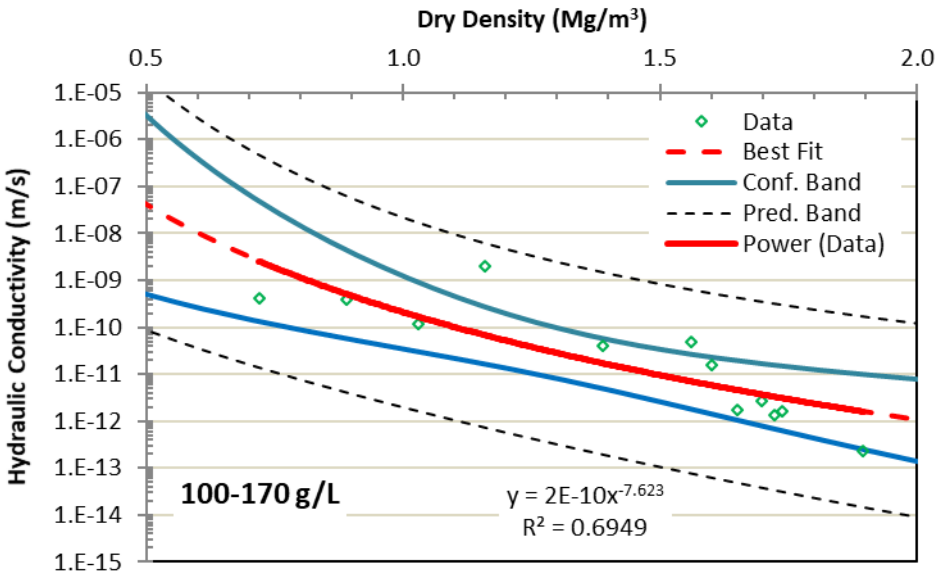

Figure D10. Power-Fit and Confidence Bands for k in 100-160 g/L TDS

>225 g/L TDS

Derived values			
Slope, m	m	-14.204	SLOPE(y,x)
Intercept, b	b	-20.089	INTERCEPT(y,x)
Observations, n	n	43	COUNT(x)
Std error in estimate, S_{yx}	SYX	1.756	STEYX(y,x)
Average x	XAVG	0.354	AVERAGE(x)
SSX	SSX	3.267	DEVSQ(x)
t(a/2,df)	t	2.327	TINV(a/2,df)
Degree of confidence (%)		95	
	a	0.05	
	df	41	n-2

Regression line		Confidence interval			Prediction interval			Invers X & Y		upper	lower	upper	lower
x	y	CI	y+CI	y-CI	PI	y+PI	y-PI	EMDD	Best Fit	Conf. Band	Conf. Band	Pred. Band	Pred. Band
-4.605	45.323	11.230	56.553	34.093	11.950	57.273	33.372	0.01	4.82E+19	3.63E+24	6.40E+14	7.47E+24	3.12E+14
-2.207	11.263	5.824	17.087	5.439	7.115	18.378	4.148	0.11	7.79E+04	2.64E+07	2.30E+02	9.58E+07	6.33E+01
-1.561	2.079	4.373	6.452	-2.295	5.986	8.064	-3.907	0.21	7.99E+00	6.34E+02	1.01E-01	3.18E+03	2.01E-02
-1.171	-3.453	3.504	0.051	-6.957	5.383	1.930	-8.836	0.31	3.16E-02	1.05E+00	9.52E-04	6.89E+00	1.45E-04
-0.892	-7.424	2.884	-4.541	-10.308	5.002	-2.423	-12.426	0.41	5.96E-04	1.07E-02	3.34E-05	8.87E-02	4.01E-06
-0.673	-10.524	2.404	-8.120	-12.929	4.742	-5.783	-15.266	0.51	2.69E-05	2.98E-04	2.43E-06	3.08E-03	2.34E-07
-0.494	-13.068	2.016	-11.052	-15.084	4.557	-8.511	-17.625	0.61	2.11E-06	1.59E-05	2.81E-07	2.01E-04	2.22E-08
-0.342	-15.224	1.693	-13.531	-16.917	4.424	-10.800	-19.648	0.71	2.45E-07	1.33E-06	4.50E-08	2.04E-05	2.93E-09
-0.211	-17.096	1.420	-15.675	-18.516	4.327	-12.769	-21.422	0.81	3.76E-08	1.56E-07	9.09E-09	2.85E-06	4.97E-10
-0.094	-18.749	1.189	-17.560	-19.938	4.256	-14.493	-23.005	0.91	7.20E-09	2.37E-08	2.19E-09	5.08E-07	1.02E-10
0.010	-20.230	0.996	-19.234	-21.226	4.206	-16.023	-24.436	1.01	1.64E-09	4.44E-09	6.05E-10	1.10E-07	2.44E-11
0.104	-21.571	0.840	-20.731	-22.411	4.172	-17.399	-25.743	1.11	4.28E-10	9.93E-10	1.85E-10	2.78E-08	6.60E-12
0.191	-22.796	0.724	-22.072	-23.520	4.150	-18.646	-26.947	1.21	1.26E-10	2.60E-10	6.10E-11	7.98E-09	1.98E-12
0.270	-23.924	0.651	-23.273	-24.575	4.138	-19.786	-28.062	1.31	4.07E-11	7.81E-11	2.12E-11	2.55E-09	6.50E-13
0.344	-24.969	0.624	-24.345	-25.593	4.134	-20.835	-29.103	1.41	1.43E-11	2.67E-11	7.68E-12	8.94E-10	2.29E-13
0.412	-25.942	0.637	-25.305	-26.579	4.136	-21.806	-30.078	1.51	5.41E-12	1.02E-11	2.86E-12	3.39E-10	8.65E-14
0.476	-26.853	0.682	-26.171	-27.535	4.143	-22.710	-30.996	1.61	2.18E-12	4.31E-12	1.10E-12	1.37E-10	3.46E-14
0.536	-27.709	0.748	-26.961	-28.457	4.155	-23.554	-31.864	1.71	9.25E-13	1.95E-12	4.38E-13	5.90E-11	1.45E-14
0.593	-28.516	0.826	-27.690	-29.342	4.169	-24.347	-32.686	1.81	4.13E-13	9.42E-13	1.81E-13	2.67E-11	6.38E-15
0.647	-29.280	0.910	-28.370	-30.190	4.187	-25.093	-33.467	1.91	1.92E-13	4.78E-13	7.74E-14	1.27E-11	2.92E-15
0.698	-30.005	0.997	-29.007	-31.002	4.207	-25.798	-34.212	2.01	9.31E-14	2.52E-13	3.43E-14	6.25E-12	1.39E-15
0.747	-30.695	1.085	-29.609	-31.780	4.228	-26.466	-34.923	2.11	4.67E-14	1.38E-13	1.58E-14	3.21E-12	6.81E-16
0.793	-31.352	1.173	-30.180	-32.525	4.252	-27.101	-35.604	2.21	2.42E-14	7.82E-14	7.49E-15	1.70E-12	3.45E-16
0.837	-31.981	1.258	-30.722	-33.239	4.276	-27.705	-36.257	2.31	1.29E-14	4.54E-14	3.67E-15	9.29E-13	1.79E-16
0.880	-32.583	1.343	-31.240	-33.925	4.302	-28.281	-36.884	2.41	7.07E-15	2.71E-14	1.85E-15	5.22E-13	9.58E-17

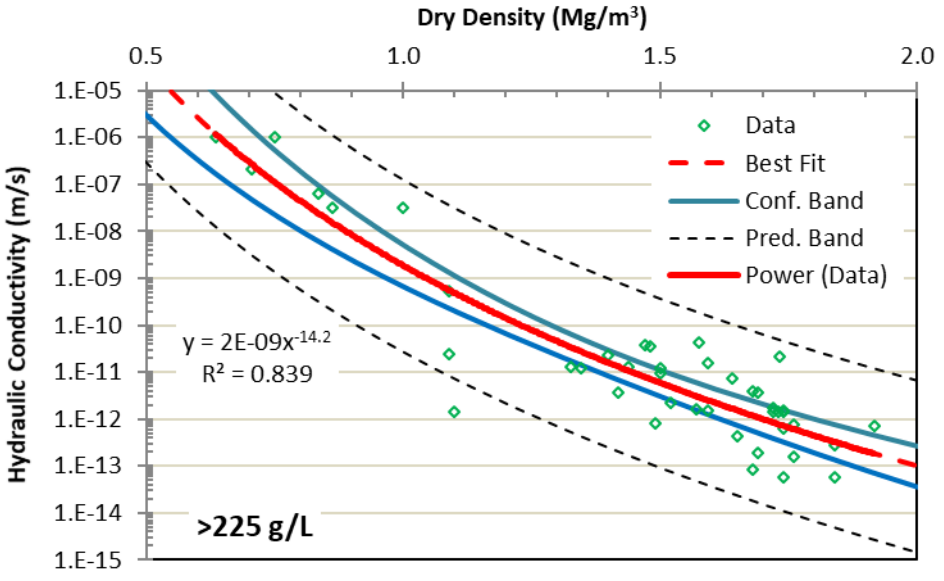

Figure D11. Power-Fit and Confidence Bands for k in >225 g/L TDS

>325 g/L TDS

Derived values			
Slope, m	m	-16.819	SLOPE(y,x)
Intercept, b	b	-18.362	INTERCEPT(y,x)
Observations, n	n	13	COUNT(x)
Std error in estimate, S_{yx}	SYX	0.808	STEYX(y,x)
Average x	XAVG	0.371	AVERAGE(x)
SSX	SSX	0.743	DEVSQ(x)
t(a/2,df)	t	2.593	TINV(a/2,df)
Degree of confidence (%)		95	
	a	0.05	
	df	11	n-2

Regression line		Confidence interval			Prediction interval			Invers X & Y		upper	lower	upper	lower
x	y	CI	y+CI	y-CI	PI	y+PI	y-PI	EMDD	Best Fit	Conf. Band	Conf. Band	Pred. Band	Pred. Band
-4.605	59.095	12.109	71.204	46.985	12.289	71.384	46.805	0.01	4.62E+25	8.39E+30	2.54E+20	1.00E+31	2.12E+20
-2.207	18.763	6.294	25.058	12.469	6.634	25.397	12.130	0.11	1.41E+08	7.63E+10	2.60E+05	1.07E+11	1.85E+05
-1.561	7.888	4.731	12.619	3.156	5.174	13.062	2.713	0.21	2.66E+03	3.02E+05	2.35E+01	4.71E+05	1.51E+01
-1.171	1.337	3.794	5.131	-2.457	4.334	5.671	-2.997	0.31	3.81E+00	1.69E+02	8.57E-02	2.90E+02	5.00E-02
-0.892	-3.365	3.124	-0.241	-6.489	3.761	0.396	-7.127	0.41	3.45E-02	7.85E-01	1.52E-03	1.49E+00	8.03E-04
-0.673	-7.036	2.605	-4.432	-9.641	3.342	-3.694	-10.379	0.51	8.79E-04	1.19E-02	6.50E-05	2.49E-02	3.11E-05
-0.494	-10.048	2.183	-7.865	-12.230	3.025	-7.023	-13.073	0.61	4.33E-05	3.84E-04	4.88E-06	8.91E-04	2.10E-06
-0.342	-12.601	1.830	-10.772	-14.431	2.781	-9.820	-15.382	0.71	3.37E-06	2.10E-05	5.41E-07	5.44E-05	2.09E-07
-0.211	-14.817	1.529	-13.288	-16.347	2.593	-12.224	-17.411	0.81	3.67E-07	1.69E-06	7.96E-08	4.91E-06	2.74E-08
-0.094	-16.775	1.272	-15.503	-18.047	2.451	-14.325	-19.226	0.91	5.18E-08	1.85E-07	1.45E-08	6.01E-07	4.47E-09
0.010	-18.529	1.053	-17.476	-19.582	2.344	-16.185	-20.873	1.01	8.97E-09	2.57E-08	3.13E-09	9.36E-08	8.61E-10
0.104	-20.117	0.871	-19.246	-20.988	2.268	-17.848	-22.385	1.11	1.83E-09	4.38E-09	7.68E-10	1.77E-08	1.90E-10
0.191	-21.568	0.728	-20.840	-22.296	2.218	-19.350	-23.785	1.21	4.30E-10	8.90E-10	2.07E-10	3.95E-09	4.68E-11
0.270	-22.903	0.631	-22.272	-23.534	2.188	-20.716	-25.091	1.31	1.13E-10	2.12E-10	6.01E-11	1.01E-09	1.27E-11
0.344	-24.141	0.585	-23.556	-24.725	2.175	-21.966	-26.315	1.41	3.28E-11	5.89E-11	1.83E-11	2.89E-10	3.73E-12
0.412	-25.293	0.589	-24.704	-25.882	2.176	-23.117	-27.469	1.51	1.04E-11	1.87E-11	5.75E-12	9.13E-11	1.18E-12
0.476	-26.372	0.634	-25.737	-27.006	2.189	-24.183	-28.560	1.61	3.52E-12	6.65E-12	1.87E-12	3.14E-11	3.95E-13
0.536	-27.385	0.706	-26.679	-28.091	2.211	-25.175	-29.596	1.71	1.28E-12	2.59E-12	6.31E-13	1.17E-11	1.40E-13
0.593	-28.341	0.793	-27.548	-29.134	2.240	-26.101	-30.581	1.81	4.92E-13	1.09E-12	2.22E-13	4.62E-12	5.24E-14
0.647	-29.246	0.887	-28.358	-30.133	2.275	-26.971	-31.520	1.91	1.99E-13	4.83E-13	8.20E-14	1.94E-12	2.05E-14
0.698	-30.104	0.984	-29.120	-31.088	2.314	-27.790	-32.418	2.01	8.43E-14	2.26E-13	3.15E-14	8.53E-13	8.34E-15
0.747	-30.921	1.082	-29.839	-32.002	2.357	-28.563	-33.278	2.11	3.73E-14	1.10E-13	1.26E-14	3.94E-13	3.53E-15
0.793	-31.699	1.178	-30.521	-32.878	2.403	-29.296	-34.103	2.21	1.71E-14	5.56E-14	5.27E-15	1.89E-13	1.55E-15
0.837	-32.444	1.273	-31.171	-33.717	2.451	-29.993	-34.895	2.31	8.13E-15	2.90E-14	2.28E-15	9.43E-14	7.00E-16
0.880	-33.156	1.365	-31.791	-34.522	2.500	-30.656	-35.657	2.41	3.98E-15	1.56E-14	1.02E-15	4.86E-14	3.27E-16

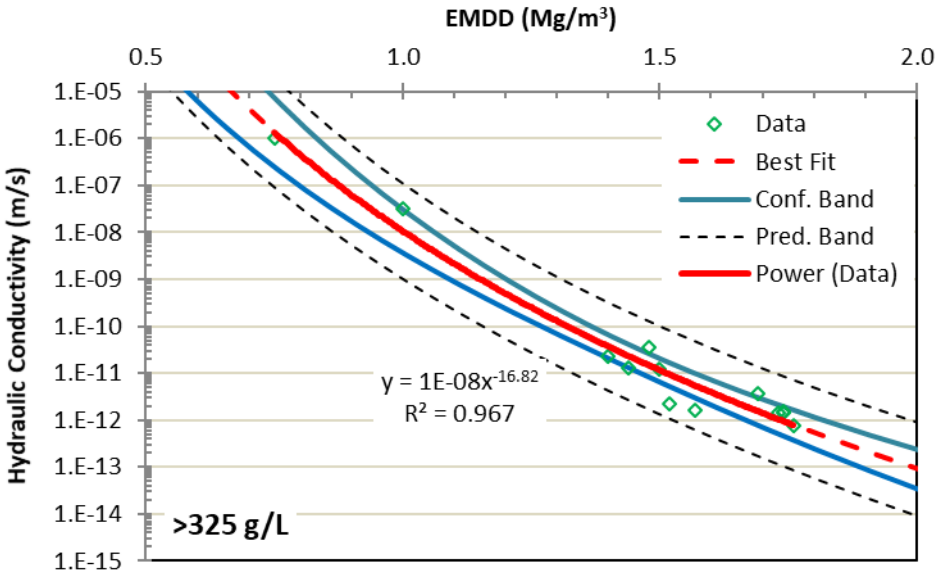

Figure D12. Power-Fit and Confidence Bands for k in >325 g/L TDS

APPENDIX E. STATISTICAL ANALYSES OF SWELLING PRESSURE DATA

Swelling Pressure Statistical Analyses to Determine Confidence and Prediction Intervals

Freshwater Conditions			
Derived values			
Slope, m	m	5.139	SLOPE(y,x)
Intercept, b	b	-6.197	NTERCEPT(y,x)
Observations, n	n	109	COUNT(x)
Std error in estimate, S_{yx}	SYX	0.534	STEYX(y,x)
Average x	XAVG	1.347	AVERAGE(x)
SSX	SSX	11.841	DEVSQ(x)
t(a/2,df)	t	2.273	TINV(a/2,df)
Degree of confidence (%)		95	
	a	0.05	
	df	107	n-2

Regression line		Confidence interval			Prediction interval			Invers X & Y		Upper	Lower	Upper	Lower
x	y	CI	y+CI	y-CI	PI	y+PI	y-PI	Dry Density (Mg/m^3)	Best Fit MPa	Conf. Band MPa	Conf. Band MPa	Pred. Band MPa	Pred. Band MPa
0	-6.197	0.489	-5.708	-6.686	1.308	-4.889	-7.506	0	0.002	0.003	0.001	0.008	0.001
0.1	-5.683	0.455	-5.228	-6.138	1.296	-4.387	-6.979	0.1	0.003	0.005	0.002	0.012	0.001
0.2	-5.169	0.421	-4.749	-5.590	1.284	-3.885	-6.454	0.2	0.006	0.009	0.004	0.021	0.002
0.3	-4.655	0.387	-4.268	-5.043	1.274	-3.382	-5.929	0.3	0.010	0.014	0.006	0.034	0.003
0.4	-4.141	0.354	-3.788	-4.495	1.264	-2.877	-5.406	0.4	0.016	0.023	0.011	0.056	0.004
0.5	-3.628	0.320	-3.307	-3.948	1.255	-2.372	-4.883	0.5	0.027	0.037	0.019	0.093	0.008
0.6	-3.114	0.288	-2.826	-3.402	1.247	-1.866	-4.361	0.6	0.044	0.059	0.033	0.155	0.013
0.7	-2.600	0.256	-2.344	-2.856	1.240	-1.359	-3.840	0.7	0.074	0.096	0.058	0.257	0.021
0.8	-2.086	0.225	-1.860	-2.311	1.234	-0.851	-3.320	0.8	0.124	0.156	0.099	0.427	0.036
0.9	-1.572	0.196	-1.376	-1.768	1.229	-0.342	-2.801	0.9	0.208	0.253	0.171	0.710	0.061
1	-1.058	0.169	-0.889	-1.227	1.225	0.167	-2.283	1	0.347	0.411	0.293	1.182	0.102
1.1	-0.544	0.145	-0.399	-0.689	1.222	0.678	-1.766	1.1	0.581	0.671	0.502	1.971	0.171
1.2	-0.030	0.127	0.097	-0.157	1.220	1.190	-1.250	1.2	0.971	1.102	0.855	3.288	0.286
1.3	0.484	0.117	0.601	0.367	1.219	1.703	-0.735	1.3	1.623	1.825	1.443	5.492	0.479
1.4	0.998	0.118	1.116	0.880	1.219	2.217	-0.221	1.4	2.713	3.052	2.412	9.182	0.802
1.5	1.512	0.128	1.640	1.384	1.220	2.732	0.292	1.5	4.536	5.156	3.990	15.367	1.339
1.6	2.026	0.147	2.172	1.879	1.222	3.248	0.804	1.6	7.583	8.780	6.549	25.745	2.233
1.7	2.540	0.170	2.710	2.370	1.225	3.765	1.314	1.7	12.678	15.032	10.692	43.176	3.723
1.8	3.054	0.198	3.251	2.856	1.230	4.283	1.824	1.8	21.196	25.826	17.395	72.481	6.198
1.9	3.568	0.227	3.795	3.341	1.235	4.802	2.333	1.9	35.437	44.469	28.239	121.796	10.310
2	4.082	0.258	4.340	3.824	1.241	5.322	2.841	2	59.246	76.683	45.774	204.866	17.133
2.1	4.596	0.290	4.886	4.306	1.248	5.843	3.348	2.1	99.052	132.362	74.124	344.928	28.444
2.2	5.110	0.323	5.432	4.787	1.256	6.365	3.854	2.2	165.603	228.631	119.950	581.298	47.178
2.3	5.624	0.356	5.979	5.268	1.265	6.888	4.359	2.3	276.868	395.117	194.008	980.561	78.176
2.4	6.137	0.389	6.527	5.748	1.274	7.412	4.863	2.4	462.890	683.092	313.672	1655.569	129.422

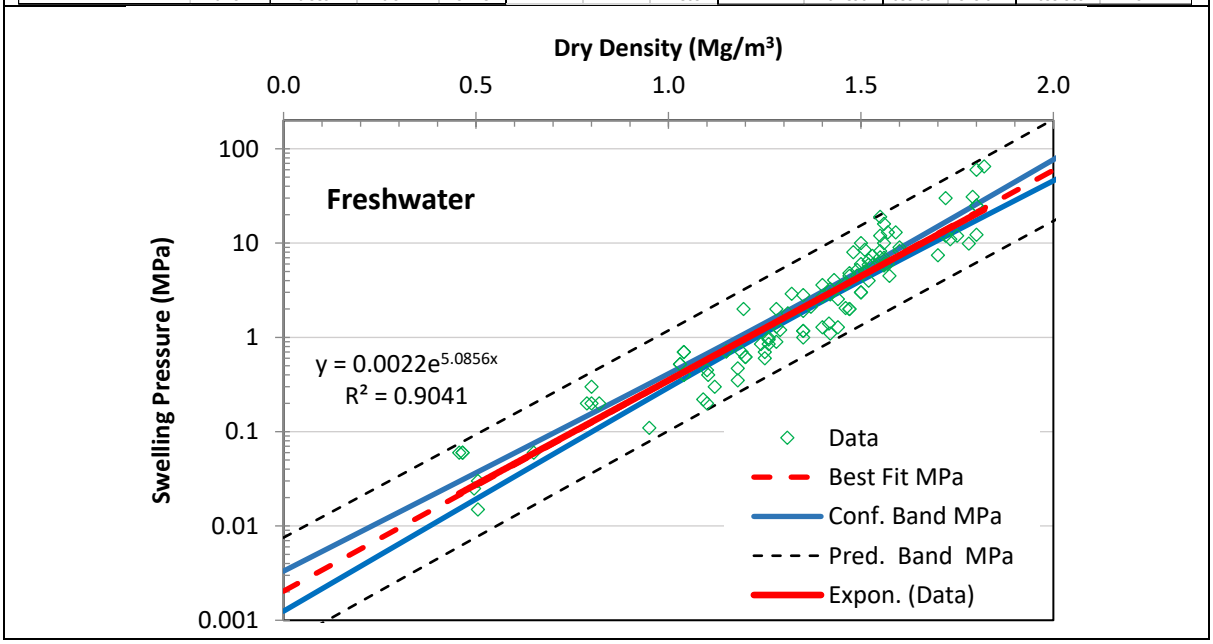

Figure E1. Best-Fit and Confidence Bands for Swelling Pressure in Freshwater

TDS = 5 to 12 g/L			
Derived values			
Slope, m	m	5.222	SLOPE(y,x)
Intercept, b	b	-6.995	NTERCEPT(y,x)
Observations, n	n	40	COUNT(x)
Std error in estimate, S_{yx}	SYX	0.620	STEYX(y,x)
Average x	XAVG	1.361	AVERAGE(x)
SSX	SSX	2.623	DEVSQ(x)
t(a/2,df)	t	2.334	TINV(a/2,df)
Degree of confidence (%)		95	
	a	0.05	
	df	38	n-2

Regression line		Confidence interval			Prediction interval			Invers X & Y					
x	y	CI	y+CI	y-CI	PI	y+PI	y-PI	Dry Density (Mg/m^3)	Best Fit MPa	Upper Conf. Band MPa	Lower Conf. Band MPa	Upper Pred. Band MPa	Lower Pred. Band MPa
0	-6.995	1.237	-5.758	-8.232	1.903	-5.092	-8.898	0	0.001	0.003	0.000	0.006	0.000
0.1	-6.473	1.149	-5.324	-7.622	1.847	-4.626	-8.320	0.1	0.002	0.005	0.000	0.010	0.000
0.2	-5.951	1.062	-4.889	-7.012	1.794	-4.156	-7.745	0.2	0.003	0.008	0.001	0.016	0.000
0.3	-5.428	0.975	-4.454	-6.403	1.744	-3.684	-7.172	0.3	0.004	0.012	0.002	0.025	0.001
0.4	-4.906	0.888	-4.018	-5.794	1.697	-3.209	-6.603	0.4	0.007	0.018	0.003	0.040	0.001
0.5	-4.384	0.802	-3.582	-5.186	1.654	-2.730	-6.038	0.5	0.012	0.028	0.006	0.065	0.002
0.6	-3.862	0.717	-3.145	-4.579	1.614	-2.248	-5.476	0.6	0.021	0.043	0.010	0.106	0.004
0.7	-3.340	0.633	-2.707	-3.973	1.579	-1.761	-4.918	0.7	0.035	0.067	0.019	0.172	0.007
0.8	-2.818	0.551	-2.267	-3.368	1.548	-1.270	-4.365	0.8	0.060	0.104	0.034	0.281	0.013
0.9	-2.295	0.471	-1.824	-2.766	1.521	-0.774	-3.816	0.9	0.101	0.161	0.063	0.461	0.022
1	-1.773	0.395	-1.378	-2.168	1.499	-0.274	-3.272	1	0.170	0.252	0.114	0.760	0.038
1.1	-1.251	0.327	-0.924	-1.578	1.483	0.232	-2.734	1.1	0.286	0.397	0.206	1.261	0.065
1.2	-0.729	0.270	-0.459	-0.999	1.471	0.742	-2.200	1.2	0.482	0.632	0.368	2.101	0.111
1.3	-0.207	0.235	0.028	-0.442	1.465	1.259	-1.672	1.3	0.813	1.029	0.643	3.520	0.188
1.4	0.316	0.231	0.547	0.084	1.465	1.780	-1.149	1.4	1.371	1.728	1.088	5.931	0.317
1.5	0.838	0.260	1.098	0.578	1.469	2.307	-0.632	1.5	2.311	2.998	1.782	10.046	0.532
1.6	1.360	0.313	1.673	1.047	1.480	2.840	-0.120	1.6	3.896	5.326	2.850	17.108	0.887
1.7	1.882	0.379	2.261	1.503	1.495	3.377	0.387	1.7	6.567	9.597	4.494	29.290	1.472
1.8	2.404	0.454	2.858	1.950	1.516	3.920	0.889	1.8	11.070	17.428	7.032	50.401	2.432
1.9	2.926	0.533	3.459	2.394	1.541	4.468	1.385	1.9	18.661	31.794	10.953	87.157	3.996
2	3.449	0.615	4.063	2.834	1.571	5.020	1.877	2	31.457	58.166	17.013	151.421	6.535
2.1	3.971	0.698	4.669	3.272	1.606	5.577	2.365	2.1	53.028	106.609	26.376	264.231	10.642
2.2	4.493	0.783	5.276	3.710	1.645	6.138	2.848	2.2	89.389	195.639	40.842	462.993	17.258
2.3	5.015	0.869	5.884	4.146	1.687	6.702	3.328	2.3	150.682	359.335	63.186	814.392	27.880
2.4	5.537	0.956	6.493	4.582	1.733	7.271	3.804	2.4	254.004	660.422	97.693	1437.602	44.879

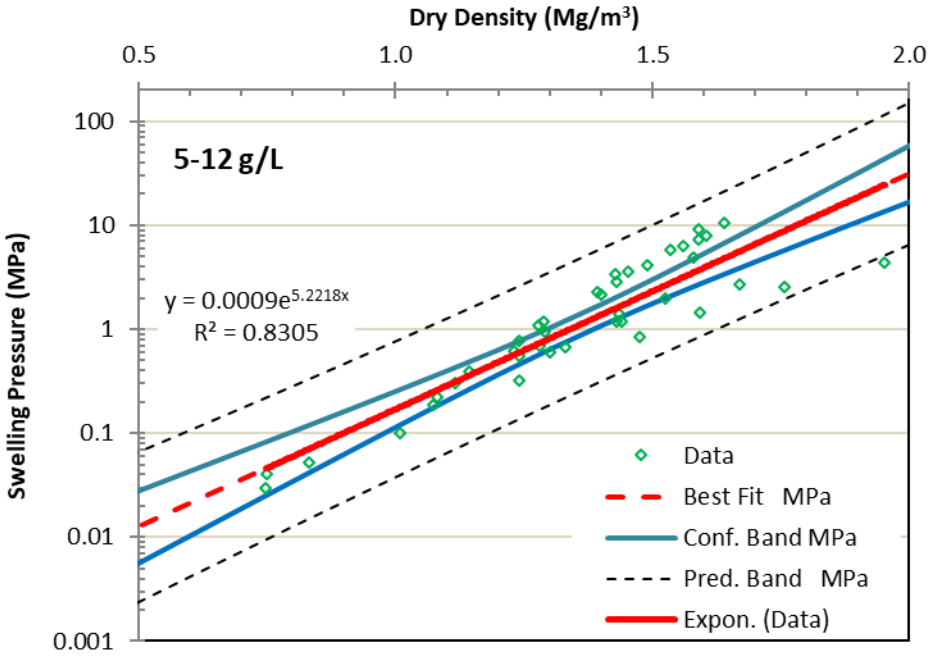

Figure E2. Best-Fit and Confidence Bands for Swelling Pressure in 5 to 12 g/L TDS

50 to 60 g/L TDS			
Derived values			
Slope, m	m	6.302	SLOPE(y,x)
Intercept, b	b	-8.549	NTERCEPT(y,x)
Observations, n	n	21.000	COUNT(x)
Std error in estimate, S_{yx}	SYX	0.618	STEYX(y,x)
Average x	XAVG	1.395	AVERAGE(x)
SSX	SSX	1.238	DEVSQ(x)
t(a/2,df)	t	2.433	TINV(a/2,df)
Degree of confidence (%)		95	
	a	0.05	
	df	19.000	n-2

Regression line		Confidence interval			Prediction interval			Invers X & Y					
x	y	CI	y+CI	y-CI	PI	y+PI	y-PI	Dry Density Mg/m^3	Best Fit MPa	Upper Conf. Band MPa	Lower Conf. Band MPa	Upper Pred.Band MPa	Lower Pred. Band MPa
0	-8.549	1.914	-6.634	-10.463	2.434	-6.114	-10.983	0	0.000	0.001	0.000	0.002	0.000
0.1	-7.918	1.781	-6.137	-9.700	2.331	-5.587	-10.250	0.1	0.000	0.002	0.000	0.004	0.000
0.2	-7.288	1.648	-5.640	-8.937	2.232	-5.057	-9.520	0.2	0.001	0.004	0.000	0.006	0.000
0.3	-6.658	1.516	-5.142	-8.174	2.136	-4.522	-8.794	0.3	0.001	0.006	0.000	0.011	0.000
0.4	-6.028	1.385	-4.643	-7.412	2.044	-3.983	-8.072	0.4	0.002	0.010	0.001	0.019	0.000
0.5	-5.397	1.254	-4.144	-6.651	1.958	-3.439	-7.356	0.5	0.005	0.016	0.001	0.032	0.001
0.6	-4.767	1.124	-3.643	-5.891	1.878	-2.890	-6.645	0.6	0.009	0.026	0.003	0.056	0.001
0.7	-4.137	0.995	-3.142	-5.132	1.804	-2.333	-5.941	0.7	0.016	0.043	0.006	0.097	0.003
0.8	-3.507	0.869	-2.638	-4.376	1.737	-1.770	-5.244	0.8	0.030	0.072	0.013	0.170	0.005
0.9	-2.877	0.746	-2.131	-3.622	1.679	-1.198	-4.555	0.9	0.056	0.119	0.027	0.302	0.011
1	-2.246	0.627	-1.619	-2.873	1.630	-0.617	-3.876	1	0.106	0.198	0.057	0.540	0.021
1.1	-1.616	0.517	-1.099	-2.133	1.590	-0.026	-3.206	1.1	0.199	0.333	0.119	0.975	0.041
1.2	-0.986	0.421	-0.565	-1.407	1.562	0.576	-2.548	1.2	0.373	0.569	0.245	1.779	0.078
1.3	-0.356	0.353	-0.003	-0.708	1.545	1.189	-1.900	1.3	0.701	0.997	0.493	3.284	0.149
1.4	0.275	0.328	0.603	-0.054	1.539	1.814	-1.265	1.4	1.316	1.827	0.948	6.135	0.282
1.5	0.905	0.357	1.262	0.547	1.546	2.451	-0.641	1.5	2.471	3.533	1.729	11.597	0.527
1.6	1.535	0.429	1.964	1.106	1.564	3.099	-0.029	1.6	4.642	7.130	3.021	22.180	0.971
1.7	2.165	0.527	2.692	1.639	1.594	3.759	0.572	1.7	8.717	14.761	5.148	42.901	1.771
1.8	2.796	0.638	3.433	2.158	1.634	4.429	1.162	1.8	16.371	30.985	8.650	83.871	3.195
1.9	3.426	0.757	4.183	2.669	1.684	5.110	1.742	1.9	30.745	65.550	14.421	165.604	5.708
2	4.056	0.881	4.937	3.175	1.743	5.799	2.313	2	57.741	139.324	23.930	329.961	10.104
2.1	4.686	1.008	5.694	3.679	1.810	6.497	2.876	2.1	108.440	296.995	39.594	662.838	17.741
2.2	5.316	1.136	6.453	4.180	1.885	7.201	3.431	2.2	203.655	634.341	65.383	1341.290	30.922
2.3	5.947	1.266	7.213	4.680	1.966	7.913	3.981	2.3	382.473	1356.709	107.824	2731.792	53.549
2.4	6.577	1.397	7.974	5.180	2.053	8.630	4.524	2.4	718.300	2904.532	177.638	5595.638	92.207

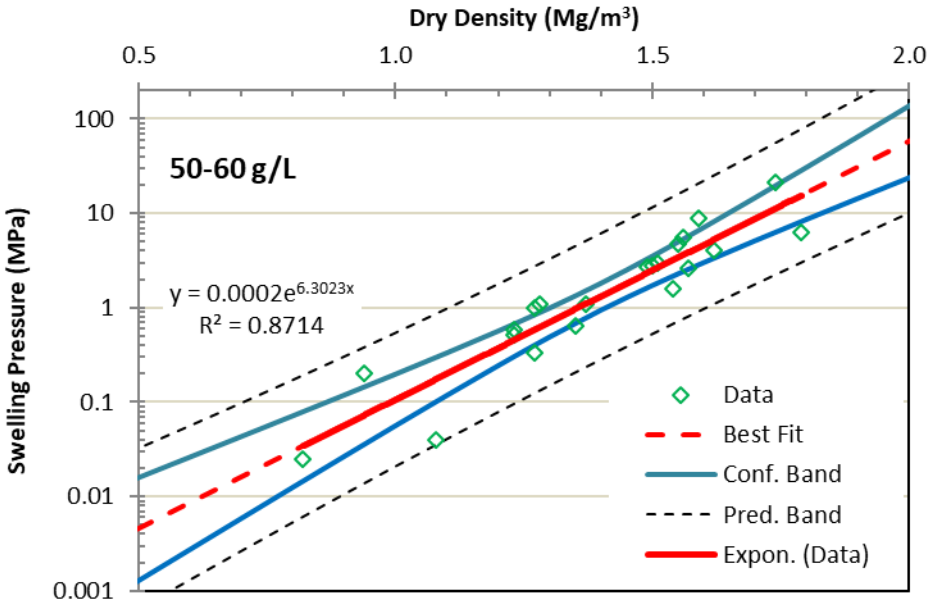

Figure E3. Best-Fit and Confidence Bands for Swelling Pressure in 50 to 60 g/L TDS

100 to 150 g/L TDS			
Derived values			
Slope, m	m	6.144	SLOPE(y,x)
Intercept, b	b	-8.569	INTERCEPT(y,x)
Observations, n	n	25.000	COUNT(x)
Std error in estimate, S_{yx}	SYX	0.650	STEYX(y,x)
Average x	XAVG	1.319	AVERAGE(x)
SSX	SSX	3.068	DEVSQ(x)
t(a/2,df)	t	2.398	TINV(a/2,df)
Degree of confidence (%)		95	
	a	0.05	
	df	23.000	n-2

Regression line		Confidence interval			Prediction interval			Invers X & Y					
x	y	CI	y+CI	y-CI	PI	y+PI	y-PI	Dry Density Mg/m^3	Best Fit MPa	Upper Conf. Band MPa	Lower Conf. Band MPa	Upper Pred. Band MPa	Lower Pred. Band MPa
0	-8.569	1.215	-7.354	-9.784	1.976	-6.593	-10.545	0	0.000	0.001	0.000	0.001	0.000
0.1	-7.954	1.129	-6.825	-9.083	1.925	-6.030	-9.879	0.1	0.000	0.001	0.000	0.002	0.000
0.2	-7.340	1.044	-6.296	-8.384	1.876	-5.464	-9.216	0.2	0.001	0.002	0.000	0.004	0.000
0.3	-6.726	0.959	-5.766	-7.685	1.830	-4.895	-8.556	0.3	0.001	0.003	0.000	0.007	0.000
0.4	-6.111	0.876	-5.236	-6.987	1.788	-4.323	-7.899	0.4	0.002	0.005	0.001	0.013	0.000
0.5	-5.497	0.793	-4.704	-6.290	1.749	-3.748	-7.246	0.5	0.004	0.009	0.002	0.024	0.001
0.6	-4.882	0.712	-4.170	-5.594	1.714	-3.168	-6.596	0.6	0.008	0.015	0.004	0.042	0.001
0.7	-4.268	0.633	-3.635	-4.901	1.683	-2.585	-5.950	0.7	0.014	0.026	0.007	0.075	0.003
0.8	-3.653	0.557	-3.096	-4.211	1.656	-1.998	-5.309	0.8	0.026	0.045	0.015	0.136	0.005
0.9	-3.039	0.486	-2.553	-3.525	1.633	-1.406	-4.672	0.9	0.048	0.078	0.029	0.245	0.009
1	-2.424	0.422	-2.003	-2.846	1.615	-0.810	-4.039	1	0.089	0.135	0.058	0.445	0.018
1.1	-1.810	0.368	-1.442	-2.178	1.602	-0.208	-3.412	1.1	0.164	0.236	0.113	0.812	0.033
1.2	-1.196	0.329	-0.866	-1.525	1.593	0.398	-2.789	1.2	0.303	0.421	0.218	1.488	0.061
1.3	-0.581	0.312	-0.269	-0.893	1.590	1.009	-2.171	1.3	0.559	0.764	0.409	2.742	0.114
1.4	0.033	0.320	0.353	-0.287	1.591	1.625	-1.558	1.4	1.034	1.424	0.751	5.077	0.211
1.5	0.648	0.351	0.999	0.297	1.598	2.246	-0.950	1.5	1.911	2.714	1.346	9.446	0.387
1.6	1.262	0.400	1.662	0.863	1.609	2.871	-0.347	1.6	3.533	5.268	2.369	17.662	0.707
1.7	1.877	0.461	2.337	1.416	1.625	3.502	0.251	1.7	6.531	10.351	4.121	33.184	1.285
1.8	2.491	0.529	3.020	1.962	1.646	4.137	0.845	1.8	12.074	20.501	7.111	62.639	2.327
1.9	3.105	0.604	3.709	2.502	1.672	4.777	1.434	1.9	22.320	40.819	12.204	118.767	4.195
2	3.720	0.681	4.401	3.038	1.701	5.421	2.019	2	41.261	81.561	20.873	226.159	7.528
2.1	4.334	0.762	5.096	3.573	1.735	6.069	2.599	2.1	76.276	163.371	35.612	432.409	13.455
2.2	4.949	0.844	5.792	4.105	1.773	6.721	3.176	2.2	141.006	327.818	60.651	829.927	23.957
2.3	5.563	0.927	6.490	4.636	1.814	7.377	3.750	2.3	260.666	658.645	103.162	1598.626	42.503
2.4	6.178	1.011	7.189	5.166	1.858	8.036	4.320	2.4	481.874	1324.627	175.296	3089.665	75.155

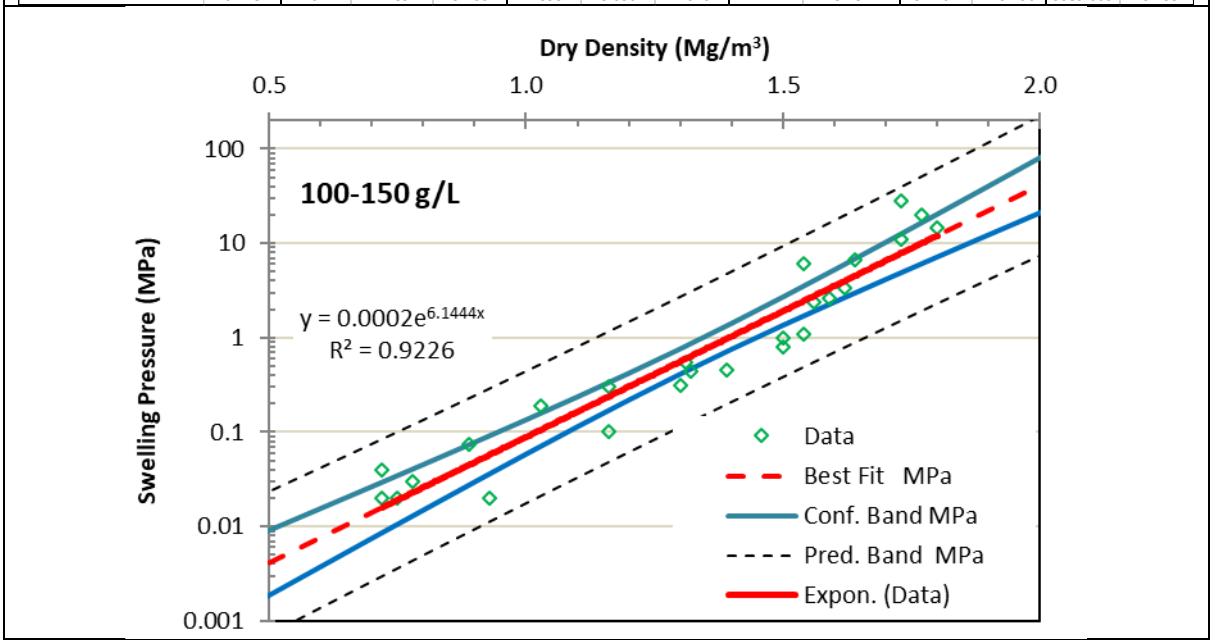

Figure E4. Best-Fit and Confidence Bands for Swelling Pressure (100 to 150 g/L TDS)

200-225 g/L TDS (SR-L)			
Derived values			
Slope, m	m	5.150	SLOPE(y,x)
Intercept, b	b	-7.475	INTERCEPT(y,x)
Observations, n	n	14	COUNT(x)
Std error in estimate, S_{yx}	SYX	0.691	STEYX(y,x)
Average x	XAVG	1.589	AVERAGE(x)
SSX	SSX	0.819	DEVSQ(x)
t(a/2,df)	t	2.560	TINV(a/2,df)
Degree of confidence (%)		95	
	a	0.05	
	df	12	n-2

Regression line		Confidence interval			Prediction interval			Invers X & Y		upper	lower	upper	lower
x (Mg/m^3)	y (MPa)	CI	y+CI	y-CI	PI	y+PI	y-PI	Dry Density Mg/m^3	Best Fit MPa	Conf. Band MPa	Conf. Band MPa	Pred. Band MPa	Pred. Band MPa
0	-7.475	3.141	-4.334	-10.615	3.604	-3.871	-11.079	0	0.001	0.013	0.000	0.021	0.000
0.1	-6.960	2.948	-4.012	-9.907	3.437	-3.523	-10.397	0.1	0.001	0.018	0.000	0.030	0.000
0.2	-6.445	2.755	-3.690	-9.200	3.273	-3.171	-9.718	0.2	0.002	0.025	0.000	0.042	0.000
0.3	-5.930	2.563	-3.367	-8.493	3.113	-2.817	-9.043	0.3	0.003	0.034	0.000	0.060	0.000
0.4	-5.415	2.371	-3.044	-7.786	2.957	-2.457	-8.372	0.4	0.004	0.048	0.000	0.086	0.000
0.5	-4.900	2.180	-2.720	-7.080	2.807	-2.093	-7.707	0.5	0.007	0.066	0.001	0.123	0.000
0.6	-4.385	1.990	-2.395	-6.375	2.661	-1.724	-7.046	0.6	0.012	0.091	0.002	0.178	0.001
0.7	-3.870	1.800	-2.070	-5.670	2.523	-1.347	-6.393	0.7	0.021	0.126	0.003	0.260	0.002
0.8	-3.355	1.613	-1.742	-4.968	2.393	-0.962	-5.748	0.8	0.035	0.175	0.007	0.382	0.003
0.9	-2.840	1.427	-1.413	-4.267	2.272	-0.568	-5.112	0.9	0.058	0.243	0.014	0.567	0.006
1	-2.325	1.244	-1.081	-3.570	2.162	-0.163	-4.487	1	0.098	0.339	0.028	0.849	0.011
1.1	-1.810	1.066	-0.744	-2.876	2.064	0.254	-3.875	1.1	0.164	0.475	0.056	1.289	0.021
1.2	-1.295	0.895	-0.400	-2.191	1.982	0.686	-3.277	1.2	0.274	0.670	0.112	1.986	0.038
1.3	-0.780	0.737	-0.044	-1.517	1.915	1.135	-2.695	1.3	0.458	0.957	0.219	3.110	0.068
1.4	-0.265	0.600	0.335	-0.865	1.867	1.601	-2.132	1.4	0.767	1.397	0.421	4.960	0.119
1.5	0.250	0.504	0.753	-0.254	1.838	2.088	-1.588	1.5	1.284	2.124	0.776	8.066	0.204
1.6	0.765	0.473	1.237	0.292	1.830	2.594	-1.065	1.6	2.148	3.447	1.339	13.389	0.345
1.7	1.280	0.520	1.799	0.760	1.842	3.122	-0.563	1.7	3.595	6.044	2.138	22.692	0.570
1.8	1.794	0.627	2.421	1.168	1.875	3.670	-0.081	1.8	6.016	11.258	3.215	39.251	0.922
1.9	2.309	0.769	3.079	1.540	1.928	4.237	0.382	1.9	10.069	21.729	4.666	69.218	1.465
2	2.824	0.931	3.756	1.893	1.998	4.822	0.826	2	16.851	42.758	6.641	124.258	2.285
2.1	3.339	1.104	4.443	2.235	2.084	5.423	1.255	2.1	28.201	85.057	9.350	226.665	3.509
2.2	3.854	1.283	5.138	2.571	2.184	6.039	1.670	2.2	47.196	170.302	13.080	419.350	5.312
2.3	4.369	1.467	5.836	2.903	2.297	6.666	2.072	2.3	78.986	342.387	18.221	785.413	7.943
2.4	4.884	1.653	6.537	3.231	2.420	7.304	2.464	2.4	132.188	690.248	25.315	1486.641	11.754

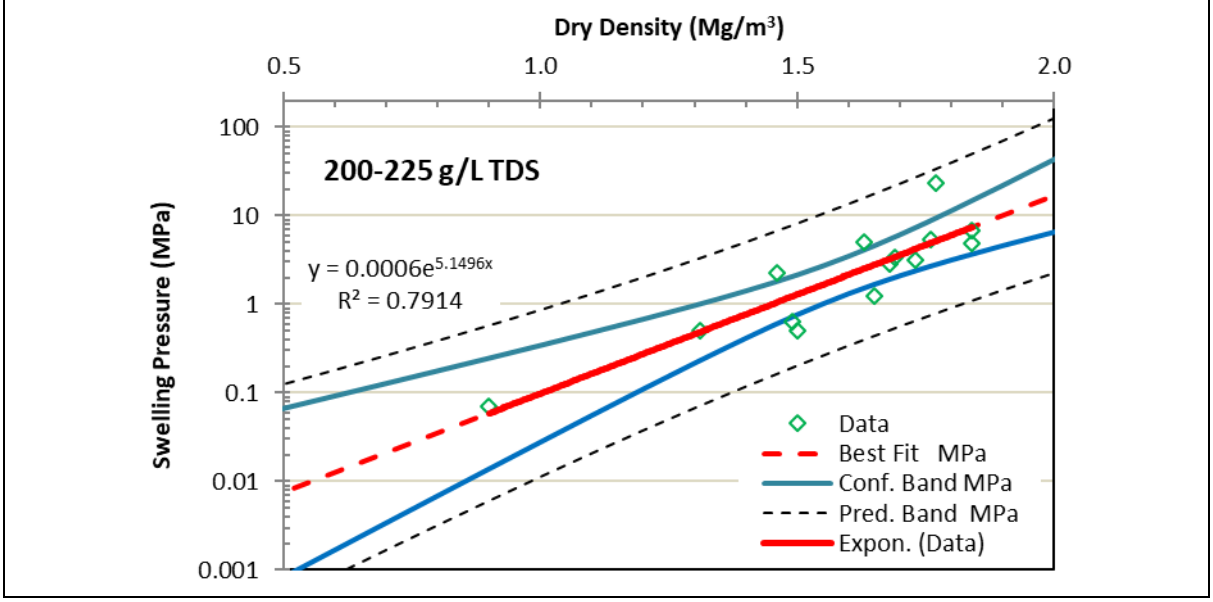

Figure E5. Best-Fit and Confidence Bands for Swelling Pressure (200-225 g/L TDS)

>335 g/L TDS			
Derived values			
Slope, m	m	7.186	SLOPE(y,x)
Intercept, b	b	-11.142	INTERCEPT(y,x)
Observations, n	n	16	COUNT(x)
Std error in estimate, S_{yx}	SYX	0.815	STEYX(y,x)
Average x	XAVG	1.342	AVERAGE(x)
SSX	SSX	1.182	DEVSQ(x)
t(a/2,df)	t	2.510	TINV(a/2,df)
Degree of confidence (%)		95	
	a	0.05	
	df	14.000	n-2

Regression line		Confidence interval			Prediction interval			Invers X & Y		upper	lower	upper	lower
x (Mg/m^3)	y	CI	y+CI	y-CI	PI	y+PI	y-PI	Dry Density Mg/m^3	Best Fit MPa	Conf. Band MPa	Conf. Band MPa	Pred. Band MPa	Pred. Band MPa
0	-11.142	2.577	-8.565	-13.718	3.290	-7.851	-14.432	0	0.000	0.000	0.000	0.000	0.000
0.1	-10.423	2.393	-8.030	-12.816	3.148	-7.275	-13.571	0.1	0.000	0.000	0.000	0.001	0.000
0.2	-9.704	2.209	-7.495	-11.914	3.011	-6.693	-12.716	0.2	0.000	0.001	0.000	0.001	0.000
0.3	-8.986	2.027	-6.959	-11.012	2.880	-6.106	-11.866	0.3	0.000	0.001	0.000	0.002	0.000
0.4	-8.267	1.845	-6.422	-10.112	2.755	-5.512	-11.023	0.4	0.000	0.002	0.000	0.004	0.000
0.5	-7.549	1.665	-5.884	-9.214	2.638	-4.911	-10.187	0.5	0.001	0.003	0.000	0.007	0.000
0.6	-6.830	1.487	-5.343	-8.317	2.529	-4.301	-9.360	0.6	0.001	0.005	0.000	0.014	0.000
0.7	-6.112	1.312	-4.800	-7.424	2.431	-3.681	-8.542	0.7	0.002	0.008	0.001	0.025	0.000
0.8	-5.393	1.141	-4.252	-6.534	2.343	-3.050	-7.736	0.8	0.005	0.014	0.001	0.047	0.000
0.9	-4.675	0.976	-3.698	-5.651	2.267	-2.407	-6.942	0.9	0.009	0.025	0.004	0.090	0.001
1	-3.956	0.822	-3.134	-4.778	2.205	-1.751	-6.161	1	0.019	0.044	0.008	0.174	0.002
1.1	-3.237	0.685	-2.553	-3.922	2.158	-1.080	-5.395	1.1	0.039	0.078	0.020	0.340	0.005
1.2	-2.519	0.577	-1.942	-3.096	2.126	-0.393	-4.645	1.2	0.081	0.143	0.045	0.675	0.010
1.3	-1.800	0.518	-1.283	-2.318	2.111	0.310	-3.911	1.3	0.165	0.277	0.098	1.364	0.020
1.4	-1.082	0.523	-0.559	-1.605	2.112	1.030	-3.194	1.4	0.339	0.572	0.201	2.802	0.041
1.5	-0.363	0.592	0.229	-0.955	2.130	1.767	-2.493	1.5	0.695	1.257	0.385	5.853	0.083
1.6	0.355	0.705	1.061	-0.350	2.164	2.520	-1.809	1.6	1.427	2.889	0.705	12.426	0.164
1.7	1.074	0.846	1.920	0.228	2.214	3.288	-1.140	1.7	2.927	6.822	1.256	26.795	0.320
1.8	1.793	1.003	2.795	0.790	2.279	4.071	-0.486	1.8	6.005	16.364	2.203	58.624	0.615
1.9	2.511	1.168	3.679	1.343	2.356	4.867	0.155	1.9	12.318	39.624	3.829	129.978	1.167
2	3.230	1.340	4.570	1.890	2.446	5.676	0.784	2	25.271	96.520	6.616	291.674	2.189
2.1	3.948	1.516	5.464	2.432	2.546	6.495	1.402	2.1	51.842	236.033	11.387	661.613	4.062
2.2	4.667	1.694	6.361	2.973	2.657	7.323	2.010	2.2	106.353	578.761	19.543	1515.159	7.465
2.3	5.385	1.874	7.260	3.511	2.775	8.160	2.610	2.3	218.181	1421.878	33.479	3499.184	13.604
2.4	6.104	2.056	8.160	4.048	2.901	9.005	3.203	2.4	447.594	3498.182	57.270	8141.081	24.609

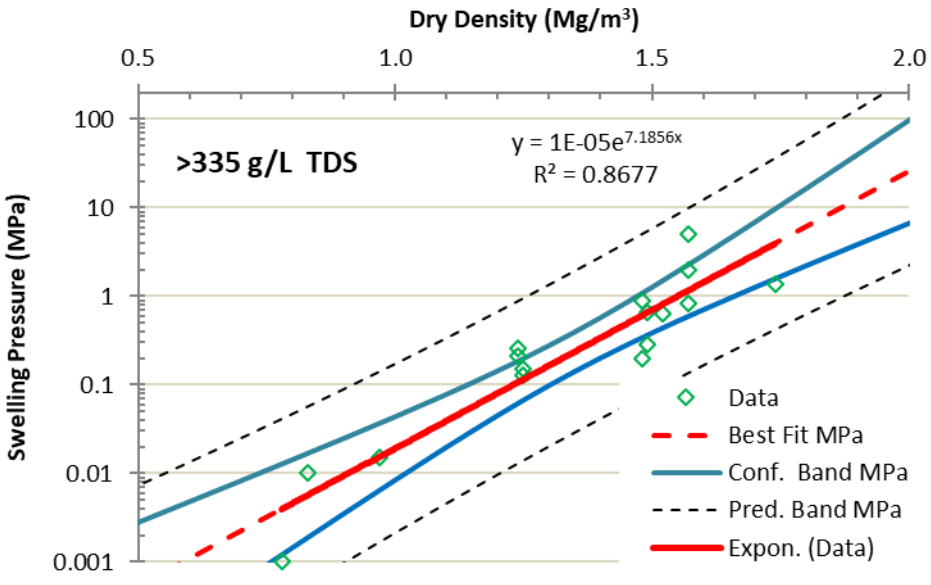

Figure E6. Best-Fit and Confidence Bands for Swelling Pressure (>335 g/L TDS)

APPENDIX F. EFFECTS OF VARYING PLACEMENT ROOM AND SPACER BLOCK DIMENSIONS ON HOMOGENIZED DRY DENSITY OF SEALING MATERIALS

Table F-1: Influence of Tunnel Dimension and Bentonite Density on Average Density of Tunnel Fill (0.3 m spacer blocks)

0.3 m spacer block geometry						0.3 m spacer block geometry					
		Volume (m3)	Units per m of tunnel	Vol per m tunnel	Bentonite volume per m tunnel			Volume (m3)	Units per m of tunnel	Vol per m tunnel	Bentonite volume per m tunnel
Tunnel height	2.2		1	7.040		Tunnel height	2.55		1	8.543	
Tunnel width	3.2					Tunnel width	3.35				
UFC volume	0.577	0.577	1.538	0.887		UFC volume	0.577	0.577	1.538	0.887	
Buffer Box length	2.9	2.9	1.538	4.460	3.573	Buffer Box length	2.9	2.9	1.538	4.460	3.573
Buffer Box height/width	1					Buffer Box height/w	1				
Spacer block length	2.9					Spacer block length	2.9				
Spacer block width	0.3					Spacer block width	0.3				
Spacer block height	1	0.87	1.538	1.338	1.338	Spacer block height	1	0.87	1.538	1.338	1.338
Spacer block volume						Spacer block volume					
Tile fill thickness	0.15					Tile fill thickness	0.15				
Tile width	3.2					Tile width	3.35				
Tile floor volume	0.480	0.480	1.000	0.480	0.48	Tile floor volume	0.503	0.503	1.000	0.503	0.5025
Concrete floor thickness	0					Concrete floor thickr	0				
Concrete floor volume		0	1	0.000		Concrete floor volume		0	1	0.000	
Gap Volume				0.762	0.762	Gap Volume				2.242	2.242
HCB volume / m tunnel					5.391	HCB volume / m tunnel					5.414
Gap Fill volume / m tunnel					0.762	Gap Fill volume / m tunnel					2.242
HCB density	**1.7**	**Mass per m tunnel**			**9.165**	**HCB density**	**1.7**	**Mass per m tunnel**			**9.203**
GF density	**1.41**	**Mass per m tunnel**			**1.074**	**GF density**	**1.41**	**Mass per m tunnel**			**3.161**
Average Density of Tunnel Fill (Mg/m3)					**1.664**	**Average**					**1.615**

0.3 m spacer block geometry						0.3 m spacer block geometry					
		Unit Volume	Units per m of tunnel	Vol/ m tunnel	Bentonite volume/m tunnel			Volume	Units per m of tunnel	Vol/ m tunnel	Bentonite volume/m tunnel
Tunnel height	2.2		1	7.040		Tunnel height	2.55		1	8.543	
Tunnel width	3.2					Tunnel width	3.35				
UFC volume	0.577	0.577	1.538	0.887		UFC volume	0.577	0.577	1.538	0.887	
Buffer Box length	2.9	2.9	1.538	4.462	3.575	Buffer Box length	2.9	2.9	1.538	4.460	3.573
Buffer Box height/width	1					Buffer Box height/w	1				
Spacer block length	2.9					Spacer block length	2.9				
Spacer block width	0.3					Spacer block width	0.3				
Spacer block height	1	0.87	1.538	1.338	1.338	Spacer block height	1	0.87	1.538	1.338	1.338
Spacer block volume						Spacer block volume					
Tile fill thickness	0.15					Tile fill thickness	0.15				
Tile width	3.2					Tile width	3.35				
Tile floor volume	0.48	0.48	1	0.480	0.48	Tile floor volume	0.5025	0.5025	1	0.503	0.503
Concrete floor thickness	0					Concrete floor thickr	0				
Concrete floor volume		0	1	0.000		Concrete floor volume		0	1	0.000	
Gap Volume				0.760	0.760	Gap Volume				2.242	2.242
HCB volume / m tunnel					5.393	HCB volume / m tunnel					5.414
Gap Fill volume / m tunnel					0.760	Gap Fill volume / m tunnel					2.242
HCB density	**1.73**	**Mass per m tunnel**			**9.329**	**HCB density**	**1.73**	**Mass per m tunnel**			**9.366**
GF density	**1.48**	**Mass per m tunnel**			**1.125**	**GF density**	**1.48**	**Mass per m tunnel**			**3.318**
Average Density of Tunnel Fill (Mg/m3)					**1.699**	**Average**					**1.657**

Table F-2: Influence of Tunnel Dimension and Bentonite Density on Average Density of Tunnel Fill (0.5 m spacer blocks)

0.5 m spacer block geometry-base case							0.5 m spacer block geometry-base case						
		Volume (m3)	Units per m of tunnel	Vol per m tunnel	Bentonite volume per m tunnel				Volume (m3)	Units per m of tunnel	Vol per m tunnel	Bentonite volume per m tunnel
Tunnel height (m)	2.2		1	7.040			Tunnel height	2.55		1	8.543	
Tunnel width (m)	3.2						Tunnel width	3.35				
UFC volume	0.577	0.577	1.333	0.769			UFC volume	0.577	0.577	1.333	0.769	
Buffer Box length (m)	2.9	2.9	1.333	3.866	3.097		Buffer Box length	2.9	2.9	1.333	3.866	3.097
Buffer Box height/width	1						Buffer Box height/w	1				
Spacer block length (m)	2.9						Spacer block length	2.9				
Spacer block width (m)	0.5						Spacer block width	0.5				
Spacer block height (m)	1	1.45	1.333	1.933	1.933		Spacer block height	1	1.45	1.333	1.933	1.933
Spacer block volume	1.45						Spacer block volume	1.45				
Tile fill thickness (m)	0.15						Tile fill thickness	0.15				
Tile width (m)	3.2						Tile width	3.35				
Tile floor volume	0.48	0.48	1	0.480	0.48		Tile floor volume	0.503	0.503	1	0.503	0.503
Concrete floor thickness	0						Concrete floor thickr	0				
Concrete floor volume		0	1	0.000			Concrete floor volume		0	1	0.000	
Gap Volume				0.761	0.761		Gap Volume				2.241	2.241
HCB volume / m tunnel fill					5.510		HCB volume / m tunnel					5.532
Gap Fill volume / m tunnel fill					0.761		Gap Fill volume / m tunnel					2.241
HCB Density	**1.7**	**Mass per m tunnel**			**9.367**		**HCB density**	**1.7**	**Mass per m tunnel**			**9.405**
GF density	**1.41**	**Mass per m tunnel**			**1.074**		**GF density**	**1.41**	**Mass per m tunnel**			**3.160**
Average Density of Tunnel Fill (Mg/m3)					**1.665**		**Average Density of Tunnel Fill (Mg/m3)**					**1.616**

0.5 m spacer block geometry-higher density fill							0.5 m spacer block geometry-higher density fill						
		Volume (m3)	Units per m of tunnel	Vol per m tunnel	Bentonite volume per m tunnel				Volume (m3)	Units per m of tunnel	Vol per m tunnel	Bentonite volume per m tunnel
Tunnel height	2.2		1	7.040			Tunnel height	2.55		1	8.543	
Tunnel width	3.2						Tunnel width	3.35				
UFC volume	0.577	0.577	1.333	0.769			UFC volume	0.577	0.577	1.333	0.769	
Buffer Box length	2.9	2.9	1.333	3.866	3.097		Buffer Box length	2.9	2.9	1.333	3.866	3.097
Buffer Box height/width	1						Buffer Box height/w	1				
Spacer block length	2.9						Spacer block length	2.9				
Spacer block width	0.5						Spacer block width	0.5				
Spacer block height	1	1.45	1.333	1.933	1.933		Spacer block height	1	1.45	1.333	1.933	1.933
Spacer block volume	1.45						Spacer block volume	1.45				
Tile fill thickness	0.15						Tile fill thickness	0.15				
Tile width	3.2						Tile width	3.35				
Tile floor volume	0.480	0.480	1.000	0.480	0.480		Tile floor volume	0.503	0.503	1	0.503	0.503
Concrete floor thickness	0						Concrete floor thickr	0				
Concrete floor volume		0	1	0.000			Concrete floor volume		0	1	0.000	
Gap Volume				0.761	0.761		Gap Volume				2.241	2.241
HCB volume / m tunnel					5.510		HCB volume / m tunnel					5.532
Gap Fill volume / m tunnel					0.761		Gap Fill volume / m tunnel					2.241
HCB density	**1.73**	**Mass per m tunnel**			**9.532**		**HCB density**	**1.73**	**Mass per m tunnel**			**9.571**
GF density	**1.48**	**Mass per m tunnel**			**1.127**		**GF density**	**1.48**	**Mass per m tunnel**			**3.317**
Average Density of Tunnel Fill (Mg/m3)					**1.700**		**Average Density of Tunnel Fill (Mg/m3)**					**1.658**